RENEWABLE OCEAN ENERGY: THE USE OF HYDRO-KITES IN THE AGULHAS CURRENT TO GENERATE ELECTRICITY

Tasha Giulia Smith

Submitted in fulfillment of the requirements for the degree of

Master of Science in Engineering

In the

Civil Engineering program

School of Engineering

University of KwaZulu-Natal

Durban

2016

Supervisor: Professor D. D. Stretch

ABSTRACT

Using fossil fuels to generate electricity is an unsustainable and environmentally damaging practice. Renewable energy is a more sustainable alternative which harnesses the earth's natural processes with minimal environmental impact. Ocean currents can be used to produce energy using turbines. Ocean currents are more consistent than wind with a much higher power producing potential due to the larger density of water. Hydro-kites are a lightweight and aerodynamic design consisting of a turbine mounted on a rigid wing which is tethered to the seabed. They can be fully submerged and controlled to fly in a 'figure of 8' shape making use of cross currents and increasing energy producing potential. The Agulhas current located on the East coast of South Africa experiences high velocities. However, energy generation is compromised due to inconsistencies as a result of Natal Pulses propagating southwards through the current. A statistical analysis is presented using measured ADCP current data, Cape Morgan was identified as the location with the highest power producing potential. A concentrated farm of hydro-kites may not be able to generate a considerable power output for up to a month at a time. Implementing a distributed system of hydro-kites along the coast can address the issue of intermittent power, where one location experiences a Natal Pulse, power can be supplied by other unaffected kites. Data from the HYCOM ocean model, verified against the ADCP data, was used to investigate the power potential using smaller kite systems distributed along the coastline as opposed to one main concentrated kite farm. A concentrated system can generate more energy but is inconsistent. The overall feasibility of kite systems and arrays was considered with a focus on submarine power cables within the kite array and grid connection on land. Implementing this project could have a significant social impact in local communities and create jobs in production and maintenance, vital in a country with high unemployment.

PREFACE

As the candidate's Supervisor I agree/do not agree to the submission of this thesis.

…… ……

Prof. D.D. Stretch Date

COLLEGE OF AGRICULTURE, ENGINEERING AND SCIENCE

DECLARATION – PLAGIARISM

I, Tasha Giulia Smith, declare that:

1. The research reported in this thesis, except where otherwise indicated, is my original research.
2. This thesis has not been submitted for any degree or examination at any other university.
3. This thesis does not contain other persons' data, pictures, graphs or other information, unless specifically acknowledged as being sourced from other persons.
4. This thesis does not contain other persons' writing, unless specifically acknowledged as being sourced from other researchers. Where other written sources have been quoted, then:
    a. Their words have been re-written but the general information attributed to them has been referenced
    b. Where their exact words have been used, then their writing has been placed in italics and inside quotation marks, and referenced.
5. This thesis does not contain text, graphics or tables copied and pasted from the Internet, unless specifically acknowledged, and the source being detailed in the thesis and in the References sections.

…… ……

T. G. Smith Date

ACKNOWLEDGEMENTS

I would like to acknowledge the following:

Prof. D. D. Stretch, supervisor and eThekwini Chair for guidance on the research and the subsistence funding.

Wimpie van Rooy from Eskom, for providing the ADCP data that was used in this study.

Dr. Andrew Swanson, for his advice on step-up transformers

All the MSc students for their constant encouragement and philosophical debates.

Michael van der Ham for his patience, love and support.

Members of the band, Not Fat Just Fluffy, for their motivation.

My parents for their support.

Table of Contents

List of Figures

List of Tables

List of symbols

Kite

α	=	Washout (twist)	(°)
A_k	=	Kite area	(m^2)
A_T	=	Turbine area	(m^2)
AR	=	Aspect ratio	
b	=	Wingspan	(m)
B	=	Blockages	
C_{TIP}	=	Tip chord	(m)
C_{ROOT}	=	Root chord	(m)
C_D	=	Drag coefficient	
C_L	=	Lift coefficient	
C_L*	=	Design lift coefficient	
$C_{L\,max}$	=	Maximum lift coefficient	
$\frac{C_L}{C_D}$	=	Lift to drag ration	
C_m	=	Moment coefficient	
cg	=	centre of gravity	
L	=	Length	(m)
μ	=	Dynamic viscosity	(Ns/m^2)
v	=	Kinematic viscosity	(m^2/s)
np	=	Neutral point	
PFW	=	Sweep angle at quarter chord line	(°)
R_e	=	Reynold's number	
STM	=	Stability proportion	
z	=	Taper ratio	

Power

α_{20}	=	Temperature coefficient of resistance of a conductor material at 20°C	
C	=	Capacitance	(F/m)
C_P	=	Betz power coefficient	
d_c	=	Diameter of conductor	(mm)

D_i	=	External diameter of insulation including screen	(mm)
D_T	=	Turbine drag	(N)
ϵ	=	Relative permittivity of insulation	(F/m)
ϕ	=	Phase angle between voltage and current	(°)
f	=	Frequency	(Hz)
F_T	=	Tether tension	(N)
Fi	=	Cable derating factor	
Υ_i	=	Roll, pitch, and yaw rates	(rad/s)
I	=	Current	(A)
k_s	=	Constant for cable type	
k_p	=	Constant for cable type	
L	=	Inductance	(mH/km)
L_i	=	Roll, pitch, and yaw torques	(Nm)
$\dot{m}$	=	Mass flow rate	(kg/s)
n	=	number of cores	
ω	=	Angular velocity	(rad/s)
P	=	Electrical load (kW)	
PF	=	Power factor	
q	=	Dynamic pressure	(Pa)
ρ	=	Density	(kg/m^3)
R’	=	DC Resistance	(Ω/m)
R	=	AC Resistance	(Ω/m)
R_t	=	Conductor resistance at t°C	(Ω/m)
R^2	=	Correlation coefficient	
S*	=	Apparent Power	(VA)
S	=	Cross-sectional Swept Area	(m^2)
s	=	Spacing between conductor centres	(mm)
t	=	Temperature	(°C)
tanδ	=	Loss factor	
v	=	velocity	(m/s)
v_A	=	Apparent velocity	(m/s)

v_{avg}	=	Average velocity	(m/s)
v_{max}	=	Maximum velocity	(m/s)
V_{LL}	=	Line to line voltage	(V)
V_{LN}	=	Line to neutral voltage	(V)
W_d	=	Dielectric loss per phase	(W/m)
X	=	Reactance	(ohm/km)
y_s	=	Skin factor	
y_p	=	Proximity factor	

CHAPTER 1

1. INTRODUCTION

1.1. Introduction

The majority of electricity produced in South Africa is from the burning of coal in power stations. Eskom is the highest contributor of carbon emissions. South Africa had the 13th highest carbon emissions in the world in 2014; 6th in terms of carbon emissions from coal at 395 $MtCO^2$, and 3rd regarding carbon emissions per capita from coal at 7.3 tCO^2 per person (Global Carbon Atlas, 2015). The current energy production system leaves many environmental problems in its wake. Currently, energy demand outweighs what can be supplied. Electrical power is not constant, many areas have experienced blackouts which will only be exacerbated placing a strain on the economy and productivity of the country.

1.2. Renewable and Sustainable Energy

The world needs to migrate to more renewable and sustainable practices of harnessing the world's resources to protect and conserve the earth for the future. Electricity is fundamental and essential to productivity and economic growth. Sustainable power generation aims to take advantage of resources occurring naturally with the objective of producing an unlimited, constant supply of electricity without harming the environment. By the year 2013, South Africa's goal was to be able to generate 10, 000 GWh of completely renewable energy from sources such as biomass, wind power, solar power and small scale hydro-power (Department of Energy, 2003). Only 6,575 GWh of renewable energy was produced in 2014, approximately two-thirds of the target set for 2013. The various types of renewable energy in South Africa are portrayed in Figure 1.1, actual values are shown in Appendix A (Internation Energy Agency, 2014). It can be seen that tidal and wave energy do not feature within the renewable energy mix. Renewable energy makes up only 2.6 % of total energy produced, whereas coal energy contributes 92 %. These values only take modern practices into consideration, ignoring energy generated through other means such as the burning of firewood and dung. Since 2011, when solar power was introduced, and wind power had no significant contribution, solar and wind power have grown substantially (Internation Energy Agency, 2014).

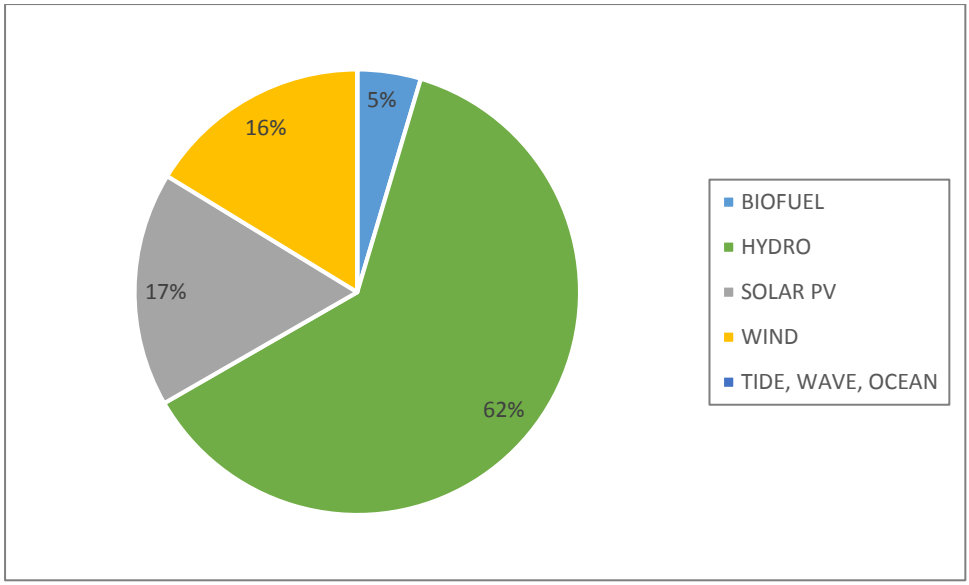

Figure 1.1. The percentage of Renewable Energy Generation 2014 (Internation Energy Agency, 2014).

1.2.1. Fossil Fuels

Eskom is the sole supplier of electrical power in South Africa. Coal power makes up the substantial majority of electricity produced, with nuclear also contributing to the energy mix. The combustion of coal makes up the majority of carbon dioxide emissions which is the main greenhouse gas culprit.

In 2003 when the white paper on renewable energy was released it could be predicted that there would not be sufficient capacity to produce enough electrical power to facilitate the growing demand. To service this demand, a new electrical power plant was required. However, renewable energy projects involve less lead time - the time between initiation and implementation of the project, than for a coal power plant (Department of Energy, 2003).

Coal power involves costs such as the construction of new power stations. Power plants at Medupi and Kusile have been commissioned with a capacity of 4, 764 MW and 4, 800 MW respectively. This form of energy not only carries installation and maintenance costs but incurs additional indirect future expenditure regarding harmful environmental effects. Carbon emissions can lead to health risks and are associated with climate change. Acid mine drainage can compromise water quality by polluting limited water supplies, and in the pursuit of coal extraction from the ground, rivers are drained. Coal power requires large amounts of water to wash coal and cool power stations, during the energy production process Eskom uses approximately 10, 000 litres per second. Water is a precious resource, especially at the present time where the country is advised to conserve water as reserves are limited. The use of coal power has many damaging environmental effects and consequences (Gets, 2013).

1.2.2. Nuclear

Nuclear power has various adverse effects including environmental damage from waste storage, radioactive waste is a serious health and safety hazard (Time for Change, 2007). It is not an affordable source of energy as costs of building new stations and infrastructure are high.

1.2.3. Environmental Impacts

The Kyoto protocol outlined the dire need for developed countries to minimise their greenhouse gas emissions. Coal based power stations can run efficiently for 40 years or more. If more power plants are commissioned, and within their active lifespan there is a requirement to limit the amount of greenhouse gas emissions, more focus will be on renewable energy systems and coal power stations would not be required to function to their full capacity. Big investments in coal power could be lost that could have been used to fund renewable energy projects. South Africa has the largest greenhouse gas emissions in Africa. In 1999, the total amount of renewable energy produced was 9%, mostly from firewood and dung which do not make use of modern technologies. The burning of firewood also adding carbon dioxide into the atmosphere (Department of Energy, 2003).

1.2.4. Politics and Legislation

A significant obstacle in moving towards a more renewable energy system is that the government has invested interest in the fossil fuel and mineral sector. There is a lack of interest in renewable energy schemes due to economic benefits of continued exploitation of fossil fuels. This is evident by the commissioning of two new power stations and the promotion of nuclear energy. A target of 17.8 GW of renewable power is to be met by 2030, yet the government has only approved 3.725 MW. Eskom is funded by the public and should be indebted to the citizens of the country to promote and invest in more sustainable means of energy generation that are not harmful, thus incorporating the need for renewables (Gets, 2013).

The government acknowledged the fact that solar water heating was feasible on a financial level in 2005. Due to the lack of information available to the public on the technology and its benefits coupled with the government having little interest in pursuing these ventures. There is no drive to make renewable energy a more dominant power source. (Gets, 2013)

It should be made easier for more renewable energy projects to enter the industry. A feed-in tariff system could be implemented in which operators of renewable energy are paid per kWh that is fed into the grid. It is hard for any small or medium sized projects to be implemented due to the cost and set up procedures required for renewable energy initiatives (Gets, 2013).

1.2.5. Electricity Grid

Another crucial barrier to renewable energy is access to the national electricity grid controlled by Eskom. There are legal, regulatory, organisational issues in attempting to develop a market for new renewable energy technology including the need for open access to the required infrastructure such as the national electricity grid, to implement the system.

The electricity baseload is the minimum amount of power required over a 24-hour period and is approximately 35 % to 40 % of the maximum load observed during a year. It becomes problematic in attempting to match peak demand with supply. Nuclear power stations are designed to function at full load due to safety concerns and restrictions, coal stations take 8 hours from starting up cold to reach full load capacity and therefore only powered down when maintenance is required. When renewable energy plants are in operation and supplying more energy than is needed, they are shut down so that baseload stations can operate at full power. Renewable energy should be given preference regarding grid access (Gets, 2013).

Operating costs can be kept low when renewable energy plants function with a continuous supply of power. Coal and nuclear power can only accommodate 25 % of variable renewable energy. If the energy generated from renewable sources increases, coal and nuclear power will be required to operate on a diminished scale with renewables having priority, the load factor for these means of power production will change having an increased effect on their cost (Gets, 2013).

The electricity grid needs an upgrade; current electricity generating stations are not economical and waste energy. A more sophisticated grid system is required where energy usage can be tracked and managed, creating a flexible power system that matches supply with demand. The government should motivate for an upgrade of the electricity grid, allowing access to renewable energy systems and overall improved efficiency with minimised wastage (Gets, 2013).

1.2.6. Job Creation

There is more potential for job creation under a large-scale renewable energy development than in the fossil fuels industry. This would benefit the country, addressing a problematic social issue of mass unemployment. Jobs can be created during the manufacturing of components, the installation process, operations and maintenance. The predicted number of potential jobs that could be created by each energy sector up to 2030 are visible in Figure 1.2: displaying objectives for IRP which is an Integrated Resource Plan; E[R] is the Energy Revolution; and AdvE[R] represents the Advanced Energy Revolution (Gets, 2013).

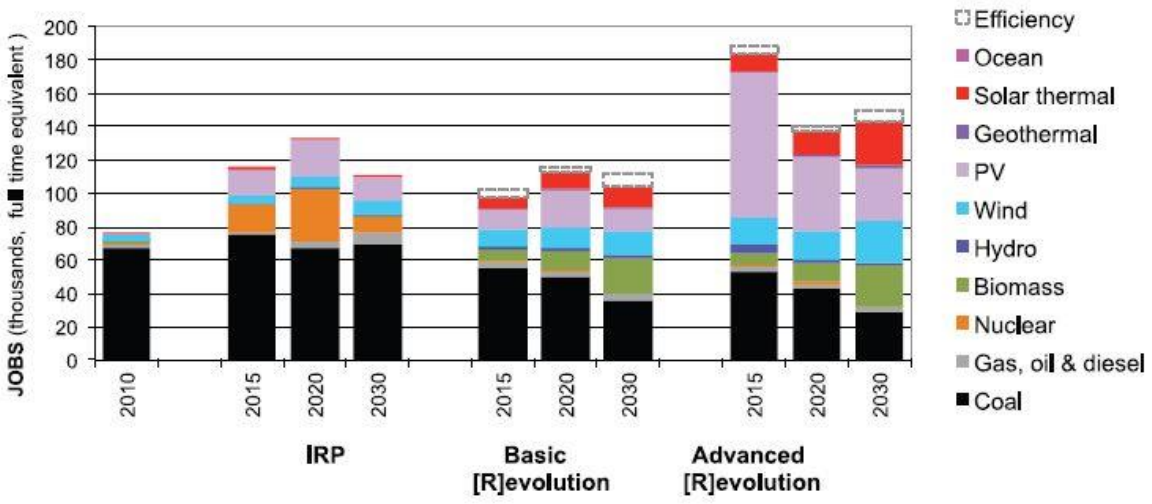

Figure 1.2. Electricity sector jobs projected to 2030 in South Africa (Rutovitz, 2010)

1.2.7. Costing

Renewable energy requires higher investment costs compared with the current electricity supply. However, the current coal-based energy is promoted and supported by the government and is subsidised. After initial capital injections, there is a lengthy waiting period before profit begins to accumulate making it less appealing to investors. The burning of fossil fuels is the dominant electricity production system where much of the infrastructure is already in place, however, new power stations need to be built to continue meeting the growing demand (Gets, 2013).

There is a preconceived notion that using energy from fossil fuels and nuclear power is more cost effective than renewable energy. However, the cost of using fossil fuels and nuclear power does not always reflect the actual cost. It ignores the negative impacts that arise from their use regarding environmental damage and climate change impacts. From a Life Cycle cost perspective, renewable energy is relatively cheap in comparison to the entire cost of nuclear and fossil fuel energy. Coal and nuclear power are significantly subsidised by government capital, creating an uneven playing field in the energy industry (Gets, 2013).

In Australia, a new wind farm is cheaper per megawatt-hour of energy produced at R747 than a new gas plant costing R1 083 or using coal which amounts to R1 336. There is a similar trend in South Africa with wind energy costing 89c per kWh. Eskom's coal-based energy costing 97c per kWh and the new Kusile power station providing energy at R1.38 per kWh upon commissioning in 2019 (Gets, 2013).

Implementing renewable energy schemes is initially expensive. Therefore, it is limited to larger projects backed by corporate or international funding. There are many risks involved in the early stages of renewable energy projects making them appear unattractive to investors who could

jeopardise losing all their initial investment in a failed project, opposed to the reduced risk investing in older, more established methods of energy production (Gets, 2013).

The following are required to reduce reliance on fossil fuels with their attendant sustainability issues:

1. Government promotion of renewable energy sources as opposed to reliance on coal and nuclear with their associated adverse environmental impacts.
2. Implementation of financial and economic incentives to make renewable energy a more cost-effective solution.
3. Improved grid access, allowing priority to renewables.
4. Total upgrade of the electricity network system to efficiently manage energy usage.
5. Government subsidies such as those with coal and nuclear, for renewable energy projects to compensate for high start-up costs.
6. Flexible legislation to allow participation of smaller renewable energy projects in industry (Gets, 2013).

1.3. Ocean Currents

An ocean current is a consistent, uninterrupted flow of moving water created through wind forcing and ocean density differences as a result of non-uniform heat and salinity conditions. Ocean currents are affected by water depth, bathymetry, ocean basin shape, the location and extent of land around which it flows, and the deflection force of the Coriolis Effect (NOAA, 2016).

Ocean currents have a high energy potential as they are more constant and unidirectional in relation to wind which is unpredictable and diurnal with overall varying speeds. Ocean energy can be more consistent and therefore more reliable which is an advantage over wind power which is subject to much change in speed and direction. Water has a greater power density over air as it is far denser. Ocean currents should be investigated for possible energy production.

1.3.1. Wind Forcing

The ocean surface layer moves due to the stress exerted upon it by wind. Coriolis force balances the stress within the Ekman layer which is the water surface layer between approximately 10 m to 200 m. Ekman transport describes the movement of the Ekman layer where the resultant movement is not parallel with the direction of the wind as a result of the Coriolis effect and is thus deflected by 90°: to the right in the northern hemisphere and in the southern hemisphere it is deflected left. The convergence and divergence of Ekman transport influence ocean circulation (Ocean Motion, 2007).

The convergence of Ekman transport induces Ekman pumping which describes the flow beneath the surface layer. As a result, the upper ocean layer becomes thicker and the depth of the thermocline

increases. The created subsurface pressure gradients generate cyclonic gyres within subpolar areas, and near the equator anticyclonic subtropical gyres are evident (Ocean Motion, 2007).

The Ekman spiral is a condition where at the base of the Ekman layer the current experiences a change in direction compared with the current flowing on the surface. It also describes the decrease in velocity as the depth increases (Bowditch, 2002; Ocean Motion, 2007; Price, et al., 1987).

1.3.2. Geostrophic Flow

The water density is a function of salinity and temperature. The water surface is higher in a region where the density is low compared to an area with larger water density. Water attempts to move from a high pressure to a low pressure, but Coriolis force has an effect and deflects the water. When the pressure gradient force balances the Coriolis force, geostrophic equilibrium is created. The speed of the geostrophic current is dependent on the density gradient. A high-density gradient produces a faster current (Bowditch, 2002; Ocean Motion, 2007).

Western boundary currents lie on the west side of sub-tropical gyres and flow at higher speeds than eastern boundary currents. The Coriolis Effect appears stronger in the latitude regions that experience the westerly winds opposed to areas influenced by the trade winds. The transport of surface waters towards the western boundary of the ocean basin creates a steep ocean-surface slope near the west side of the gyre resulting in the geostrophic flow being faster on the western side (Ocean Motion, 2007).

1.3.3. Currents around South Africa

South Africa has a prime position at the southern tip of Africa surrounded by oceans with direct access to marine resources to potentially exploit for renewable energy. The cold Benguela current travels northward towards the equator along the west coast, and along the east coast the warm Agulhas current flows southward.

1.3.3.1. Benguela Current

The Benguela current is an Eastern boundary current passing along the West coast of South Africa and can be seen in Figure 1.3. These currents tend to be slower, more shallow and wider than western boundary currents, transporting cold water as they flow towards the equator from higher latitudes (Ocean Motion, 2006). The Benguela current experiences low velocities of between 0.11 to 0.23m/s and a 15 to 20Sv transport capacity. The Benguela current is not a potential source of renewable energy as the speed of the current is not sufficient to feasibly generate energy. (Meyer, et al., 2014).

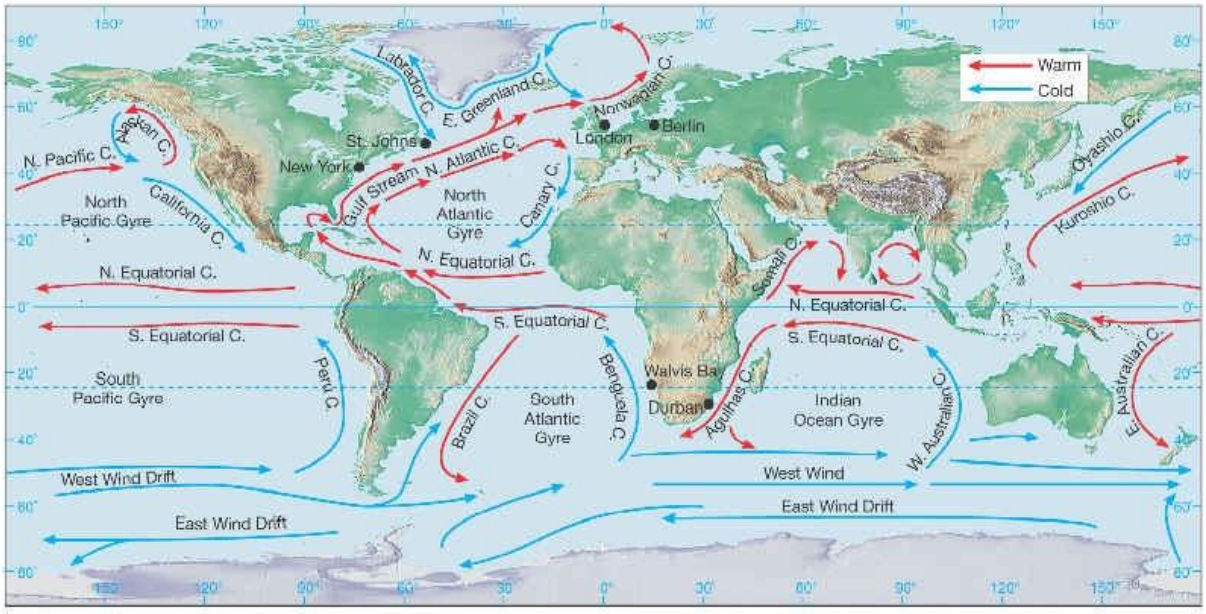

Figure 1.3. Map showing ocean circulation and currents (Nirman, 2014).

1.3.3.2. Agulhas Current

The Agulhas current is a warm Western boundary current located between 27° and 40°S on the East coast of South Africa flowing in proximity to the shoreline. The Agulhas current is the second fastest ocean current in the world and has a transport capacity of approximately 70Sv, where 1Sv is equivalent to 1 x $10^6 m^3/s$ (Gyory, et al., 2016). The core of the Agulhas current is steered strongly by the topography of the coastline and follows the continental shelf closely. For 80% of the duration the current is known to lie within 31km of the coast with surface currents reaching speeds of up to 2m/s based on information gained from a current meter mooring placed at approximately 32°S (Bryden, et al., 2005). Natal Pulses are large infrequent solitary meanders that propagate southwards within the Agulhas current, destabilising it and pushing it further offshore, limiting the consistency of the current.

1.4. Underwater Kite Turbine Technology

Underwater kites are a technology that can be used to generate energy from moving water along the eastern coastline of South Africa. The shelf is narrow which may provide a better location in the shallower water for kites to function and allow for easy maintenance. Kites can move across the current, increasing speeds and generating more power (Loyd, 1980). An array of kites placed within the current is a similar concept to offshore wind energy which incorporates large turbines and submarine cables. However, kites are located beneath the water surface where they cannot be seen and create no visual pollution, situated at depths so as not to interfere with shipping routes. Underwater kites can be small devices with less weight per kilowatt generated compared with large stationary marine turbines and do not require the construction of foundations. Due to their small size they are also better suited to co-exist with the marine environment. Ocean energy has the potential

to create electrical power and supply a portion of the electricity demand causing less environmental harm and alleviating the pressures placed on coal-fired electricity plants.

1.5. Motivation

The current inconsistent energy supply compromises the economy, productivity and quality of life. Coal-based electricity generation methods undermine the environment with unsustainable practices and links to climate change. Renewable energy must be considered, to supply part of the electricity demand and as a foundation for possible future expansion. For a sustainable and renewable future, alternative energy sources need to be investigated that can function in harmony with the environment creating less pollution and greenhouse gas emissions while finding a stable and reliable source of constant, uninterrupted electrical power. Wind and solar energy have grown substantially over the last few years, but the energy potential from marine sources has not been investigated fully.

The Agulhas current should be explored as to whether it is feasible to generate renewable energy from this resource with regards to the technology available for energy extraction. The social impacts it may have regarding local job creation and the impact on communities, environmental effects associated with technology operating in a marine environment as well as the cost aspect of such a renewable energy project should be examined.

1.6. Key Questions

What effect does the presence of Natal Pulses have on the implementation strategy for harnessing energy from the Agulhas current?

How can underwater kites be implemented sustainably to harness energy from the Agulhas current?

How much energy can underwater kite systems potentially generate?

Are underwater kite farms feasible regarding installation?

1.7. Aims and Objectives

1. Locate optimal position for energy extraction using hydro-kites within the Agulhas current observing current using ADCP measurements.
2. Validate ocean current data provided by the HYCOM model for the Agulhas current between Port Edward and Port Alfred using ADCP data and determine the model's accuracy for predicting Natal Pulse events.
3. Investigate the scale of installation regarding a concentrated system or using distributed kites along the coast.
4. Determine potential power output per kite and possible kite design.
5. Determine optimal configuration of hydro-kites regarding submarine cables.

6. Investigate suitable and feasible hydro-kite array and concept in terms of turbine placement and anchoring.
7. Consider overall sustainability of kites regarding technology, social factors, economic effects and the effects on the environment.

1.8. Dissertation Outline

The outline of the dissertation is as follows:

Chapter 2 presents a literature review focussing on the Agulhas Current system and Natal Pulses, reviewing HYCOM and ROMS ocean models and their performance. Various technologies available for marine energy extraction were investigated with emphasis on TUSK systems as well as the design of a flying wing. Turbines and submarine cables were also studied.

Chapter 3 describes the methods used and relevant calculations performed to attain the relevant results.

Chapter 4 is made up of the results and discussion including an analysis of available ADCP data, Natal Pulse events observed at various locations and HYCOM model predictions. The findings of using a distributed hydro-kite system compared to a concentrated system are presented with hydro-kite arrays and submarine cable configurations.

Chapter 5 presents the conclusions of this research and recommendations for further studies

CHAPTER 2

2. LITERATURE REVIEW

Chapter 2 comprises of a literature review observing aspects of a hydro-kite system within the Agulhas current. The review briefly looks at alternative renewable energy including the Sere Wind Farm project, with a more detailed enquiry into the workings of the Agulhas current with a focus on Natal Pulses and limitations with regards to marine power generation. Eskom ocean current data as well as various ocean models were investigated. Various marine energy extraction technologies were explored with the focus being on TUSK systems. Basic rigid kite wing design was considered as well as turbine motors and submarine power cables regarding installation and design.

2.1. Alternative Renewable Energy

Resources need to be thoroughly investigated to determine their feasibility for renewable energy production. Factors to be considered include the technology involved to extract the resource, the conversion system to transform the resource into electrical power and the costs associated with these. The cost of transporting the energy generated from the source to users, as well as the location and size of the demand required are contributing features.

There are many renewable energy solutions available: solar power predominantly through the use of photovoltaic systems, biomass using organic matter such as fuelwood, hydropower incorporates moving water under the gravitational force to rotate turbines and produce power, with wind power through the use of windmills or wind turbines. These various forms of renewable energy make up part of South Africa's total renewable energy. At present marine energy does not contribute to the renewable energy mix and should be further investigated. Energy from ocean currents is a similar concept to that of wind energy which is a fast growing market in South Africa. Marine energy using ocean currents may demonstrate significant advantages over wind power (Department of Energy, 2003).

2.1.1. Wind Energy

Wind is a naturally occurring element, although it is not constant and therefore not always reliable. Certain zones along the coast of South African have been identified as potential wind turbine locations. Vast areas of open space are required to create a wind farm where the resultant landscape is not aesthetically pleasing. Wind farms connected to the national grid can be supplement electricity. Farms need to be located far away from other activities as they create noise and visual pollution. Wind farms with massive wind turbines take up space that cannot then be used for any other activities, so there is competition for land (Department of Energy, 2003).

2.1.2. Sere Wind Farm

The Sere wind farm is the first wind energy development implemented by Eskom on a commercial scale. The farm is situated near Koekenaap, Lutzville and Vredenda on the west coast of South Africa over an area of 3700 km^2. This wind energy project is an attempt to show Eskom's commitment to minimising their negative environmental impact regarding carbon emissions by investing in a renewable and sustainable power source. Over the 20-year lifespan of the plant carbon emissions could be reduced by up to 6 million tonnes (ESKOM, 2014). The wind farm requires little or no water for the production of energy as opposed to coal-based power where water is necessary for cooling systems. Precious water resources are therefore also conserved by this renewable energy project (ESKOM, 2011).

The wind farm consists of 46 turbines that generate 2.3 MW each to achieve a 100 MW capacity. The anticipated energy generation is 298, 000 MWh for this project in 2014, the energy will be fed into the grid at the Skaapvlei substation at a voltage of 132 kV and then transported to the Juno substation through a new cable line distribution (ESKOM, 2011).

Eskom's Renewable Energy Business unit implemented this wind farm project and anticipates involvement in other similar renewable energy projects in the future, hoping the success of this farm will encourage renewable energy development in South Africa and within the African continent (ESKOM, 2011; ESKOM, 2014). This project helped to create more than 400 jobs during the construction phase with the local community experiencing increased economic activity. Full-time skilled technicians were sourced from the local community and received adequate training to operate and maintain the plant (ESKOM, 2014).

The Sere wind farm project was funded by Developing Finance Institutions (DFI) with capital sourced through the Clean Technology Fund and had government support. The cost of the project compared with the market costs of capital and levelised cost of energy was found to be favourable (ESKOM, 2014). Siemens Wind Power A/S was involved in the construction of the farm using Siemens wind turbines SWT-2.3-108. The turbines have three blades, 108m in diameter covering a swept are of 9144m^2, the turbine has a cut-in speed of between 3 m/s and 4 m/s and a cut-out speed of 25 m/s. The weight of the rotor and nacelle is 60, 000 kg and 82, 000 kg respectively (Siemens, 2012).

2.1.3. Disadvantages of Wind Energy

There are some drawbacks of wind energy regarding overall cost, consistency and environmental effects. The production cost per kWh of wind power is larger than that of coal produced electricity. The capacity of wind turbines is small ranging from 25 kW to around 2, 000 kW whereas a thermal unit producing coal-based power has a maximum load in the range of 200 MW to 600 MW. It would

require a considerable number of wind turbines to replicate the power output of just one thermal unit. As wind has an inconsistent and unpredictable nature, the power generated is not constant where power can only be produced at certain higher wind speeds and is, therefore, an unreliable energy source. Wind farms have certain environmental effects such as noise and visual pollution, with vast areas of land that are unable to be utilised for other activities, turbines can also have adverse effects on bird life (ESKOM, 2011).

A relatively new concept similar to that of wind power exists, where ocean current energy can be used to drive underwater turbines that harness power from moving water. The improved advantages of this system are that ocean currents are generally constant and can offer increased reliability, they would not occupy space that could be utilised for other activities and are located below the water surface where they are not visible. Power from ocean currents should be investigated as a suitable sustainable and renewable energy resource (Department of Energy, 2003). The Sere wind farm can later be used to compare wind turbine power to that of a proposed underwater hydro-kite system regarding potential energy, the area required, overall size and configuration.

2.2. The Agulhas Current System

The Agulhas current will be investigated for potential power generation. The current is not always consistent as it experiences Natal Pulse events which cannot be predicted and move the core of the current, thus reducing the reliability of power available.

As the South Equatorial current nears the African coast it starts to flow south-westward; part of the current flows between the African mainland and Madagascar; the rest flows along the Eastern coastline of Madagascar. When these waters reach the Southern part of Madagascar, they join again to form the Agulhas current. In the South West Indian Ocean sub gyre, part of the current is recirculated. At a latitude of 40°S the current retroflects, known as the Agulhas Retroflection, and sheds eddies south of South Africa and starts to flow south and then east together with the Western Wind Drift as the Agulhas return current (Lutjeharms, 1988). Some of the current flows around the south end of Africa and helps to form the Benguela current. In the retroflection region, large anticyclonic Agulhas Rings are created, break away from the current and moving westward. The rings allow salty and warm water to leak into the Atlantic Ocean from the Indian Ocean (Beal, et al., 2011).

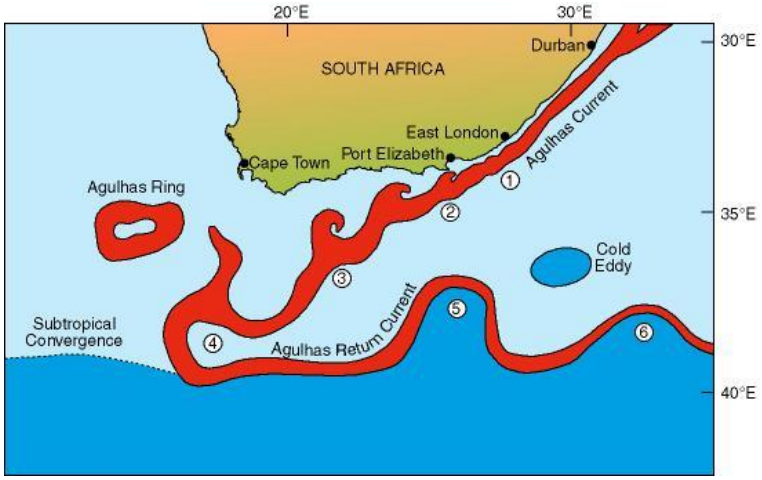

Figure 2.1. Diagram showing circulation of the Agulhas current system including the Agulhas Return Current and the spawning of Agulhas Rings. 1. The inception of small meanders. 2. The core of the Agulhas Current starts to diverge from the coastline. 3. Meanders. 4. The Agulhas Current retroflection region. 5. And 6. Are Agulhas Return Current meanders. This diagram is adapted from (Boebel, et al., 2003) and sourced from (Bayworld Centre for Research and Education, 2005).

2.2.1. Natal Pulses

The bathymetry of the South African coastline with a narrow shelf, steep continental slope and relatively non-complex topography aids in stabilising the current. Along the coast between Maputo in Mozambique and Port Elizabeth, the continental shelf narrows where the current flows closer to the shoreline at a high velocity which is ideal for power generation.

Natal Pulses are characterised as infrequent and unpredictable large cyclonic meanders with approximately a 150 km diameter that migrate down the coastline which can affect the amount of electricity able to be produced as the current is not constant. The Natal Bight occurs between Durban and Richard's Bay where the continental shelf widens, the shelf's change in morphology induces a destabilisation in the current (Lutjeharms, et al., 2003). Due to variability within the Mozambique channel and South of Madagascar, anticyclonic deep-sea eddies are produced and fed into the Northern Agulhas current region. The interaction of these large anticyclonic eddies with the Agulhas current in the Natal Bight region results in the formation of Natal Pulses (deRuijter, et al., 1999; deRuijter, et al., 2002; Schouten, et al., 2002; Tsugawa & Hasumi, 2010).

Natal pulses are meanders with a core of cold water circulating cyclonically inshore of the current. As the pulses propagate. South Westwards along the continental slope, they increase in diameter and relocate the core of the current seaward (Leber & Beal, 2014). Natal Pulses are small near the Natal Bight at around 30km, as the pulses move southwards they can reach 200km offshore near Port Elizabeth (Leeuven & deRuijter, 2000; Rouault & Penven, 2011). Natal Pulses propagate down the coast at speeds between approximately 10 and 20km per day (Vaart & deRuijter, 2001). The speed of the pulse reduces to around 4km per day after the Agulhas Bank near Port Elizabeth at 34°S (Lutjeharms & Roberts, 1988).

A Natal Pulse causes the velocity of the current to decrease suddenly near the coast, coupled with a direction reversal as the pulse passes over pushing the core of the current further offshore. The pulses can be present for 50 to 70 days within the system and on average 1.6 Natal Pulses reach Port Elizabeth in a year (Rouault & Penven, 2011). One of the requirements set out by Rouault & Penven (2011) in identifying Natal Pulse events was that they persisted for a duration of 10 days.

Smaller eddies also migrate through the ocean current system similar to that of Natal Pulses, experiencing a sharp drop in the velocity magnitude with an accompanying change in the direction. However, these do not last as long as Natal Pulses and are commonly only present for approximately one day.

There is an undercurrent present that flows in the opposite direction to the Agulhas current with much lower velocity magnitudes than those experienced near the surface. It occurs below 800m in depth which would be far beyond the location of the turbine technology and is therefore not a concern. Moored underwater kites would be anchored to the seabed on the shelf which is usually within 100m (Beal & Bryden, 1999; Donohue, et al., 2000).

2.2.2. Technical Analysis of Energy Extraction

Certain areas within the Agulhas current were studied for possible energy extraction regarding economic feasibility and potential extractable energy. The locations investigated were Port Edward, Gonubie (north of East London), East London (south) and Port Alfred.

The energy that is theoretically available within a cross-sectional area is defined as the theoretical resource and is a function of density, area and velocity. The part of the theoretical resource that is physically extractable after taking hydrodynamic factors into consideration is the extractable resource. The technical resource is the portion of the theoretical resource that can actually be accessed that is determined by the technology available. Designing technology accordingly to operate efficiently can increase this resource (Moodley, et al., 2012).

Based on the cross-section profiles and ocean current velocities, higher speeds occurred closer to the sea surface. At deeper depths, lower speeds may be seen due to a friction force between the seabed and flowing ocean current. Where there is minimal friction, higher velocities are experienced and where there is a smaller surface area available an inversely proportional relationship exists between contact surface length and ocean current speed. Cross-section profiles of the study locations can be seen in Appendix B (Moodley, et al., 2012).

The results showed that Gonubie was the area with the highest theoretical resource. It is possible that an area with low velocities but a large theoretical resource could yield a lower technical resource than

an area with high velocities yet lower theoretical resource. The speed of the current is proportional to the efficiency and type of technology chosen to extract ocean energy (Moodley, et al., 2012).

2.2.2.1. Location

In establishing the prime location for a potential pilot study, there are many elements to consider. The power density is the highest further offshore and at shallow depths. There are greater costs involved when implementing technology at deeper depths beyond 100m, with the cost of cabling increasing with distance offshore. Ocean current velocities should be high enough for the technology to be able to capture energy efficiently. If the technology is placed at deep depths maintenance will prove challenging and costs will be higher. Shipping routes must be avoided, or a clear distance must be allowed for ships to pass over the technology. Large marine mammals may be injured by the implemented system or may pose a threat to the system regarding potential damage (Meyer, et al., 2014; Moodley, et al., 2012). Commercial fishing should be taken into consideration so that this activity is not negatively impacted. The existing power grid and infrastructure already in place can affect the location, if the plant is located closer to the grid, less cost regarding submarine cables will be incurred.

2.2.2.2. Environmental

37 species of whale and dolphin are found along the coast over 2000km between Durban and Doring on the West Coast. These mammals can be found close to the coast, within 50m from the shore and travel between the surface and a depth of 3km. It would be impossible to avoid implementing technology at a site that will not interfere with the wildlife (Whale Route, 2014).

In the event of large marine life colliding with the technology, considerable damage can be incurred. Repairs can be expensive and time wasted where the system would be incapacitated. Marine animals are also at a greater risk of injury or death if an underwater renewable energy system is installed.

Implementing sensors that shut down the technology in the presence of marine animals will compromise the overall efficiency and produce a lower capacity factor. However, the potential threat to marine wildlife cannot be overlooked. To protect the natural environment, preventative measures should be taken, minimising adverse effects of implementing technology in a marine environment.

Marine protected areas must be avoided, turbine systems should not be placed near areas of conservation, and electrical cables should be diverted to avoid these locations. The Marine Living Resources Act is in place to ensure the protection of marine environments and biodiversity.

Pondoland is an MPA located south of Port Edward which spans approximately 90km along the coast and extends offshore to around 15km restricting the placement of hydro-kites near Port Edward. The boundaries of the MPA extend to the water, seabed and air space up to 1000m above sea level. The

area provides a sanctuary in which overexploited fish species can recover and breed, supporting and controlling eco-tourism and scientific research while not posing a threat to the environment (Marine Living Resources Act of 1988). Pondoland includes subtropical reefs and nursery areas for young fish in estuaries, and whales and dolphins offshore. The area offers protection to overexploited line-fish including red steenbras and black musselcrackers. There are different zones within the MPA; some are no-take areas where no fishing is allowed while others allow limited amounts of harvesting (South African Tourism, 2011).

2.2.2.3. Shipping

Along the East Coast of South Africa is one of the busiest shipping routes where over 5000 trips are made each year. Figure 2.2 shows the global shipping routes. Ships save fuel and are more economical by travelling in the core of the Agulhas current where speeds are the fastest. Large container ships have a draft, the hull length below the sea surface, of 16m, therefore as a safety measure a minimum depth of 20m should be allowed for clearance, the shallowest depth at which technology can be safely implemented (Moodley, et al., 2012). The passing over of ships on the water surface above installed marine turbine technology would create a disturbance within the water column and could temporarily compromise the efficiency of the system.

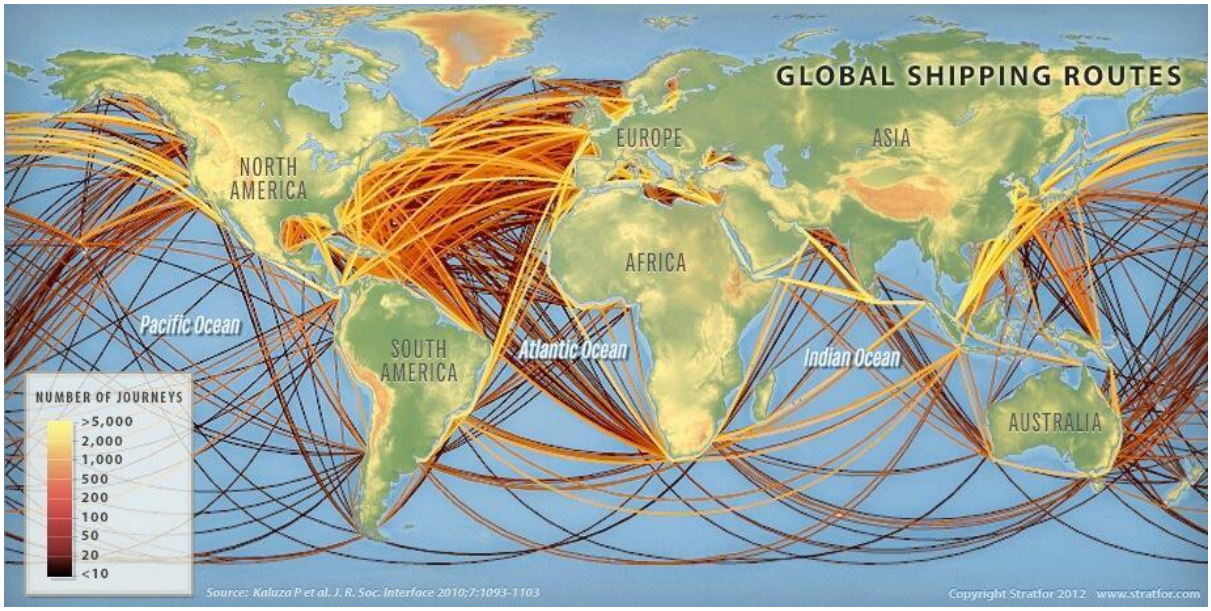

Figure 2.2. Map showing the global shipping routes (Kaluza, et al., 2010).

2.3. Eskom DATA

An investigation was conducted along the East coast between Port Edward and Port Alfred to determine the best possible location to implement an underwater plant to generate electricity based on the current velocity, distance to the power grid and potential power production (Meyer, et al., 2014).

2.3.1. Locations investigated

Four sites were studied using ADCP velocity data averaged over time. A full temporal analysis including information on the variability of the current and Natal Pulses was conducted on more favourable sites where the mean velocity measured above 1.2 m/s: at Locations 1 and 2. Figure 2.3 shows the four investigated locations. The location north of East London at Cape Morgan, Location 1, had higher velocities, however, East London, Location 2, was closer in proximity to the substation (Meyer, et al., 2014). Utilising Location 2 would require less cable length and thus decrease the overall cost. Figure 2.4 shows the proximity of the various ADCPs around Cape Morgan and East London and their relative distance to substations where energy can be fed into the grid and transported for use. Figure 2.5 shows the South African power network and possible future grid connections including a line near the coast running from Durban to East London which could be beneficial for a marine energy project where offshore cables within that region could link into the grid.

Figure 2.3. Map showing the investigated locations along the Agulhas current where ADCPs were deployed: Location 1: Cape Morgan, Location 2: East London, Location 3: Port Edward and Location 4: Fish River (Meyer, et al., 2014).

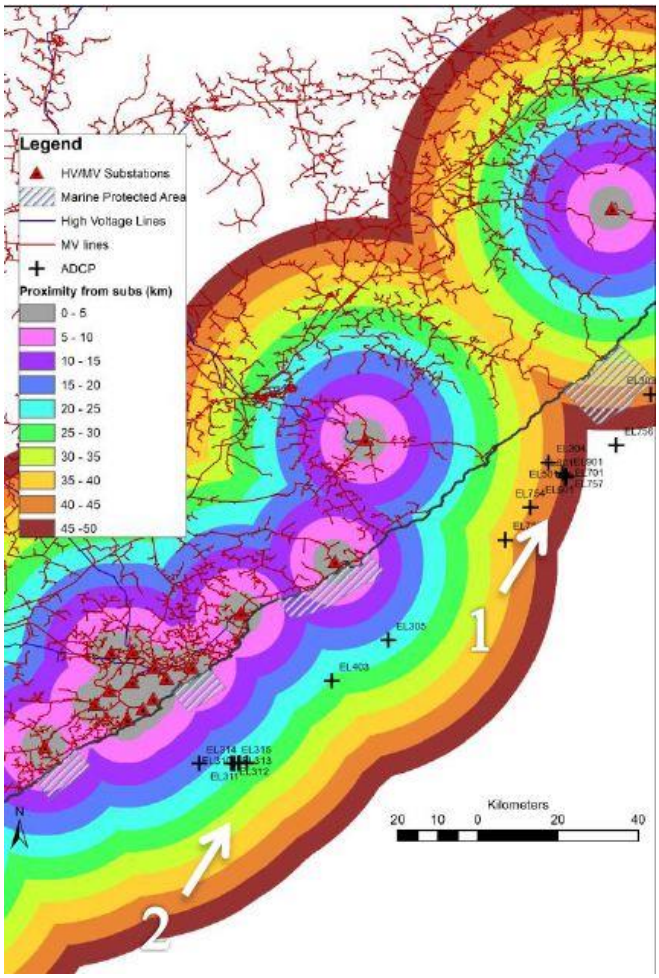

Figure 2.4. Map showing the proximity of Locations 1 and 2 to the electricity grid and marine protected areas (Meyer, et al., 2014).

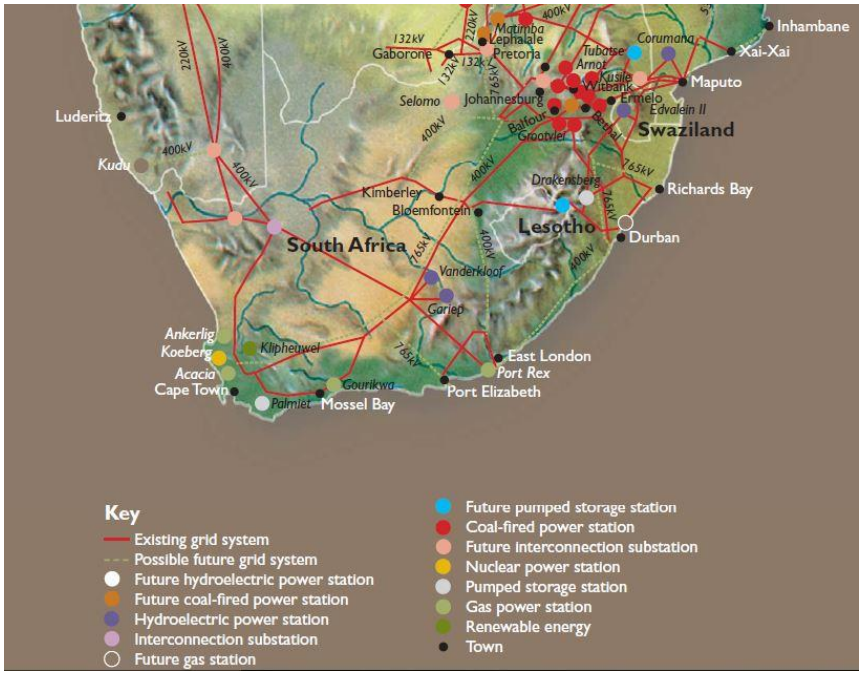

Figure 2.5. Map showing the South African power network with possible future grid system connections (Eskom Holdings Limited, 2009).

The current direction appeared constant without the presence of natal pulse events, yet the magnitude of the velocities tended to fluctuate with more variability. Overall, the low velocities experienced within the data set would adversely affect the potential power production.

Renewable energy is extractable from the Agulhas current, however, speed and direction are not always constant as a result of current meanders and Natal Pulses. Location 1 would be better suited to extracting energy due to the presence of higher velocities and lower variability, but is situated further away from the nearest substation, whereas Location 2 has the benefit of being closer to onshore substations (Meyer, et al., 2014). The potential to extract energy from the Agulhas should be investigated together with a suitable technology to maximise power potential.

2.4. Ocean Models

Various ocean models are available which attempt to simulate the ocean environment using bathymetry and forcing mechanisms. The models' applicability in modelling the Agulhas current system was investigated to attain data outside the range of the ADCP measurements for further investigations concerning energy potential within the system.

2.4.1. ROMS model

The Regional Ocean Modelling System (ROMS) is a free surface, split explicit ocean model which incorporates stretched grid σ coordinates where the vertical layers follow the ocean topography (Shchepetkin & McWilliams, 2003). It uses the Boussinesq approximation and the hydrostatic vertical momentum balance to solve incompressible hydrostatic primitive equations. The model uses curvilinear coordinates in the horizontal and in the vertical direction terrain-following coordinates are used.

The South African Experiment (SAfE) provided a higher resolution child model within the domain of 27.7° to 39°S and 11.5° to 27.4°E. The resolution is 1/12°, about 8km, refined by a factor of 3 from the parent model which had a resolution of only 1/4°. The model incorporates 32 vertical layers. The bathymetry is sourced from the GEBCO dataset with surface forcing obtained from the COADS wind dataset which was not resolved well near the coast and is, therefore, biased towards the open ocean. The duration of the model run was for ten years, but the model required the first two years to reach a statistical equilibrium so only years 3 to 10 were used (Penven, et al., 2006).

2.4.2. HYCOM model

The Hybrid Coordinate Ocean Model (HYCOM) is a three-dimensional hybrid ocean prediction simulator which uses isopycnic coordinates and a fixed grid (Bleck, 2002). Similar to the ROMS SAfE model it incorporates 1/12° resolution in both the longitudinal direction and the latitude direction for the area of the Agulhas current to be studied. There are 32 vertical layers within the model ranging

from the surface to a depth of 5500m. Bathymetry for the model input is supplied by the NRL DBDB2 dataset which is quality controlled. Surface forcing used is from Navy Operational Global Atmosphere Prediction System (NOGAPS) providing information on wind stress, wind speed, precipitation and heat flux (HYCOM, 2015).

The model runs at NAVO HPC every day making use of data assimilation to produce a five-day hindcast and forecast, experiments used were GLBa0.08 and were sourced from https://hycom.org/dataserver/glb-analysis. The data includes the following variables: surface downward heat flux in the air, water flux into the ocean, surface temperature and salinity, sea surface height (SSH), the ocean mixed layer thickness, sea water salinity and potential temperature, as well as the eastward and northward velocity components which are of pivotal importance in this current study. Due to the isopycnal structure of the model, it can be used for deep ocean modelling, mixed layer modelling using constant depth and pressure schemes, in coastal regions with a terrain-following coordinate approach, as well as in shallow areas using level co-ordinates. The HYCOM global model provides data from August 2008 to present day.

The HYCOM Reanalysis model is available from October 1992 to the end of 2012, data for experiments GLBu0.08 are available at https://hycom.org/dataserver/glb-reanalysis. The reanalysis attempts to recreate the ocean environment from previous years by assimilating the temperature and salinity profiles in HYCOM. The reanalysis is similar to that of the analysis, however, the input forcing varies. The reanalysis uses bathymetry from the General Bathymetric Chart of the Oceans (GEBCO) and surface forcing from the National Centre for Environmental Prediction (NCEP) Climate Forecast System Reanalysis (CFSR) which includes wind speed and stress, heat flux and precipitation. From the temporal frequency of the input forcing mechanisms, the diurnal cycle is resolved. The model uses the same resolution as the analysis but is integrated to 40 z levels and presents data for only the sea surface height (SSH), water temperature, sea water salinity and the ocean current velocity components. The reanalysis contains more depths within shallower regions above 100 m (HYCOM, 2015).

2.4.2.1. Evaluation of HYCOM Model

The accuracy and drawbacks of the HYCOM model were investigated, evaluating the model as an instrument to predict ocean current energy. A direct comparison was made between HYCOM model data and in situ ADCP measurements. The accuracy of the model around the Agulhas region was investigated and used to predict KEF, flow speeds and the variability of the current direction; with the aim of determining the suitability of pursuing ocean current energy based on available kinetic energy (VanZweiten, et al., 2014).

HYCOM data was available daily for entire years between 2009 and 2012. To ensure the elimination of seasonal bias complete successive dates were used, as well as using most recent data extracted from the latest HYCOM model.

An indication of the energy that is potentially extractable from an ocean current turbine is the KEF which is calculated per unit area perpendicular to the flow. This value quantifies the available power in the current flow per unit time per unit volume, not to be confused with the total energy extracted (VanZweiten, et al., 2014).

$$KEF = \frac{1}{2}\rho v^3 \tag{2.1}$$

Using the mean eastward and northward velocities the mean flow direction was calculated:

$$\bar{\varphi} = \tan^{-1}\left(\frac{\overline{V_E}}{\sqrt{\overline{V_N + \overline{V_E}} + \overline{V_N}}}\right) \tag{2.2}$$

Only if the current flowed more than 90° from the mean flow direction was it considered a current reversal

HYCOM data is available at fixed depth intervals over the dates that were simultaneous with the ADCP deployments, statistics were calculated at each HYCOM grid point and were available at four grid points surrounding the ADCP location. The results were then bi-linearly interpolated to the ADCP location removing spatial averaging effects of current velocity magnitudes.

Bin depths were linearly interpolated to a vertical grid with 1 m spacing due to the vertical bin depths of ADCP measurements not being equal. A depth of 20 m was chosen to evaluate the modelled and measured datasets as this is considered the shallowest height for turbine placement. Depths below 20m could be used for larger turbines, or where vessel traffic is observed and has an impact or where large sea surface waves could have a damaging impact on technology (VanZweiten, et al., 2014).

At a depth of 20 m, approximately 0.3 % of the earth's sea surface (1, 064, 600 km^2) possesses a KEF larger than 0.5 kw/m^2 which is considered the base KEF and corresponds to a velocity of approximately 1 m/s. If turbines are designed to be more efficient in slower current velocities, they could be suited to many areas of the world.

The ability of HYCOM to simulate ocean currents is quantified to determine if the model can perform well as a tool to assess ocean current energy. Areas were investigated regarding KEF, current speed and the number of current direction reversals that occur (VanZweiten, et al., 2014).

2.4.2.2. Agulhas Current

HYCOM has a tendency to predict the core of the Agulhas current near the 1000 m isobaths which lie approximately 50 km offshore. A study through SEVIRI SST (Sea Surface Temperature) data showed the core to be positioned 20km offshore at East London (Rouault & Penven, 2011).

The maximum mean KEF observed in the HYCOM model for the Agulhas current was 1.83 kW/m^2 where there were 1.5 % current reversals; this location is north of the ADCPs so this cannot be verified. A similar value of 1.76 kW/m^2 near the ADCP at the Fish River was experienced where the current reverses for 1 % of the duration (VanZweiten, et al., 2014).

At the three ADCP locations investigated at Cape Morgan, East London and the Fish River, that HYCOM predicts the mean current speed fairly accurately except for depths above 50m which are the depths where turbines are required. The average current flow estimated by HYCOM was compared with the ADCP measurements for the three locations at depths of 20 m and 50 m. The Fish River was the only position showing an overprediction in the mean current speed, by 38 % for a depth of 50 m and by 14% at 20 m depth. At East London, the current speed was overpredicted by 1% for a depth of 50m, but underpredicted by 26 % for a depth of 20 m. At Cape Morgan, the current speed was underpredicted by 5 % for 50 m depth, and by 23 % for a 20 m depth (VanZweiten, et al., 2014).

HYCOM fails to perform during extreme conditions due to the discrepancies between the modelled and the measured maximum current speeds throughout the water column. HYCOM underpredicts the maximum current flow by 30 %, 31 % and 19 % for areas at the Fish River, East London and Cape Morgan respectively (VanZweiten, et al., 2014).

2.4.2.2.1. Kinetic Energy Flux

The average KEF was calculated at each ADCP location at a depth of 20 m using the HYCOM model. It overpredicted the KEF at the Fish River by 18 % while underpredicting the KEF by 58 % and 54 % for East London and Cape Morgan respectively. At all locations at depths below 50m, the model overestimates the KEF. The severe inability of HYCOM to predict the KEF can be accredited partly to the fact that KEF is related to the cube of the current speed and the error is also cubed. These results can, therefore, be highly misrepresentative of the actual ocean current conditions and ocean developers need to be wary of the model results (VanZweiten, et al., 2014).

HYCOM alone cannot be used to predict locations where there is a high KEF as it fails to estimate the KEF of shallow areas efficiently. Therefore, the points at which ADCP measurements were taken would be neglected. At East London that the average KEF for the considered period was 1.58 kW/m^2, and 2.164 kW/m^2 was calculated for the location at Cape Morgan which is higher than any point predicted by the HYCOM model (VanZweiten, et al., 2014).

2.4.2.2.2. Direction Variability

HYCOM tends to predict the direction of the current to vary less than it does with regards to the direction measured at a depth of 20 m. It seriously underpredicts the percentage of current reversals by 73 %, 31 % and 61 % for locations at the Fish River, East London and Cape Morgan respectively. This inability to successfully estimate the amount of current reversals that occur leads to the impression that the Agulhas current is more consistent than it truly is, indicating a greater suitability for renewable technology to be implemented which is again misleading (VanZweiten, et al., 2014).

2.4.2.2.3. Natal Pulse predictions

It is of significant interest as to whether the HYCOM model can accurately predict the occurrence of Natal Pulses. These meanders are a major drawback of installing turbine technology where up to 40 day periods at specific locations the system can be incapacitated as velocities decrease to almost zero in the presence of a pulse event.

HYCOM appears to be able to model the occurrence of Natal Pulses coinciding with the dates at which they occur within the ADCP data. Natal Pulses seem to have an effect on the entire water column, seen as velocity near zero through the depth that persists for approximately a 30-day duration. The duration and frequency of a turbine's inability to operate and produce electricity is a necessary factor in the feasibility analysis of installing renewable energy technology (VanZweiten, et al., 2014).

2.4.2.3. Overall HYCOM Assessment

VanZweiten et al. (2014) investigated the HYCOM model as a tool to predict ocean currents and the potential extractable energy. The current speed variability is underpredicted as well as the mean current speed at most locations and consequently the power available. HYCOM fails to model the position of the core of the Agulhas current, assuming it is further offshore than in reality. Current velocities near the surface are not well modelled, and the variability of the current direction is also not well assessed which are critical for this study regarding ocean energy potential. However, HYCOM can be beneficial in locating areas to investigate for prospective power generation. It is more favourable for a model to underpredict values that to give overpredictions indicating great potential that does not exist. It is advised that long-term in situ measurements be recorded of possible development sites and used in conjunction with HYCOM model results.

There are various reasons as to HYCOM's incompetence in efficiently predicting the magnitude of the current velocity and the flow direction: the ADCP locations are positioned close to the coastline, the bathymetry changes significantly from 100 m to 1000 m over a short distance of approximately 25 km, and the resolution of the model is coarse. Possible reasons for the inconsistencies between modelled results and measured ADCP data in shallower depths may be due to surface shear arising from wind forcing that increases the current speed, but the model fails to take this into consideration. Another

possibility for the errors is that HYCOM tends to estimate the core of the Agulhas to be further offshore than it is, thus providing slower speeds at the locations concerned (VanZweiten, et al., 2014).

2.4.3. Model Comparison

A study was conducted by Backeberg et al. (2010), comparing the HYCOM model and the ROMS model which included the SAfE as well as a higher resolution nested model of the Agulhas Bank. The HYCOM model used within the comparison is an older coarser resolution model not used in this study. The various models were compared using estimated surface velocities derived from ENVISAT's Advanced Synthetic Aperture Radar (ASAR). The ability of the models to predict the strength of the current in the upper water column layers, and the topographic steering of the model, was investigated and compared.

Satellite altimetry was used to validate the ocean circulation models; it is the only available dataset ranging over a prolonged time period able to represent global ocean circulation. However, in close proximity to coastal regions factors such as the atmospheric conditions, tidal model inaccuracies, land contamination and limitations of the geoid and projections can impact the data received from satellite altimetry. Therefore, inaccuracies within the data may be evident due to the Agulhas current flowing the coastline closely. Satellite altimetry observations are shown to underestimate the magnitudes of velocities within the Agulhas current. Both satellite altimetry, as well as ASAR observations, are used to validate the ocean models (Backeberg, et al., 2010).

The HYCOM model tended to underpredict ocean velocities within the Agulhas current core. The model showed the core to lie around the 4000 m isobaths after the continental shelf separates whereas the core is seen to flow around the 1000 m isobaths in observations from the ASAR data. The SAfE model also underpredicted current velocities but showed a better correlation to actual results than the HYCOM model. This ROMS model displayed improved topographical steering and a stronger current core. The low resolution of the ROMS parent model leads to an unrealistic smoothed input bathymetry for the SAfE model (Backeberg, et al., 2010).

The models' performance in the vertical structure was observed. HYCOM shows maximum velocities above 0.7 m/s between depths of 100 m and 200 m where the Agulhas core is around the 4000 m isobath at a latitude of 35° S. The SAfE model displays maximum velocities larger than 0.9 m/s above a depth of 100m where the Agulhas core at a latitude of 34.5° S is in agreement with the 1000 m isobaths. The SAfE model correlated well with the velocity profile from a mooring South East of Durban near 32° S that provided data for the duration of a year. The high resolution nested ROMS model of the Agulhas Bank predicted similar results to that of the SAfE model regarding the Agulhas core

position. The model showed current velocities with magnitudes above 1.0 m/s for depths above 100m (Backeberg, et al., 2010).

There is no undercurrent present within the SAfE model due to its coarse resolution, but it is apparent in the high resolution nested model at depths beyond 1000 m. The HYCOM model experiences a strong undercurrent that follows the continental slope closely between depths of 100 m to 2000 m; the undercurrent shifts the Agulhas core further offshore in the model (Backeberg, et al., 2010).

The ROMS models are a better prediction of ocean events. There is a more uniform vertical layer distribution within the ROMS models whereas HYCOM contains most layers above depths of 200 m. The HYCOM model uses z-level co-ordinated where each isopycnal layer is assigned reference densities which cause an uneven distribution of vertical layers and is a poor method for modelling the Agulhas current system. All models investigated provided underpredictions of the mean velocity in the Agulhas current. HYCOM performed the worst while ROMS produced a superior model regarding topographic steering in comparison to that of HYCOM (Backeberg, et al., 2010). The latest version of the HYCOM model GLBa0.08 used in this study may achieve improved model predictions due to its finer resolution and more even distribution of vertical layers. However, it still appears to have the same problem in predicting the core of the Agulhas further offshore (VanZweiten, et al., 2014).

2.5. Power from Marine Currents

Turbines can be used to generate electricity from ocean currents. They can be relatively small in size as water is a dense medium. Ocean currents are mostly constant, the movement is predictable, and thus ocean currents can be considered a reliable renewable energy resource (Department of Energy, 2003).

There are technology systems available that have been designed and can convert energy from moving ocean currents into electrical power. These relatively new technologies include the SeaGen tidal turbine, Minesto Kite, HydroRun and Ceto.

As the current is nearly constant, high load factors are produced (Meyer, et al., 2014). Minesto claims that marine energy and the hydro-kite technology used to extract it are competitive with other electricity production methods. Ocean energy is reliable and predictable and can be produced locally. Potential impacts on the environment and marine life must be investigated before implementing underwater technology and a thorough EIA should be conducted.

2.5.1. TUSK Systems

A Tethered Undersea Kite (TUSK) obeys similar principles to that of Airborne Wind Energy (AWE) systems which are utilised to achieve power from higher wind speeds at high altitudes and minimise infrastructure required. TUSK systems represent an alternative to wind energy and could be more

economical and efficient. TUSKs may have larger forces acting upon them compared with AWE systems as water is denser than air, even though the velocities at which the ocean current flows at are much smaller than those of wind. It is recommended that a rigid wing system should be used to resist these forces imposed by ocean currents.

The TUSK system can either be tethered to a buoy floating on the ocean surface as in Figure 2.6 or, anchoring the tether to the sea floor as in Figure 2.7. In either case, submarine cables are necessary to transmit energy to the shore. Where TUSK systems are placed at depths beyond 50m floating buoys should be used, whereas in shallower regions it is better to moor the tether to the seabed. It is more advantageous to position the turbine on-board the kite as more energy can be produced when the turbine moves at a higher speed than the ocean current using principles of cross current motion. An alternative is to place the generator either on the buoy or on the seabed where it would remain stationary. The tether is subject to a high tension force and is allowed to reel out from a rotating generator shaft, the tether is then pulled back in by a motor, by reducing the kite's attack angle the tether tension is decreased. A small percentage of the power produced would be used to drive the motor. Due to TUSK systems being able to achieve higher velocities due to cross current motion, they are more effective for ocean currents that have lower velocities where smaller sized systems can also be used to reduce material and installation costs.

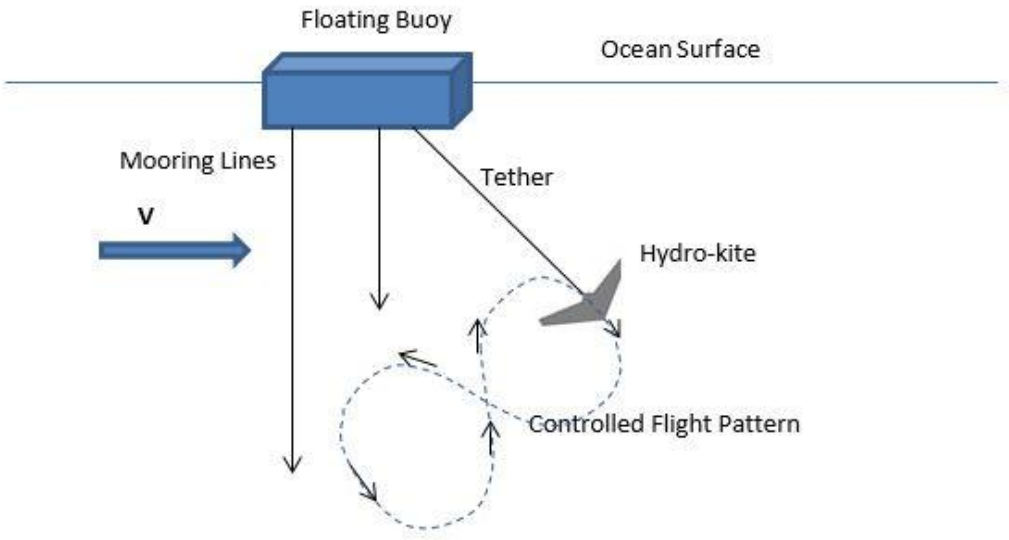

Figure 2.6. Diagram showing the components of a TUSK system using a tether to a floating buoy on the sea surface (Olinger & Wang, 2015).

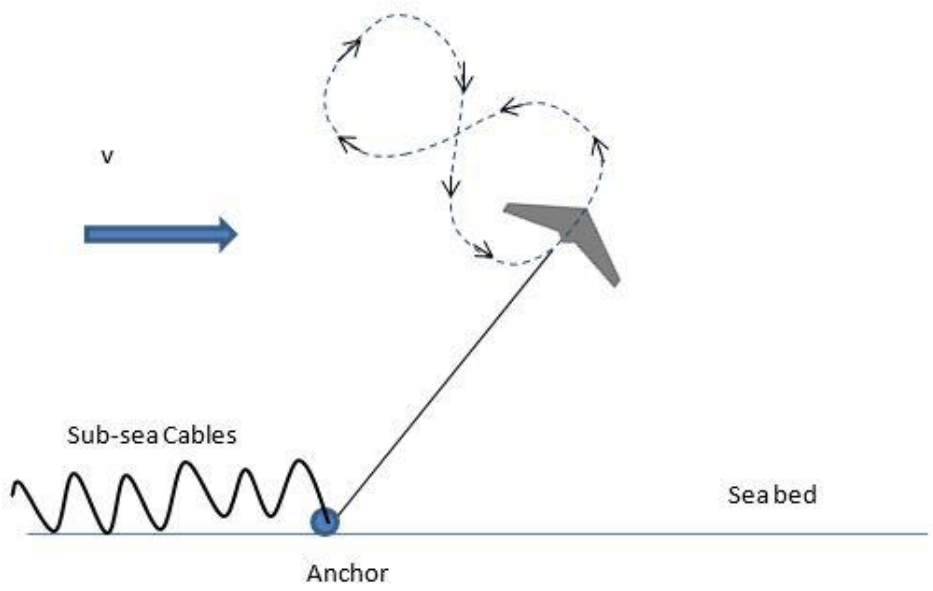

Figure 2.7. Diagram showing an alternative TUSK system using a tether and anchor on the seabed to secure the hydro-kite (Olinger & Wang, 2015).

The apparent velocity that the kite experiences by moving in cross-current motion is a function of the kite's lift to drag ratio $\left(\frac{C_L}{C_D}\right)$ as well as the actual current velocity. Figure 2.8 shows the ocean current velocity and apparent velocity in relation to a moving hydro-kite.

$$v_A = \left(\frac{2C_L v}{3C_D}\right) \tag{2.3}$$

(Olinger & Wang, 2015)

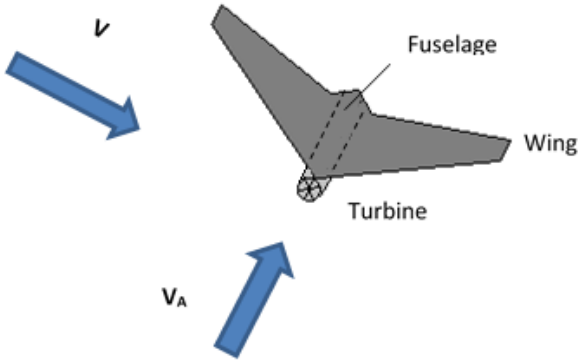

Figure 2.8. Diagram showing the velocity and apparent velocity in relation to the kite (Olinger & Wang, 2015).

Power density, also known as KEF is the theoretical power that can be produced per unit area dependent on the velocity cubed. Apparent velocity can be much higher than the actual velocity and is then cubed and the swept area of a turbine flowing across the current is greater. Therefore, the

potential power output from a kite exploiting cross-current motion will be significantly larger than a stationary kite (Olinger & Wang, 2015).

$$P' = \frac{1}{2}\rho {v_A}^3 \tag{2.4}$$

The density of sea water is taken as 1027kg/m^3 (Hyperphysics, 2016) (Windows To the Universe, 2016).

For AWE systems to be effective, they make use of high wind speeds located at high altitudes beyond 500 m. In attempting to achieve a minimal tether length and weight, the angle between the tether and the ground should be large. Maximum power is achievable when the tether is horizontal with the wind direction. Using a large tether angle reduces the possible power output. Due to there being higher velocities near the ocean surface, using a buoy connected to a kite flying in shallow depths achieves a smaller tether angle with a shorter tether length and producing more power. The buoy can also be submerged below the sea surface. Figure 2.9 and Figure 2.10 show hydro-kite systems using a tether connected to the seabed, and a tether to a floating buoy which is also anchored to the seabed, respectively.

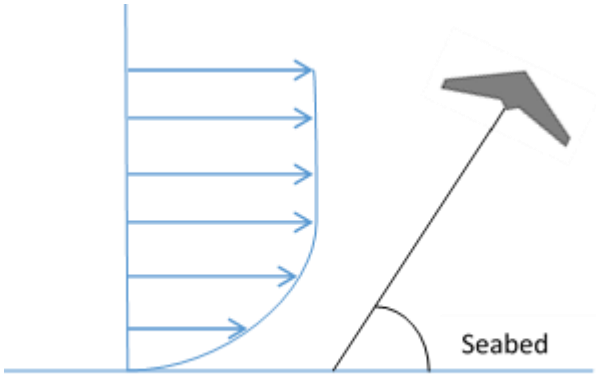

Figure 2.9. Diagram showing a TUSK system, where a long tether at a large tether angle is required to maintain the kite at the required water depth.

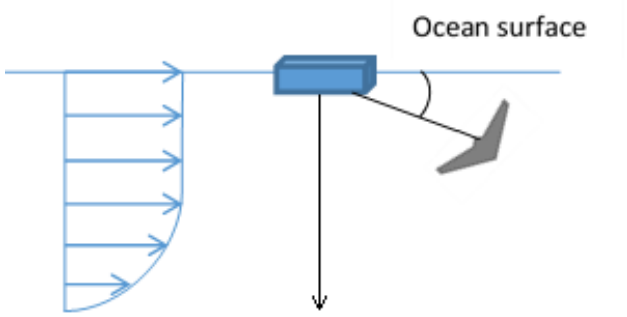

Figure 2.10. Diagram showing a TUSK system tethered to a floating buoy; higher velocities occur near the ocean surface, so a shorter tether at a smaller tether angle is used.

The drawbacks of using TUSK systems is that they require advanced control systems to guide the kite in the "figure of 8" cross-current motion. Kite materials are fully submerged within a marine environment and will deteriorate with time eventually requiring replacement. Undesirable effects from turbulence within ocean currents could affect both the kite and the efficiency of the turbine.

Stall characteristics of the kite wing and turbine blades must be investigated, as well as the structural loading and fatigue effects on the kite constituents. TUSK systems must resist effects of major storms, effects experienced will be on a smaller scale as the kite is fully submerged compared to if it were

located closer to the surface. Kites tethered to floating buoys may be more affected by storms as the tether point is on the sea surface and subjected to more impact. However, the hydro-kite can be reeled in during a storm or for maintenance purposes.

Many factors need to be taken into consideration when implementing TUSK systems; placement needs to avoid shipping routes, in this regard a hydro-kite tethered to the seafloor directly would be a more suitable option so as not to interfere with surface activities. The system will also have an influence on the environment and could impact marine life and habitats, as rotating turbines could pose a threat and increase fish mortality, therefore, steps must be taken to minimise these effects. A TUSK system should be investigated for possible deployment within the Agulhas current to generate energy (Olinger & Wang, 2015).

2.5.2. Power output

The maximum theoretical power (*P*) as suggested by Loyd can be calculated as Eq. (2.5), this can be applicable for either TUSK system of using an on-board generator or a stationary generator with a kite moving in uniform high-speed cross-current motion. However, using a stationary generator does not produce as much power as there is a loss of power in the tether retraction stage where the tether reels out and back in (Loyd, 1980).

$$P = \frac{2}{27}\rho v^3 A_k C_L \left(\frac{C_L}{C_D}\right)^2 \tag{2.5}$$

Where A_k is the kite wing area and C_L is the lift coefficient.

Dynamic pressure (q) is calculated using the following equation:

$$q = \frac{1}{2}\rho {V_A}^2 \tag{2.6}$$

TUSK, AWE and stationary marine turbines were compared by Olinger & Wang (2015). For the same size kite area, the TUSK system was capable of producing far more energy than that of the AWE as well as generating more energy than the marine turbine. The dynamic pressure of the TUSK system was found to be significantly higher when compared to the others, demonstrating the requirement for the TUSK to be rigid using materials of high strength.

2.5.3. Technology Available

There are various types of ocean current turbine technologies available that can efficiently harness energy from ocean currents including TUSKs as well as other systems.

2.5.3.1. MINESTO

Minesto AB is a company that uses TUSKs to harness electrical power from tidal and ocean currents. Kites are composed of a wing, turbine and rudders anchored by a tether to the seabed. Kites are propelled forward by the hydrodynamic lift force acting on the wing created by the water current. The kites move in the "figure of 8" shape to make use of cross-currents as described in TUSK systems. As water moves through the turbine mounted on the kite electrical power is generated which is then transmitted through a cable within the tether and further transmitted to shore via submarine cables located on the seabed. Figure 2.11 shows Minesto's TUSK system (Minesto, 2011).

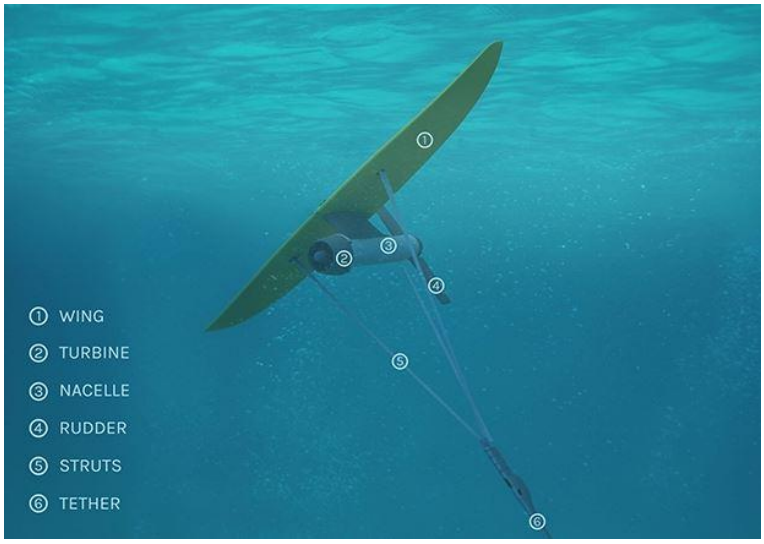

Figure 2.11. DeepGreen technology from Minesto (Minesto, 2011)

Minesto's project DeepGreen was running long-term trials in Northern Ireland at a 1: 4 scale that commenced in 2013 and has managed to generate electricity. The overall goal is to produce 1.5 MW in 2017. The prototypes were tested regarding functionality as well as the competitiveness of this type of power generation compared with other technologies available (Minesto, 2011). Minesto has been able to generate energy at a similar price similar to that for offshore wind power (Minesto, 2015).

The advantages of using this technology to produce electricity are that it is cost-effective and can operate in low-velocity currents between 1.2 m/s and 2.5 m/s in shallow depths from 60 m to 120 m. It is a relatively lightweight technology being 10 to 25 times less weight per MW than other technologies. Installation, servicing and maintenance can be performed by small boats, reducing offshore operations which would increase costs. Kites cause minimal visual impact as they are submerged below the sea surface (Minesto, 2011).

2.5.3.1.1. Holyhead Deep Project

Minesto has plans to implement the first commercial scale power plant off the west coast of Anglesey in Wales in 2017, a £25 million venture. The 10 MW kite array is predicted to be able to supply energy

to 8000 homes. The location chosen is close to the coast and experiences a mean peak flow between 1.5 m/s and 2.0 m/s at depths 80 m to 100 m. Energy can be transferred into the grid at Holy Island, accessibility through good transport links will aid the installation and maintenance processes (Minesto, 2015).

The implementation of this project aims to address socio-economic issues regarding local job creation over a wide range of disciplines including manufacturing, project development, engineering, marketing and sales as well as research and development. Due to marine energy being a relatively new technology, there is much risk associated with it, capital investment and long term political strategies are necessary. The market for marine energy has grown substantially, increasing 600% from 2010 to 2014, until 2020 it is anticipated to expand by 2300 % (Jansson, 2015). Initially, the cost of generating energy with this technology will be high but as the technology and industry develop costs should decrease and upon success investors should see a profit. Minesto predicts the sale of energy to be £250 per MW at the start of the project but costs should decrease and eventually this energy should be cheaper than that of nuclear power which is below £100 per MW. Over the next 15 years, this development has the potential to contribute £12 billion to the Northern Wales economy (Dickins, 2015).

2.5.3.2. SeaGen

SeaGen is a large scale commercial tidal energy generator that includes two rotors both 16m in diameter, connected through a gearbox to a generator. A crossbeam that supports the rotors is connected to and supported by a 3 m diameter pile as shown Figure 2.12.

Figure 2.12. Diagram showing the underwater turbines of the SeaGen technology (Sea Generation LTD, 2013).

The rotors are pitch controlled and able to move through 180° optimising power output as the angle can be changed to suit the velocity of the tidal stream, this can reduce forces exerted on the equipment. The rotors are placed within the top third of the water column where flow is the fastest to maximise energy output. The electricity produced by the turbine is grid compliant as the support structure contains electrical infrastructure eliminating the need for external power conditioning. Maintenance is quick and easy as the turbines can be raised up out of the water by the crossbeam which can slide along the support incurring minimal repair time, and there are no additional costs such as transport.

The first commercial marine renewable energy project by SeaGen was implemented in Strangford Lough, east of Northern Ireland in the UK in 2008. Over a wide range of current velocities, the system reached 48 % efficiency. The SeaGen S is capable of producing 20 MWh per day and has generated more than 9 GWh. The SeaGen system underwent three years of environmental monitoring which showed that the structure had not had a significant effect on marine life in the testing area of Strangford Lough.

Advantages of this energy system are that it has been thoroughly tested, maximum energy output is achieved, there are minimal operational and maintenance costs due to the design, the electricity produced is compliant with the grid, and it causes little environmental damage. However, this energy system requires the installation of massive infrastructure offshore, and part of the structure is visible above the water surface which could interfere with surface activities and shipping routes (Sea Generation LTD, 2013)

2.5.3.2.1. Numerical Turbine for Agulhas Current

A numerical turbine model was investigated by Meyer et al. (2014) to determine the capacity factor using data provided for the Agulhas current. The capacity factor is the ratio of the average power and the peak power produced. A simple marine turbine was used based on those from SeaGen with the same rotor diameter of 16m but with operating speeds between 0.6 m/s and 2.0 m/s, the power coefficient of the turbine was taken as 0.4. The value of the power coefficient is determined by the ratio of actual power able to be produced by the turbine and the theoretical power that could be generated by the current.

The SeaGen turbine technology attains a capacity factor of 66 % over 1000 hours of being in operation (Siemens, 2012). The capacity factors for Location 1 were 50.8 % for the first time period from April 2006 to March 2009, and 50.9 % for the second period from March 2009 until September 2010 derived from calculations. The capacity factors are approximately equal regardless of the number of natal pulses experienced with only two Natal Pulses were seen in the first time period, whereas three

occurred during the second. The capacity factor at Location 2 was slightly lower than that for Location 1, at 47.5 %. All calculated capacity factors were lower than what the technology is capable of producing, this could be attributed to the fluctuating nature of the Agulhas current and lower experienced velocities. However, the predicted capacity factors are relatively high regarding variable renewable energy (Meyer, et al., 2014).

2.5.3.3. HydroRun

HydroRun is a technology that uses the natural water flow in rivers to generate consistent and cost-competitive electricity. The system uses a glider attached to a tether that connects to a turbine; a submerged generating station is present and secured to the riverbed where electricity travels to the shore via a power cable.

The HydroRun system operates in rivers with a minimum depth of 5m and an ideal sweep distance of 40 m. The freestream glider moves underwater like a pendulum, back and forth in a controlled computer pattern. The water produces a lift force which pulls the tether and generates electricity. Figure 2.13 shows the system and components The movement of the glider increases the river velocity by a factor of 8 creating more power and being more hydrodynamic than if it were stationary. A foil with a span of 3 m and area of 3 m^2 operating at a velocity of 2.5 m/s is capable of producing 40 kW.

The system has a minimal environmental impact. Marine wildlife stays where river flow is weaker and avoid stronger flows, this is ideal as HydroRun works better in stronger flows where more power can be created. The system does not interfere with spawning locations and the ecology remains intact. The natural river flow is unchanged as there is no large infrastructure on the riverbed.

The electricity produced is compatible with the grid system and can also be used in communities that are not grid connected. There is radar, sonar and vision software located on the device which can sense and detect objects or boats nearby and change the flight path to avoid them (HydroRun, 2014).

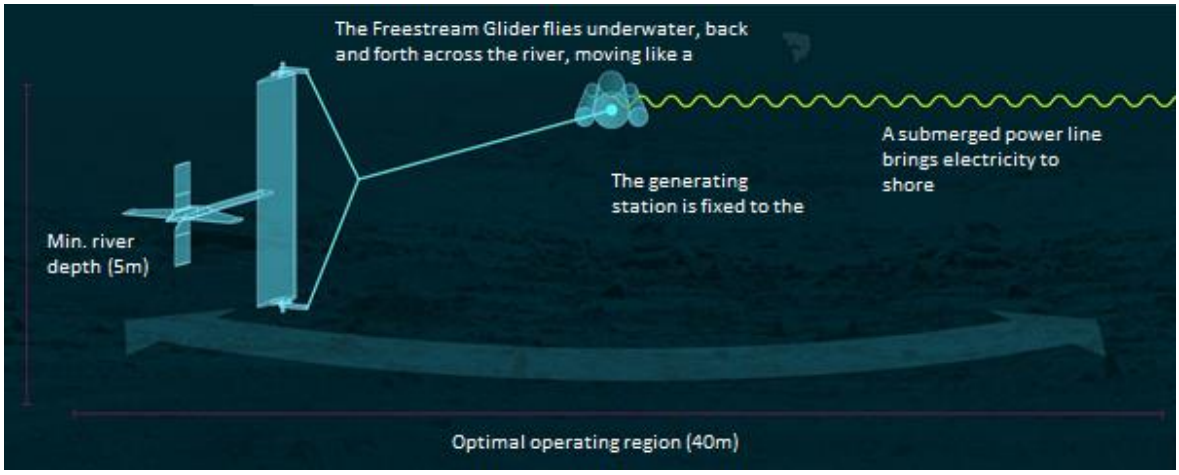

Figure 2.13. Diagram showing how the HydroRun hydro-kite is designed to operate in a river environment (HydroRun, 2014)

2.5.3.4. CETO

Carnegie Wave Energy Limited is an organisation which was the first to produce a wave energy system connected to the electrical grid on a commercial scale, it is also capable of producing desalinated water. CETO technology comprises of a fully submerged buoy tethered to a pump on the seabed. This project commenced in April of 2012 offshore of Garden Island in Western Australia.

This project was introduced to reduce the dependence on fossil fuels to produce energy and to provide a solution to the issue of high power tariffs imposed upon defence bases and remote islands, as well as the inefficiency to provide sufficient freshwater. The first power revenues received by Carnegie for the sale of green wave energy were from the Department of Defence HMAS Stirling, Australia's largest naval base at Green Island.

The CETO Buoyant Actuator seen in Figure 2.14 moves in harmony with ocean waves. The tether extends and contracts as it transmits energy to the pump. The pump pressurises the water which is then sent to shore through a submarine pipeline. Once this highly-pressured fluid reaches the shore it is used to run a hydroelectric power plant located off the shelf where the production of electricity takes place, the resulting low-pressure water is pumped back offshore. After three years of designing, financing, development and construction, CETO 5 was implemented successfully with plans for a new project with a higher electricity generation capacity (CETO 6).

The high-pressure water created can also be the input for a desalination plant using reverse osmosis to produce fresh water. Limited amounts of greenhouse gas emissions are produced as electrical pumps had been previously used to facilitate this process.

CETO causes no visual impact as it is submerged in relatively deep water avoiding damaging effects of breaking waves and storms, therefore having no impact on recreational activities. This technology has been tested and can function at various depths, tides, swell directions and seafloor conditions. It provides a reliable supply of electrical energy and freshwater while co-existing with the natural marine environment (Carnegie, 2015) (Triton Renewable Energy, 2016).

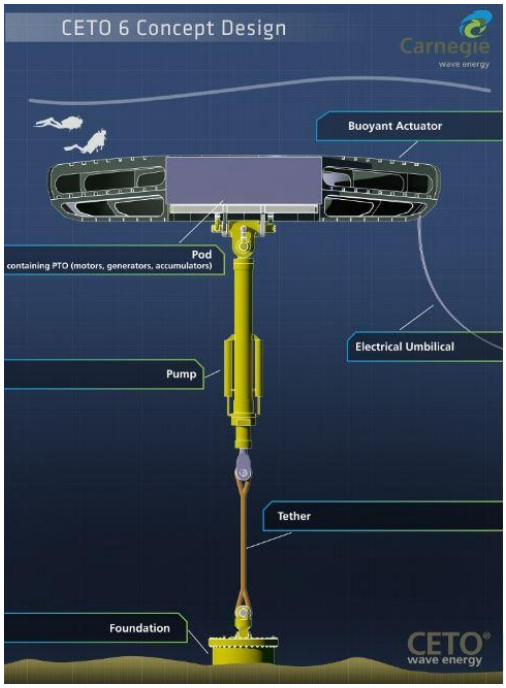

Figure 2.14. Diagram showing the working CETO 6 buoy system (Carnegie, 2015).

2.6. Kite Design

The design of the hydro-kite is paramount to the efficiency of the energy system and amount of power that it can potentially generate. Kites must be designed according to their environment to function optimally in the marine setting at low current speeds taking into consideration the variability of the current speed and direction.

There are a number of considerations regarding kite design: the area of the kite wing, the aspect ratio, taper ratio, the amount of sweep of the wing, the size of the control surface, position of the centre of gravity, type of airfoil used, turbine weight, inlet area and nacelle design, the number of turbine blades used and location of the tether connection. Neutral buoyancy may be required and can be created by placing volumes of buoyant air or foam on the kite which could be situated in the fuselage.

2.6.1. Kite Tether

The tension of the tether (F_T) can be calculated using:

$$F_T = C_L q A_k \tag{2.7}$$

Tethers that have been used successfully in AWE systems are commercial High Modulus Polyethylene (HMPE) which can apply to TUSK systems. They can withstand up to 6 x 106 N at breaking strength with diameters of up to 120 mm and 300 kg per 100 m in weight. These tethers are neutrally buoyant and adequately water resistant. Tests should be performed on tethers investigating effects of dynamic loads, fatigue and creep, estimates of tether lifespan must also be considered. Tether drag will add to the total drag on the system: using a tether diameter of 60mm could make up approximately 60 % of

the total kite drag (Olinger & Wang, 2015). Recommendations by Olinger & Wang (2015) suggest that the weight of the tether should not exceed more than 5 % of the total kite weight using a tether of approximately 100 m in length. A tether connecting a kite with an on-board turbine requires a power cable connection from the kite to the distribution point either located on the seabed or a floating buoy, therefore, the cable may have to be embedded in the tether material. A Power cable will add significant weight to the tether and increase the drag force experienced.

2.6.2. Turbine

The efficiency of the turbine is a limiting factor which determines the amount of energy that is practically extractable from the flow stream. The Betz equation is a similar concept to the thermodynamic Carnot cycle efficiency whereby a heat engine is not capable of harnessing the total amount of energy available from a source and must, therefore, emit some heat (Ragheb & Ragheb, 2011). A Betz turbine assumes that the maximum amount of extractable energy available is not a function of the turbine design but uses conservation of mass and momentum of a fluid stream flowing through an idealised "disc" (Olinger & Wang, 2015). The reduction of speed in the movement from the upstream region to the downstream area restricts the efficiency of turbines. The braking action induced by the turbine occurs as a result of mechanical energy extraction where the kinetic energy of the flow is reduced from the upstream to the downstream wake region. Viscous and pressure drag forces on turbine blades, swirl caused by the rotor in the streamflow and overall power losses within the transmission system makeup other efficiency losses (Ragheb & Ragheb, 2011).

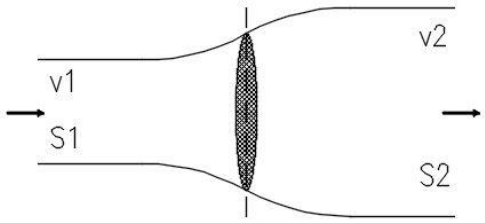

Figure 2.15. The ideal model of a wind turbine where v1 and S1 are the upstream ocean current velocity and cross-sectional swept area respectively, and v2 and S2 represent the velocity and swept area of the downstream region respectively.

The flow stream is considered to be incompressible where $\dot{m}$ is the mass flow rate. And the continuity equation is

$$\dot{m} = \rho S_1 v_1 = \rho S_2 v_2 \tag{2.8}$$

Figure 2.15 shows the change in swept area and velocity from upstream of the turbine to the downstream region. The cross-sectional area swept by the turbine blade (S) is greater downstream

where the velocity at that location is lower since from the continuity equation the product of swept area and velocity must be constant.

The Betz limit restricts the maximum power coefficient to 59.26 % which is the theoretical power harnessed from an ideal flow. Only 35 % to 40 % of available power is extractable when considering losses from friction, the roughness of the blade surface and mechanical imperfections (Ragheb & Ragheb, 2011).

Calculating the drag (D_T) created by a Betz turbine where A_T is the area of the turbine

$$D_T = \frac{4\rho {V_a}^2 A_T}{9} \tag{2.9}$$

(Olinger & Wang, 2015)

Turbine efficiency and turbine arrays will be discussed later in the chapter.

2.6.3. Wing Design

A hydro-kite must be able to withstand hydrodynamic effects due to the large density of water. The shape of the wing is the airfoil, certain types of airfoils perform better for specific conditions. As the wing passes through a fluid an aerodynamic force is created. Lift is the component of this force in the direction perpendicular to the direction the wing is moving in, the drag being the force component in the direction parallel to that of motion. The angle of attack controls the lift produced. Using a cambered airfoil can generate a lift force even when the angle of attack is at 0°. As the attack angle surpasses that of the critical angle, stall occurs and the lift force experienced is reduced. As the angle of attack changes the moment remains almost constant, but the force changes. A larger attack angle will result in a higher lift force (Hepperle, 2002). Figure 2.16 shows the forces acting on an airfoil and Figure 2.17 shows the airfoil properties.

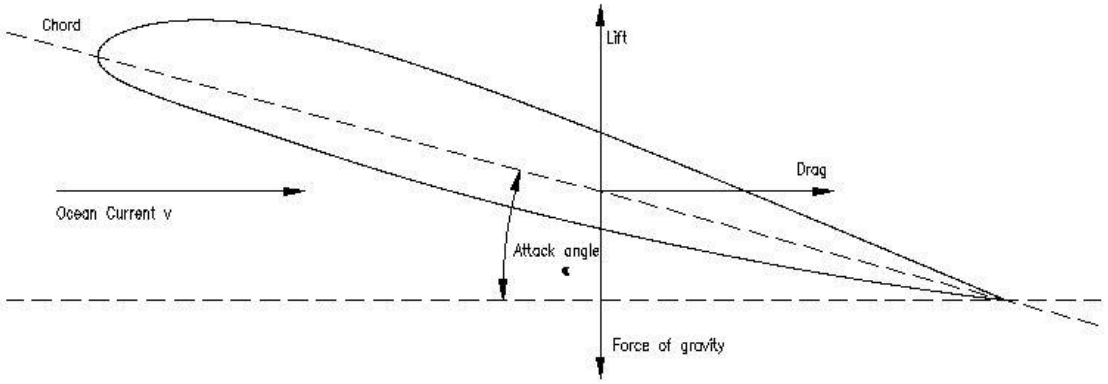

Figure 2.16. Diagram indicating the forces on an airfoil: lift, drag, angle of attack and weight due to gravity. Lift occurs perpendicular to the flow stream and drag is in the direction of the flow stream. The force of gravity will always act downwards.

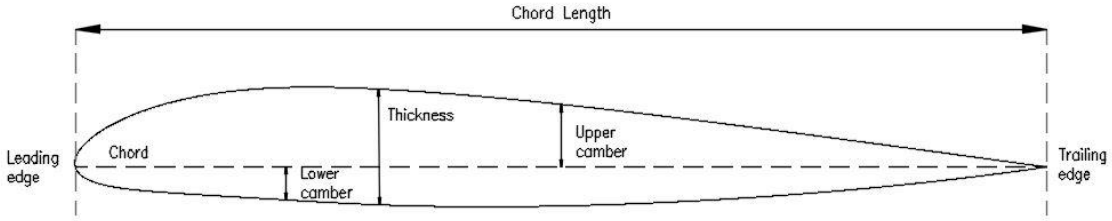

Figure 2.17. Diagram displaying the properties of an airfoil.

2.6.3.1. Wing design types

Types of aircraft include the plank which has an unswept wing and in plan view is a rectangular shape. Minesto uses a similar type of underwater kite. Stability in an unswept wing is attainable by placing the centre of gravity (*cg*) in front of the neutral point (*np*). Longitudinal stability is achieved within the airfoil alone, and the C_m should be positive. This airfoil can incorporate a heavy reflexed camber line. However, the addition of twist would only improve stall properties and not add stability.

The swept wing can incorporate any airfoil as adjusting the sweep and twist creates longitudinal stability. The C_m used for this type of aircraft must be close to zero where a small twist angle is required so the plane can perform at a variety of speeds. An ideal airfoil would be slightly cambered incorporating a small reflex with some amount of twist as swept and tapered wings tend to have higher loading near the wing (Hepperle, 2002).

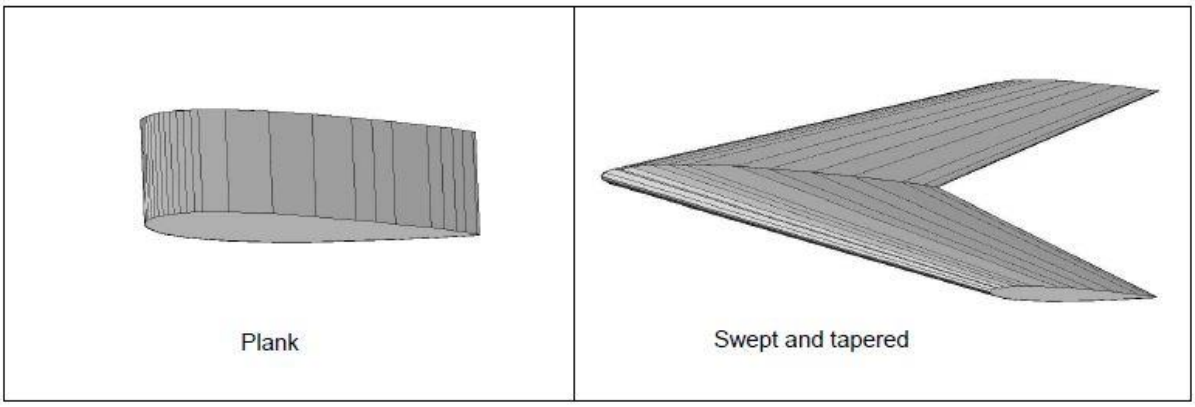

Figure 2.18. Diagrams showing a plank wing design and a swept and tapered flying wing.

2.6.3.2. Wing Properties

The Aspect Ratio (AR) has an influence on the kite design and its overall performance. The use of a higher AR will result in the design of a sleeker wing and there will be less induced drag which can add to better operation. However, a high AR can lead to smaller Reynolds numbers which reduce the kite performance (Haas, 2014).

$$AR = \frac{b^2}{A_k} \tag{2.10}$$

Where *b* is the wingspan of the kite.

The taper ratio ($_z$) has an impact on the kite design regarding washout (twist) and performance. A low taper ratio with a larger difference between dimensions of the chord and the tip results in less washout required. However, calculations yield smaller Reynolds numbers for the wingtip, and worse stall characteristics can be experienced (Haas, 2014).

$$z = \frac{C_{Root}}{C_{Tip}} \tag{2.11}$$

Where C_{ROOT} is the root chord and C_{TIP} is the tip chord.

The hydro-kite will fly in the ocean current in a controlled “figure of 8” flight pattern perpendicular to the direction of the current. Therefore, the aircraft will be subject to many angles of attack, and this must be included in the design.

Camber of an airfoil is defined as the asymmetry between the top and bottom airfoil surfaces and is shown in the Figure 2.17, a symmetrical airfoil has no camber. The camber line is a curve located halfway between the upper and lower surfaces. Using a cambered airfoil increases the maximum C_L and reduces the stalling speed. An airfoil in which the camber line curves up near the trailing edge is a reflexed cambered airfoil which is used to produce a positive moment coefficient (C_m).

Twist, or washout, is used to adjust the lift distribution along the aircraft win, ensuring that the wing tip will be the last to stall. If the attack angle is higher at the root than at the wingtip, the root will stall before the tip. The geometric twist is the difference between the x-axis of the root and that of the tip, it aids in stabilising wings with angles of sweep and airfoils with a large camber. If the wing functions outside of its design parameters, the addition of twist will induce a drag force (Hepperle, 2002).

2.6.3.3. Airfoil Design

Important factors to consider in aircraft design is the lift coefficient (C_L), drag coefficient(C_D) and moment coefficient (C_m) which have a large influence on longitudinal stability. The addition of a horizontal tail can balance the wing moment. However, in this case, a simple kite design without the use of a tail will be utilised.

Longitudinal stability is the ability of the aircraft to return to a stable position after experiencing a disturbance and can be reached by placing the cg before the np. The aircraft will fail to stabilise on its own after a disturbance if the cg and np are the same points.

The amount of camber and reflex must be chosen adequately in order to design a suitable aircraft, effects of increasing the reflex and camber as well as moving the camber can be seen in Table 2.1 (Hepperle, 2002).

Table 2.1 Table showing the advantages and disadvantages of modifying certain parameters of an airfoil.

	Advantages	Disadvantage
Increase reflex	C_m increases	Lift decreases. Probability of stall increases
Increase camber	Lift increases	C_m decreases; not as stable if C_m below 0
		Increased stress on boundary layer.
Maximum camber located closer	C_m increases; airfoil	Increased pressure on boundary layer

2.6.3.4. Elevons

Elevons are flaps located on the trailing edge of the wing and can move and assist in aircraft steering and turning manoeuvres. They are surfaces used to control pitch, roll and yaw movements, aiding to stabilise the aircraft where no tail is present (Actforlibraries.org, 2008). Elevons combine the

properties of elevators and ailerons, where elevators control pitch and ailerons regulate roll (The Aviation History Online Museum, 2002). Recommendations by (Haas, 2014) suggest that the length of the elevon be approximately 70 % of the half-span $\left(\frac{b}{2}\right)$ for a larger AR above 10, but for smaller AR values can be around 40 % of the half-span. The elevon can extent to 50% of the chord at the tip, whereas on the root side it can be between 18 % and 25 % of the local chord at that point. Elevons can be seen in Figure 2.19.

2.6.3.5. Flaps

Flaps are incorporated in the wing design at the tail of the wing in the centre near the root chord. Flaps are useful in increasing lift and washout. They cause the aircraft to slow but do not essentially increase the drag force. If the flap length is too long the nose will pitch down whereas if the length is too short the nose will pitch up and not create a large enough lift force. The desired flap length should incur no moments either up or down. The flap should extend between 30 % and 50 % of the chord along the root chord but only between 18 % and 25 % of the local chord on the side closer to the tip. Flaps are shown in Figure 2.19.

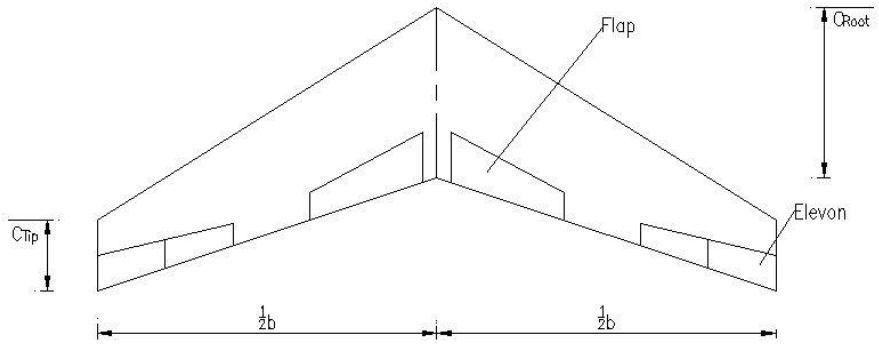

Figure 2.19. Diagram showing tip chord (C_{Tip}), root chord (C_{Root}), wingspan (b), elevons and flaps.

2.6.4. Kite Simulation Results

Simulations were performed by Olinger & Wang (2015) for a kite using the "figure of 8" flight pattern for six consecutive cycles over 200 seconds. Outcomes showed that using a simple control can achieve stable periodic trajectories. The kite's effective angle of attack did not vary much despite kite turning manoeuvres and remained at low angles below those at which stall would occur. Pitch angles remained near the selected pitch trim angle. Both yaw and pitch angles oscillate between minimum and maximum specified values during a cycle.

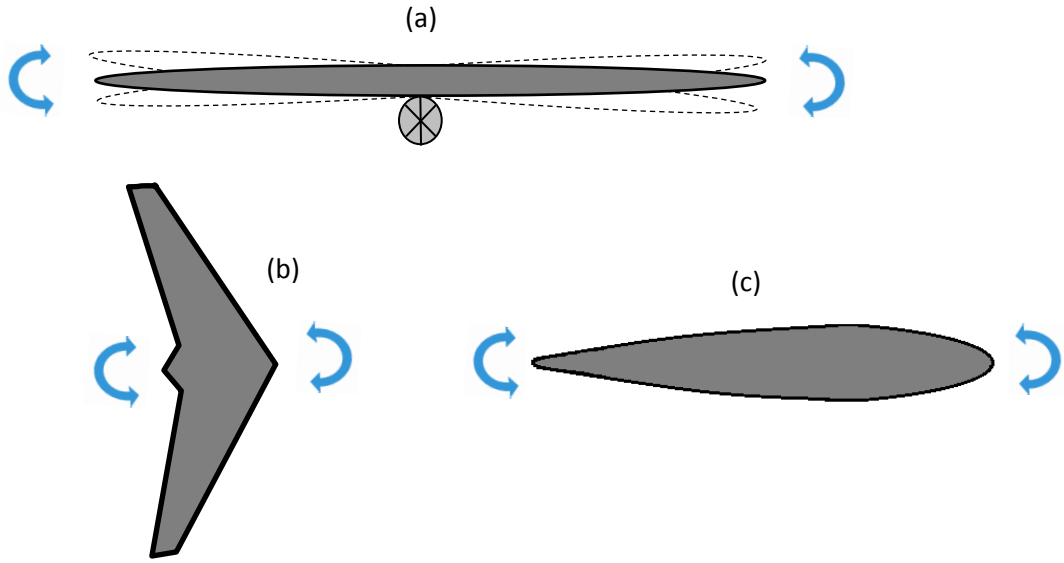

Figure 2.20. Diagram showing (a) roll, (b) yaw and (c) pitch movements of the kite. (Smithsonian National Air and Space Museum, 2015)

The calculation for Instantaneous power output for the kite:

$$P = C_P \frac{1}{2} \rho {V_a}^3 A_T - L_i \dot{\gamma}_i \tag{2.12}$$

Where C_P is $\frac{16}{27}$ for an idea, Betz turbine.

The last term in Eq. (2.12) represents the power lost due to controlling the kite's flight pattern. $\frac{C_L}{C_D}$ values are less than the initial predicted values during the cross-current flight motion reducing power output. Simulations results showed that the actual power produced was found to be approximately 50 % of the theoretically predicted output. Power output is not constant throughout the kite's simulated movement where there were two peaks per cycle. Improvements can be made by using a more advanced control system to regulate the kite's course and velocity. As the kite turns, the power produced is low, this coupled with the higher power input required to control roll, pitch and yaw indicate that the power produced will be negative in these instances. Approximately 20% of the average power produced is thought to be lost due to the power required to control the kite's movement. Peak power is not affected as it will occur when the kite is in a high-speed cross-current motion where virtually no power input is necessary for control.

Observing the simulation results, during kite turns the lift to drag ratio and the C_L also became negative as the kite's angle of attack becomes negative. Tether tensions remain positive during the entire movement but decrease during a turning movement. There is a variation in tether tension which occurs periodically, therefore, dynamic loading and effects of fatigue in the tether must be investigated (Olinger & Wang, 2015).

2.7. Turbines

Turbines are tools used to convert mechanical energy into electrical energy. A comparison is conducted between AC induction motors and Permanent Magnet Generators observing the various components and how they operate and regarding overall efficiency.

2.7.1. AC Induction Motor

An AC induction motor depicted in Figure 2.21 uses magnetism to generate rotary motion. It is made up of a fixed outer stator joined to an electrical power source that feeds into the poles of the rotor and facilitates magnetic field revolutions within the motor. There is an induction of current in the conducting bars in the rotor that work with the stators' magnetic fields, the current that attracts the magnetic fields of the stator produces magnetic fields. The rotors induce current, and the magnetism forces it to follow the magnetic field of the stator producing rotary motion. The motor increases the flux which the fixed coils enclose. Torque is generated by the effect of the induced current in the rotor on the air gap which provides magnetic resistance.

The drawbacks of this system are its inefficiency. The waste heat generated can damage insulation and compromise reliability. Induction can restrict the power density; it is generated within the induction rotor squirrel cage made up of connected aluminium or copper conducting bars. The back EMF is the voltage produced by the rotating permanent magnet motor, when the rotor spins faster, it creates a higher back EMF. Back EMF is more predominant in induction motor (IM) systems where there is a reduction in current and the motor slows down. The initial cost is of a moderate nature, but can incur high operating expenses. A motor that is too small will suffer electrical stresses and could lead to failure whereas an oversized motor may damage the driving, therefore, motors should be sized accordingly equipment and operate at less than the rated load and become inefficient (Penton, 2012).

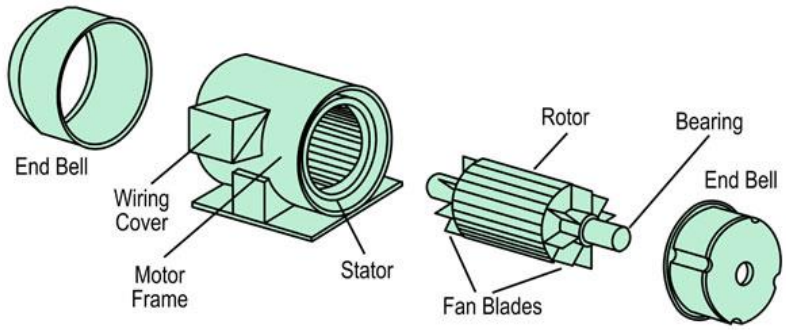

Figure 2.21. Diagram showing components of AC induction motor including stator windings, rotor, support bearings, cooling fan (Electronic Design, 2013).

2.7.2. Permanent Magnet Generator (PMG)

A permanent magnet generator is dependent on the magnetic field produced by the permanent magnet. It poses an alternative to traditional IMs where permanent magnets replace the rotor

windings. PMGs can generate AC. In an AC system, the induction is at the rotor with an array of permanent magnets where the stator and rotor magnetic fields rotate at equal speeds and it is synchronous. There is no requirement for a gearbox as the generator is directly coupled (transfer of electrical energy through contact) to the turbine and can generate a high power output at a low rotating speed.

The PMG system experiences fewer losses in the rotor than conventional systems and thus experiences a lower rise in the temperature requiring a smaller and simpler cooling system. The temperature at the bearings is also lower which increases reliability and the bearing lifespan. PMGs are energy efficient, operationally flexible and can be small and lightweight with a low life cycle cost; failure should not occur as permanent magnetic fields are constant. PMGs can function in any environment including wind and water. The demand for renewable alternative energy has increased the need for these systems as they do not consume of environmental resources to produce energy (ALXION, 2011; PM, 2013).

All PMGs require a variable frequency drive to function. The motor and electrical components are designed to withstand a maximum voltage above that of the rated drive voltage but are intended to operate far below the maximum voltage. Failure could occur in a PMG if the motor speed is greater that the speed ranges for which the design allows, where the maximum voltage surpasses that of the drive components. Permanent magnets that are subject to high currents or high operating temperatures may become demagnetised losing their magnetic properties, if this occurs the magnets cannot return to their previous state and must be replaced. Permanent magnet drives can provide over current protection limiting the threat of high current demagnetization. The use of high-temperature magnets restricts the operating temperature of the motor, and the use of integrated thermostats can ensure permanent magnet protection (Penton, 2012).

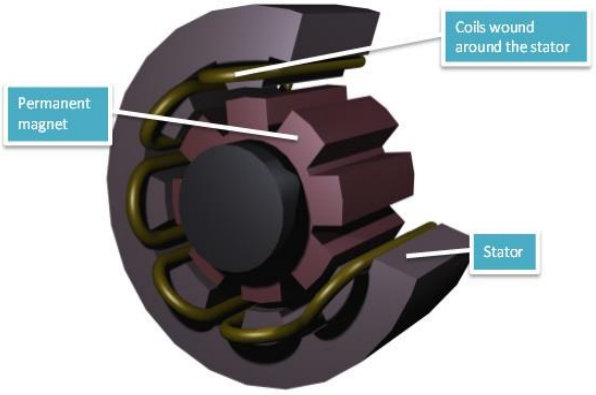

Figure 2.22. Diagram showing cross section of a PMG including stator and coils (Comsol, 2012).

Figure 2.23. Diagram showing longitudinal cross section of a PMG (Penton, 2012)

2.7.2.1. Advantages of PMG

The power density of PMGs is greater than that of conventional IMs. Permanent magnets can produce more flux for their size in comparison to that generated by an IM. The PMG uses permanent magnets on the rotor avoiding the need for coils and input energy to the coils, brushes are not required to supply power to the rotor, so there are no heat losses. There is a reduction in the resistance losses as there are fewer windings in the coils with the magnets forming the current. PMGs are lightweight and capable of operating from cold having the potential to produce a higher energy output (PM, 2013).

PMGs are superior to conventional DC motors and generators regarding efficiency and losses. Ohmic losses in conventional generators are caused by the current flowing through resistance in the armature winding, the field windings and the brushes and brush contacts. PMGs have reduced ohmic losses, designed without armatures or brushes. The field coils have low inductance with smaller coils so the system has less copper resistance which can produce the same power output. Other losses present in conventional generator systems include core losses, mechanical losses and stray load losses. These losses are either eliminated or much smaller using the PMG due to its design (PM, 2013).

Overall, PMGs are more efficient than other systems at the required voltage level incurring fewer losses than conventional IMs while exhibiting a higher power density. PMGs are reliable offering a low life cycle cost and a potentially greater life span than conventional IMs. PMG technology is well suited to use within the hydro-kite system as it can operate in any environment and is lightweight so it can be submerged underwater and positioned on the hydro-kite.

2.7.3. Siemens Electric Motor

Siemens has developed a lightweight motor for use in aircraft which can produce a power of 260 kW with a weight of 50 kg, generating more than 5 kW per kilogram - about five times more than what conventional systems are capable of producing where they can achieve less than 1 kW per kilogram. The electric motor operates at 2, 500 rpm and without the use of gears it can drive the aircraft propellers.

Using a cobalt iron alloy in the motor's stator can achieve high magnetisability. The configuration of the permanent magnets is in a Halbach array, within the rotor: four magnets placed near each other to orientate each magnetic field in a different direction reducing the amount of material required as the magnetic flux is optimally directed. An electrically non-conductive cooling liquid such as silicon oil or galden can be used for the direct-cooled conductors and direct discharge loss of the copper (Drives & Controls, 2015). It would be advantageous for the hydro-kite system to install turbines which are as efficient as possible with a low weight to power ratio. However, the cost of the system must be kept low to compromise between cost and efficiency.

2.8. Turbine Arrays and Efficiency

Turbine efficiency has a large impact on the amount of power that can be produced as was previously discussed. The Betz limit is found to be 59% where the maximum extractable power is restricted to this percentage of the total theoretical energy. To make a considerable energy contribution, a significant number of turbines are required. Turbines can be arranged relatively close together in farms. The arrangement of turbines can have an influence on the efficiency at which they operate and the power generated. The best array should be found and used with minimal environmental impact.

The turbines described are large tidal turbines similar to those of SeaGen. Models consider turbines as discs offering resistance to flow. A line of turbines within the flow stream is defined as a fence. Hydro-kites have an entirely different application as they are much smaller devices which move within the current and will have different effects on the flow stream (Nishino, 2013).

2.8.1. Wake Mixing

Wake mixing describes the effect of the flow stream downstream of turbines where the resistance of turbine structures causes disturbances within the flow stream which can interact with each other. Core flow describes the flow that enters the turbine 'disc', and bypass flow is the flow that does not flow through the turbine but flows around it.

Wake effects limit the efficiency of multiple fences of turbines where fences downstream can be influenced by upstream fences and their resulting wake impacts unless the distance between fences is large enough for wake effects not to have an impact downstream. The transfer of energy and heat loss occurs in the near wake region between bypass and core flows as a result of wake mixing which can affect the efficiency of a lone fence and possibly even one turbine. The effect of near wake mixing could be negligible for a single turbine as the near wake area, depending on blockages, is only a few turbine diameters in length. However, the effect is prominent where many devices are laid across the stream and the length of the array increases (Nishino, 2013).

2.8.2. Blockages

A full tidal fence includes turbines arranged over the whole width of a channel. In the applied situation of implementing turbines within ocean currents, the arrangement is considered a partial tidal fence as the channel width is assumed to be infinitely wide. There is scale separation between flow around each turbine and flow around the complete turbine array. The limit of extractable energy can be increased for an infinitely wide channel from that of 59.26 % to 79.8 % if the spacing of turbines is optimal (Nishino & Wilden, 2013).

The blocking effect of turbines occurs when they are spaced closely within a lateral array to maximise the amount of power produced. The blockage effect model considers the turbine to be in a uniformly

confined flow stream as a disc. It assumes the conservation of energy for core and bypass flows and the mixing of core and bypass flows, in the far wake located downstream of where the pressure equalises between these flows. Far downstream, the flow reverts to a steady stream. The limit of extractable power experiences an exponential relationship with the channel blockage ratio, *B* which is ratio of cross-sectional area of turbines to the cross-sectional channel area, this is also considered to be the global blockage. The power coefficient (C_P) is defined as

$$C_P = \frac{P}{\frac{1}{2}\rho {v_0}^3 A} \tag{2.13}$$

Where the maximum power coefficient ($C_{P\,max}$) is

$$C_{P_{max}} = \frac{16}{27}(1 - B)^{-2} \tag{2.14}$$

The Betz limit occurs when B = 0. The turbine is only capable of extracting the available kinetic energy where the pressure upstream is equivalent to the pressure downstream. As B increases above zero, pressure head is created between the far upstream and downstream regions, from this pressure difference additional energy can be extracted. The power coefficient can increase over that of the Betz limit, as B tends to unity C_P can approach infinity where power is produced by pressure head only; Eq. (2.14) in this case, does not apply (Nishino & Draper, 2015).

The local blockage is the ratio of single turbine area to the cross-sectional area of the local flow stream. Investigating the effect of local blockage on the turbines' efficiency the model assumed a large number of turbines arranged in both the vertical and lateral directions within a wide flow path. The model combines the effect of local and global blockages. The model incorporates complete scale separation between local - around the device, and global - around the entire array, flow events and includes mixing within the far wake region. This assumption is only valid if there are enough turbines within the array. The model is usable even when global blockages are zero, and the channel is considered to be infinitely wide. The local blockage ratio is found to be optimal at 0.4 with a C_P of 0.798. The effect of local blockage can also apply to wind turbines as it is not possible to arrange these turbines in the vertical direction the blockage effects will be less severe, and the power coefficient will be lower than the optimal case. The influence of local blockages on wind turbines is similar to the application of hydro-kites within the Agulhas current, both assume an infinitely wide 'channel' area but can potentially still make use of local blockages to increase extractable power (Nishino & Draper, 2015).

2.8.3. Turbine Arrays

Research into optimising turbine arrays has been done observing centred and staggered arrangements as well as the effect of the number of fences used. Models ignore losses such as those associated with

angular momentum, wake and hydrodynamic losses. The model assumes ideal turbines with a steady flow ignoring bed friction presenting an upper bound for the extracted power.

The spacing of turbines should be great enough so that pressure can equalise between rows but small enough to avoid wake mixing upstream before the next row of turbines. Observing two rows of turbines in a centred and a staggered formation, the average power extracted is larger for the staggered arrangement, however, placing all turbines in one row would yield an even bigger power output. The use of more than one row of turbines requires larger inter-turbine spacing compared to the use of only one row to maximise power. Increasing the number of rows of turbines may result in a greater wake mixing effect. Turbines cause resistance to the flow stream as it diverts locally at individual turbines. The diversion of the flow limits efficiency and power production.

In practice where it is not possible to place all turbines within a single row, a large number of turbines are used, situated within the ideal flow stream experiencing high velocities and using multiple rows facilitates a spatially dense array. The number of fences used determines the optimal inter-turbine spacing within rows. The local blockage effects are seen to reduce with the addition of fences from 0.4 using one partial fence to 0.12 using two partial fences. A further decrease in these effects will occur with added rows due to local blockage effects being greater in upstream rows but will be less downstream due to wake velocities and less power generated in downstream fences (Draper & Nishino, 2013).

2.9. Submarine Power Cables

Due to the increasing demand to extract renewable marine energy resources there is a larger demand for more subsea cables to facilitate the transportation of electrical power generated. Cables incorporate either a single or three core cable, which is more flexible, through which large amounts of energy can be transported (Attwood, 2000). Investigations were undertaken into submarine cables regarding general specifications, methods of installation, environmental concerns as well as their design and components.

2.9.1. General Cable Specifications

There are many basic requirements for the use of submarine cables installed on the seabed. High safety factors should be incorporated to keep repair operations to a minimum avoiding the high costs associated. Over long distances operating power loss is a problem and compromises maximum energy generation, therefore, transmission losses should be reduced. Subsea cables can be manufactured to a maximum of 100km in continuous length reducing the amount of discontinuities occurring at jointing locations and allow for continuous cable laying. However, it may prove difficult to manage larger lengths of cable where the manufacturing process must be capable of insulating, sheathing,

armouring, storing and off-loading and cables may weigh up to 8000 tonnes. Flexible joints can be used to combine shorter lengths of cable. Cables are subjected to forces including extreme bending under tension, twisting and coiling and must be designed to endure these imposed forces. They should be balanced regarding torque to resist twisting forces when lowering the cables into position. They must resist external pressure applied by water at their operating depth, as well as being impermeable to prevent water entry. The design should consider the case of damage to the metal sheath where water may be able to pass through. The length of cable affected should be limited, so overall damage is less. Cable armour must be sufficiently durable to prevent damage. Cables will be subject to movement under tidal currents on the seabed which may cause abrasion damage, therefore, cables must be weighted appropriately to counteract this force. They should also be equipped to withstand potential corrosion and designed for a sufficient flexural fatigue life (McAllister, 1982).

2.9.2. Installation

An advanced cable laying vessel can be used to install cables, placing cables in desired positions while avoiding impediments that may occur on the seabed. Jointing can take place where lengths exceed the loading capacity of the laying vessel. It is imperative that before installation commences that conditions of the seabed are analysed to determine successful installation of subsea cables and prevent possible environmental damage. Depths below 100m require specialised vessels to perform installations, due to the implementation of hydro-kites in shallower waters this is not a concern. Tethers must be anchored along the coastal shelf which is within a depth of 100m in most areas making the operation less challenging (McAllister, 1982).

There are two techniques of cable installation. The first involves laying cables from large coils stored in the hold of the laying vessel. The other method lays cables from a large turntable or drum situated on the deck of a laying barge. This process ensures that cables are exposed to less severe bending and is a preferred method (McAllister, 1982).

Difficulties may arise in cable installation. Cables must resist mechanical forces imposed on them by ocean currents and their own weight (Attwood, 2000). There is a high risk of damage to cables during the installation process where stresses produced can occur immediately or can only be seen years later when the cable is in service (Subsea Cables UK, 2014). After installation, cables are subject to potential external damage that can occur from fishing activities, anchors, an impact from vessels, possible movement and terrain of the seabed (Attwood, 2000) (Subsea Cables UK, 2014). To minimise the risk to cables through fishing activities. Fisherman can be provided with information and be made aware of cable locations and depths to avoid those areas (Subsea Cables UK, 2014). Cables can be protected by metallic armour wires during the construction process and can be buried in the seabed to minimise the risk of damage. There is little probability of internal cable damage (Attwood, 2000).

A cable plough can be used to bury the cable in the seabed. The cable is taken from the ship and fed through to the plough towed by the cable ship or by a ship following behind it. The plough digs a trough in the seabed and lays the cable inside, when the plough passes over the part of excavated seabed it covers it, burying the cable. Jetting and trenching are alternative methods to cover cables. Where it is not possible to bury the cable, protection of the cable then involves covering it with overburden, materials used can include polyurethane or concrete (Attwood, 2000; Subsea Cables UK, 2014).

Submarine power cables require repair if damage or a fault occurs. Repair time is reliant on ship and cable availability and can take weeks to months. During the repair process, the cable is taken up to the surface in two parts as there is not enough slack available to directly join the two pieces, an additional length of cable is used to splice into the original cable joining the two ends. Each repair thus adds length to the cable (Subsea Cables UK, 2014).

2.9.3. Environmental Concerns

As with the environmental impact of the renewable energy extraction technology, there is also the concern of possible environmental impact from the submarine power cables. Power cables seem to have no significant effect on the environment: cables are relatively small in diameter with only a small amount of disturbance to the seabed during installation and reparation processes which affect only a narrow seabed section where the cable is laid. Research has shown the effects of Electromagnetic Fields (EMF) are incredibly small. Thermal temperature rises as a result of the power cables are also not significant as they are not detectable from natural temperature fluctuations (Subsea Cables UK, 2014). The use of sea electrodes could potentially result in seawater pollution due to the electrolysis of seawater and corrosion of steel elements, therefore, these are avoided (Attwood, 2000).

The MPA of Pondoland near Port Edward where ADCP deployments have previously taken place should be investigated regarding installing a submarine cable through that area, initially, it will cause disturbances to the seabed due to the installation process but will have no impact afterwards, and fish species can remain protected.

2.9.4. Cable Properties

Submarine cables are underground cables with the addition of a lead sheath and steel armouring to ensure they are impermeable from water and protected from damage. The additional weight of the cables aids to inhibit cable movement where strong currents may be present (Windenergie-Institut, 2001).

2.9.4.1. Conductors

An electrical conductor allows the free flow of energy. Metals are good conductors with low resistivity. Copper and aluminium are commonly used conductors due to their high conductivity potential and cost (Thue, 2005). Copper conductors have a higher current density reducing the required cable diameter where aluminium conductors have up to only 62 % of the conductivity of copper and require a diameter increase of 60 % to operate at the same resistivity (Thue, 2005). Copper also shows a higher resistivity to corrosion, if the cable is subject to damage with water being able to enter, copper cables will perform better (McAllister, 1982). Aluminium has a weight advantage over copper for the same resistivity as it has a lower density, less than 50 % of that for copper. However, aluminium also requires more insulation for the same resistivity, with more surface area to insulate over as it has a greater diameter. Copper tends to operate better in short circuit conditions whereas aluminium is prone to metal creep and oxidises at a fast pace when exposed to air (Thue, 2005).

2.9.4.2. Insulation material

XLPE is a material which is made up of polyethylene linked chains, it operates well at higher temperatures as the cross-linked chains aid in inhibiting the material from separating or melting but can be prone to thermal expansion. XLPE has relatively low dielectric losses, but higher than those of Polyethylene (PE) but ages better and has more resistance to water treeing.

Ethylene Propylene Rubber (EPR) is an elastomer, a copolymer of ethylene and propylene. EPR is more flexible than PE or XLPE materials with a lower risk of thermal expansion compared to XLPE and resists water treeing, however, EPR has higher dielectric losses. (Open Electrical, 2012)

For AC cables with voltage ratings of up to 34.5 kV, the insulation thickness for land cables can apply. The design for higher voltage cables can incorporate a lower maximum design stress than that which is used for land cables as submarine cables are subject to extreme bending and tension during the laying process before they are even in use. (McAllister, 1982)

2.9.4.3. Current Ratings

The current rating of the submarine cable is a function of the recommended maximum conductor temperature, the thermal resistivity of the dielectric material and the laying environment. As an additional safety factor the maximum conductor temperature should be about 15° to 20°C below that used for land cables, this results in the need for larger conductors which increase the cost but reduce cable losses. Site conditions and the method of installation influence the thermal resistivity: 0.3 Km/W for cables on the seabed surface, and between 0.3 and 1.0 Km/W for buried cables (McAllister, 1982).

2.9.4.4. Water Pressure

Cables that are non-pressurized and of circular design do not experience any distortion at depths above 150 m. The installation of cables occurs at a depth of approximately 100m on the coastal shelf, distortion from water pressure will not be a concern (McAllister, 1982).

2.9.4.5. Fibre optics

The design of submarine power cables should include a fibre optic cable linked to the hydro-kites to remotely control their movement and angles of attack.

2.9.5. Power Transmission

The diameter of submarine power cables can vary from 70 mm to over 210 mm and can be used in an Alternating Current (AC) or Direct Current (DC). Cable selection is dependent on the required length of the cable, the voltage, its transmission capacity and grid synchronisation. AC power is a more economical system compared to DC until longer route lengths are required. For path lengths up to 80km AC is a better solution and over longer distances DC should be incorporated. In a system that transmits lower amounts of power at shorter distances, HVDC transmission would not be feasible due to the added cost of converter stations required. Wind farms closer to the shore make use of AC, whereas further offshore wind farms of a larger size would require HVDC. A DC system can create magnetic compass errors which are particularly prominent when cables are laid North to South (ESRU, University of Strathclyde, 2002; Subsea Cables UK, 2014).

AC supplies power in 3 phase which can be in three separate cables or can be combined in one cable with a three core formation. DC can be delivered in mono-polar or bi-polar where it is usually two conductors that can also be separate or together in a coaxial arrangement (Subsea Cables UK, 2014).

The transmission of electrical power can be through a 3 phase system or a single phase system in AC. Domestic households and small businesses that are not industrial use single phase transmission systems. 3 phase systems are used in larger businesses, in industrial applications and manufacturing. 3 phase systems are smaller incorporating less wiring compared to single phase systems reducing cost; it can use lower voltages and is safer and more economical. Single phase includes two wires: one live wire and one neutral wire and 3 phase uses four wires: three live wires with one neutral. Figure 2.244 shows that for the single phase when the wave is at 0 V there is no power supplied at that time. Using a three phase system where there are three wave cycles present each being 120° out of phase with the one before so at no time will there be no power available. Figure 2.24 and Figure 2.25 show single phase and three phase power respectively (Tripp Lite, 2015).

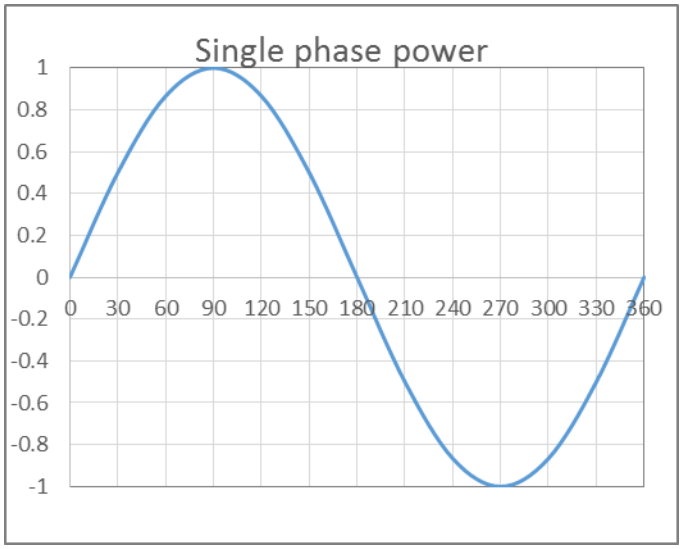

Figure 2.24. Diagram showing single phase power over one wave cycle

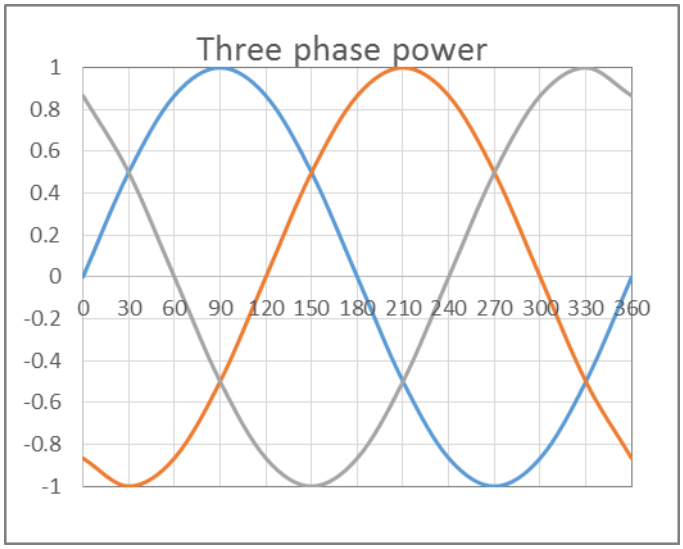

Figure 2.25. Diagram showing three phase power over one wave cycle.

Three phase power is the more common system used for power transmission and has many advantages over the single phase system. In transmitting the equivalent amount of electrical energy, 3 phase uses less conducting material, i.e. copper or aluminium.

Three phase motors are preferred over those used in single phase as they are smaller for the same current rating, they can start on their own producing a rotating magnetic field whereas single phase motors require a starting winding that can only generate a pulsating magnetic field. Uniform power can be transmitted during the entire course of the cycle using 3 phase motors, unlike single phase in which the transmitted power is based on the fluctuating instantaneous current. These motors are then subject to more vibrations (Tripp Lite, 2015).

Submarine circuits that make use of 3 core cables can have a voltage rating of up to 132 kV and can be economical regarding cable costs and those associated with the installation. Unjointed continuous lengths of cable are not possible. Flexible joints can be used but add to the cost proving expensive for long cable lengths.

If the cable is subject to damage, it is possible that all three cores within could be affected. To achieve security of the electricity supply, it would be advantageous to implement two three-core cables that are spaced approximately 250 m apart. If only one cable is damaged, the other cable will still function, and at least some of the electricity supply can be transmitted until repair operations can take place (McAllister, 1982).

AC power transmission can be achieved using three single conductors, but they must not intersect, allowing a safe distance between each cable to allow for a repair loop. It is not possible to lay all cables in one process, therefore, installation costs are increased (Windenergie-Institut, 2001).

2.9.6. Cost

Submarine cables have a lifespan of 25 years where they could potentially function for up to 40 years assuming they are not subject to failure. The repair of submarine cables can be expensive. Due to commercial confidentiality, it is hard to attain an estimate of cable costs. Submarine cable installation is also very particular to each project. Transmission of power from an offshore source is costly, and it is, therefore, more economical to transport large amounts of energy.

The cost of submarine cables far outweighs that of overhead cables, ranging from £50 to £125 per metre (approximately R870 to R2170 per metre) in the range of medium voltage cables. A submarine cable connecting the North Sea platform Beatrice to the shore spanning a distance of 26km at an AC voltage of 33kV cost £100 per metre (around R1735 per metre). The construction of cables becomes more difficult with an increase in voltage, as the voltage increases so do the costs. The cost of installing submarine cables is highly dependent on the depth at which the cable is laid as well as the nature of the seabed. Installation costs can be between £2 million and £5 million per km of cable (approximately between R35 million and R87 million).

Cables up to a voltage of 300kV can use XLPE as an insulation material, beyond this value at around 500kV mass-impregnated cables are used with an insulation of oil impregnated paper which are far more expensive. The cost of HVAC cables ranges from $0.74 million to $1.08 million per km (R10.4 million to R15.2 million). The cost of HVDC cables is between $1.5 million and $1.9 million per km (R21.1 million and R26.8 million) (Carbon Copy Communications, 2011).

2.9.7. Submarine Cables in Wind Farms

Offshore wind farms which are of a similar nature to offshore hydro-kite arrays require submarine cables to transport power from the offshore location to land. Small cables connect each turbine within the farm and link up to an offshore substation. Power is then transmitted through a high capacity cable to the shore.

Wind energy is not a reliable source due to its intermittent nature with an availability of only 40 – 50%; while nuclear, coal, oil and gas energy have an availability of between 82 – 92%. In the UK at times when renewable energy technology can function at its full capacity, the UK has the option of selling the additional electricity to Europe through interconnector cables (Subsea Cables UK, 2014). Due to ocean currents within the Agulhas current being more reliable than wind, security of supply might be higher for the hydro-kite project than wind farms.

Wind power incorporates the use of small individual turbine systems connected into a distribution network at a low voltage. Due to wind energy being of a variable nature it results in fluctuation in power output. However, this does not cause a problem in electrical systems as the variation is not distinct as there are already fluctuations from the supply and demand of electricity.

Wind turbine technology includes a rotor converting wind energy into mechanical energy; the mechanical power is absorbed by the generator and converted into electrical energy which feeds into the electricity supply grid. A gearbox adjusts the rotor to the speed of the generator.

Connecting the wind turbines to the grid incorporates the use of transformers and a substation which includes a circuit breaker and electricity meter. High losses are incurred using low voltage cables. Each turbine requires a transformer, located nearby to limit the length of the LV cable. The transformer increases the voltage level of the turbine which is usually between 400V and 690V to a medium voltage of up to 36kV. There are no standard products available to increase the voltage further (Windenergie-Institut, 2001).

2.9.7.1. Grid Connection

Large offshore wind farms would require an offshore substation to transform an MV line to an HV line to further limit losses in long cables to the shore. The substation is an offshore structure implemented at shallower water depths requiring a foundation. The top structure of the substation can be constructed offshore and brought to site by a floating crane and assembled. High voltages of up to 400kV are attainable for cables transporting energy to the shore; for higher voltages, the transformer must be oil cooled or insulated.

Offshore wind turbines require foundations upon which to construct the turbine structure. The foundation cost increases with the depth of the water, but shallow waters limit the access for boats. Foundations and the wind turbine structure make up a considerable percentage of the cost required. The turbines also need to be placed far offshore so as to cause no visual impact making installation more difficult. The hydro-kites are a suitable alternative compared to offshore wind farms, requiring no foundations or large turbine structure causing no visual impact (Windenergie-Institut, 2001).

2.9.7.2. Cost of Grid Connection

The cost of connecting an offshore wind farm to the grid involves the local electrical installation as well as the expenses involved in connecting the wind farm to the electrical grid. The local electrical installation incorporates the MV cable system within the wind farm, the cost of local equipment required, the technology needed, existing soil conditions to lay cables, the distance between turbines, the size of the wind farm and voltage level of the existing onshore grid. If the distance to the shore from the farm is long, the system requires an offshore transformer substation which would increase

costs. It is necessary to consider the distance to the closest onshore HV substation to connect the farm to the electricity grid.

The submarine cable system of a hydro-kite array can be designed similar to that of an offshore wind farm. Short lengths of LV cables are required connecting the hydro-kites. Power produced by a turbine operating at a low voltage is transmitted to a transformer positioned on the seabed in proximity to the hydro-kite. The transformer steps the voltage up to an MV line to transmit energy along longer distances at a low current to minimise losses incurred. Various cable configurations and hydro-kite arrangements will be investigated including the use of an offshore substation and without (Windenergie-Institut, 2001).

2.9.8. Power Cable Properties

2.9.8.1. Resistance

2.9.8.1.1. DC resistance:

DC resistance can be calculated from the resistivity of the conductor material and the area of the conductor.

$$R' = \frac{\rho l}{A} \tag{2.15}$$

$$R_t = R_{20}[1 + \alpha_{20}(t - 20)] \tag{2.16}$$

α_{20} = 0.00393 (Copper)

α_{20} = 0.00403 (Aluminium)

2.9.8.1.2. AC resistance:

When AC flows through a conductor and currents are relatively high. Skin effect and proximity effect influence the current distribution resulting in an uneven distribution within the conductor cross-section. Skin effects and proximity effects are considered negligible with small conductors carrying smaller current magnitudes, these effects increase with the size of conductors. Therefore, from technical and economic perspectives it is more advantageous to design conductors so as to reduce skin and proximity effects.

$$R = R'(1 + y_s + y_p) \tag{2.17}$$

The skin factor yields small values where conductor sizes are below 150mm^2 operating at frequencies of 50/60 Hz.

Skin effect factor:

$$y_s = \frac{{x_s}^4}{192 + 0.8{x_s}^4} \tag{2.18}$$

where:

$$x_s{}^2 = \frac{8\pi f}{R'} \times 10^{-7} k_s \tag{2.19}$$

X_s should not exceed 2.8.

K_s = 1 for circular, stranded, compacted and sectored conductors.

Proximity effect factor: for 3-core cables

$$y_p = \frac{{x_p}^4}{192 + 0.8{x_p}^4} \times \left[\left(\frac{d_c}{s}\right)^2 \times \left[0.312 \times \left(\frac{d_c}{s}\right)^2 + \frac{1.18}{\left[\frac{{x_p}^4}{\left(192 + 0.8{x_p}^4\right)} + 0.27\right]} \right] \right] \tag{2.20}$$

where:

$$x_p{}^2 = \frac{8\pi f}{R'} \times 10^{-7} k_p \tag{2.21}$$

k_p = 1 for circular, stranded, compacted and sectored conductors.

2.9.8.2. Reactance

Reactance calculated for each core of a 3-core cable.

$$X = 2\pi f L \times 10^{-3} \tag{2.22}$$

2.9.8.3. Electrical Losses

Losses are a critical element of electrical cable system design. Therefore, an efficient system must be designed minimising potential losses.

2.9.8.3.1. Conductor Losses

Conductor losses are calculated:

$$nI^2 R_t \tag{2.23}$$

Losses are proportional to conductor resistance, and the square of the current travelling through the conductor. Resistance decreases with an increase in conductor size, however, it would prove uneconomical to increase the conductor size to minimise losses as this would add significantly to the

material cost. Transmitting electrical power at higher voltages can reduce the current flowing through the conductor.

2.9.8.3.2. Dielectric Losses

The dielectric loss in AC cables in each phase is calculated:

$$W_d = \omega C {V_{LN}}^2 tan\delta \tag{2.24}$$

where:

$$\omega = 2\pi f \tag{2.25}$$

tanδ = 0.008 for XLPE

tanδ = 0.04 for EPR

Capacitance for cables which use circular conductors can be calculated:

$$C = \frac{\epsilon}{18 \ln\left(\frac{D_i}{d_c}\right)} \times 10^{-9} \tag{2.26}$$

ε = 2.5 for XLPE

ε = 3 for XLPE

Dielectric losses are considered negligible for cables with a line to neutral voltage of 15 kV for EPR; 37 kV for XLPE.

(McAllister, 1982)

2.9.9. Cable Design Calculations

2.9.9.1. Total Derating Current

The total derating current of a cable is the total derating factor multiplied by the current-carrying capacity of the cable. The derating factor is calculated by multiplying correction factors that apply to various situations such as cable laying environment, ground temperature, thermal resistance or soil type, depth, distance and grouping (Parmar, 2014).

2.9.9.2. Voltage Drop

In a single phase power supply the voltage is the line to neutral voltage whereas in a three phase system, the voltage is a line to line voltage. The relationship between line to neutral voltage and line to line voltage is as follows:

$$V_{LL} = \sqrt{3}\, V_{LN} \tag{2.27}$$

The power factor relates the actual power generated to the apparent power:

$$PF = cos\varphi = \frac{P}{P^*} \tag{2.28}$$

Power generated from single phase:

$$P = VIcos\varphi \tag{2.29}$$

Power generated from 3 phase:

$$P = \sqrt{3}VIcos\varphi \tag{2.30}$$

Apparent power:

$$P^* = \frac{P}{PF} \tag{2.31}$$

The current in each phase of a three-phase system:

$$I = \frac{P^*}{V_{LN}} \tag{2.32}$$

Simplifying:

$$I = \frac{P}{\sqrt{3}\, PF \times V_{LL}} \tag{2.33}$$

The voltage drop is one of the limiting factors regarding cable design and sizing. The permissible voltage drop is usually 5 %.

$$Voltage\ drop(\%) = \frac{\sqrt{3} \times I \times (Rcos\varphi + Xsin\varphi) \times Length \times 100}{V \times No.of\ cable\ runs \times 1000} \tag{2.34}$$

(McFadyen, 2009) (Parmar, 2014)

CHAPTER 3

3. METHOD

This chapter describes the methods involved in attaining the relevant results. Data used in this study and analysis includes ADCP observations and data retrieved from the HYCOM model. Information regarding submarine cable design is also presented.

3.1. Eskom Data

Eskom data was retrieved directly from the Eskom renewable energy division. The data included observations at 51 ADCP points located along the coast of South Africa between Port Edward and the Fish River for various time periods between 2005 and 2010. A list of ADCP deployments can be found in Appendix C. The provision of data was in the form of excel spreadsheets for each depth interval with an indication of the validity of the results.

3.1.1. Acoustic Doppler Current Profiler

Acoustic Doppler Current Profilers (ADCP) are used to measure the speed at which water moves across the water column. They can be fixed to the seafloor and can measure the current speed at intervals up to the sea surface. The device makes use of the Doppler Effect using sound. Sound waves have a higher frequency pitch as they move closer to an object. The ADCP releases 'pings' of sound into the water at a steady constant frequency, the sound waves travel through the water until they come into contact with suspended particles within the water where they reflect back to the ADCP device. The sound waves resonate at lower frequencies from particles moving away, and at higher frequencies by particles moving closer to the profiler.

The Doppler shift can be used to calculate the speed of the particles and the surrounding water by using the differences in frequency between the sound waves transmitted and those received. The current speed at different depths can be calculated as sound waves that hit particles further away from the device take longer to reflect back than the time it takes for particles in closer proximity. Current speeds at various depths can be calculated using the Doppler shift and measuring the time required to reflect.

The ADCP can take readings for a water column of 1000 m. The disadvantage of this device is that high frequency 'pings' result in more accurate data readings, but low frequencies can travel further; compromising between accuracy and distance. The ADCP requires suspended particles to be present in the water for sound waves to reflect off of. Problems arise if the water is clear, there may not be enough particles available therefore data collected may not be precise. Other issues that may result in unreliable data is the presence of bubbles from turbulent water or marine life passing through the

water column. The ADCP instrument is also susceptible to algae growth or barnacles attaching to it (Ocean Instruments, 2004).

ADCP instruments used in the study by Eskom included Nortek devices with an East London nametag but are located near the ADCPs deployed at Cape Morgan. All other ADCPs used are RDI.

Figure 3.1. Image of an RDI ADCP device used to measure ocean current magnitudes and directions (Sentinel, 2013).

3.1.2. Analysis of Eskom Data

The water column for which the ADCP collected ocean current data was divided into bins according to depth, bin 1 being the closest bin to the ADCP device. Bins were included only if more than 75 % of the data collected was considered 'good data', other data was discarded.

ADCP Data was received from Eskom in the format of excel spreadsheets for each bin depth for each ADCP device. Information available included the range, depth, direction of the current and velocity magnitude supplied in cm/s. The percentage 'good' of the data was also included for each date and time entry. The data quality was provided listing the calculated averages for each bin. The information collected from the Nortek ADCPs near East London do not contain an indication of the data quality. The longest duration that a single ADCP collected data during this investigation was for six months.

The central locations were selected where ADCPs were grouped together so that ocean current velocities could be observed over a longer period. Locations observed included Port Edward with three offshore positions, Cape Morgan, East London and the Fish River with one main area and another location further south. At each main ADCP location, the bin closest to the 20m depth was selected. Data from different time periods was combined at the relative locations. The date and time for each entry was combined and ocean current velocities were converted into m/s. Certain ADCPs contained data recorded every half hour whereas others were only recorded every hour. Data was filtered to the

same time step where necessary to compare data. At each central location, the average, maximum, median, mode and standard deviation of the current velocity was calculated.

At Port Edward, ADCPs at the different offshore locations were compared against each other for the same time series. A probability of non-exceedance graph was generated for each position so that the distribution of current velocities and distance offshore could be compared.

A statistical analysis was performed on the ADCP data available at a depth of approximately 20 m, the minimum depth at which hydro-kites would operate, for the prime locations where most of the ADCP data was available. Statistical analysis included using a probability of non-exceedance graph generated for all locations and normal distribution graphs to investigate the distribution of ocean current velocities at the various sites and compare them. Frequency distribution graphs were generated for each time series at the relevant positions to investigate the consistency of the current. Further comparisons were performed for different points along the coast with the same time series, relating position to the velocities produced. Ocean current roses were generated for the main locations and can be seen in Appendix C.2.

3.1.3. Natal Pulses

Natal Pulse events were observed within the data, identified as a sudden drop in current velocity coupled with a direction change. These were found through observations in both the current and direction data, some verified through Meyer, et al. (2014) and Rouault & Penven (2011). Images of Sea Surface Temperature (SST) in Appendix C.4 confirm and show the presence of some of these cyclonic pulses as they result in a drop in temperature. The occurrence of Natal Pulses during the data collection period was observed, recording when Natal Pulses were experienced at various locations. The average occurrence of Natal Pulses was calculated as well as the duration of the pulses and speed at which they propagated down the coast. The speed of the Natal Pulses as they moved southwards was calculated observing the lag time - the time between the date the pulse commenced in one region and the date the same pulse was experienced in an area further south. The distance between them was calculated from the relative geographical coordinates using a python script (Appendix G).

$$speed(km/day) = \frac{distance\ (km)}{time\ (days)} \tag{3.1}$$

The magnitude and direction of the ocean current changes during Natal Pulse events at the various locations through observations of the ADCPs for the same time series. The average duration of a Natal Pulse was calculated for each location, and the average speed between locations was determined from the limited observations available. Comparing the various locations, it is observed which sites

experience Natal Pulses at the same time and the duration that the event occurs simultaneously. This is a key factor for developing a distributed system

3.2. HYCOM data

HYCOM data was sourced from the organisation's database available at http://hycom.org/dataserver/glb-analysis. The data was provided in the form of netCDF4 files which were analysed with Python open source software where data could be extracted and analysed. HYCOM model experiments expt_90.6, 90.8, 90.9, 91.0 and 91.1 were extracted where data was available from September 2008 to present. Therefore, only three main locations were able to be compared: Cape Morgan, East London and the northern Fish River location. Information provided and extracted was the magnitude of the velocity components, in the northward (u) and eastward (v) direction captured daily as a snapshot at 00:00.

HYCOM data was extracted at three depth intervals: 20 m, 30 m and 50 m. Other vertical depths up to 5500m were available, but comparisons could not be made with the measured data as in most cases ADCPs were placed at depths above 100m, most capturing data between 80 m and 90 m. The critical zone to be observed is near the surface at the shallower depths where hydro-kites should be placed for ease of installation and to optimise their power potential from higher currents near the surface.

The HYCOM model has a resolution of 1/12° which correlates to a distance of around 8km. Data provided from HYCOM for the required geographical location lay between -27° and -35° South and 19° and 34° East at the required depths. The NetCDF4 files were opened using Spyder, a version of Python where ocean current data was retrieved. Data was available in a grid format, the closest grid reference locations to where the main ADCPs were deployed were determined and data was extracted from these. The resultant velocity, as well as the ocean current direction, were attained through calculations performed using the velocity components provided.

The resultant velocity (v_R) was calculated from the vector components using:

$$v_R = \sqrt{u^2 + v^2} \tag{3.2}$$

Direction was calculated by first determining the quadrant in which the velocity vector lies and then using a formula to determine the direction:

Quadrant 1: u > 0; v > 0 $\quad Direction = 90^\circ - tan^{-1}\left(\frac{v}{u}\right)$

Quadrant 2: u > 0; v < 0 $\quad Direction = 180^\circ + tan^{-1}\left(\frac{v}{u}\right)$

Quadrant 3: u < 0; v < 0 $\quad Direction = 270^\circ - tan^{-1}\left(\frac{v}{u}\right)$

Quadrant 4: u < 0; v > 0 $$Direction = 360^{\circ} + tan^{-1}\left(\frac{v}{u}\right)$$

3.3. HYCOM Model Validation

3.3.1. Direct Data Comparison

The HYCOM data was compared with the available Eskom data for the same time series to validate the model for locations at Cape Morgan, East London and the more northern Fish River. The datasets were investigated to determine a correlation between them. This was done for the three depth intervals available: 20 m, 30 m and 50 m. The depth against current velocity relationship was also investigated.

Factors were determined to relate the HYCOM data to the measured ADCP data for the considered time period. The relationship between the factors applied and the depth was also investigated. Factors were determined by plotting a scatter graph of the actual distribution against the modelled distribution of the velocity magnitudes.

Eskom data was filtered to contain only one entry per day at as close to 00:00 as possible to match it with the daily snapshot provided by the HYCOM model. Data that was missing from the Eskom data set was removed from the HYCOM dataset for the same time period. A scatter plot was generated with a trend line ensuring that it passed through the origin to obtain the gradient and therefore the scaling factor relating the two data sets. The correlation coefficient (R^2) was also obtained to determine the similarity of the data sets' distribution. To avoid overprediction in terms of unrealistic energy potential, if the factor obtained through the scatter plot and applied to the model data generated maximum values larger than the measured maximum velocity for that data set, that factor was then discarded. A new factor was calculated using the maximum values from each dataset.

$$New\ Factor = \frac{measured\ v_{max}}{modelled\ v_{max}}$$

This procedure was performed for locations at Cape Morgan, East London and the Fish River for depths of 20 m, 30 m and 50 m using the HYCOM data.

3.3.2. Assumptions for Unavailable Data

Locations at Port Edward and the more southern Fish River only supplied data for short periods before the HYCOM model commencement date. Comparisons cannot be conducted at these locations and assumptions needed to be made to determine possible scaling factors. These factors would later be verified using the HYCOM Reanalysis model and the relationship between the various locations and their required factors. The data was filtered at each location providing one data entry per day closest to 00:00. HYCOM data available from the model start date until September 2010, the date at which the last Eskom ADCPs were retrieved, was extracted at these locations. The average and maximum

velocities were calculated for the HYCOM data set at each location. The factor was found using the average velocity values from each dataset.

$$Factor = \frac{measured\ v_{avg}}{modelled\ v_{avg}}$$

If the factor found using the average velocity resulted in a maximum value higher than that of the actual data set, then the factor was recalculated using the maximum values as before.

3.4. HYCOM Reanalysis

Another HYCOM model was available, the HYCOM Reanalysis which attempted to refine model results and present a more accurate depiction of real ocean events. This model ran from 2005 until 2010, therefore, all main locations including Port Edward and the more southern Fish River location could be compared with the model data.

The same procedure as for the HYCOM model validation was conducted for the Reanalysis using the Eskom data. Appropriate scaling factors were determined to apply to the model for it to resemble that of actual events, this was performed at a depth of 20 m only.

3.5. HYCOM Alternative Positions

Rouault and Penven (2011) proposed that the core of the Agulhas current occurs approximately 20km offshore. HYCOM tends to predict this core approximately 50 km offshore due to the coarse resolution of the model and inability to accurately model ocean events near the coast as well as the Agulhas Undercurrent present which forces the core further offshore (Backeberg, et al., 2010). Extracted data from the closest point to the ADCP could yield incorrect results if the actual corresponding point within the current is a further 30 km offshore.

Taking this suggestion into account, data was extracted from other positions surrounding the ADCP points further offshore. Comparisons were made between the new offshore points, the measured data and the HYCOM data closest to the ADCP to determine whether the new locations yielded more accurate results. All data at a depth of 20m was extracted.

3.6. Potential Power Output

The extractable power available for a hydro-kite is a function of the density of sea water, the ocean current velocity, the wing area of the kite, the design lift coefficient and the lift to drag ratio of the kite as seen in Eq. (2.5) (Loyd, 1980). The amount of power produced is highly dependent on the technology available: the kite design and its flight properties. The current velocity cannot be altered. Therefore, the kite design must incorporate the velocities that are experienced and the design must

accommodate for this. The relationship between power and kite wing area according to current velocity was investigated and displayed graphically.

3.7. Distributed vs. Concentrated system

A distributed hydro-kite system incorporates the use of many hydro-kites spaced out along the coastline within the Agulhas current. A concentrated system would include only one main hydro-kite farm with kites placed within the same spatial area. The power potential and consistency of these two systems was evaluated.

The KEF was used as an indicator for power producing potential. It is possible to adjust the kite design to improve performance and energy generation, but the velocity cannot be altered. Therefore, the KEF is a useful guideline. The total number of days as a percentage that a certain location would not be operational for was also used as an indicator, as well as the longest consecutive duration that the system would be inactive. KEF values, as well as days inoperational, were calculated for two time intervals where ADCP measurements were available at three different locations

The area of potential extraction was broken up into four sections using the known locations from which data was extracted: Port Edward, Cape Morgan, East London, Fish River and Fish River South. Points within each section were to be extracted as one point per kilometre commencing from the known location at Port Edward. The coordinates where one section began and ended were known. Therefore, the required number of points and their coordinate locations could be calculated. A Spyder script was used to determine the coordinates of each point where information was required, and thus also the HYCOM grid references were attained.

Due to the resolution of the model being coarse, many points fell into the same spatial grid location within the HYCOM model. The number of each point required was also calculated using Spyder. Delft3D was used to extract all points required using the quickplot function. Factors were interpolated and applied to each point based on the known factors at the investigated locations and the distance between those locations. The average of the factors for each point was calculated using a pivot table. The calculated factors were applied to the velocity data accordingly.

3.7.1. Cut-in speed

The cut-in speed was determined by investigating various cut-in speeds from 0 m/s in intervals of 0.2 m/s. The KEF was calculated for each cut-in speed scenario, and the potential power output was determined. A graph of cut-in speed vs. the power produced was plotted to determine which cut-in speed provided enough significant power. A cut-in speed of 0.8 m/s was used in further calculations, the findings of using a cut-in speed of 1 m/s were also considered, which had been recommended by Olinger & Wang (2015) and vanZweiten et al. (2014). A cut-out speed of 2.4 m/s was specified.

3.7.2. KEF

The KEF was calculated using the current velocity from the data provided and the density using Eq. (2.1). Slight changes in velocity can significantly affect the KEF as it is related to the cube of the velocity. All entries within the factored data that yielded a current velocity below the cut-in speed were discarded and considered too low to produce a considerable energy contribution, data above the cut-out speed was also filtered out. Locations were only considered to be 'working' if they generated a current velocity between the specified parameters. Other sites were considered 'not working' if they failed to meet the requirements. Omitting the low-velocity values would ensure that natal pulse events are not considered as velocities are relatively low.

The total sum of the KEF for each section was calculated as well as the total sum of the KEF using the best point in each section which was multiplied by the number of points used in each section to equate the distributed system to that of the concentrated. The percentage of the KEF of using all points compared to using only the best point within each section was calculated to determine the percentage of power that the distributed system would make up of the concentrated system. This was also calculated using all points from all sections.

A test was performed converting KEF values to a binary system of operational as 1 and non-operational as 0 instead of actual KEF values. The percentage of KEF of using all points as opposed to the best point alone was calculated using the binary system and denoted as the "working percentage". The working percentage gives a better indication of the working potential as KEF is proportional to the velocity cubed where small changes in velocity yield substantial changes in KEF which may produce misleading results. The working percentage of KEF was done for each section and using the total number of points.

3.7.3. Days Inoperational

The number of days within the model data set that the best points in each section would be considered inoperational, where the velocity does not meet the cut-in and cut-out speed requirements, was calculated and converted to a percentage. The number of days that each sector would not be working was also calculated based on the sum of the KEF for all points within the section. This was done using all locations as well. The number of consecutive days that the system would be inoperational for was calculated for the best points within each section and entire sections.

3.7.4. Calculated Power

The potential power was calculated for each section, the best point in each section and using the total number of points. The average power output was calculated using the average KEF values. The properties of the kite assumed for calculating the power output included a design C_L of 1 and a lift to drag ratio of 15. The distributed system used smaller kites of a 3 m^2 area, whereas fewer, larger 6 m^2

kites were incorporated in the concentrated array. The realistic power output was assumed to be 50% of the value calculated using Eq. (2.5) (Olinger & Wang, 2015).

3.7.5. Working Percentage of Distributed Array

An analysis of using all the points included investigating the percentage of the duration that a certain number of kites would be operational. The duration for which a specified percentage of kites would be functional was calculated using intervals of 25 % of kites i.e. the duration that 0-25 % of kites are working was calculated, as for 25-50 % etc. A pie chart was created using the various intervals with the percentage of the duration that would be operational to give a better visual indication of the overall functionality of a distributed system. A probability of exceedance graph was also generated.

This procedure of calculating KEF values, days inoperational, power output and the working percentage of a distributed array was repeated using the other datasets: the factored HYCOM Reanalysis and the best approximate location extracted from HYCOM. The unfactored HYCOM model data would yield unrealistic results due to the incorrect prediction of the velocity distribution along the coast and should not be used to base any sound findings. The results from the factored HYCOM model were compared against those of the factored HYCOM reanalysis, verifying the factors used in the HYCOM model where no data was available. The results from the datasets were compared against each other.

3.8. Kite Design

3.8.1. Kite Wing

The same principles for the design of a tailless flying wing model aircraft were applied to the design of a potential hydro-kite to determine a rough estimation of properties. The dynamic loading of a TUSK system was calculated and compared to that of a marine turbine and a wind turbine using Eq. (2.6).

The design incorporates a swept kite wing. The dimensions for the wingspan, the root chord and the root tip were selected to produce an initial kite design with an area of $1m^2$. The quarter chord and quarter tip were found to calculate the PFW, which is the angle of the quarter chord line. Figure 3.2 shows the kite wing and dimensions required.

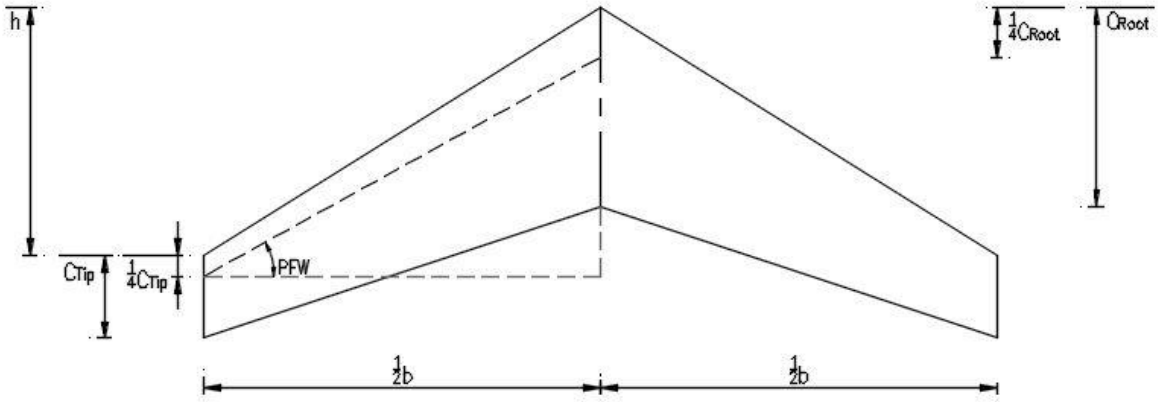

Figure 3.2. Diagram showing dimensions of swept and tapered wing design.

$$PFW = \frac{(h - \frac{1}{4}C_{Root} + C_{Tip})}{\frac{1}{2}b} \tag{3.3}$$

The aspect ratio was calculated as in Eq. (2.10) and the maximum C_L was estimated. Estimations for the C_{Lmax} can be between 0.7 and 1.0 for airfoils 8 % to 12 % thick with low c_m values. Thicker airfoils with higher Reynold's numbers can attain a higher C_{Lmax}.

$$C_{L_{max}} \approx (0.9 \times Airfoil\ thickness) + (0.1\alpha) \tag{3.4}$$

The Reynolds number (R_e) was calculated at the chord and the wingtip using the density and kinematic viscosity (ν) of seawater. A speed of 1m/s is used.

$$R_e = \frac{vL}{\nu} \tag{3.5}$$

Where *v* is calculated using the dynamic viscosity (μ) and the density.

$$\nu = \frac{\mu}{\rho} \tag{3.6}$$

μ = 0.00108Ns/m^2

The taper ratio was determined as per Eq. (2.11). Calculations were performed to find values for *k1* and *k2*.

$$k_1 = \frac{1}{4}\frac{(3 + 2z + z^2)}{(1 + z + z^2)} \tag{3.7}$$

$$k_2 = 1 - k_1 \tag{3.8}$$

The design lift coefficient (C_L*) was estimated and taken as 0.4 for acrobatic aircraft as the hydro-kite will be subject to turning manoeuvres with many angles of attack. The stability proportion (STM) is a function of the cg and np with respect to the average chord length. The STM is approximately 0.1 for a typical wing with vertical stabilisation. A value of 0.15 is assumed for the STM, recommended by Haas, (2014).

$$STM = \frac{(cg - np)}{\left(\frac{(C_{Root} + C_{Tip})}{2}\right)} \tag{3.9}$$

A suitable airfoil was chosen from the Airfoil Tools database (Airfoil Tools, 2016) based on the R_e and $C_{L\,max}$ appropriate to the design requirements of the kite. The c_m values at the root and wingtip were sourced from the polar diagrams using the R_e for the chosen airfoil. The washout (α) required was calculated

$$\alpha = \frac{k_1 \times c_{m_{Root}} + k_2 \times c_{m_{Tip}} - C_L{}^* \times STM}{1.4 \times 10^{-5} \times AR^{1.43} \times PFW} \tag{3.10}$$

A washout of less than 4° results in the wing being unstable and a washout higher than 15° exhibits poor performance at higher speeds. Therefore, if the washout calculated was more than 15° or below 4°, a new airfoil was to be chosen with different moment coefficients in order to produce a better washout value, or the entire kite design process was repeated with different kite dimensions. The amount of twist applied varies along the wingspan of the kite.

3.8.2. Kite Turbine

A potential turbine for use on the 3 m^2 hydro-kite could be similar to the 315 kW 10,000 rpm high-speed brushless PM synchronous motor. The turbine produces a power of 315 kW at a voltage of 380V with a current rating of 506 A. The voltage, power and motor speed could be altered according to design specifications. It is advisable to keep the speed below 15, 000 rpm where the maximum speed possible is 24, 000 rpm. The size of the motor and the output shaft can also be changed to accommodate design requirements. The motor can be AC or DC and can be water cooled (Xinda Green Energy Co., LTD, 2016). The weight of the motor is 180 kg, a turbine weight of 200 kg will be assumed and used in design calculations.

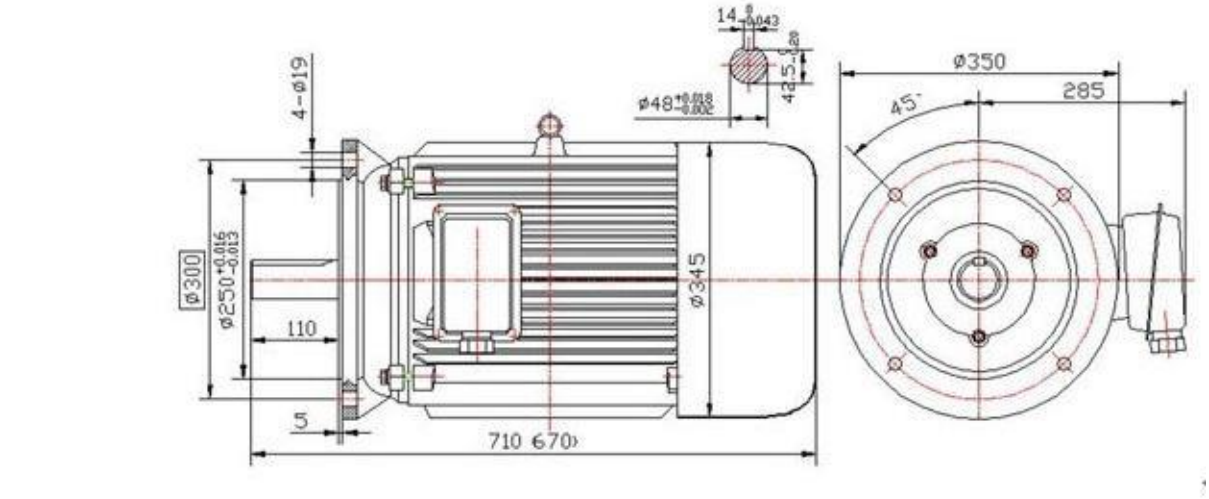

Figure 3.3. 315kW 10000 high-speed brushless PM synchronous motor (Xinda Green Energy Co., LTD, 2016).

3.9. Submarine Power Cables

3.9.1. Cable and Kite Configurations

Various cable and kite configurations were investigated and designed which included scenarios for both concentrated and distributed systems using Medium Voltage (MV) and High Voltage (HV) cables. Each system aims to have a maximum design capacity of 100 MW. The hydro-kite also requires a tether to connect the kite to the seabed and a cable to transmit energy from its point of origin at the turbine to the seafloor. A step-up transformer near the anchor point then increases the voltage from that of a Low Voltage (LV) to an MV to transport energy to shore.

3.9.1.1. Concentrated Array

The concentrated arrays were designed to be made up of larger 6 m^2 kites, the maximum power produced by one kite can be calculated using the cut-out velocity. The number of kites required was then determined based on the maximum design capacity chosen and the maximum potential power of each kite. The kite array is made up of kites connected by a cable line, a few lines are used in the configuration where each line of kites within the arrangement is identical for ease of construction. The number of kites in each cable configuration scenario may not be the same and will differ slightly. The load is calculated as the sum of the maximum capacity of each kite within the line, this value is then rounded up as a measure of safety.

Option 1 is a kite and cable configuration which makes use of a concentrated hydro-kite farm at the prime location with the highest experienced ocean current velocities. MV cables are required to connect the kite array. It incorporates the installation of an offshore substation close to the array which is the endpoint of the MV cables. HV cables are then used to transfer electricity to the shore

from the substation. The effect of using different HV voltages on the cable size and losses was investigated as well as using two runs of HV cable compared to only one.

Option 2 is also a concentrated farm at the prime location. However, it uses MV cables throughout the entire system to transport electricity from the generation point to the shore. Each line of kites will have its own MV cable connected it to the shore.

3.9.1.2. Distributed Array

The distributed arrays use smaller kites of 3 m^2 spread out along the coast within the Agulhas current over regions that experienced relatively high velocities to address the issue of intermittent power as a result of Natal Pulse events. The cables are arranged in segments as one line along the coast would not be feasible due to the voltage drop being exceeded as the generated load is transmitted over long lengths. Smaller lengths of cable must be used to connect hydro-kites within the distributed array with central lines to the shore. Due to areas experiencing different current velocities, designing the power cable to carry the sum of the maximum load of each kite would be an over design as all kites within a line segment will not be operating at full capacity at the same time. The number of kites required cannot be calculated using the maximum power capacity of the kite and applied to all locations.

The distributed kite array had to be designed to avoid Marine Protected Areas (MPAs) along the coastline which were sourced and presented in a shapefile imported into Google Earth. The main MPA that needed to be avoided entirely was the large area of Pondoland near Port Edward. Hydro-kites were therefore unable to be placed at Port Edward, the first line could only start at Port St. Johns. Other MPAs could be avoided using cable lines at angles to the coastline (not perpendicular) or by shifting the line segment and adjusting the hydro-kite spacing.

An initial test with a set number of hydro-kites distributed along the coast was performed, MPAs were avoided and hydro-kites were spaced equally within line segments. The velocity at the locations of these hydro-kite positions was observed using the factored HYCOM data. The total maximum potential power output was observed for each line segment using the sum of the power at each of the locations within the line from the factored HYCOM velocities for each time entry. The total maximum power was determined for each line and was rounded up to the nearest 500 kW as a margin of safety. The total maximum power of that system produced by the initial number of kites incorporated was then used to calculate the number of kites that would be required for a system with a total capacity of 100MW. The spacing of the kites was chosen based on the number of kites required and the available distance along the coast. Again, the locations of the hydro-kites for the new 100 MW system were extracted using HYCOM and their current velocities and maximum potential power output was investigated. Locations further north have shorter distances offshore compared to those located

further south. Each line segment of the distributed array was designed separately with respect to load and distance offshore.

Option 3 is a distributed system which incorporates the use of hydro-kites spaced out along the coastline within the Agulhas current. MV cables will be required to transmit energy from the kites to the shore. Hydro-kite locations in the distributed systems were imported into Google Earth as a kml file.

The voltage drop and losses for Option 3 were calculated at each kite position within the line segment using the load carried from that point and the relevant distance to shore. Due to uncertainty with regard to the combined loading of the kites, the load of one kite was assumed as the maximum capacity for these calculations, therefore results attained may be conservative. The maximum capacity for the entire segment was used for the voltage drop and loss calculation for the central line to the shore. The losses calculated were a sum of all losses between kites within the segment and the loss in the central line.

3.9.1.3. Distributed Concentrated Array

Option 4 attempts to modify the concentrated array system by combining it with the concept of a distributed array. It incorporates three main hydro-kite farms at locations with high electricity generation potential opposed to only one farm, these farms are spread out along the coast at a spacing of approximately 90km. Farm sites were selected observing the best positions within the area segments regarding high current velocities between validated model points. Farm 1 between Port Edward and Cape Morgan, Farm 2 between Cape Morgan and East London – the main concentrated farm from Options 1 and 2, and Farm 3 located between East London and the Fish River. MV cables are to be used to connect the hydro-kites and transport the electricity generated to the shore, similar to that of Option 2 for each farm.

3.9.2. Cable Design

3.9.2.1. Design Calculations

The cable design incorporated the use of a copper conductor with an XLPE insulation which is used in calculations. The frequency, maximum ambient temperature and maximum conductor temperature were provided. The electrical load required was calculated and the cable distance from the source to the endpoint was estimated using Google Earth imagery with an additional 5km assumed for overland transport. The demand factor was assumed to be 1 with a power factor (PF) taken as 0.5 where the value of ϕ was calculated from the PF using Eq. (2.28). The total derating factor was calculated by multiplying the correction factors from ground temperature, thermal resistance or soil cable depth.

The voltage was chosen and the consumed load (P*) in KVA was calculated using Eq. (2.31). The full load current was determined from Eq. (2.33) where a cable size was chosen based on the calculated load current. The total derating current was calculated multiplying the cable current rating and the total derating factor. The total derating current must be higher than the full load current carried through the cable, if this was not satisfied then the cable size was increased. The reactance of the cable was calculated from the inductance value using Eq. (2.22). The number of cable runs was specified. The voltage drop was calculated from Eq. (2.34), if the voltage drop was below 5% then the cable was of an adequate size, otherwise, the cable size must be adjusted to a larger cable to ensure an acceptable voltage drop. The voltage drop is the limiting factor when long lengths of cable are used as in Options 2 to 4, whereas in shorter lengths of cable the current capacity becomes the limiting factor as in the short MV cables of Option 1. The amount of power lost due to the resistance of the cable was calculated from Eq. (2.23) using the copper cable resistance and the current, and converted to a percentage of the total load.

Comparisons were made between the various cable configurations regarding cable length required, cable size specified and the ohmic losses incurred.

3.9.2.2. NEXANS MV Cables

The data for MV power cables used was sourced from one of the major cabling companies, NEXANS. NEXANS medium voltage submarine cable catalogue provides information on submarine MV cables using copper conductors. Cable sizes range from a conductor area of 35 mm^2 to 240 mm^2 with rated voltages from 12 kV to 36 kV. The catalogue provided constructional data of the cable: the cable composition and thickness of the various elements as well as the overall cable weight. Electrical data was supplied providing information on resistance, both DC and AC, the capacitance, inductance and the current rating. This information is crucial to designing a cable fit for purpose (NEXANS, 2013).

Figure 3.4. Submarine power cable elements (NEXANS, 2013).

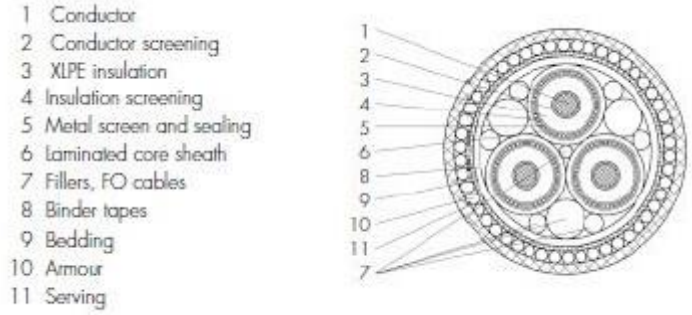

Figure 3.5. Diagram showing the cross-section of the submarine power cable and its composition (NEXANS, 2013).

3.9.2.3. ABB Cables

The electrical data for MV and HV cables was sourced from another prominent company in the cabling industry, ABB. Cable resistances needed to be calculated based on the conductor area and copper resistivity as they were not provided.

The insulation used for all the submarine cables is XLPE where dielectric losses are found to be less than in cables where the insulation material is EPR or fluid filled. The current ratings were determined under the assumptions that the maximum temperature at the seabed is 20°C, the thermal resistivity in the seabed is 1.0 Km/W and that the seabed laying depth is 1 m. Aluminium cables made up of an aluminium conductor and aluminium alloy armouring could be used to replace the copper cables, however, the current rating would be approximately 75 % -80 % of that calculated for a copper

conductor for the same conductor area. ABB can provide larger cables with conductor areas beyond that of 1000 mm^2 on request (ABB, 2013).

3.9.2.4. High Voltage Cables

ABB cables were used in the design of HV cables, they are XLPE insulated and armoured with a lead sheath, they are armoured more intensely compared to the MV cables. The ABB cable catalogue provided constructional data as well as some electrical data on the HV submarine cables, however, the resistance of each cable was not specified and was therefore, calculated. Firstly, the DC resistance at 20°C for the cable size was calculated using Eq. (2.15), which was then used to determine the DC resistance at 90°C from Eq. (2.16). The skin effect factor and proximity effect factors were determined using Eq. (2.17) and Eq. (2.18) respectively. The AC resistance at 90°C was then calculated for the cable sizes using the conductor area from Eq. (2.17). The cable design was performed through the same process as described for the MV cables.

3.9.2.5. Larger size MV cables

MV cables were required that exceeded sizes of 240 mm^2, which is the largest size available from the NEXANS catalogue. Similar cables were available from the ABB catalogue which included larger size cables with conductor areas of up to 1000 mm^2 at the same voltage of 36 kV. An approximation of the properties for the NEXANS cables using larger conductor sizes is gauged using information provided on the ABB cables. The properties of the ABB cables were adjusted to resemble that of the NEXANS cables which can be found in Appendix E.6. Properties differ between the cables from different companies due to their composition and different amounts of armouring.

A scatter plot of ABB current was plotted against NEXANS current carrying capacity for the smaller cable sizes that could be compared. Scatter plots were generated for inductance, conductor diameter and the diameter over the insulation. Relationships were determined for all properties described. The relationships and equations generated using trendlines were used to determine the equivalent NEXANS cable property values for the larger cable sizes.

The AC resistance was calculated for the ABB cables using the same procedure outlined for the HV Cables. A scatter plot of AC resistance was generated from NEXANS and ABB where ABB resistances were adjusted to determine equivalent resistances for larger NEXANS cables. Cables were designed using these assumptions.

3.9.2.6. Low Voltage Cables

The hydro-kite requires a tether cable to connect the on-board turbine to the step up transformer located on the seabed. Energy is transmitted from the source where it is generated at a low voltage through the tether cable to the step-up transformer increases the voltage to transport energy to shore

at low current with minimal losses. The cable tether connects the hydro-kite to the seabed so that the kite can fly at a depth of 20 m below the water surface in the ocean current. The tether length is assumed from the seabed depth and kite spacing as well as assumption on the effect of the current which will influence the tether. The tether cable must be designed to carry the maximum potential load that the kite could generate.

Data for marine LV cables was sourced from Prysmian and used in calculations; the data provided was limited with the lowest voltage of 1 kV which was used. Resistance had to be calculated as before. The tether cable was designed using both the unarmoured and armoured cables. The requirement for the tether cable is that it needs to be supported by the kite. The self-weight of the kite and its components, the turbine and the tether weight must be less than the displaced weight of the kite for it to be supported. Further calculations were performed to find the new kite dimensions or minimum voltage for smaller cables to be used fulfilling the weight requirement. The possibility of using two smaller cables instead of one large cable was also investigated.

CHAPTER 4

4. RESULTS and DISCUSSION

This chapter presents the results and their analysis. It includes a study of available ADCP data, validity of the HYCOM model and appropriate scaling factors. Potential power is investigated using both concentrated and distributed kite array systems using three model datasets. Submarine cables are designed for various kite arrangements and examined regarding length, size and potential losses.

4.1. Analysis of Eskom ADCP Data

Eskom distributed 51 Acoustic Doppler Current Profilers (ADCP) along the East Coast of South Africa in the Agulhas current within approximately 400 km over a combined period between 2005 and 2010. The positions of these ADCPs are shown in Figure 4.1. ADCPs centred around four main areas: Port Edward, Cape Morgan, East London and the Fish River (near Port Alfred), the majority of these being near the areas of Cape Morgan and East London which were suspected to produce higher current velocities compared with other locations. To avoid confusion, location labels from Meyer et al. (2014) have been adopted.

Due to there only being five years of data combined from all ADCP locations it is difficult to perform a detailed comparison and analysis between positions as data is limited and not always available for the same time periods. Some areas, namely Location 1 at Cape Morgan and Location 2 at East London have data for almost the entire duration. Location 3 at Port Edward has data for less than a year at the start of the project while data from the Fish River, Location 4, was only collected during the last few years. Another hindrance is that data availability is inconsistent, at times data is absent for certain ADCP locations.

Bins closer to the sea surface are more unreliable as more information is lost. As the primary area of study is within the shallower depth regions this is a significant issue at certain ADCPs where the percentage of good data is not consistent. ADCP measurements are supplied in bin depth intervals of 2 m. Bin depths are also not consistent for all ADCPs and can vary. The closest depths to 20 m with the higher percentages of “good” data were obtained and investigated. In the event of higher percentages of data lost for depths around 20 m, data was extracted for slightly deeper depths which had better quality readings. A list of ADCPs, their data extraction depths and corresponding percentage of lost data can be found in Appendix C.1. Due to velocities near the surface being higher in magnitude than those at lower depths, extracting data from deeper depths would be a conservative approach and would not lead to unrealistic results. Although data is inconsistent and in some instances, reliability is compromised, it can still provide a good indication of ocean current conditions.

The velocity experienced at all locations fluctuates greatly even without the presence of Natal Pulses or meanders. The direction of the current is more constant with the exception of meanders and pulse events where sudden direction changes occur.

As the data is not consistent, seasonal bias will be present due to an uneven time series where it is difficult to compare locations. All dates are given as month/day/year. All durations of Natal Pulses mentioned are approximate values where a clear indication of lower velocities and direction reversals was observed.

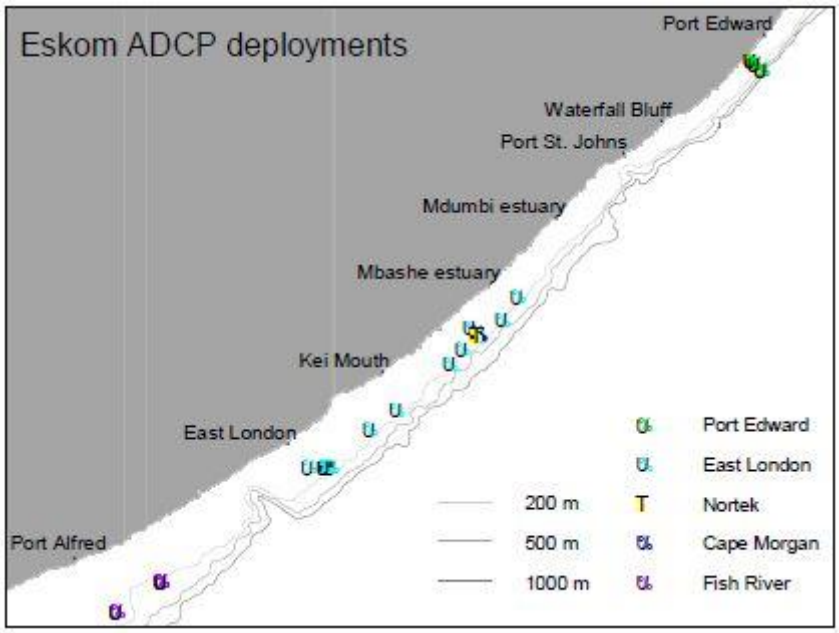

Figure 4.1. Map showing locations of ADCP deployments along the southern part of South Africa's coast between September 2005 and September 2010 from Eskom data.

4.1.1. Port Edward:

The ADCPs deployed at Port Edward (Location 3) were distributed in three places. The first site was 3km offshore with ADCPs within 20 m of each other at a mooring depth of 32 m, the second 6 km offshore at a moored depth of 60 m and the last one 10 km offshore at a fixed depth of 156 m, ADCPs at the most offshore areas were spaced within 65 m of each other. The relative positions of the three deployments are seen in Figure 4.2. The two most inshore groups of ADCPs collected data for one year from September 2005 to September 2006. The most offshore group retrieved data from the same starting time until April of 2006. Positions further offshore yielded much higher velocities than areas closer to the coastline for the same period, implying that the core of the Agulhas is located more offshore in this region. The average velocity at the most inshore point is almost half that of the nearest further offshore position, with the most offshore position yielding an average of approximately 25 % more than its closest point. The average velocities and maximum values can be seen from the table

below as well as Figure 4.3 where the probability of non-exceedance curve is plotted for each position, demonstrating the higher probabilities of larger velocities more offshore.

Table 4.1. Velocity statistics for various ADCPs around Port Edward

ADCP Position	Start Date	End Date	Average Depth (m)	V_{avg} (m/s)	V_{max} (m/s)	V_{med} (m/s)	V_{mod} (m/s)	σ (m/s)	No. NP
PE601,602	8/9/2005	10/4/2006	20.5	0.53	1.39	0.55	0.73	0.26	1
PE601,602,603	8/9/2005	9/9/2006	20.67	0.51	1.39	0.52	0.55	0.24	2
PE301,302	8/9/2005	10/4/2006	19.74	0.98	2.01	1.05	1.29	0.44	1
PE301,302, M03	8/9/2005	9/9/2006	19.83	0.93	2.01	0.96	0.91	0.41	2
PE751,752	8/9/2005	10/4/2006	23	1.27	2.47	1.40	1.63	0.57	1

The highlighted cells show data for the same period. V_{avg} is the mean velocity; v_{max} is the maximum velocity; v_{med} and v_{mod} are the median and the mode of the velocities respectively.

Figure 4.2. Google Earth image showing the relative positions of the ADCPs placed near Port Edward.

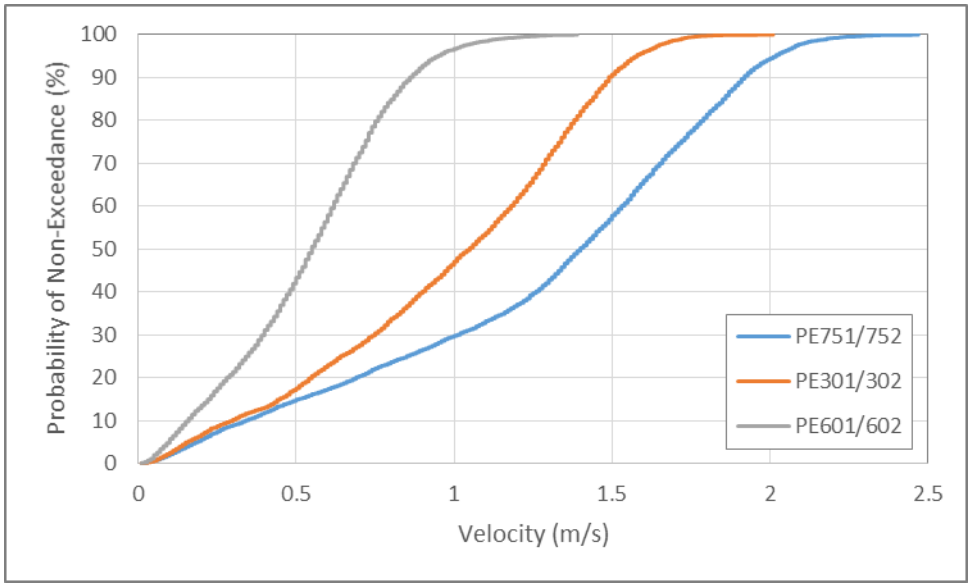

Figure 4.3. The probability of non-exceedance for velocities measured at various ADCPs near Port Edward, observing the difference between points further offshore using ADCPs at each location from 8/9/2005 to 10/4/2006 with hourly velocity recordings.

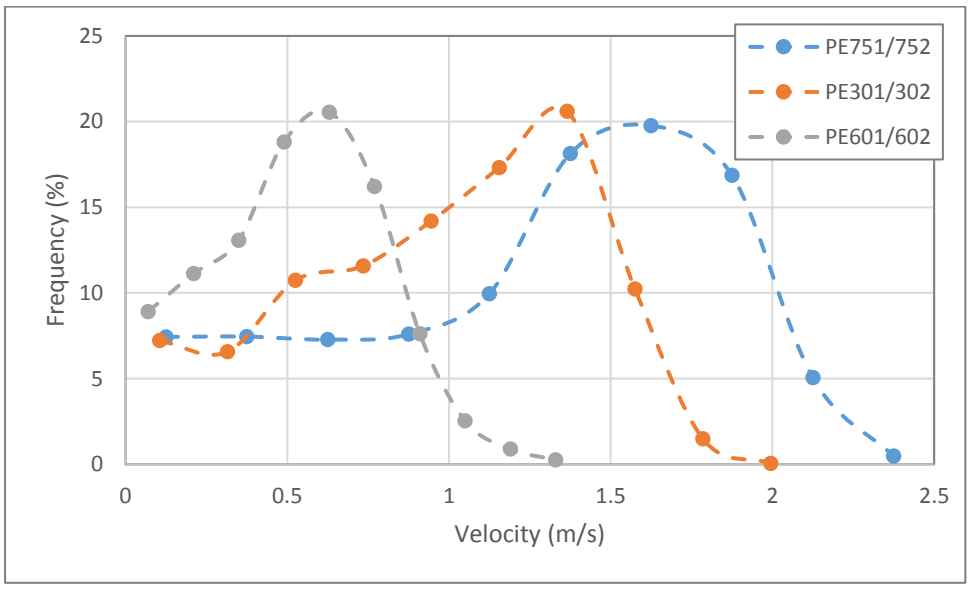

Figure 4.4. Frequency distribution of the velocity recordings from ADCP locations near Port Edward at various positions offshore using ADCPs from 8/9/2005 to 10/4/2006. Dashed lines are used to join data points.

The frequency distribution of the velocity magnitudes at the various locations around Port Edward can be seen in Figure 4.4. The most common speeds for the most offshore site accounting for 57 % are relatively high between 1.2 m/s and 2.0 m/s. At the location 6 km offshore speeds are predominantly between 0.8 m/s and 1.4 m/s, comprising approximately half the distribution. The ADCPs nearest the shore show a higher frequency of slower speeds between 0.2 m/s and 0.8 m/s making up 75 %. The ocean current rose for the most offshore ADCP site can be seen in Figure 4.9.

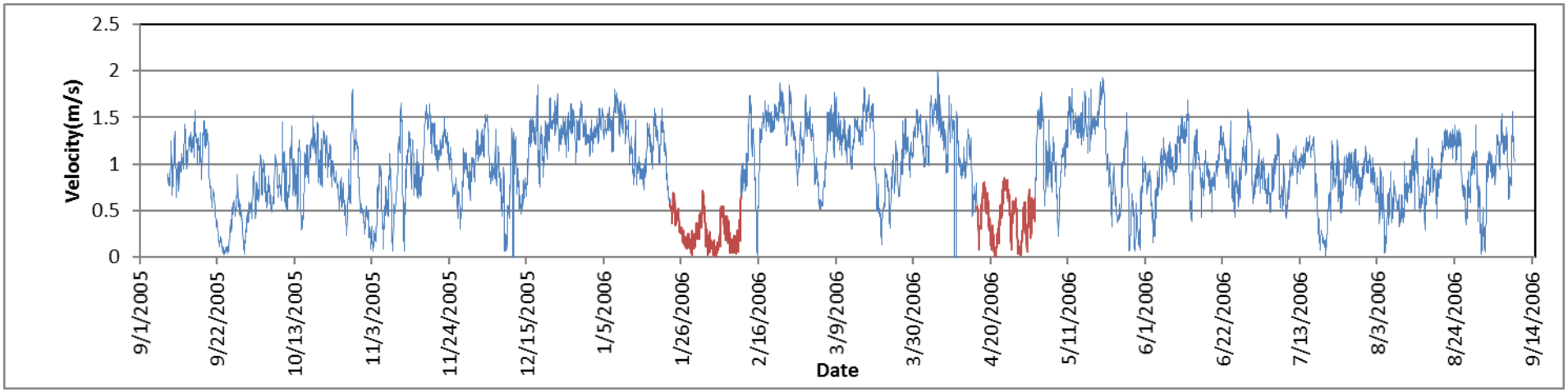

Figure 4.5. The magnitude of the velocity at the 6km offshore ADCPs near Port Edward. Natal Pulse events are highlighted.

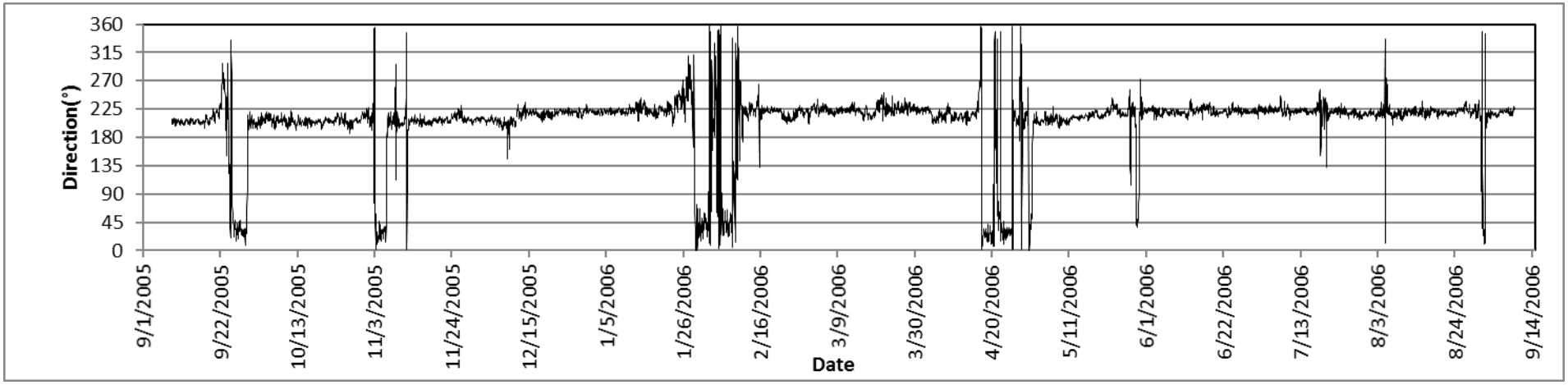

Figure 4.6. The direction of the velocities for the 6km offshore ADCPs near Port Edward. Natal pulse events are seen by the longer duration fluctuations in the current direction which correspond to the low velocities seen in Figure 4.5. Meanders are observed by the shorter duration direction changes.

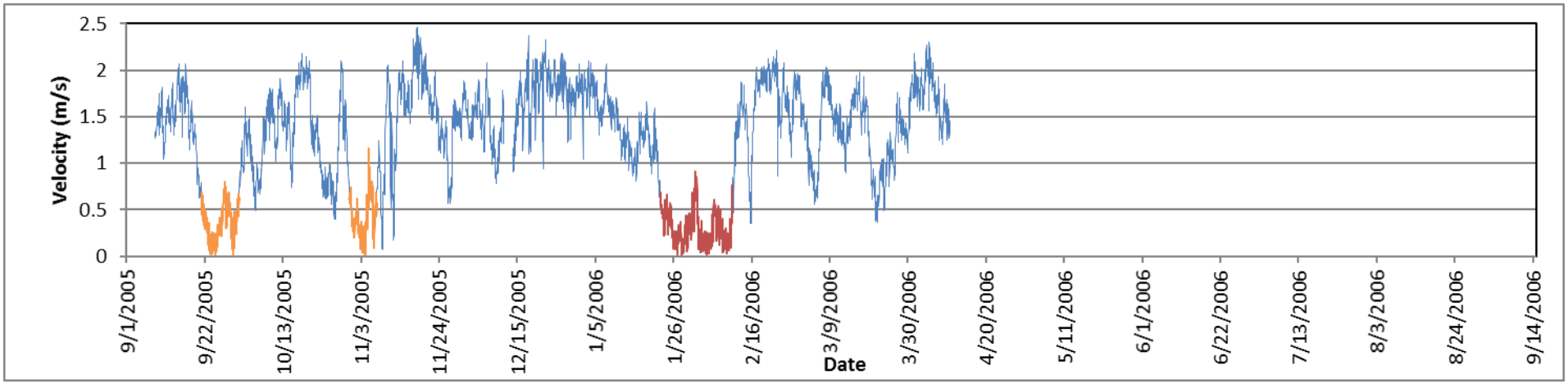

Figure 4.7. The magnitude of the velocity at the most offshore ADCPs near Port Edward. Natal Pulse events are highlighted – red is a Natal Pulse event, orange describes shorter duration meanders. Higher magnitudes for this location are observed when compared to those in Figure 4.5.

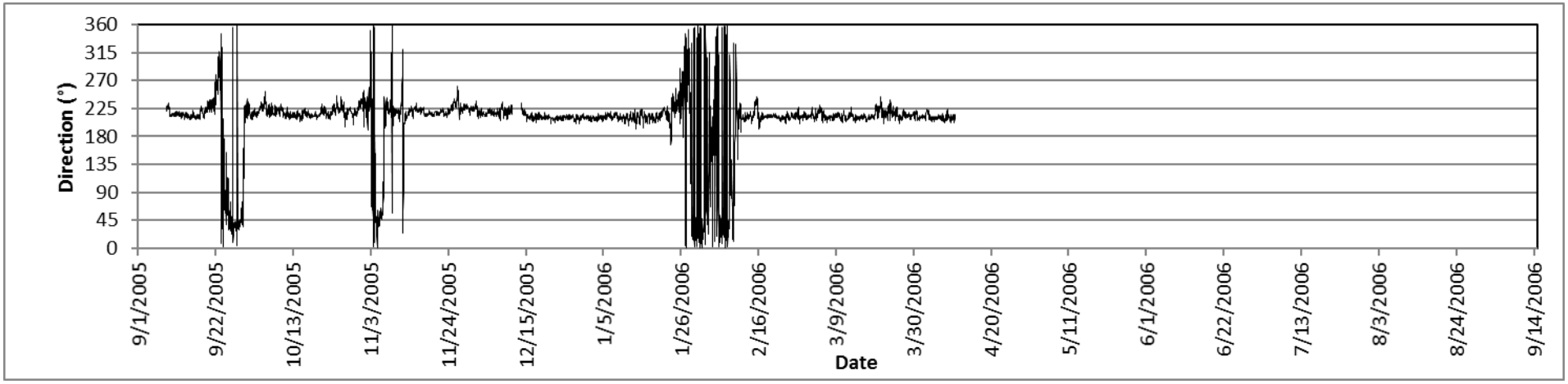

Figure 4.8. The direction of the velocity for the most offshore ADCPs near Port Edward. Natal pulse events can be seen by the fluctuations in the current direction which correspond to the low velocities seen in Figure 4.7.

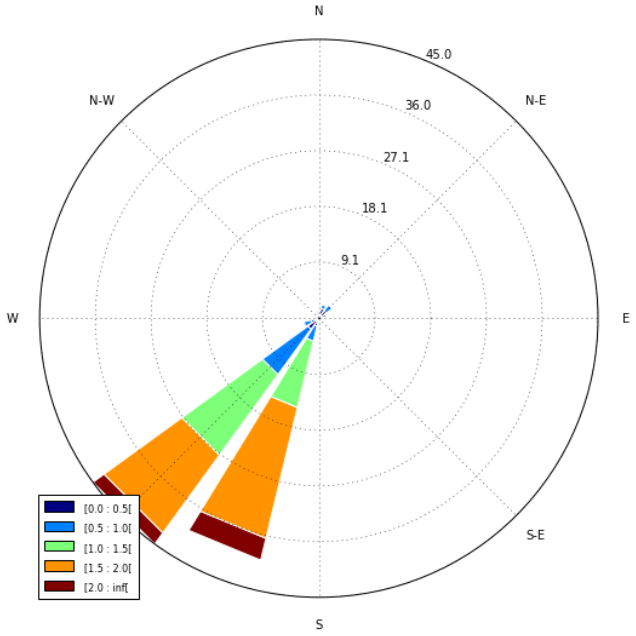

Figure 4.9. Ocean current rose depicting range and frequency of velocity magnitudes and directions at Port Edward between 8 September 2005 and 6 April 2006.

During the one-year period when data was collected, 2 Natal Pulses were experienced: the first occurring near the end of January 2006 which persisted in the region for 19 days and the second near the middle of April 2006 which lasted for approximately 16 days which can be seen in red in Figure 4.5. Natal Pulses are experienced at the same time at all locations. Other meanders were also observed within the period. For the two more inshore locations, especially that nearest to the shore, the meander is not well detected as the velocities are relatively small and fluctuating. The meanders can be seen more clearly at the most offshore site where there is a steep drop in the velocity persisting for approximately 7 to 10 days in the system, two distinct meanders such as this are noted at the most offshore location during 2005. Current direction is mostly constant between Natal Pulse and meander events.

It is recommended that if offshore kites are deployed near Port Edward that they are placed further offshore to make use of the higher currents experienced at this position, but the shelf depth is deeper than 100 m and installation may prove more challenging and costly. As there is only data collected for one year at this location it is hard to conduct a comparison between this area and the others as many of those have data that only commences after 2006 at which time data from Port Edward is no longer available. More data is required to confirm the velocities already observed to obtain an accurate view of conditions.

4.1.2. Cape Morgan:

The ADCPs placed near Cape Morgan (Location 1) were all positioned near the same area, approximately 15 km from the shore. They were divided into two time periods as some of the data

was missing or not reliable and different types of ADCPs were used. The first period ran from December 2005 to May 2008 with Nortek ADCPs located within 110 m from each other except for the first ADCP deployed, EL1901, located just less than 400 m away from the group. The second time period started from July 2009 until September 2010 where ADCPs were within a distance of 200 m from each other except for one ADCP, CM302, which was placed approximately 1.2 km on the inshore side of the others. This ADCP yielded much lower velocities, taking the presence of a Natal Pulse into consideration, other ADCPs still yielded much higher results under similar circumstances. The depth at which the ADCPs were placed was between 80 m and 90 m. The two data sets correlated well and similar frequency distributions were observed as seen in Figure 4.10. Statistics were calculated using the outlying ADCPs and without. This location produced the highest current velocities.

There were other ADCPs with similar time series to RDI ADCPs CM301 and CM302 which were Nortek ADCPs (EL901 and EL1910), but the majority of the data was missing. Therefore, comparisons could not be conducted between the different ADCPs.

Table 4.2. Velocity statistics for ADCPs at Cape Morgan.

ADCP Position	Start Date	End Date	Average Depth (m)	V_{avg} (m/s)	V_{max} (m/s)	V_{med} (m/s)	V_{mod} (m/s)	σ (m/s)	No. NP
EL201 - EL801	2006/04/11	2008/05/04	19.96	1.48	2.70	1.59	1.69	0.53	2
CM303 - CM306	2009/03/23	2010/09/13	20.50	1.46	2.82	1.59	1.76	0.59	4
EL1901-EL801	2005/12/14	2008/05/04	20.07	1.50	2.70	1.61	1.82	0.53	3
CM301 - CM306	2008/07/12	2010/09/13	20.67	1.38	2.82	1.54	1.76	0.62	7
EL1901 - CM306	2005/12/14	2010/09/13	20.33	1.44	2.82	1.58	1.76	0.58	10

For the first period 3 natal pulses were observed: the first starting in February 2006 persisting for 13 days, this Natal Pulse is not as well defined as seen when it passes Port Edward. Low velocities are experienced for a shorter duration and the direction change appears more like meander where it does not persist for long. The second Natal Pulse appears near the end of April 2006 where it is well defined similar to that at Port Edward with low velocities and a constant direction change throughout. The last Natal Pulse started from the beginning of June 2007 which was also well defined. The second and third Natal Pulses had durations of approximately 15 and 16 days respectively. The pulse evident in June 2007 shows a velocity drop with a change in direction, but within the period where the direction

change occurs the direction stabilises at around 45° and coincides with an increase in velocity which then decreases as the direction changes again. This can be seen in Figure 4.13 and Figure 4.14.

Many one day meanders were also experienced in February and March of 2007, and near the end of the period in March 2008 two meanders are seen in close consecution having a similar effect as that of a natal pulse. During the second time period 7 natal pulses were observed. The first 2 occurred during the latter half of July 2008 and the beginning of January 2009 lasting 18 and 20 days respectively where both were well defined. An unusual event occurs near the end of February 2009 where the velocity decreases gradually, coupled with a slight increase in the direction and then a sudden change like that of a meander. This event resembles that of a Natal Pulse further south near East London. During November 2009 a direction change is experienced unlike that of a Natal Pulse or a meander, where the average constant direction changes by approximately 50°, a drop in velocity is experienced at this point which lasts roughly 30 days. This Natal Pulse event can be seen more clearly at other locations further south. The other 3 distinct Natal Pulses all occurred within the year of 2010: at the end of March, end of May and the start of August. The first 2 pulses lasted 18 and 16 days respectively, whereas the last one persisted for 24 days. This can be seen in Figure 4.15 and Figure 4.16.

After the Natal Pulse event experienced in March 2009, the average direction drops by less than 20°, then near the end of 2009 there is the distinct direction shift of about 50° mentioned previously which remains throughout 2010. It is seen that there is a significant amount of fluctuation present within the velocity during 2009. In 2010, the current appears slightly more stable with high velocities but with the impact of more Natal Pulses it yields a lower average.

The frequency distribution graph seen in Figure 4.10 shows how the velocities can fluctuate over different time periods at the same location. Similar profiles are seen for EL201 to EL801 and CM303 to CM306. The addition of EL1901 adds more average velocities between 1.5 m/s and 2 m/s, whereas the inclusion of CM301 and CM302 causes a shift in the distribution graph to more low values which could be attributed to the presence of more Natal Pulse events. There are generally lower velocities for this period, also taking into consideration the distance of CM302 from the central ADCP location.

The majority of speeds for ADCPs EL201 to EL801 occur between 1.4 m/s and 2.0 m/s making up just over 50%. The distribution of speeds for the second period using ADCPs CM303 to CM306 is similar, with 48% of velocities occurring between 1.4m/s and 2.0m/s. Ocean current roses for Cape Morgan can be seen in Figure 4.11 and Figure 4.12 for the various time periods.

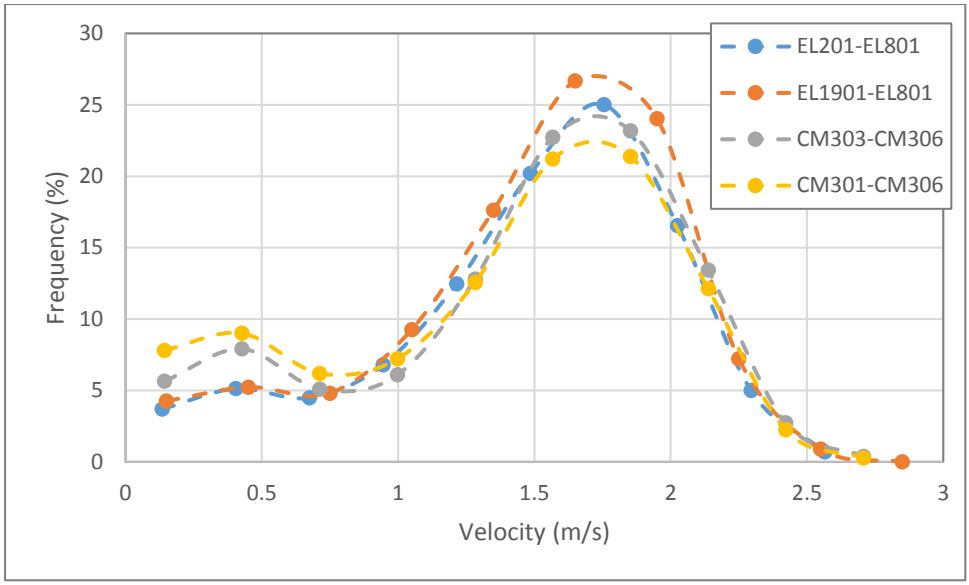

Figure 4.10. Frequency distribution of different ADCP groups using velocities recorded every half hour. Dashed lines are used to join data points.

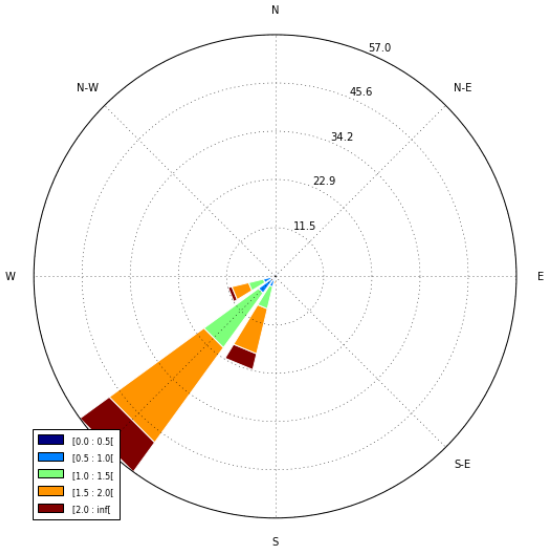

Figure 4.11. Ocean current rose for velocity magnitudes and directions at Cape Morgan between 11 April 2006 and 12 July 2008.

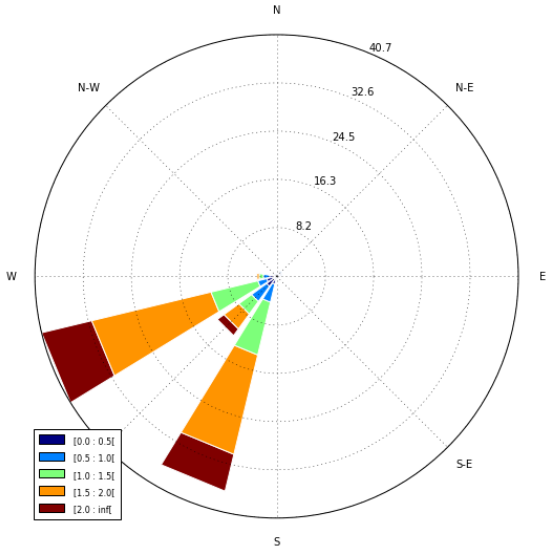

Figure 4.12. Ocean current rose showing velocity magnitudes and directions at Cape Morgan between 23 March 2009 and 13 September 2010.

If only one plant is commissioned opposed to a distributed array of kites, it should be located near Cape Morgan to take advantage of the higher velocities.

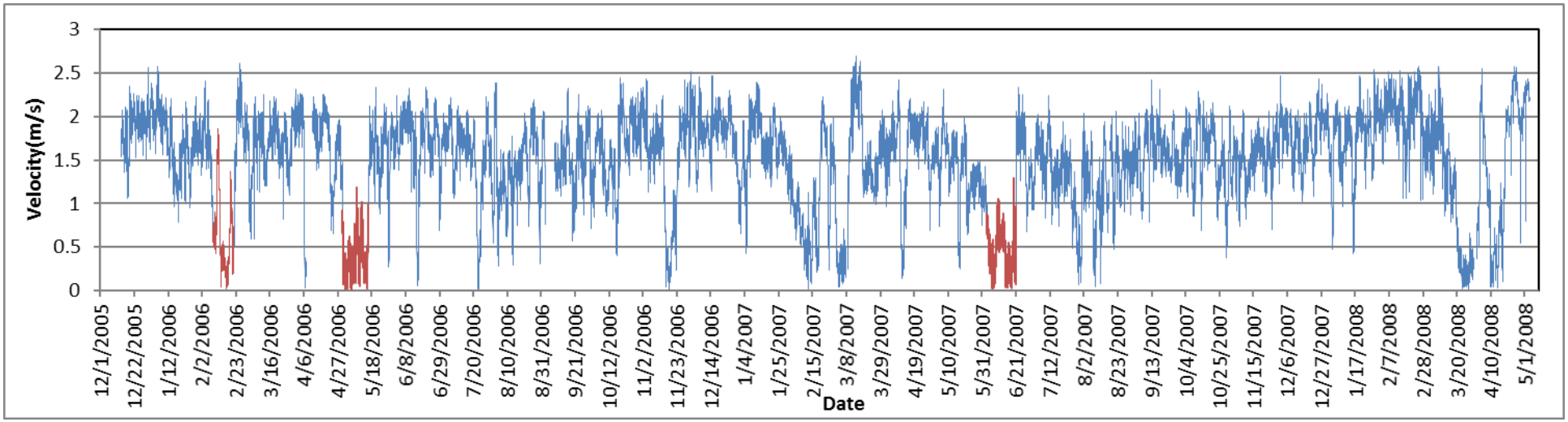

Figure 4.13. The magnitude of the velocity at Cape Morgan. Natal Pulse events are highlighted.

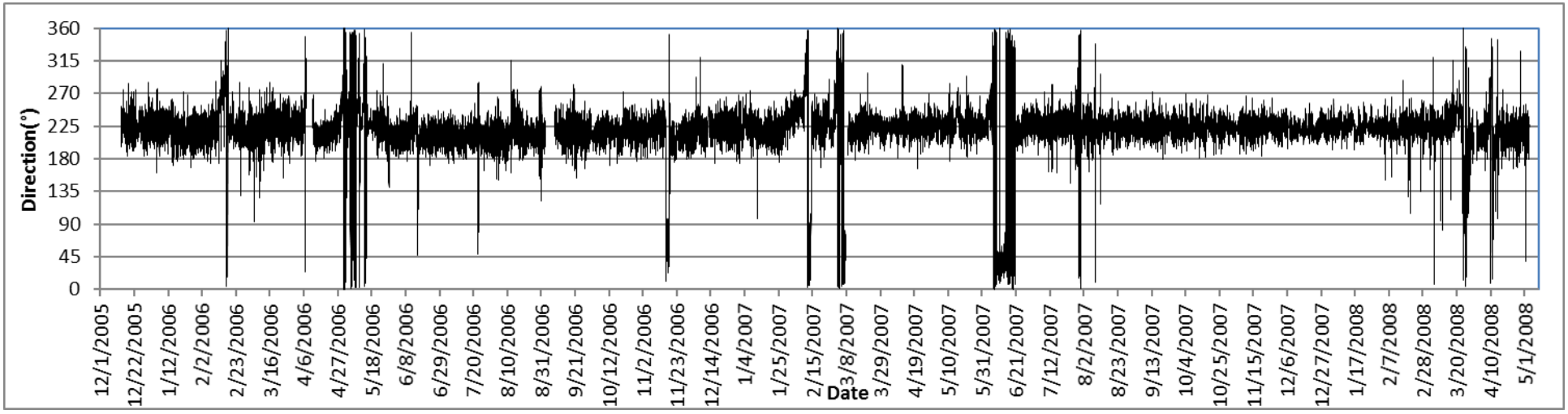

Figure 4.14. Directions which correspond to velocities in Figure 4.13. Natal Pulse events and meanders are seen by sudden direction changes.

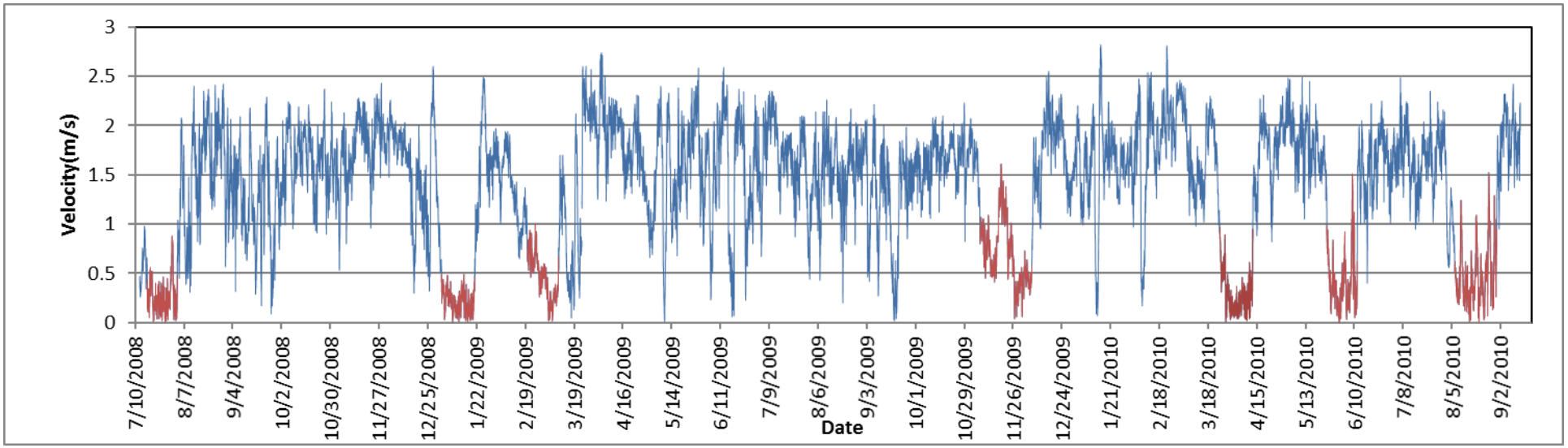

Figure 4.15. The magnitude of the velocity at Cape Morgan for the second period. Natal Pulse events are highlighted.

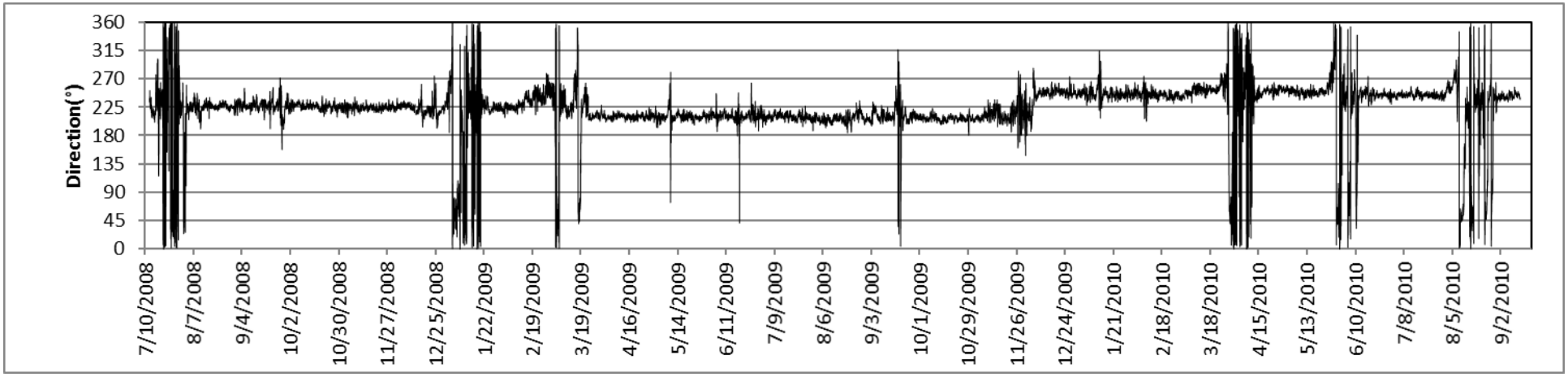

Figure 4.16. Directions that correspond to Figure 4.15 velocity magnitudes. Natal Pulse events and meanders are seen as sudden direction changes. The changes of average almost constant direction is seen where it drops during March 2009 and then after the event in November 2009 increases and continues at this average direction throughout 2010 with the exception of the Natal Pulse direction changes.

4.1.3. East London:

The ADCPs near East London were placed around the same area approximately 20 km offshore. They were split into two sets as the two groups of ADCPs were located around 1.5 km away from each other. The first set collected data from August 2007 to March 2009 where ADCPs were spaced within 300 m of each other. The other set collected data from March 2009 to September 2010. ADCPs were placed at between 80 m and 90 m depths. Velocities for the first set were noticeably higher than those for the second set. Velocities are still relatively high, making East London the location with the second highest velocities.

The inclusion of EL306, located approximately 1.7 km offshore from the first set of ADCPs at a depth of approximately 100 m does not affect the average velocity experienced even with the presence of a Natal Pulse. Likewise, with the inclusion of EL314 positioned a much further 7.5km inshore of the second group of ADCPs, it has virtually no effect on the averages calculated. The first data set has more occurrences of higher velocities than the second data set which experiences a high frequency of low velocities (below 1 m/s). This is seen in the frequency distribution graph in Figure 4.17 and could be accredited to the fact that there were more Natal Pulses present in the second data series.

Table 4.3. Velocity statistics for ADCPs at East London.

ADCP Position	Start Date	End Date	Average Depth (m)	V_{avg} (m/s)	V_{max} (m/s)	V_{med} (m/s)	V_{mod} (m/s)	σ (m/s)	No. NP
EL306 - 311	2007/03/08	2009/03/22	21.00	1.40	2.78	1.53	1.69	0.61	4
EL307 - 311	2007/08/18	2009/03/22	21.20	1.40	2.83	1.54	1.67	0.61	3
EL312 - 315	2009/03/22	2010/09/13	20.64	1.18	2.71	1.25	1.40	0.58	4
EL306 - EL315	2007/03/08	2010/09/13	20.86	1.31	2.78	1.43	1.61	0.61	8

During the first time period, 4 Natal pulses were observed within the area. The first occurs during June 2007 persisting for approximately 22 days and appearing as a meander combined with a Natal Pulse. It is not as defined as at Cape Morgan, but the same velocity profile is evident where within the Natal Pulse the direction attempts to stabilise and there is a subsequent increase in velocity, which is higher than that seen at Cape Morgan. The second pulse observed occurred near the end of July 2008 persists for about 17 days, the velocity appears to drop gradually before the pulse occurs which could be attributed to meander-like direction fluctuations. The other Natal Pulses occurred in 2009, one in January which was well-defined as at Cape Morgan and lasted around 20 days, the other in March, not as defined which appears more like a meander which lasted for roughly 17 days. Around this time at Cape Morgan the velocity experiences a gradual decrease where the lower velocities coincide with

a meander-like direction change. Data from the Fish River is missing for this period, therefore, conditions at that location are unknown and cannot be compared. These events can be seen in Figure 4.20 and Figure 4.21.

Fluctuating velocities are experienced throughout, during March and April of 2008, two meanders occurring close together create an occurrence of low velocities for approximately 3 weeks. This is also detected at Cape Morgan.

Observing the second time period, as in Cape Morgan in November 2009, an event occurred with low velocities and changing direction. At this location it appears more like a Natal Pulse, much more defined than that experienced at Cape Morgan, lasting for 21 days. The other 3 Natal Pulses seen at Cape Morgan in 2010 were also evident in East London as they migrated down the coast, occurring in April, June and August lasting 20 days, 12 days and 20 days respectively.

It can be seen for the two time series that contain the same number of Natal Pulses that velocities can differ at the same location. Generally, higher velocities are seen for the first period, possibly because Natal Pulses and meanders occur further apart so the current is allowed to stabilise more, unlike during the second period. During the second period velocities appear to fluctuate more and to lower values, this cannot be due to the inclusion of the ADCP located further inshore as the average velocity experienced there was higher than the others for this time period.

During the first period, there was a larger percentage of velocity magnitudes between 1.4 m/s and 2.0 m/s accounting for 43% of the data. Observing the second time period where the frequency distribution graph is shifted left with a more even distribution of lower speeds: 47% of readings are between 1.0 m/s and 1.8 m/s. Ocean current roses for the different time periods can be seen in Figure 4.18 and Figure 4.19.

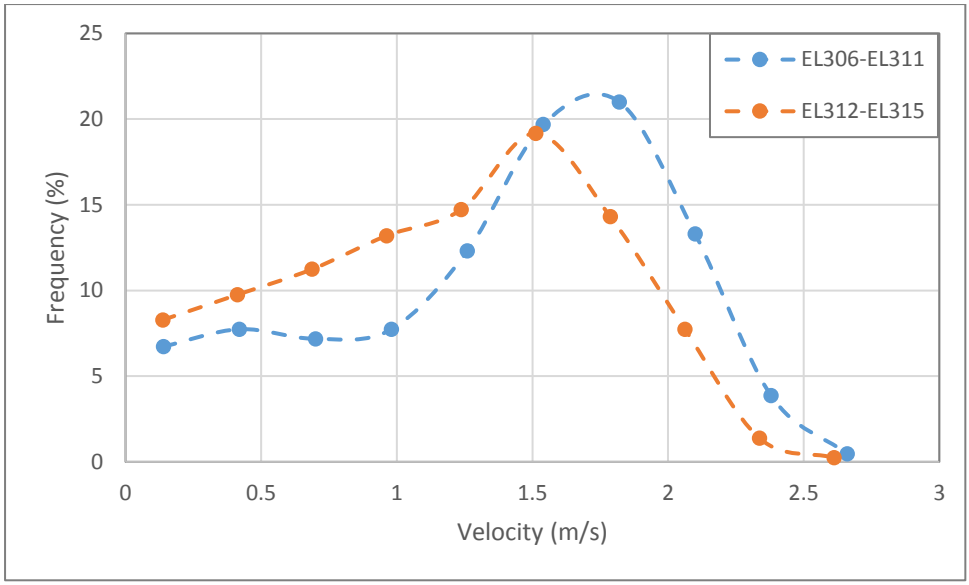

Figure 4.17. Frequency distribution of the two time series at East London. All data used is recorded hourly due to EL306 having hourly data entries. Dashed lines are used to join data points.

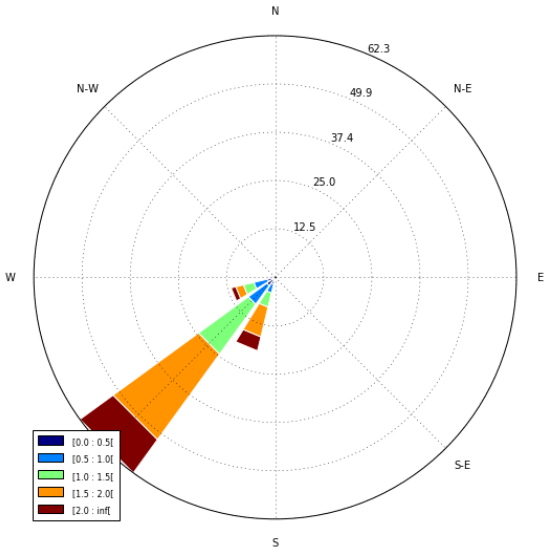

Figure 4.18. Ocean current rose depicting current speeds and directions for East London between 18 September 2007 and 22 March 2009.

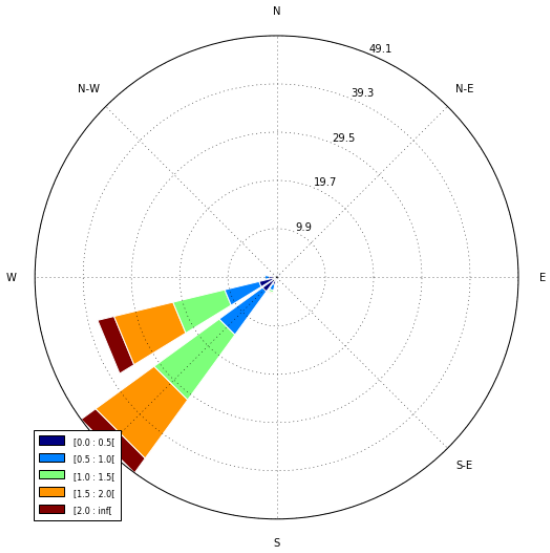

Figure 4.19. Ocean current rose showing the magnitude and direction of the current at East London between 23 March 2009 and 13 September 2010.

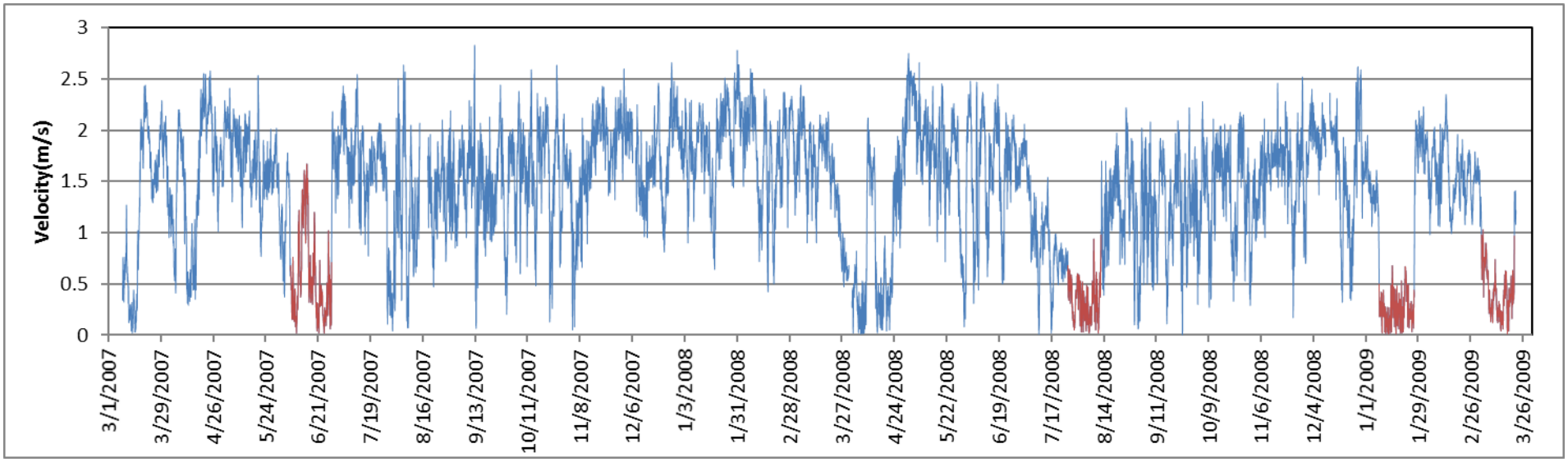

Figure 4.20. The magnitude of velocities observed at East London during the first period; Natal Pulse events are shown in red.

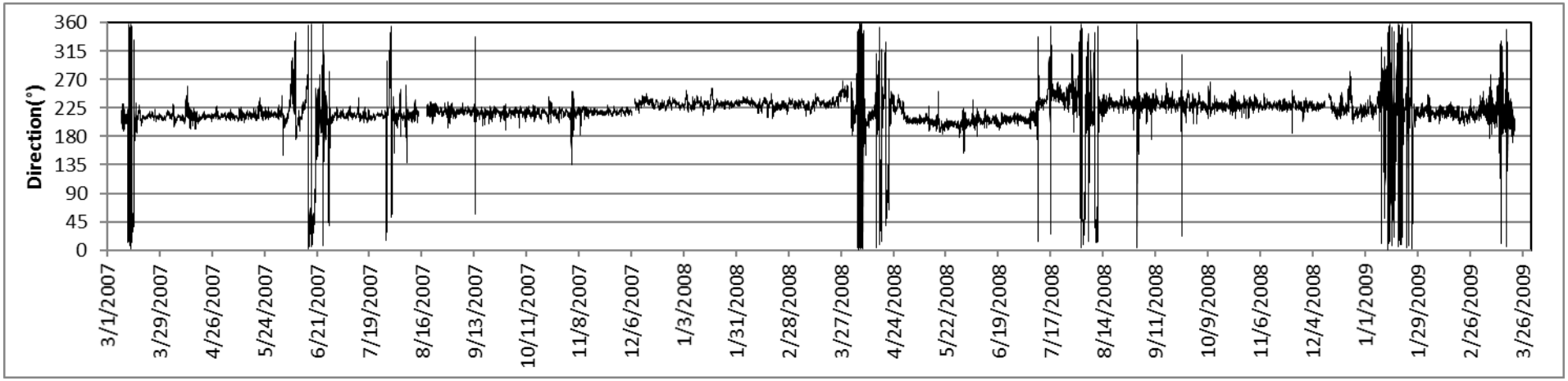

Figure 4.21. Directions corresponding to the current velocity magnitudes in Figure 4.20.

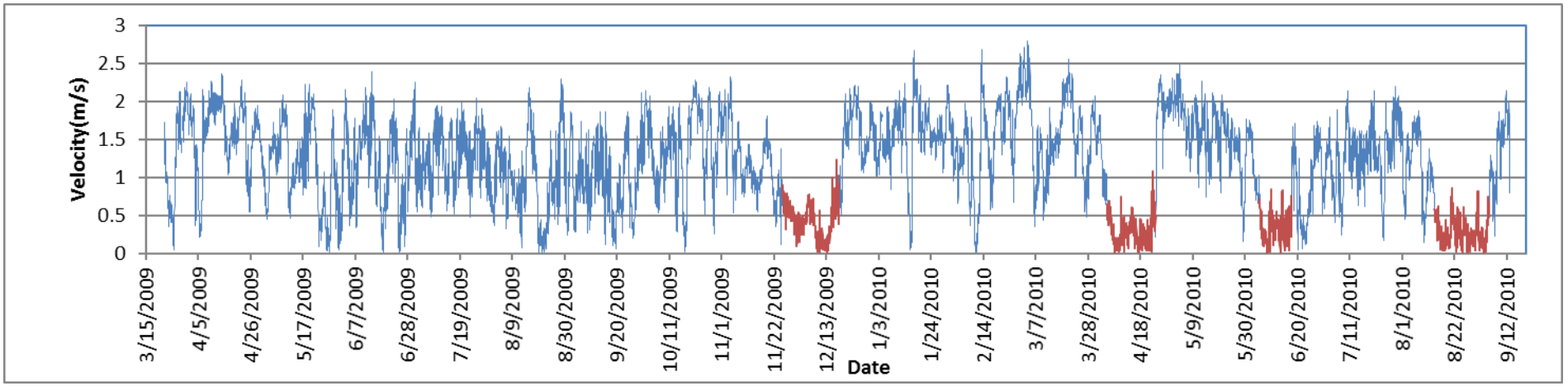

Figure 4.22. Velocity magnitude for the second period at East London; velocities appear lower than the first period seen in Figure 4.20; Natal Pulse events are identified in red.

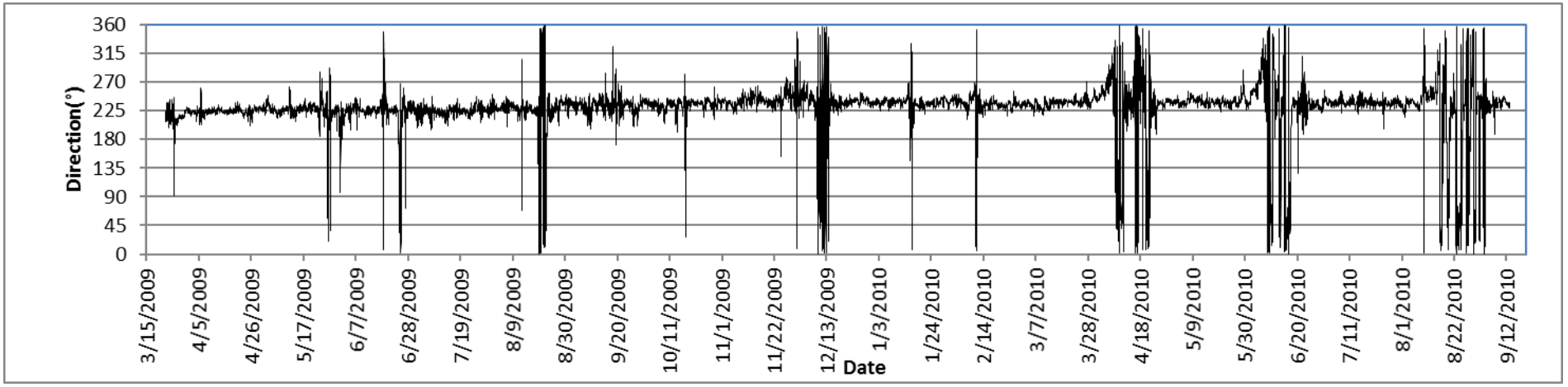

Figure 4.23. Directions relating to Figure 4.22 velocity magnitudes; distinct direction changes can be seen with the occurrence of a Natal Pulse; meander events can also be seen. Unlike at Cape Morgan there is little change in the average direction throughout the time series.

.

4.1.4. Fish River:

ADCPs near the Fish River were found around 25 km offshore within 150 m from each other between April 2008 to February 2009; and from March 2009 until September 2010; however, one ADCP is located further south from the group of ADCPs at a distance of about 1.2 km. ADCPs are placed at depths between 90 m and 100 m. Both data sets were relatively consistent with each other for the different time periods. The lowest average velocity is experienced at this location, yet could still prove high enough to become part of a distributed kite array system.

ADCPs were also deployed further south, 30km offshore at a depth of around 90 m, and at distance of just over 25 km from the main group of ADCPs. These yielded the highest current velocities within the area. This may be due to its position further south, or because no Natal Pulses were experienced during this short time from August 2007 until March 2008.

Table 4.4. Velocity statistics for ADCPs at the Fish River.

ADCP Position	Start Date	End Date	Average Depth (m)	V_{avg}	V_{max}	V_{med}	V_{mod}	Σ	# NP
FR301 - 752	2007/08/18	2008/03/29	20.5	1.29	2.69	1.32	1.52	0.50	0
FR303 - 305	2008/04/01	2009/02/04	20	0.99	2.64	0.98	1.21	0.53	2
FR306 - 308	2009/03/22	2010/03/04	21.53	0.96	2.73	0.93	1.65	0.54	1
FR303 - FR308	2008/04/01	2010/03/04	20.765	0.98	2.73	0.94	1.65	0.54	3
FR303 - FR309	2008/04/01	2010/09/03	20.7914	0.96	2.73	0.92	1.65	0.55	6

Two Natal Pulses are observed during the first time period near the main Fish River site, one during 2008 in August lasting 23 days where velocity drops to low values but the direction change appears as a series of meanders instead of a constant direction change during the event. The other Natal Pulse occurred near the last half of January 2009 lasting a shorter duration of only 10 days where the change in direction also appears more like a meander. There is evidence of the same 2 meanders that were seen at Cape Morgan and East London that created low velocities, in this area and appear to last for 16 days near the beginning of the time series. During the second period only one natal pulse is observed in December 2009 which is more defined at this location than at East London or Cape Morgan but lasts only 15 days. The last ADCP that collected data during 2010 saw the same occurrence of the 3 pulses as observed at Cape Morgan and East London. The first 2 Natal Pulses lasted 19 and 24 days respectively with an uncertainty of the last pulse as the data ends. The pulse seen in June may be coupled with a meander as low velocities persist for a while where meander like direction changes are also seen. These observations can be seen in Figure 4.27 and Figure 4.28.

The frequency distribution graph can be seen in Figure 4.24 for the two locations at the Fish River. The profiles of FR303 to FR305 and FR306 to FR308, even incorporating FR309 do not vary much from the graph visible including all ADCPs. The area further south yields a much better frequency distribution profile with a larger percentage of higher values around 1.5 m/s. The primary location investigated produced a higher percentage of lower values with many below 1 m/s which would not prove feasible for the desired power extraction. Ocean current roses for the Fish River locations can be seen in Figure 4.25 and Figure 4.26 for the more southern and northern areas respectively.

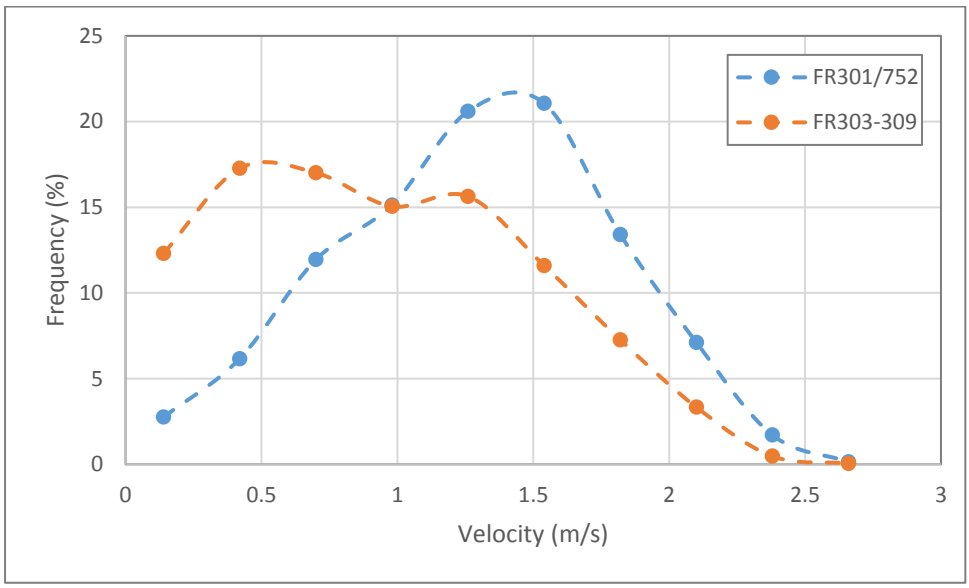

Figure 4.24. Frequency distribution using half-hourly entries. There is little difference incorporating FR309. Dashed lines are used to join data points.

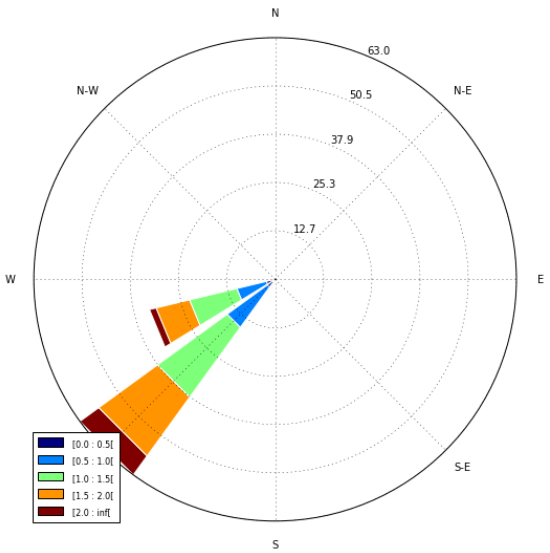

Figure 4.25. Ocean current rose displaying velocity magnitudes and directions at the more southern Fish River location between 18 September 2007 and 29 March 2008.

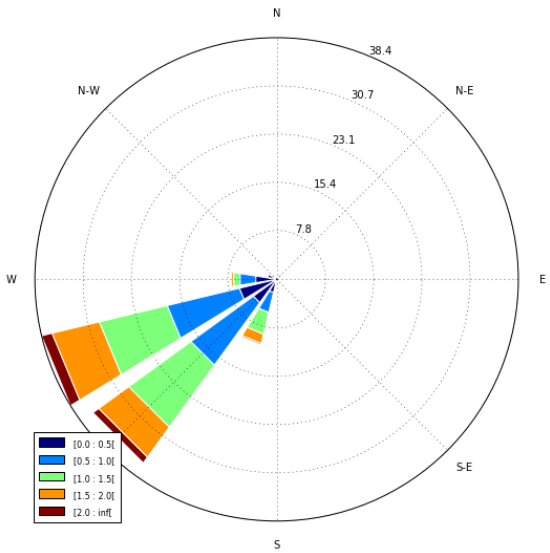

Figure 4.26. Ocean current rose showing the magnitude and direction of the ocean current at the more northern Fish River location between 1 April 2008 and 4 March 2010.

The frequency distribution of velocities around the Fish River shows that most velocities for the more northern ADCPs occur with an even distribution between 0.2 m/s and 1.4 m/s making up for 69 % of the data. Whereas, at the more southern location velocities are relatively much higher with 65 % occurring within the range of 0.8 m/s and 1.8 m/s.

Overall it should be noted that velocities at the Fish River appear to fluctuate more than locations further north. Higher velocities are observed for the site further south, although no Natal Pulse events were present so this is an unrealistic situation. However, this region should be investigated further over a longer duration to determine if higher velocities are present. The only instance in which the area of the Fish River would be used is if it was incorporated into a distributed system as velocities at other locations further north are much higher making those areas a more attractive option for power production regarding a concentrated farm.

The distribution of velocities fluctuates with respect to the various locations. Regarding the more southern Fish River location it can be seen that at least 50 % of the velocities fall between 1.0 m/s and 2.0 m/s. At Locations 1 and 2, as well as the most offshore position at Location 3 it is observed that at least 60 % of the data falls within the 1.0 m/s to 2.4 m/s interval. The distribution of data for each location is presented in Appendix C.3. An operating range of between 1.0 m/s and 2.4 m/s could be used for a kite turbine system.

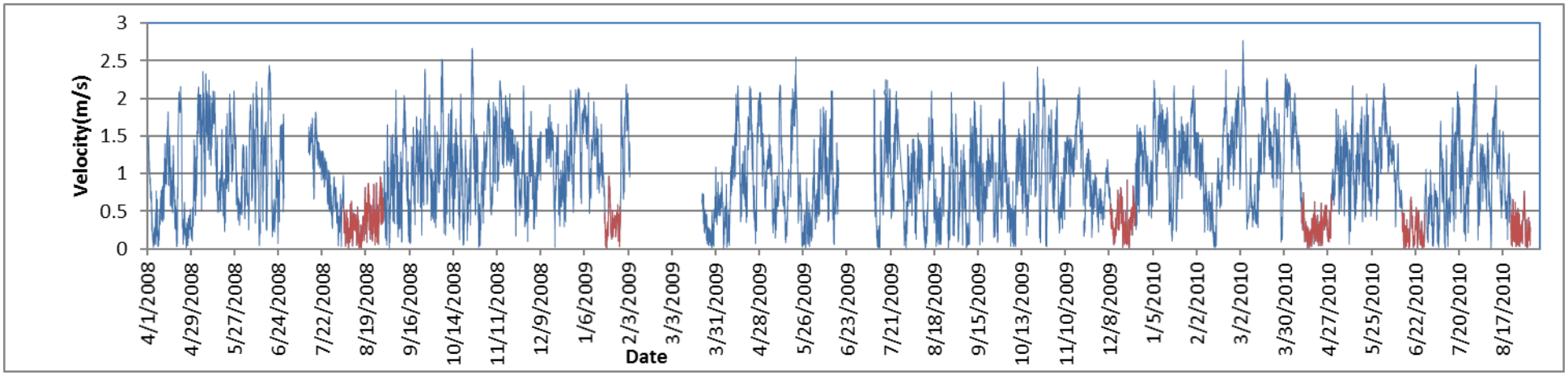

Figure 4.27. Current velocity magnitudes for the ADCPs near the Fish River; Natal Pulse events are visible, gaps in the data are present. Velocities are observed to be lower and more fluctuation is present within the dataset than at other locations.

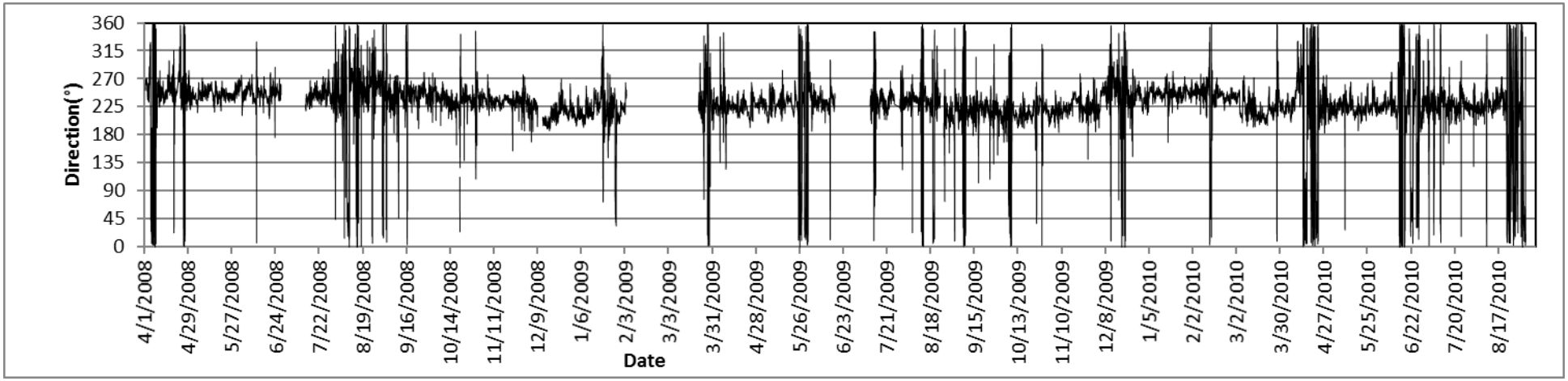

Figure 4.28. The directions that correspond to Figure 4.27. velocity magnitudes. Directions appear to fluctuate a lot more at this location than is seen at the other areas

4.2. Inter-location Comparison

Figure 4.29 shows the velocity non-exceedance probabilities for five locations. The data used to generate the graph was taken from the available ADCPs. The northern Fish River site yielded the lowest velocities while Cape Morgan produced the highest. Locations 2, 3 and 4 South all yield similar curves and do not differ significantly from Location 1. Due to this graph using different time series for the various locations, it is not an accurate representation but can be used as a general guideline. Locations 3 and 4 South have very limited data available and will, therefore, need to be investigated further for more accurate results.

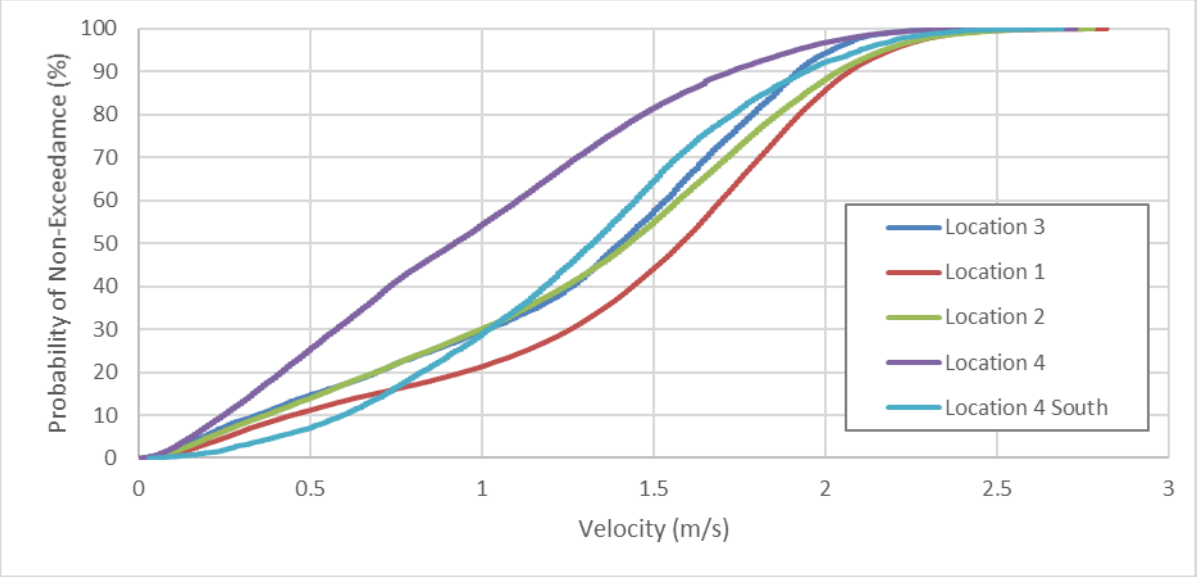

Figure 4.29. The probability of non-exceedance graph showing data collected at each location over the period where data was available. Location 3: 08/09/2005 – 10/04/2006. Location 1: 14/12/2005 – 13/09/2010. Location 2: 08/03/2007 – 13/09/2010. Location 4: 01/04/2008 – 03/09/2010. Location 4 South: 18/08/2007 – 29/03/2008.

Observing Figure 4.29, Location 4 has a 55 % probability of not exceeding a velocity of 1 m/s, Location 1 has only a 21 % chance of not reaching a velocity of 1m/s, with Locations 2, 3 and 4 South have non-exceedance probabilities for a velocity of 1 m/s of approximately 30 %.

The normal distribution profiles generated as seen in Figure 4.30 demonstrate the velocity distribution amongst the different ADCP locations. Location 4 South has the lowest standard deviation, whereas Location 2 has the highest. Location 4 has the lowest mean, with Locations 2, 3 and 4 South having a similar mean velocity, Location 1 experiences the highest mean velocity.

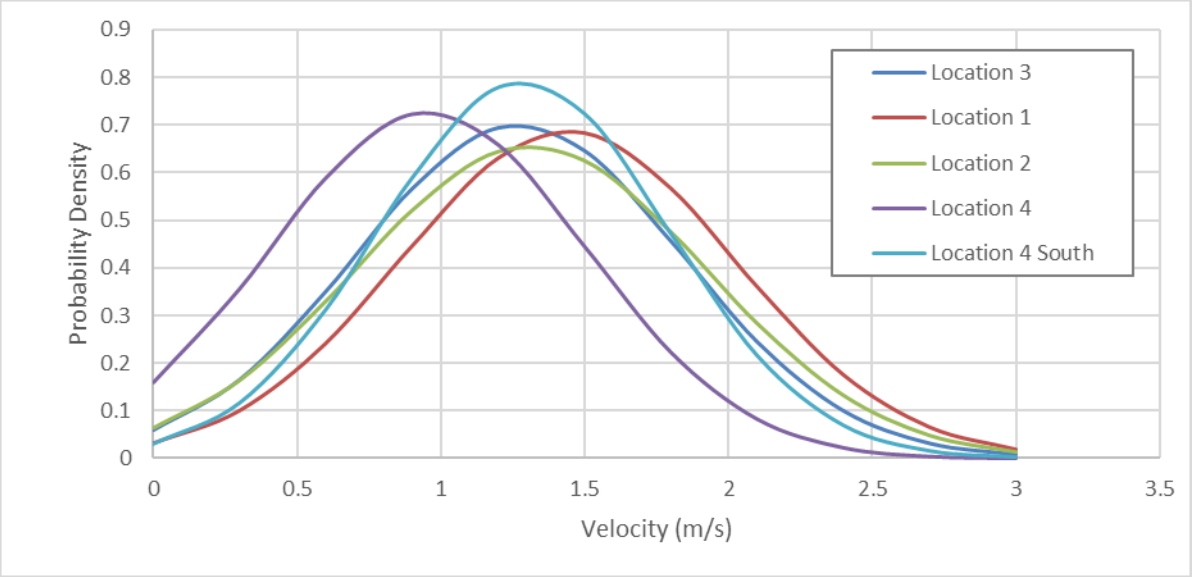

Figure 4.30. Normal distribution using the mean and standard deviation derived from data at all locations where available.

ADCPs at different locations with the same period were compared against each other to investigate how they differ in general and in terms of Natal Pulse events.

ADCP point PE752 at Port Edward was compared against EL1901 at Cape Morgan from mid-December 2005 to early April 2006. The Port Edward site appeared more sensitive to changes with a more fluctuating velocity profile. One Natal Pulse was experienced during this period which had a far greater effect at Port Edward where it experienced a longer duration. At Cape Morgan, there is significantly less change in direction appearing more like a meander when compared with that for Port Edward where the direction change continues for almost the entire duration of the pulse effect. The pulse affects both locations simultaneously for approximately two days as it travels at around 11 km per day down the coast over a distance of 193km.

Three ADCP points were compared, EL303 north of Location 1, EL201 at Location 1 and EL403 between Locations 1 and 2 from April to August 2006. Velocities for EL303 and EL201 were very similar in magnitude and slightly higher in relation to EL403. One Natal Pulse event was observed during the period that persisted for approximately 15 days at the two more northern locations and around 19 days at EL403. It was noted that the speed of propagation within this area segment was faster than averages calculated through the entire system, travelling an average of 25 km per day between EL303 and EL403. The direction of the current experienced a change for the whole duration of the pulse event at all locations, towards the end of the Natal Pulse the direction changes appear more like a series of meanders. Another position at Port Edward using PEM03 could also be compared with these points, at this location the Natal Pulse persisted for 16 days, travelling at 13 km per day to reach EL303. It can be seen that near the initial three locations over the distance of almost 100km, that Natal Pulse

events will be experienced at approximately the same time and may travel at a faster rate between these areas. Therefore, incorporating a distributed system within this area would have little effect on the consistency of potential power production and would not prove advantageous.

Observing points at EL401 at Location 1 and EL305 a distance 55km south along the coast, even though there are no natal pulse events present, it is congruent with the faster speed within that area observing meanders that tend to occur at approximately the same time at both locations which fall within the 100 km area mentioned previously. Velocities are higher at the site further south where the direction also appears more constant.

Three ADCPs, EL756 north of Location 1, EL501 at Location 1 and EL306 near Location 2 were compared between early March and mid-August 2007. The velocities for the points at Locations 1 and 2 were almost equivalent and slightly lower than that for the more northern point. EL756 was extracted at a depth of approximately 30m which was the shallowest depth available due to large amounts of lost data. It experiences the highest velocities, above those at Locations 1 and 2, this could be due to inaccuracies within the data collected and should be investigated further. The Natal Pulse that occurred during the time frame started at relatively the same time for both northern points which were a short 13km apart. The lag time between the pulse occurring at the northern locations and Location 2 is fairly short and congruent with high speeds within this area segment.

Four locations were compared between August and December 2007 where no Natal Pulse events occurred. ADCPS at Locations 1 and 2 produced similar velocities while the point south of Location 4 yielded the lowest velocity, where a point less than half a kilometre more offshore of Location 1 yielded the highest average velocity being 20 cm/s above that of Location 1. Meander events that occurred appeared more exaggerated at the points further south than those further north, with more fluctuating velocities and lower velocities which persisted for longer. Points further offshore of Location 1 should be investigated to determine if they have higher velocity potential.

ADCPs at Locations 1, 2 and 4 were compared from July 2008 to mid-September 2010. No general trend can be seen with regards to speeds between Location 1 and Location 2 and Locations 2 and 3. There is a much variability with regards to speed of propagation of Natal Pulses. For some, Natal Pulses travel quicker from Location 1 to Location 2 and for others, they are faster between Location 2 and Location 4. The duration of the Natal Pulses experienced at each position also appears to be random, where some last for longer periods and others shorter. During one time series segment the velocities at Cape Morgan were lower than both other locations, although the position at Cape Morgan was further inshore where velocities would be lower.

It can be concluded from the inter-location comparison of various points along the coast that current velocities can fluctuate, what is observed and noted for one period could be different for another period. The duration of a Natal Pulse seems to last longer at Port Edward than Cape Morgan, however, more data would be required to verify this statement. Between these areas the pulse travels at a relatively slow speed so it takes longer to travel down the coast which is ideal for a distributed system to work in which locations are not affected by Natal Pulses at the same time. Observations are limited so this observation may not be reliable.

Observing ADCPs located between Locations 1 and 2 and those just north of Location 1, it is seen that within a distance of approximately 100 km that Natal Pulse events are experienced at relatively the same time. A distributed system would not be practical within this segment alone as all units would cease to operate simultaneously, rendering a distributed system redundant. Although, during the period where these results were calculated, there was little data available to compare from other locations to verify relative Natal Pulse speeds between other areas. Positions further south tended to experience a higher frequency of meanders which lasted longer and appeared more prominent. Therefore, due to greater fluctuations of data further south, Cape Morgan is identified as the more stable location in terms of current velocity. Positions slightly offshore of Location 1 should be investigated in terms of yielding higher velocities.

There is an average overlap of Natal Pulses for 2 days between Port Edward and Cape Morgan, i.e. when the pulse starts at Cape Morgan, 2 days later it ceases at Port Edward and the velocity increases, this is observed from the limited data available. An average overlap of 10 days is seen between Cape Morgan and East London, and 9 days between East London and the Fish River. These values are useful in determining whether a distributed hydro-kite system would be functional.

It is difficult to make defined comparisons with such limited data with few occurrences of Natal Pulse events to be compared. Data is inconsistent and most areas do not share data for the same time period. It is difficult to conduct a conclusive analysis as what was seen in this data period may differ for another period.

Table 4.5. Number of natal pulse events experienced per year throughout ADCP deployments (2005 – 2010).

YEAR	No. Natal Pulse
2006	2
2007	1
2008	1
2009	3
2010	3
Average	2.0

From Table 4.5 Natal Pulses occur randomly between the five years of data available, where some years only experience one pulse while other years experienced as many as three Natal Pulse events. Some pulses are more defined than others, persisting for longer periods whereas some are not well observed at certain locations and do not last as long. It is noted that during this five-year period where data was available the average occurrence of 2.0 Natal Pulses is higher than the average from literature, of 1.6 Natal Pulses propagating as far south as Port Elizabeth per year(Rouault & Penven, 2011) .

4.3. Speed and Duration:

The average speed between Location 1 and 2, Location 2 and 4 and Location 3 and 1 differed only slightly. Mean speeds were found to be between 11 km per day and 13km per day as the natal pulse moves down the coast through the various sites. Within an area between Cape Morgan and East London the Natal Pulses seems to travel faster, with an average speed of almost 25 km per day. However, the speed calculated between Natal Pulse events from Cape Morgan to East London yielded a much lower average speed.

Table 4.6. Average speeds calculated between locations, minimum and maximum speeds are also provided.

Location	Average Speed (m/s)	Number of observations	Minimum Speed (m/s)	Maximum Speed (m/s)
3 and 1	12.57	2	11.35	13.79
1 and 2	12.74	8	5.83	32.67
2 and 4	11.10	6	6.43	16.00
1 and 4	10.34	6	6.09	12.25

From Table 4.6 average speeds are congruent with the values found in literature of Natal Pulses propagating at between 10 and 20km per day within the Agulhas current. However, in some instances, the speed at which the pulses move is relatively slow at just over 5 km per day, and another occurrence in which the pulse moves at a high 32.67 km per day – these speeds are calculated between the same area and show how each pulse is different and fluctuations are present.

Table 4.7.The average duration of natal pulse at the locations, minimum and maximum durations are also specified.

Location	Average Duration	Number of observations	Minimum	Maximum
3: Port Edward	17.50	2	16	19
1: Cape Morgan	18.70	10	13	29
2: East London	18.38	8	12	22
4: Fish River	18.20	5	10	24

The minimum duration of a Natal Pulse in one particular area over the data period was 10 days at the Fish River, whereas the maximum duration was 29 days seen at Cape Morgan. The minimum duration correlated with recommendations from Rouault and Penven, (2011) where they only identify cyclonic meanders as Natal Pulses if they persisted for 10 days or more. The average durations at all locations were very similar at approximately 18 days.

4.4. Evaluation of HYCOM data

Data was extracted from the HYCOM model and was observed together with the measured ADCP data. A comparison could be drawn between the two data sets and thus the reliability of the HYCOM model to accurately predict ocean current velocity, as well as its sensitivity to Natal Pulses experienced, could be evaluated.

At all locations the average velocity decreases with an increase in depth, therefore to take advantage of higher velocities, shallower depths would be preferred for kite deployment, also making retrieval much easier and less costly.

It was seen that initially at a depth of 20m that the velocities from the modelled data were much lower than the measured data at many locations. To obtain an accurate representation of the actual results, a correction factor needed to be applied to the modelled data. The Eskom ADCP velocity data tended to decrease more rapidly with depth than the HYCOM data for shallow depths. The modelled data multiplied by the correction factor was able to mimic the overall distribution and the average velocity. The chosen correction factor was not to exceed the actual average velocity for that period or the maximum velocity in order to prevent an overestimation of the current which would render results inaccurate and possibly more favourable than the actual conditions. It is recommended to incorporate a lower factor that may underestimate the velocities than a higher factor which would overestimate providing unrealistic results.

4.4.1. Location 1: Cape Morgan

Data was compared for a two-year period from 18 September 2008 to 13 September 2010. Within the HYCOM data set there was little change in current velocity throughout the depth intervals investigated. The difference in velocity between depths of 20 m and 50 m within the HYCOM data was approximately 25 % of the actual difference in velocity experienced. The actual velocity decrease with depth occurred at a faster rate than the modelled data predicted. The average and maximum current velocities for Cape Morgan at all depths were considerably higher than that estimated by the model.

All depth intervals required a correction factor of more than 1.3 to resemble the average velocity of the ADCP data. However, using those factors would result in the HYCOM maximum velocity being much higher than the actual maximum value for the daily average. Maximum values do not exceed

those seen within the hourly data set at depths 30 m and 50 m, but factors were nevertheless adjusted to account for this. Therefore, the factored modelled data produces values that are slightly lower than the actual measured readings but are a better approximate. A good correlation was seen between the actual and modelled velocity as correlation coefficients were above 0.96 for all depths. The model underestimated the current velocity by more than 35 % for depths 20 m and 30 m and underestimated the velocity at 50 m by more than 25 %. At all depths the velocity was underestimated by the model. The average direction calculated from the HYCOM dataset was within 6° of the actual measured current direction at all depths.

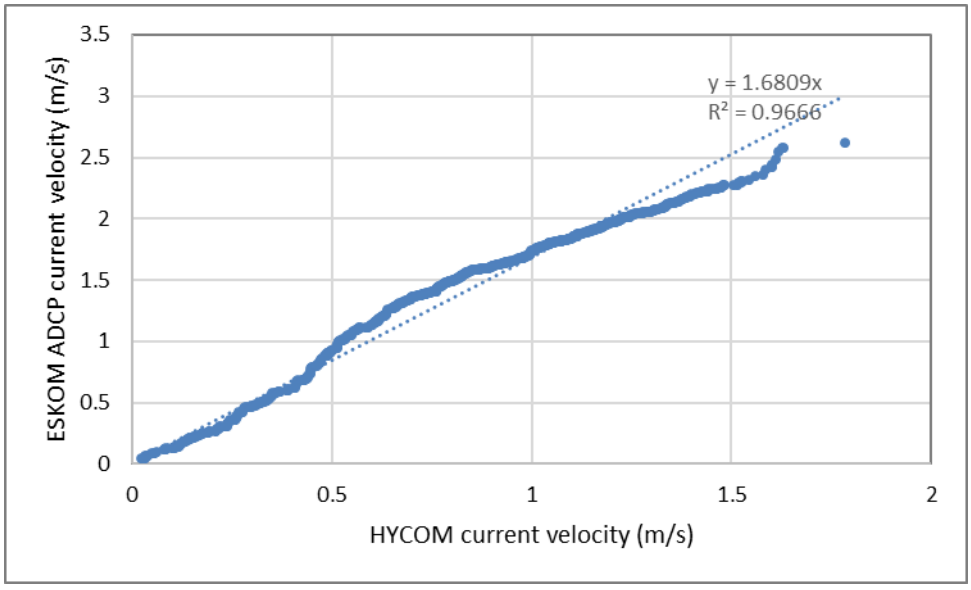

Figure 4.31. Scatter plot of two data sets at Cape Morgan for a depth of 20m to determine correction factor required. (From CM at 20m but correct snapshot values

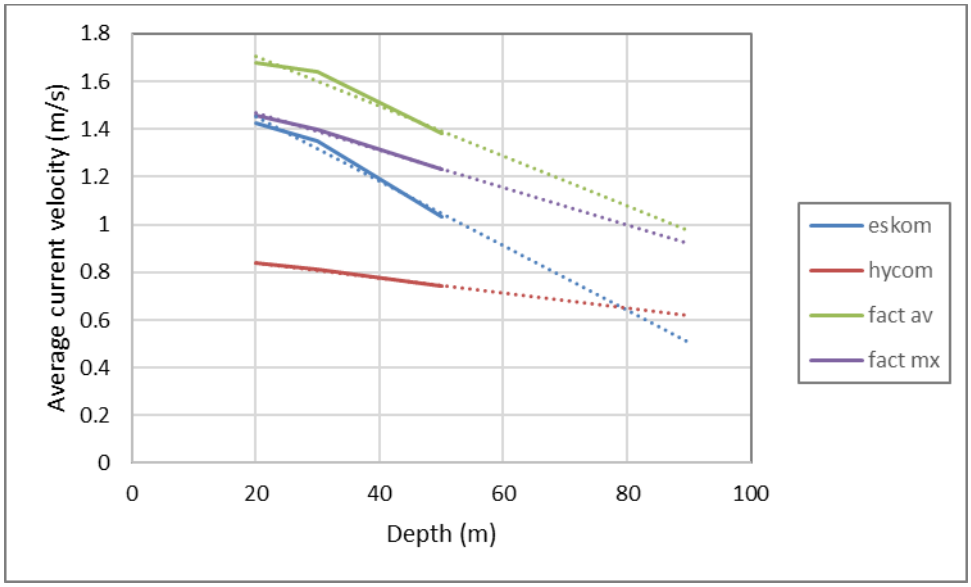

Figure 4.32. Depth vs. Average current velocity including correction factors: fact av corresponds to the factors calculated from the scatter plots, fact mx corresponds to the factors used that had to be adjusted to prevent the maximum values exceeding those of the values recorded.

Using the trendlines from the HYCOM and Eskom data in Figure 4.32Figure 4.31, the two data sets will intersect at around 79 m, after which it is assumed that the HYCOM data will start to overpredict current velocities for deeper depths. At the point of intersection where HYCOM and Eskom data yields the same average that the correction factor should be equal to 1, but it produces a slightly higher value. Correction factors are to be used as a guideline.

Observing the plot of the actual velocity against the modelled velocity with time in Figure 4.33, the model is fairly accurate in producing results close to the actual data after factors have been applied. Natal Pulses are well modelled and occur at the same time as those observed The second Natal Pulse experienced in 2010 is seen to occur slightly later, a slight lag effect. The direction change for this pulse is not well modelled. The modelled direction seen in Figure 4.34 also resembles that of actual events where direction changes are observed near the same time as they occur. HYCOM tends to predict additional direction changes not present in reality. Near the end of 2009 where the direction suddenly changes and increases by almost 50° is not replicated by the model which maintains a steady average direction.

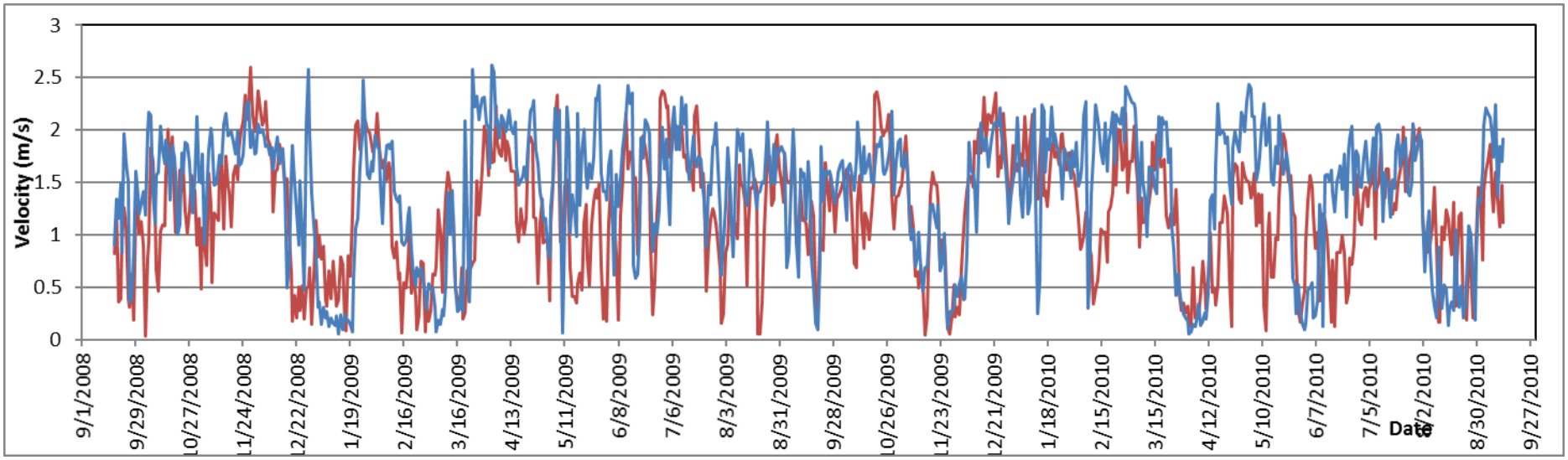

Figure 4.33. Magnitudes of velocities of the two data sets: actual ADCP measurements (blue) and factored HYCOM modelled data (red) to show how well the modelled data compares to the actual results

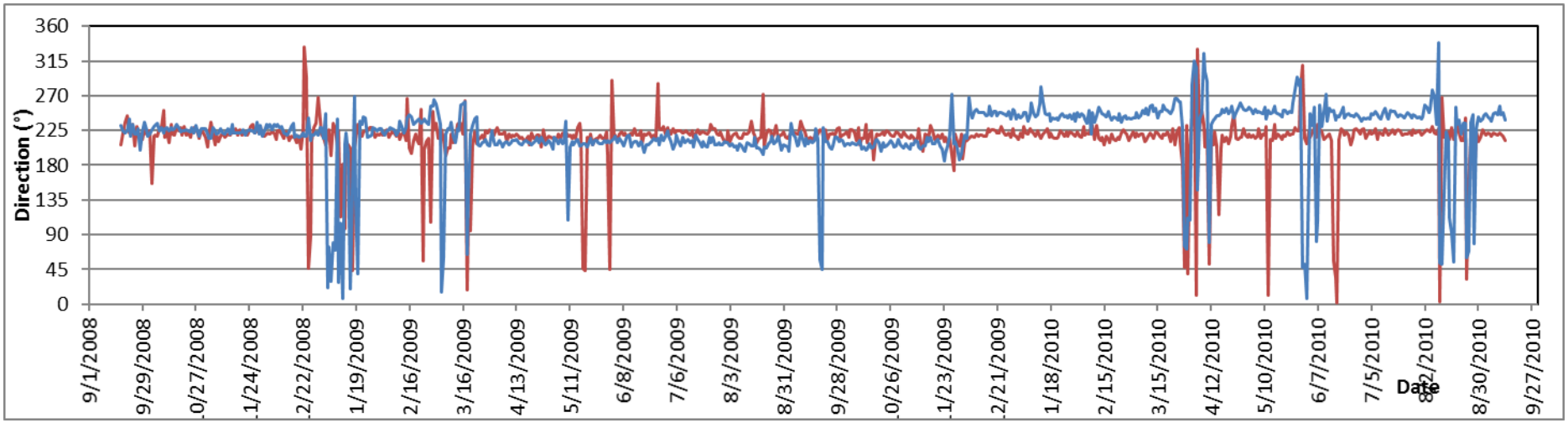

Figure 4.34. The direction of the current velocities Figure 4.33. for the different data sets: ADCP recordings (blue) and HYCOM predictions (red).

4.4.2. Location 2: East London

As with the previous observations at Cape Morgan, HYCOM underestimates the change in velocity with depth. The modelled average current velocities for this location are higher than those for Location 1 at Cape Morgan, but the measured current velocity for that region is higher than Location 2. The difference in velocity between the depths of 20 m and 50 m for HYCOM is higher than at Location 1, at approximately 30 % of the actual velocity difference.

For depths 20 m and 30 m a factor greater than 1.0 needs to be implemented where HYCOM tends to underpredict velocities. However, at a depth of 50 m HYCOM overestimates the current velocity and a factor lower than 1.0 must be incorporated. The measured data decreases at a faster rate than HYCOM predicts. The Eskom data and HYCOM data intersect and at a depth of approximately 40 m seen in Figure 4.36 where the factors applied decrease linearly with depth. At the point of intersection, the factor is equal to 1.

Regarding depths 30 m and 50 m, the factors calculated slightly overestimated the average when multiplied by the HYCOM average. The factor was adjusted accordingly. Underestimations regarding current velocity of 17 % and 9 % are observed for depths of 20 m and 30 m respectively, an overestimation of 12 % is seen at the 50 m depth. There is a high correlation observed between the Eskom and HYCOM data as all correlation coefficients calculated were above 0.98 for all depths. As seen at Location 1, the average direction is approximately equal to that seen from the actual data and is within 2°.

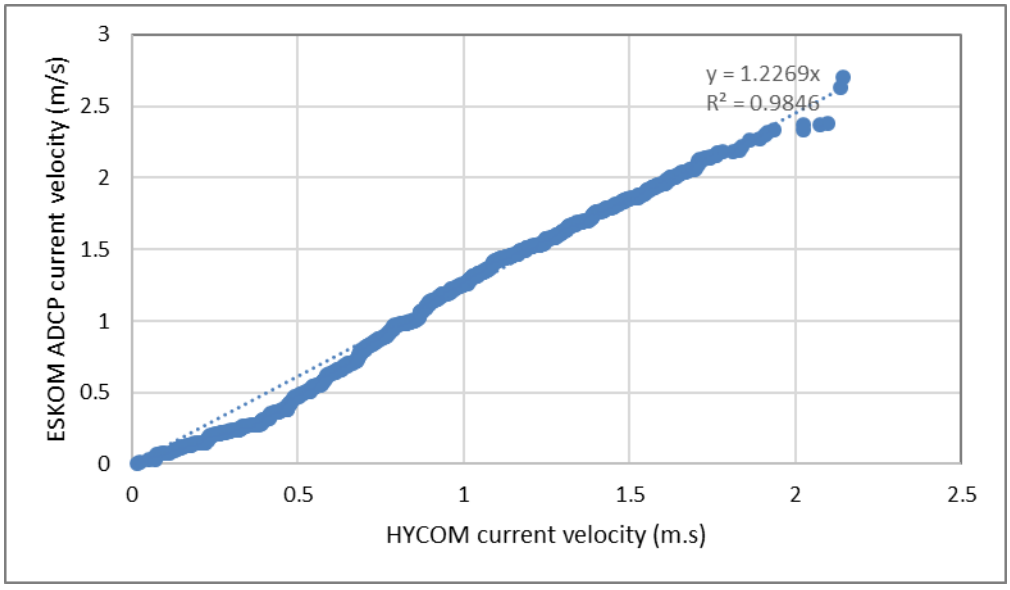

Figure 4.35. Scatter plot of the two data sets to determine the correction factor at East London at a depth of 20m.

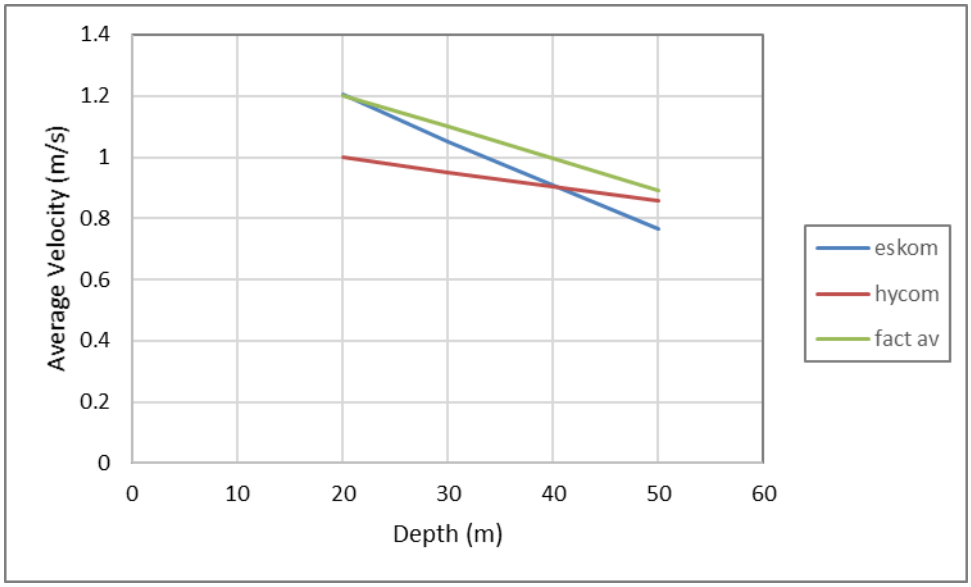

Figure 4.36. Depth vs. Average current velocity for Eskom ADCP data and HYCOM modelled data, correction factors used are included based on the results from the scatter plots.

Data produced from the HYCOM model is fairly accurate in modelling actual events captured by Eskom ADCP data. The model follows the trends seen in the actual data where drops in velocity are experienced due to Natal Pulse events. One Natal Pulse event in March 2009 is not accurately modelled by HYCOM although lower velocities are indicated they are still higher than the actual experienced. At this location, the second natal pulse that occurred in 2010 is more accurately modelled than it had been at Cape Morgan. The average direction and direction changes modelled by HYCOM are very accurate at this location and occur congruently with the actual direction changes both for Natal Pulse events and meanders.

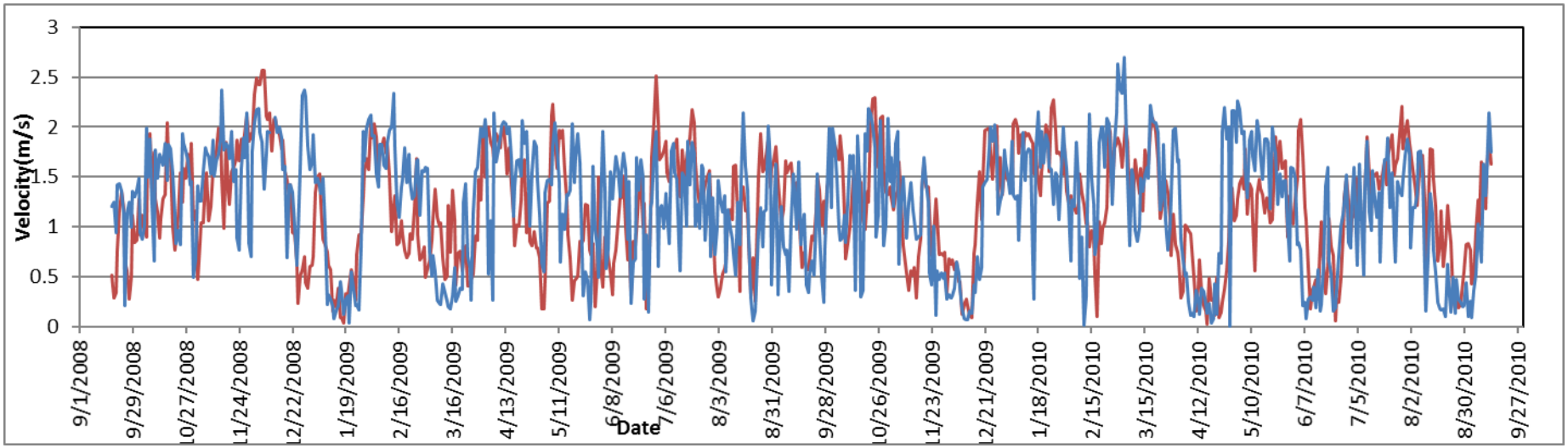

Figure 4.37. Velocity magnitudes for the two data sets: ADCP measurements (blue) and HYCOM model predictions (red), at the location of East London at a depth of 20m.

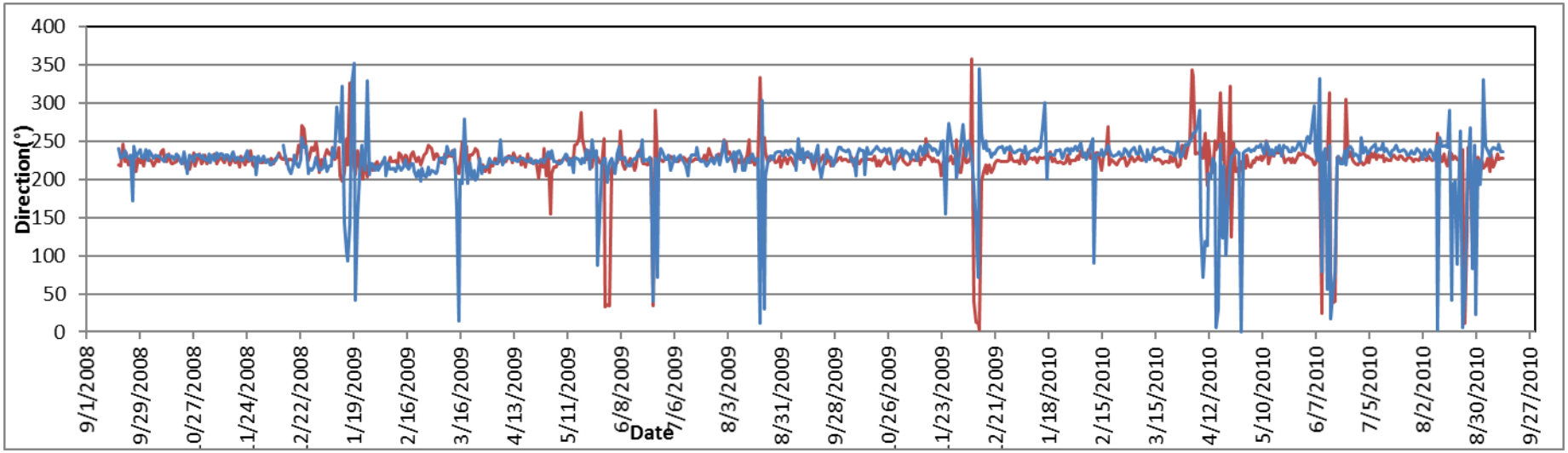

Figure 4.38. Directions corresponding to velocity magnitudes depicted in the Figure 4.37: ADCP readings (blue), HYCOM predictions (red).

4.4.3. Location 4: Fish River

Model data at the more northern Fish River location resembles the measured results for the shallower depths observed. There is still the general trend seen where measured velocity decreases at a faster rate with depth than the model data. Correction factors of approximately 1.0 are required for depths 20 m and 30 m, with no drastic change to values necessary. However, after the intersection of the HYCOM and Eskom data at 32m, HYCOM predicts higher velocities. At the 50m depth, a factor below 1.0 must be used to correct this. For all depths, factors for all locations needed to be adjusted so that they did not exceed the average velocity. At this site HYCOM underpredicts velocities by 4% and 1% for depths 20 m and 30 m respectively, with an overprediction of 9 % at 50 m depth. The velocity difference of the modelled data between depths 20 m and 50 m is approximately 65 % of the velocity difference experienced by Eskom data. There is a high correlation between measured and modelled data with correlation coefficients above 0.95 at all depths. From Figure 4.39, the correlation between the data sets is linear for the lower current velocities but deviates slightly with regard to higher velocities. The average modelled direction is within 7° of the actual observed direction.

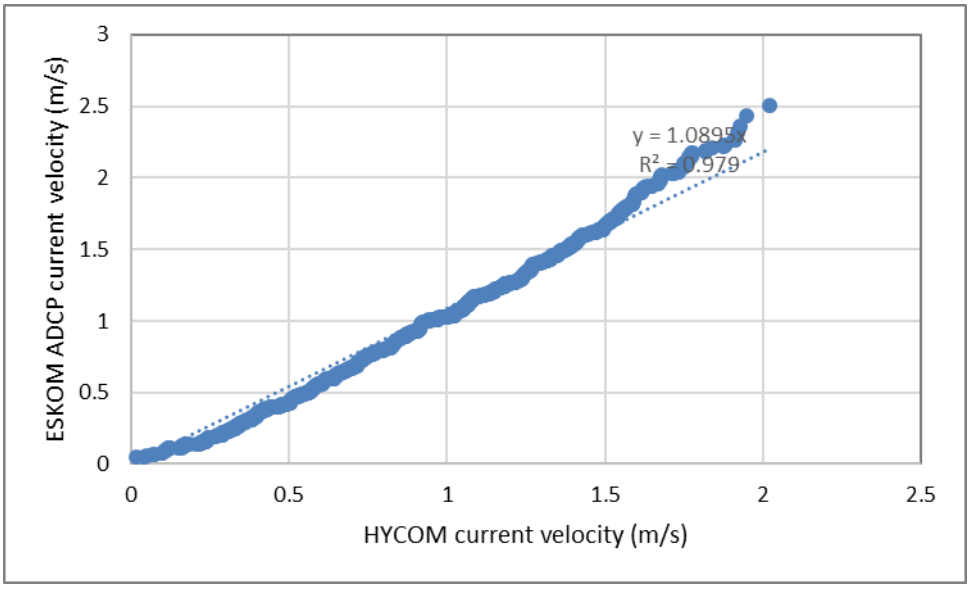

Figure 4.39. Scatter plot of the velocity magnitude distribution of the two data sets at the Fish River at 20m depth.

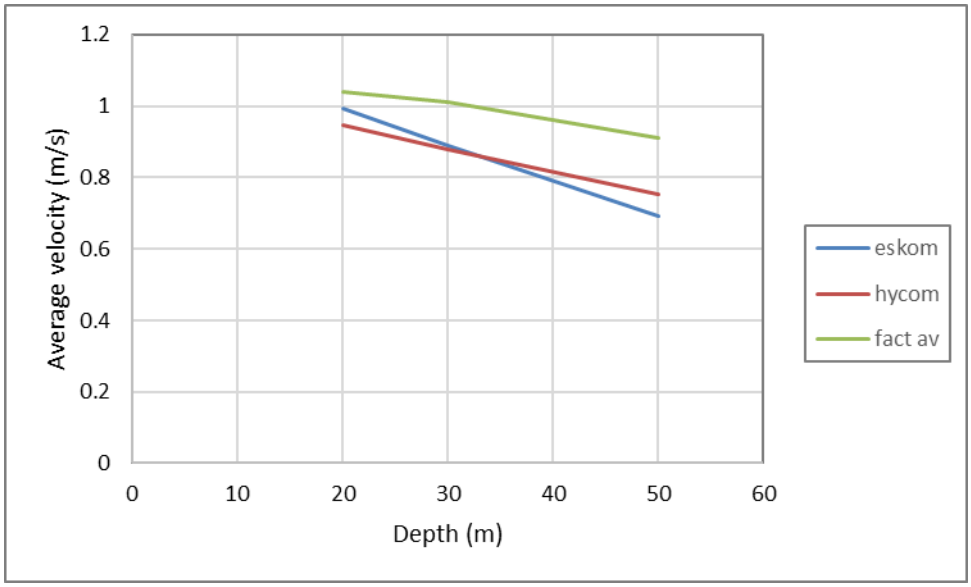

Figure 4.40. Depth vs. Average current velocity at the Fish River. Data is shown from the ADCP measurement and the HYCOM model, calculated correction factors to be applied to the HYCOM model are also depicted.

Although there is data missing from this set, it can be seen that the modelled data can predict fairly accurate current velocities for a depth of 20 m. The model can predict Natal Pulse events as they occur and low velocities as a result of meanders, however, the timing is slightly off as seen in January 2009 where there is a lag in predicting low velocities and in April 2010 where low velocities are predicted for longer than the actual duration. HYCOM can predict the direction changes associated with most Natal Pulses and meanders, but in this data set, many direction changes are modelled which do not occur in reality. There is a slight direction deviation from the average which occurs between November 2009 and February 2010 which is not predicted by the model.

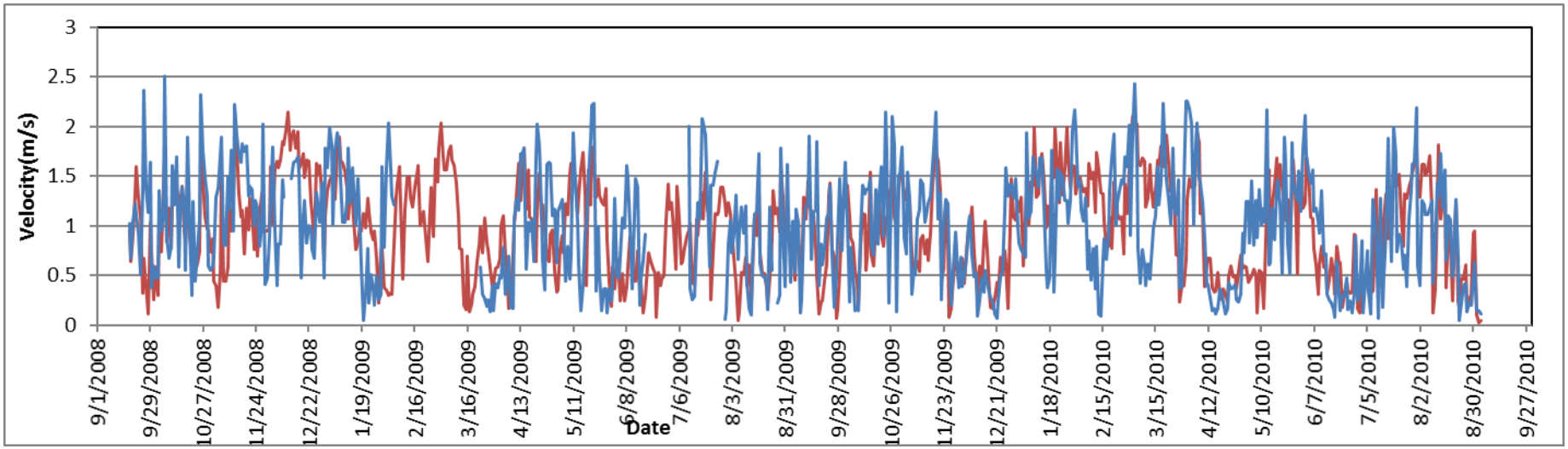

Figure 4.41. Velocity magnitudes for both data sets at the Fish River at 20m depth: ADCP recordings (blue) and HYCOM model estimates (red).

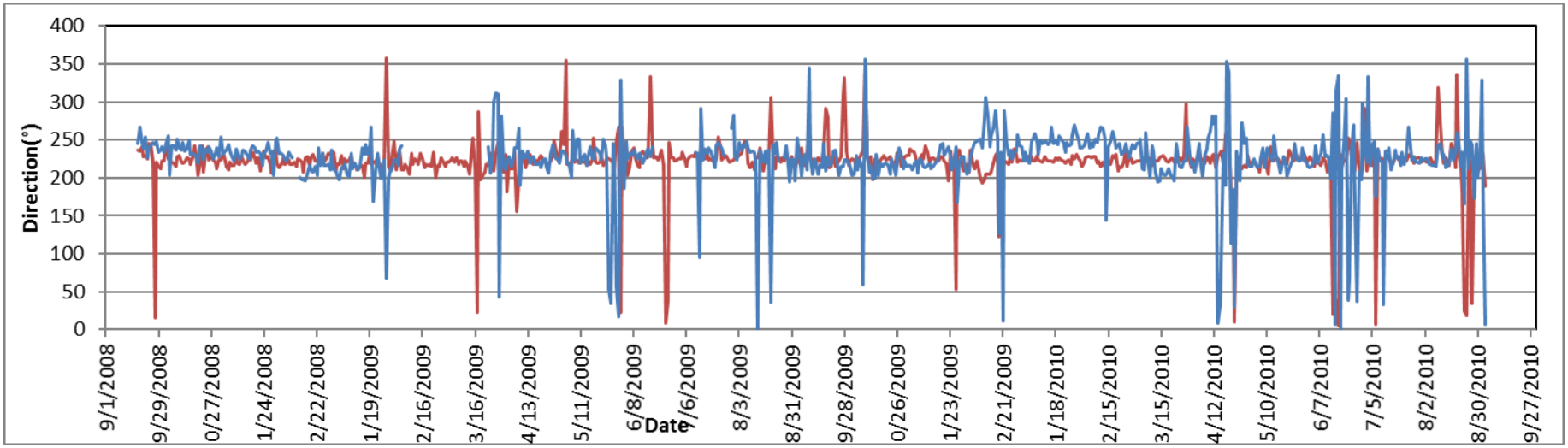

Figure 4.42. Directions of the velocities experienced at the Fish River at 20m depth: ADCP measurements (blue) compared against HYCOM model predictions (red).

4.4.4. Location 3: Port Edward and Location 4 South: Fish River South

Due to the data from Port Edward only being available for one year during 2005 and 2006, it cannot be evaluated and compared with HYCOM data only available from 2008 onwards. An assumption must be made based on the data available. The factor needed to be chosen where the maximum velocity of the factored data did not exceed that of the data available. The average velocity calculated for the period was much higher than the average factored HYCOM value but due to uncertainty, underestimations are preferred over the risk of overestimating values.

The same procedure was performed for the area further south of the Fish River where data was available for a limited time during 2007 and 2008. At this location more caution needed to be exercised as there were no Natal Pulse events present within the dataset to lower the average velocity. The velocity over a longer period would probably be lower. The average velocity provided by HYCOM was much lower than that of the actual data available. Due to the observations from the main Fish River location that could be confirmed where virtually no factor was necessary at a depth of 20m. It was decided that no factor would be applied to the further south Fish River location.

Table 4.8. HYCOM Data correction factors at various locations at a depth of 20m.

LOCATION	Correction Factor	Correlation Coefficient
3: Port Edward	1.25	-
1: Cape Morgan	1.46	0.9666
2: East London	1.2	0.9846
4: Fish River	1.04	0.9790
4: Fish River South	1.00	-

During the comparison of modelled data with the measured ADCP data, it was seen that velocity data decreases almost linearly with an increase in depth. The linear decrease occurs at approximately the same rate for Cape Morgan and East London but at a slower rate for the Fish River by observing the gradient of the trendlines for the correction factors. The measured velocities decrease at a faster rate with depth compared with the model data which decreases at a much slower rate. HYCOM data tends to start off underestimating the velocity for shallow depths, at some depth the model and measured data intersect after which the model starts to overestimate the velocity. The model does not produce consistent predictions throughout the water column for shallow depths. Through the use of correction factors the model data can represent the actual measured data more accurately but because of the data decreasing at different rates, different correction factors are needed for the corresponding depths.

It is known from previous observations that Location 1 clearly yields the highest average velocity, Location 2 yields high average velocities, but lower than Location 1, and Location 4 generates the lowest average velocities. This is not accurately represented by the model data at all. The model without any factor adjustment indicated that Location 2 produced some of the highest velocities, followed by Location 4, with Location 1 having the lowest velocities. However, there is not much difference between average velocities within these three locations in the model data, whereas there is a distinct difference in the actual measured data. It is conclusively seen that locations of seemingly high current velocities observed with the HYCOM model cannot simply be assumed and used. HYCOM fails to determine the location of the highest velocity (Location 1) and overlooks it entirely. Therefore, HYCOM cannot be used as a tool to identify probable locations of high current velocity. Without the use of measured data and implementing correction factors, the data is useless and of limited value. The model is fairly accurate in simulating Natal Pulse events which is critical to this study regarding potential power production and consistency of power. It is recommended that the model be used in conjunction with measured in-situ data sets in order for it to be used effectively.

4.5. HYCOM Reanalysis

The HYCOM Reanalysis is available from August 2005 to December 2012. All locations can be directly compared with the modelled data for that period, unlike the problem encountered with the HYCOM data. The Reanalysis required higher correction factors than those applied to the HYCOM model. The factored HYCOM model showed a slightly better correlation to the actual data than the Reanalysis.

Table 4.9. HYCOM Reanalysis correction factors at various locations at a depth of 20m.

Location	Correction Factor	Correlation Coefficient
3: Port Edward	1.76	0.8107
1: Cape Morgan	1.72	0.9629
2: East London	1.4	0.978
4: Fish River	1.14	0.9661
4: Fish River South	1.07	0.9370

There is a similar trend in the correction factors as with the HYCOM model where Cape Morgan required a higher factor, followed by East London and then the Fish River which did not need a high factor.

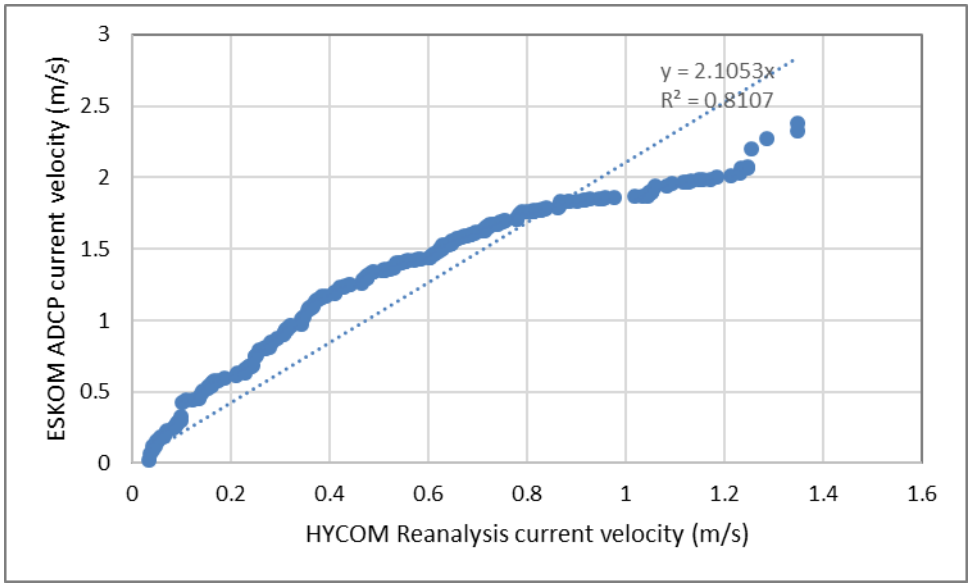

Figure 4.43. Scatter plot for two sets of data: ADCP measurements and HYCOM model reanalysis for the location at Port Edward at a depth of 20m. The data does not correlate as well at this location.

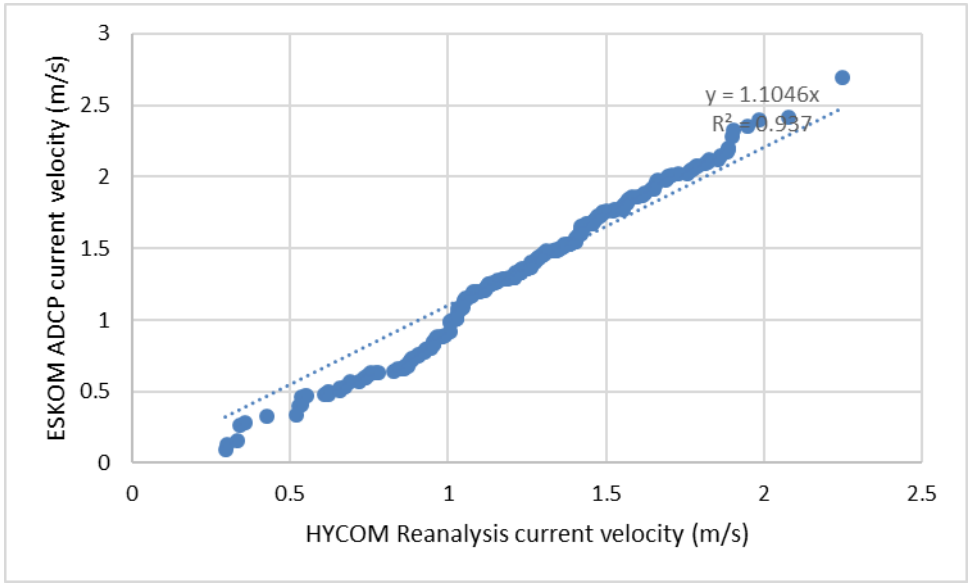

Figure 4.44. Scatter plot of two data sets at the Fish River South location at a depth of 20m: ADCP data plotted against HYCOM model reanalysis data.

The correlation coefficients were very similar for HYCOM analysis and Reanalysis. It could be assumed that the correlation factors for the unknown locations of Port Edward and the Fish River South could be similar to those produced from the Reanalysis. The correlation coefficient calculated for data at Port Edward was considerably low at a value of only 0.81, when compared to the high coefficients of at least 0.96 and above attained for other locations. This site also required a high factor to resemble the limited measured data. The position at the Fish River South produced a relatively high correlation coefficient of 0.93 but the model appears to predict more low velocities. From this observation it appears that the HYCOM model has a stronger correlation to the actual ocean current velocities from

Cape Morgan to the northern Fish River. Further north there is much less correlation and further South of the Fish River the correlation also tends to weaken.

The data used from the Reanalysis could be used to verify assumptions made for unknown locations within the HYCOM data set to ensure they follow the same general trend.

Observing the factors required, it is assumed that high factors are needed for the more northern locations and lower factors are required moving further south within the Agulhas current. As only five central locations can be examined with measured results, there is some uncertainty as to what occurs between the positions which cannot be verified without the provision of more data.

It was imperative to apply factors to the data so that they resemble real world events. As with the HYCOM model, this model needs to be used in conjunction with measured findings to refine it and gain a more accurate representation. Areas located in between the main locations could also be investigated to verify the general trends.

4.6. Alternative HYCOM extract

4.6.1. Cape Morgan

The ADCPs located near Cape Morgan are situated approximately 13 km offshore. The HYCOM data obtained closest to this position was very poorly estimated. Other sites further offshore were investigated and compared with the measured data. The best surrounding approximate was found to be a point along the same line of latitude, a distance of 15 km east from the actual point and approximately 24 km offshore. The next best approximate with little difference in velocities compared with the best location, was found to be in line with the actual ADCP position perpendicular to the coastline, around 30 km offshore. It is noted that further offshore of the site of the best approximates, the difference between the measured velocities and the modelled velocities becomes more significant and thus less accurate.

Overall the best approximate further offshore is still a poor representation of the velocities experienced at Cape Morgan as it underestimated the velocities by approximately 16 % but remains a more suitable indication than the closest extract which underestimated velocities by 41 %, 2.5 times as much as the best approximate. A similar correlation coefficient was achieved for this location, 0.97, slightly higher than for the HYCOM data.

A similar velocity profile is seen for the alternate position as the factored HYCOM data in Figure 4.45. It appears to represent the second Natal Pulse of 2010 slightly better. The direction profile was also very similar to that of the actual location with the inclusion of a few more meander events that did not occur in reality.

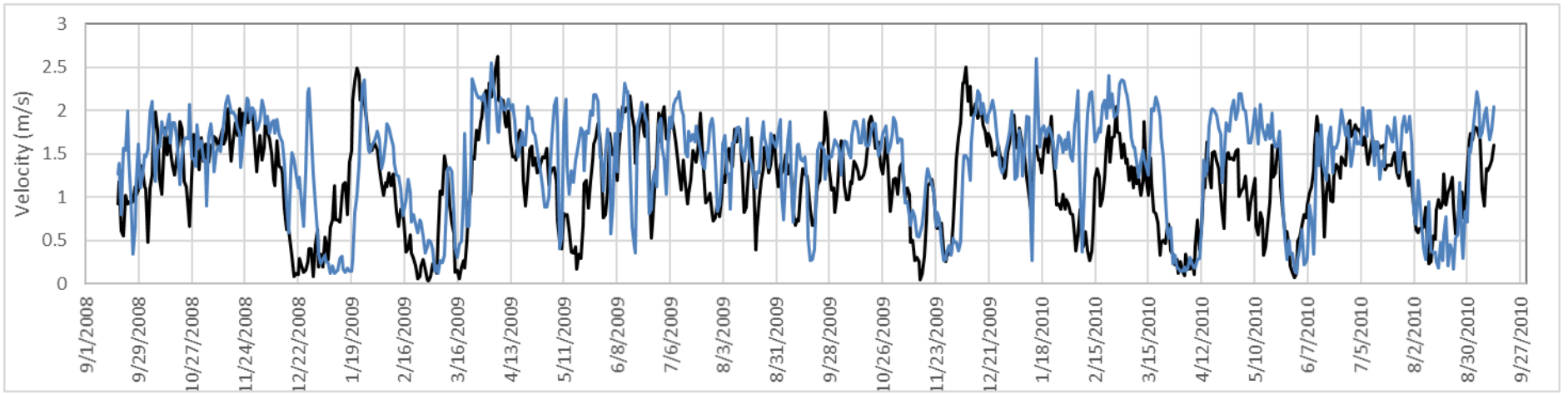

Figure 4.45. Velocity magnitudes at Cape Morgan at 20m depth for two data sets: ADCP actual measurements (blue) and HYCOM modelled data extracted at the best alternative position located further offshore (black).

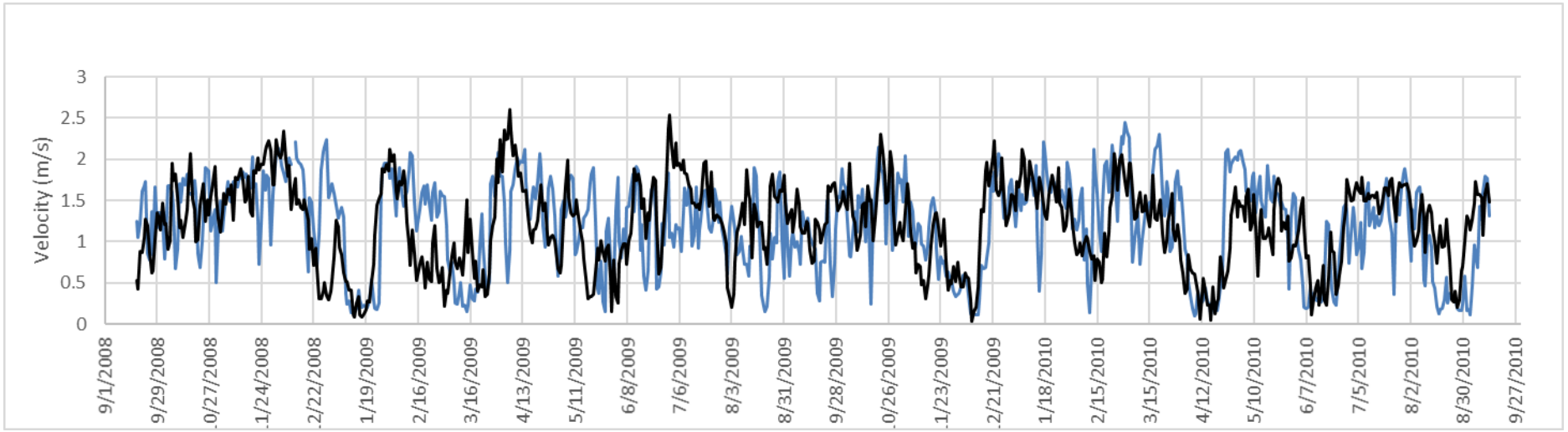

Figure 4.46. Velocity magnitudes for two data sets: ADCP actual recordings (blue) and HYCOM modelled data (black)extracted from the best alternative location at East London at a depth of 20m.

4.6.2. East London

The ADCPs near East London were situated between HYCOM points, so the closest was found to be a point slightly south of the ADCPs. HYCOM points further offshore were considered. The actual position from which data was captured was around 22 km offshore. An area north of the ADCP position yielding velocities significantly lower than the measured as well as the modelled data extracted from the nearer point. The closest approximate was a found to be 33 km offshore, 10 km from the original point of extraction and in line with the ADCP position perpendicular to the coast. Another point of more accurate results was found at the same latitude as the actual location but further east, about 28km offshore. Investigating other points further offshore (up to 55 km) yielded less accurate results. Data at the best-approximated position was fairly precise, producing an overall underestimation of only 0.7%.

4.6.3. Fish River

The ADCPs at this more northern Fish River site were located approximately 25km offshore. The actual point where modelled data was extracted yielded good results when compared with the measured data, where almost no correction factor was needed. Other surrounding more offshore positions were considered up to approximately 50km, all of which overpredicted the velocities measured at this location. The best site was a point along the same latitude as the original position but slightly further offshore, approximately 30km which underestimated velocities by just under 4%. There was little difference between this and the actual point. Therefore, the actual position could still be used.

4.6.4. Port Edward

HYCOM data was analysed to provide a general indication of the velocity distribution compared with the limited data available at Port Edward. It is assumed that the average velocity for the position at Port Edward is relatively constant, such as other locations which are fairly consistent even with fluctuating velocities. The data extracted from the HYCOM model yielded very low-velocity values for this area. The best location produced an average velocity approximately 20 % lower than the velocity from the data. This position was located 20 km offshore, 10 km from the ADCP position.

4.6.5. Fish River South

There is uncertainty regarding the location south of the Fish River. Through observations of other locations and the location of their best approximates, it is estimated that the best approximate for positions further south is found closer to the actual point than those further north. To prevent overestimations due to uncertainty, no best approximate for this site was selected as the original position was used.

Table 4.10. Approximate distances offshore for ADCP locations and locations where the best approximate was found using Google Earth imagery.

Location	ADCP distance (km)	HYCOM best approx. (km)
Port Edward	10	20
Cape Morgan	13	24
East London	22	33
Fish River	25	30
Fish River South	33	-

Overall, observing the findings of using alternative positions from the HYCOM model, for most locations, except the Fish River, a more accurate representation of the velocities experienced was found further offshore within approximately 10 km from the original ADCP position. All best approximations did not overpredict velocities and were lower than the measured results. However, no distinct correlation between the actual point and best-approximated point in HYCOM could be seen using the limited amount of positions available, apart from being further offshore. Further north from Port Edward to East London the best approximate locations are approximately 10 km further offshore from the ADCPs. Whereas further south near the Fish River, the best approximate location is only 5km further offshore which yields velocities very similar to that of the closest point to the ADCP location. This aids the theory that HYCOM tends to predict the core of the Agulhas current further offshore for points further north; until the Fish River in which the model predicts the core at the approximate location. However, since there is limited data available this cannot be applied to points that have not been investigated. An assumption is made that for the locations between Port Edward and East London that the best-approximate for all points in between would lie between those points.

Table 4.11. Percentage underestimation of current velocities at locations using various modelled data

Location	HYCOM	HYCOM REANALYSIS	HYCOM ALTERNATE POSITION
Port Edward	-	56.23	-
Cape Morgan	41.34	51.40	16.30
East London	16.85	32.56	0.68
Fish River	4.47	12.37	3.61
Fish River South	-	6.84	-

It can be seen that the percentage of underestimation or overestimation of the HYCOM data in this analysis of the data differs from that produced by vanZweiten et al. (2014). This could be attributed to the fact that in this study data was extracted from the grid location and not interpolated with surrounding grid points and their spatial locations around the ADCP.

4.7. Factors Affecting Power

The potential power that a hydro-kite can produced is dependent on the current velocity and the kite design regarding its size and flight properties.

4.7.1. Kite wing area

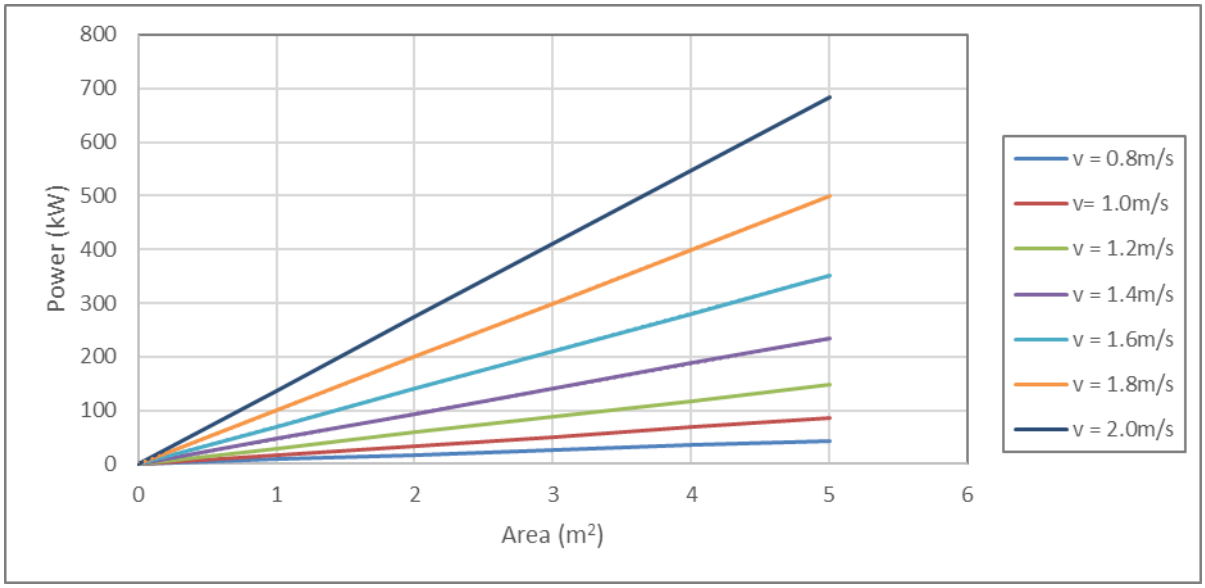

Figure 4.47. Graph showing the potential power that can be generated using the Loyd equation for a given velocity based on the kite wing area, assuming a lift to drag ratio of 15 and a lift coefficient of 1.

Figure 4.47 shows the effects of the kite wing area and the velocity on the maximum amount of power that could theoretically be produced according to Eq. (2.5). Power increases linearly with the area of the kite wing for a given current velocity. Assuming a set velocity produces a specific power output, to achieve the same power output using a lower velocity the area of the kite must be increased. From Figure 4.47, it can be seen that using lower velocities will require a greater increase in area to achieve the same amount of power.

4.7.2. Lift to drag ratio

Figure 4.48 shows the relationship between the power output and the lift to drag ratio. Current velocity is kept constant at 1 m/s, the lift coefficient is constant at a value of 1 and the kite wing area is set at $3m^2$. Small changes in the lift to drag ratio can have a large impact on the power produced. Increasing the lift to drag ratio from 10 to 15 results in more than twice the amount of power that can be generated.

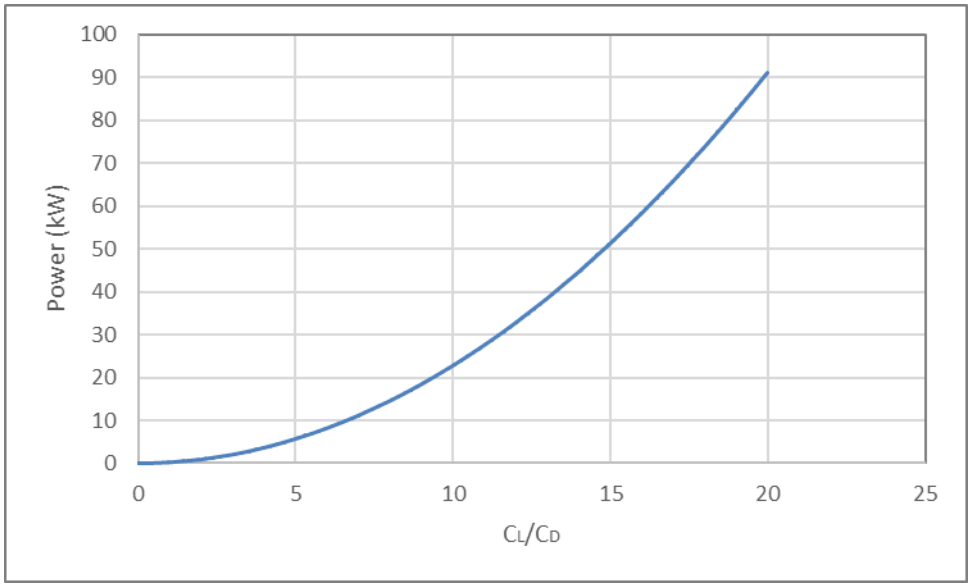

Figure 4.48. Graph showing the influence of the lift to drag ratio on the power output. The following variables were kept constant: velocity at 1m/s, kite area at 3m² and the lift coefficient of 1.

A hydro-kite should be designed according to the desired power output using the known velocity distribution along the Agulhas current. A lift to drag ratio of 15 is assumed for all power calculations.

4.7.3. Cut-in and Cut-out speeds

The distribution of the current velocities at the various ADCP locations showed that only a small percentage (less than 1 %) of the data included current speeds greater than 2.4 m/s. Therefore, it is acceptable to specify a value of 2.4 m/s as the cut-out speed at which the turbine no longer generates power. A high current speed may also pose damage to the hydro-kite, a kite should be tested to determine at what speed this occurs ensuring that it operates within safe limits. Applying this cut-out speed will also ensure that the results derived from the modelled data do not overpredict the potential power output as incorporating high values can significantly affect the average due to the velocity being cubed.

The cut-in speed was investigated with regards to power output using the Loyd equation in Eq. (2.5). The factored modelled data from HYCOM was used with various cut-in speeds by filtering the data, and the average power output was calculated for each. The results are shown in Figure 4.49, observing that the lower velocities do not significantly impact the average power and can be disregarded. After a cut-in speed of 0.8 m/s the power produced tends to drop more dramatically with an increase in cut-in speed. A cut-in speed of 0.8 m/s was used for future calculations. Results using a cut-in speed of 1.0 m/s can also be found in Appendix D.

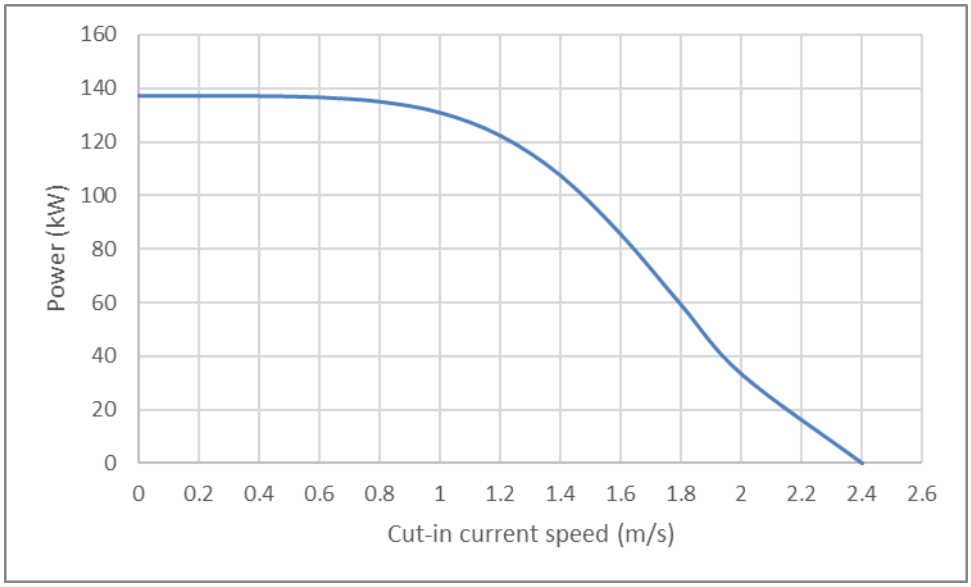

Figure 4.49. The effect of cut-in speed with regards to potential power output using the factored HYCOM model data using a 3m² kite.

4.8. Kinetic Energy Flux

4.8.1. Comparison of actual results

Two time periods were able to be directly compared using the ADCP data. The first from 19 August 2007 to 29 March 2008 was investigated for locations at Cape Morgan, East London and the more southern Fish River location. The other period from 2 April 2008 to 3 September 2010 was investigated for locations at Cape Morgan, East London and the more northern Fish River site. The first comparable time series is limited as the duration spans less than a year and is considered an ideal situation as no Natal Pulse events were observed. The second time series presents a more realistic representation of conditions over the 29-month period where six natal pulse events were witnessed.

It was also investigated as to whether the energy potential using all three locations was greater than compared to using only one position which yielded higher velocities.

4.8.1.1. Time series 1: Comparison of Cape Morgan, East London and Fish River South

As this short period contained no Natal Pulse events, the percentage that each location was operational for was high. Positions at Cape Morgan and East London were working for more than 90 %, with the site at the Fish River being active for almost 80 % of the duration. There is no time where at least one location is not working, for 96 % of the duration at least two locations were functional, with all three areas working for approximately 68 % of the time period.

During this time, East London yielded a slightly higher average KEF than Cape Morgan. There was little difference in using all three locations compared to using only Cape Morgan or only East London, achieving 86 % of the KEF at East London. However, this is a more ideal period so results will be misleading to the actual events.

Table 4.12. KEF of ADCP locations for cut-in speeds or 0.8m/s and 1.0m/s for time series 1 from 19 August 2007 to 29 March 2008.

TIME SERIES 1	KEF		
LOCATION	CUT-IN SPEED = 0.8	CUT-IN SPEED = 1.0	% CHANGE
CM	2.61	2.60	0.17
EL	2.62	2.61	0.45
FR2	1.62	1.60	1.63
ALL (3)	2.27	2.25	0.62
ALL COMPARED TO EL: PERCENTAGE OF KEF	86.64	86.21	

4.8.1.2. Time series 2: Comparison of Cape Morgan, East London and Fish River

Due to this time series being of a longer duration with a more realistic distribution of Natal Pulse events, a more accurate comparison can be achieved. However, within the data set a combined 6 % of data is missing. To gauge an accurate comparison, the missing data was removed from each location.

The site at the Fish River operates for only 57 % of the time, while positions at Cape Morgan and East London work for 77 % and 70 % respectively. For 94 % of the total duration, there is at least one location operational, which is greater than the working percentage at the optimum position at Cape Morgan. At least two of the three locations are operational for 71 % of the duration, but all three areas operational only 38% of the time.

When comparing the use of all three locations compared to using only Cape Morgan, it is seen that the average KEF is lower for all locations making up only 69% of Cape Morgan's KEF. Therefore, there is more energy potential available using Cape Morgan, however, if a more constant supply of energy is required it could be more advantageous to implement hydro-kites at more than one location.

Table 4.13. KEF of ADCP locations for cut-in speeds or 0.8m/s and 1.0m/s for time series 2 from 2 April 2008 to 3 September 2010.

TIME SERIES 1	KEF		
LOCATION	CUT-IN SPEED = 0.8	CUT-IN SPEED = 1.0	% CHANGE
CM	2.07	2.06	0.68
EL	1.54	1.50	1.98
FR2	0.92	0.89	3.47
ALL (3)	1.42	1.40	1.69
ALL COMPARED TO CM: PERCENTAGE OF KEF	68.60	67.96	

Changing the cut-in speed from 0.8 m/s to 1.0 m/s can affect the 'working' results by up to 10 %. This can be seen in Appendix D. It must be taken into consideration the limitations of these calculations,

more accurate results could be obtained if more positions were investigated and if data was more consistent for longer durations.

4.8.2. Distributed points

An investigation into whether a distributed system of small individual hydro-kites compared with a concentrated farm at only one location was undertaken using the data provided by the factored HYCOM model. Data was extracted assuming one kite placed every kilometre between Port Edward and the Fish River where a total of 414 points were investigated. Due to the resolution of the model being significantly more than 1 km (approximately 8 km in each latitude and longitude direction) the same data serves for more than one location. The data was filtered to keep only entries which fell between the relevant cut-in and cut-out speeds to attain an accurate potential power output and fair estimate in the number of days operational.

All area segments between known locations have a high count of the number of days they cannot remain operational. This is congruent with the fact that Natal Pulses persist for a number of days within the same segment where lower velocities are experienced. Combining area segments results in a decrease of the days not operational. The days that each segment is not working occur at different periods along the coast as the Natal Pulse or meanders pass over and migrate southwards. Therefore, using all points between Port Edward and the Fish River would yield the least amount of days that the hydro-kites will not be operating.

It is required that a system is chosen to find a balance between power generation and days operational in order to maximise functionality.

4.8.2.1. Factored HYCOM

4.8.2.1.1. KEF

The average KEF using all points was far less than that calculated at the location with the highest velocity which was found near Morgan's Bay between Cape Morgan and East London. Using all the points yielded 64 % of the total possible KEF that could be achieved using the best location. The inclusion of more positions decreases the number of days that the system is not operational for but at a reduced KEF. Incorporating all points yielded an average KEF of 1.35 kW/m^2. Other areas south of East London produced lower average KEF values. The average KEF for the best location was 2.11kW/m^2. Using all points made up 95 % of the best site regarding working KEF which is significantly more than that calculated using the actual values. Observations of KEF and operationality are shown in Table 4.14.

4.8.2.1.2. Days Operational

Incorporating all points indicates that the kite system will not be operational for less than 1 % of the duration. However, in using only one location at Morgan's Bay, the location would not be operational

for 23 % of the duration, which is fairly significant regarding the demand for a constant power supply. The longest consecutive duration that no kites are operational for is one day using all locations and 14 days using the best site. The longest consecutive duration in which less than 25 % of kites are not operational is 7 days using all points.

4.8.2.1.3. Kites Operational

It is of importance to investigate the number of kites that would be operational within a distributed system as it may result in the least number of days not operational, but if for a large percentage of that duration only a few kites are operational within the system it would not be feasible. The factored HYCOM data set showed that 56 % of the time more than 75 % of the hydro-kites would be functional, 50 % of the hydro-kites would be operational for 82 % of the duration and at least one-quarter of the kites would be working for 96 % of the time. The percentage of hydro-kites that are functional and the relative percentage of the duration that they would be operational for is shown in Figure 4.50.

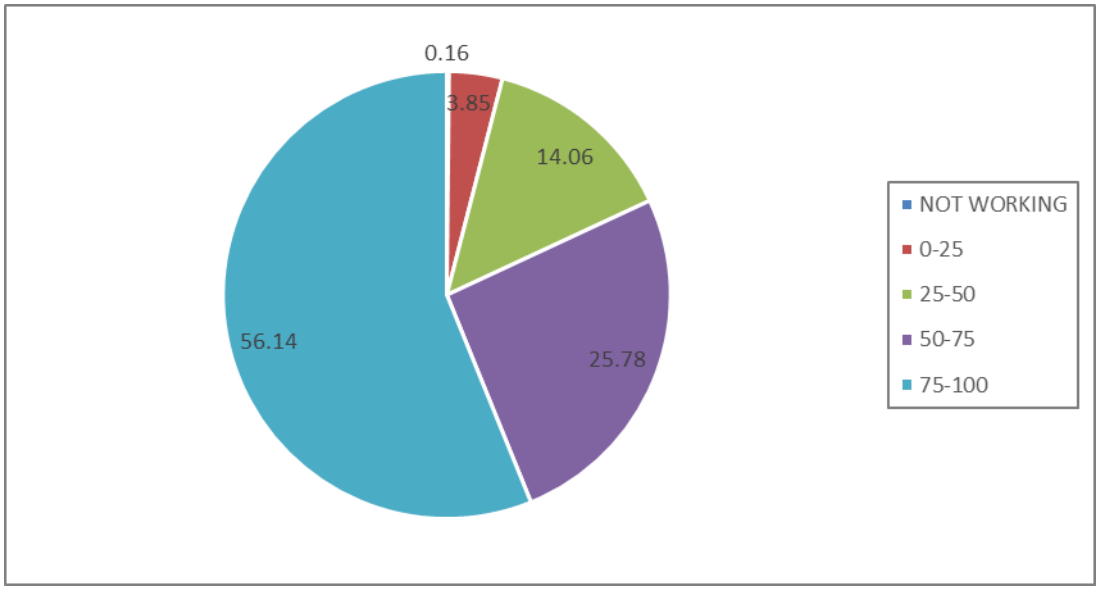

Figure 4.50. Percentage of the duration that kites will be functional for the corresponding percentage of kites working using the factored HYCOM data. (Factored/total)

There is much variability in the results between the factored and unfactored data. The factors were derived for short time periods where measured data was available, they may not be entirely accurate and it is possible that they may tend to overestimate the current velocities (or possibly underestimate them). It is known with certainty that the unfactored data tends to underestimate the current significantly and is of little value.

Table 4.14. The daily average KEF for each area segment and best point within the segment, and percentage of duration each segment or point would be inoperational for, using the factored HYCOM data set.

cut-in speed = 0.8	All Points									Best Point					
FACTORED HYCOM	Avg. KEF (kW/m^2)	Power (kW)	Not working (%)	0%<x<25%	25%<x<50%	50%<x<75%	75%<x<100%	Consecutive Days Inoperational	Consecutive Days Op.<25%	Avg. KEF (kW/m^2)	Power (kW)	Not working (%)	Consecutive Days Inoperational	KEF (%)	Working (%)
PE:CM	1.30	64.85	4.49	7.51	9.77	20.70	57.53	13	28	1.98	98.95	25.35	33	65.53	95.33
CM:EL	1.57	78.69	5.96	7.47	7.79	8.90	69.88	11	14	2.11	105.44	23.04	14	74.63	99.55
EL:FR2	1.34	66.81	7.79	7.95	6.63	12.48	65.16	19	22	1.99	99.72	18.24	22	67.00	91.94
EL:FR1	1.26	62.79	6.87	9.34	6.36	14.86	62.57	16	22	1.99	99.72	18.24	22	62.97	90.54
FR2:FR1	0.89	44.61	25.27	1.59	4.57	2.07	66.51	25	26	1.03	51.50	32.30	33	86.64	101.73
Total	1.35	67.61	0.16	3.85	14.06	25.78	56.14	1	7	2.11	105.44	23.04	14	64.13	95.23
PE:EL	1.39	69.49	1.07	6.40	12.40	22.29	57.85	4	9	2.11	105.44	23.04	14	65.91	94.85
CM:FR1	1.40	70.15	1.87	8.42	9.73	16.09	63.89	6	12	2.11	105.44	23.04	14	66.53	97.75
PE:FR2	1.38	68.84	0.24	4.29	13.47	24.59	57.41	1	7	2.11	105.44	23.04	14	65.29	95.54

The percentage of the KEF that using all points would achieve when compared to the best point from the area segment was calculated (KEF %) as well as the operational potential calculated without actual KEF values – working %. The percentage of time that the area would not be operating for was calculated (Not working %) as well as kite operationality above 0%, 25%, 50% and 75% compared with the percentage of time that the best point within the area segment that would not be functional. Average power was also calculated from the Loyd equation: average power values in the table are estimates of the average value taken as 50% of the calculated power.

4.8.2.2. Factored Reanalysis

The factored HYCOM Reanalysis can be used and compared against the factored HYCOM model to assess the results and determine if they correlate. This can attempt to provide a verification of the factors that were assumed for the HYCOM model that could not be calculated using actual data.

4.8.2.2.1. KEF

The average KEF in using all points is lower than that of HYCOM at 1.23 kW/m^2, the best location is located north of Cape Morgan yielding a KEF of 2.16 kW/m^2. The KEF calculated for the best location between Cape Morgan and East London is equal to that for the HYCOM data. The percentage KEF of the area segments compared with the best point in each is slightly lower than that calculated for the HYCOM model with slightly lower working percentages.

4.8.2.2.2. Days Operational

The number of days inoperational is greater than when compared with the factored HYCOM data; except for the case of using all points where there is no time at which no kites are operating. The best site between Port Edward and Cape Morgan is inoperational for 29 % of the duration, however, the best location between Cape Morgan and East London is congruent with that of the HYCOM data regarding both KEF and operationality. The best point will not be operational for 15 consecutive days

4.8.2.2.3. Kites Operational

There is a lower percentage of the duration where more than 75 % of the kites are working, compared to the other datasets. For only 48 % of the duration, more than 75 % of kites are operational, more than 50% of the kites are working for 80 % of the time, and over 25 % of the kites' function for 95% of the duration, this is shown in Figure 4.51.

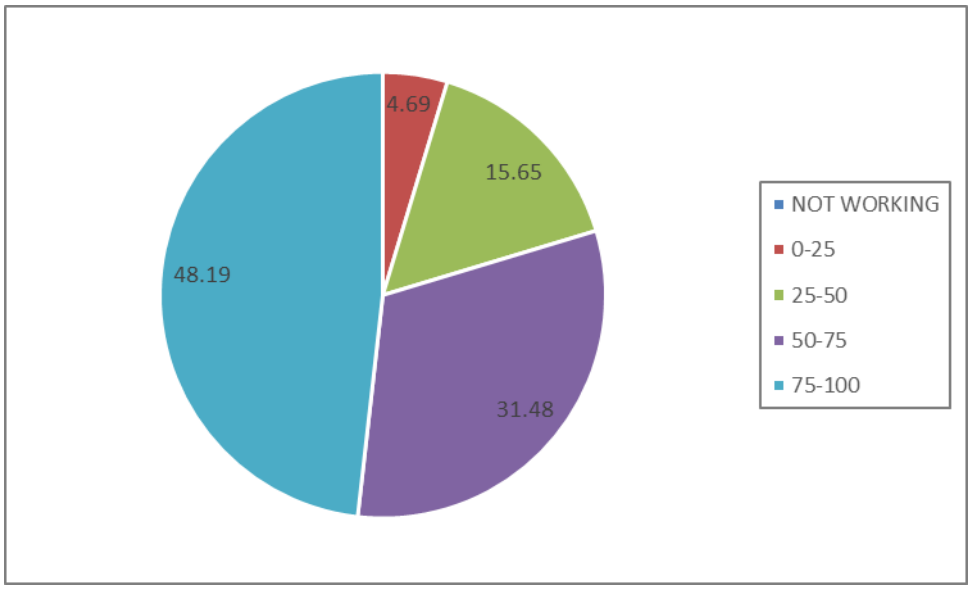

Figure 4.51. Percentage of the duration that a specific percentage of kites operates for using the factored HYCOM Reanalysis.

Table 4.15. Average KEF for area segments and best locations within segment, and percent of duration for which kites are inoperational, using data from the factored HYCOM Reanalysis.

cut-in speed = 0.8	All Points									Best Point					
FACTORED REANALYSIS	Avg. KEF	Power (kW)	Not working (%)	0<x<25%	25<x<50%	50<x<75%	75<x<100%	Consecutive Days Inoperational	Consecutive Days Op.<25%	Avg. KEF	Power (kW)	Not working (%)	Consecutive Days Inoperational	KEF (%)	Working (%)
PE:CM	1.29	64.34	2.10	8.56	13.10	33.73	42.51	5	15	2.16	108.21	28.63	15	59.45	91.95
CM:EL	1.33	66.68	6.86	7.75	8.27	13.51	63.62	12	15	2.11	105.45	22.69	13	63.23	95.08
EL:FR2	1.06	53.18	8.93	9.41	9.93	9.45	62.29	10	20	1.70	85.21	19.67	15	62.41	87.79
EL:FR1	1.05	52.57	8.15	10.55	8.89	12.44	59.96	10	20	1.70	85.21	19.67	15	61.69	87.68
FR2:FR1	1.00	49.78	24.94	0.37	4.65	0.96	69.08	22	22	1.08	53.86	26.90	26	92.42	95.81
Total	1.23	61.60	0.00	4.69	15.65	31.48	48.19	0	6	2.16	108.21	28.63	15	56.93	96.51
PE:EL	1.30	65.12	0.41	6.38	15.35	27.64	50.22	2	9	2.16	108.21	28.63	15	60.18	95.66
CM:FR1	1.18	59.10	2.66	8.89	10.85	19.26	58.34	5	14	2.11	105.45	22.69	13	56.05	92.95
PE:FR2	1.24	62.24	0.04	4.72	15.61	30.22	49.41	1	6	2.16	108.21	28.63	15	57.51	96.42

See Table 4.14. for notes.

4.8.2.3. Alternative positions HYCOM

The same number of points was extracted between the approximate locations as in the HYCOM dataset regardless of new positions and relative distances. The new locations offshore are to correspond with the actual positions. Therefore, the same number of points should be extracted.

4.8.2.3.1. KEF

The daily average KEF using all points within the system is similar to that experienced using the Reanalysis at 1.22 kW/m^2. The highest daily average of 1.68 kW/m^2 was found between East London and the Fish River offshore of Hamburg, this value is much lower than the best location from the other datasets. KEF values may be lower than those for the factored data due to the underestimation of current speeds. 73 % of the KEF at Hamburg could be achieved using a distributed system. This value is higher than that for the other datasets due to the lower KEF of the best location within the system where 89 % of the working capacity could be attained. Table 4.16 shows average KEF values and indicates operationality.

4.8.2.3.2. Days Operational

The analysis of the best approximate data yields the same outcome as the previous analyses in which using a distributed system results in the least time that hydro-kites are non-operational. No kites are working within the system for less than 1 % of the duration, whereas using the location near Hamburg, for 17 % of the duration no kites will be functioning. The longest duration of consecutive days where the entire system is not operational is 2 days using all locations and 24 days using the best position, where less than 25 % of the kites in a distributed system are not working for 13 consecutive days.

4.8.2.3.3. Kites Operational

Observing the chart in Figure 4.52, utilising all positions, it shows that for 56 % of the duration more than three-quarters of the hydro-kites are functioning, more than 50 % of the kites are working for 83 % of the time, and at least one-quarter of the kites are operating for 95 % of the time. This resembles the outcome of the factored results.

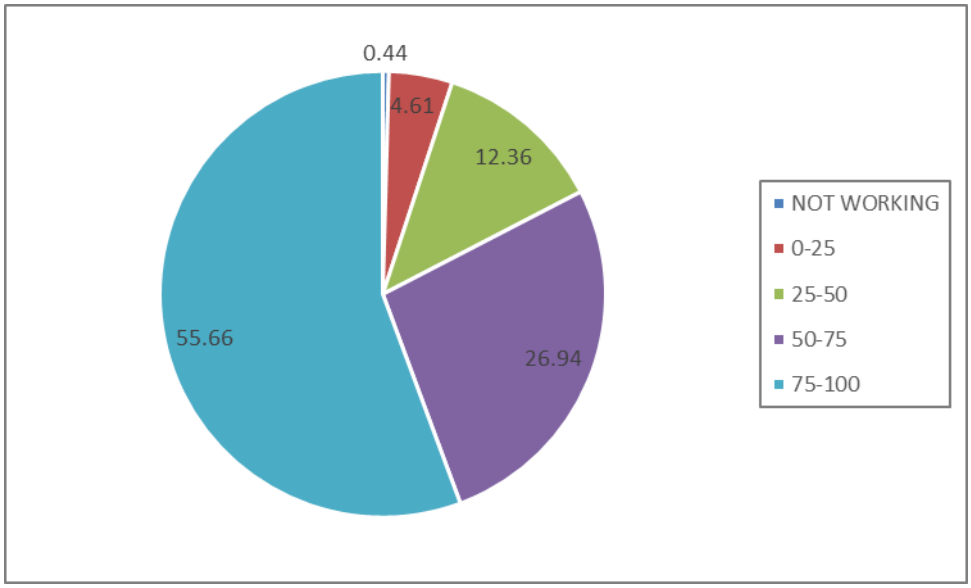

Figure 4.52. Percentage of the duration that the corresponding percentage of kites inoperational, using the best approximate locations extracted from the HYCOM model.

Table 4.16. Average KEF values calculated for area segments and best points within the segment, and percentage of duration each segment or point would not be working for using the data supplied from the HYCOM model at the best alternative positions, no factors were applied.

cut-in speed = 0.8	All Points									Best Point					
ALT HYCOM	Avg. KEF (kW/m^2)	Power (kW)	Not working (%)	0%<x<25%	25%<x<50%	50%<x<75%	75%<x<100%	Consecutive Days Inoperational	Consecutive Days Op.<25%	Avg. KEF (kW/m^2)	Power (kW)	Not working (%)	Consecutive Days Inoperational	KEF (%)	Working (%)
PE:CM	1.07	53.56	7.63	9.65	12.44	13.95	56.34	23	36	1.39	69.70	22.61	40	76.84	88.83
CM:EL	1.39	69.35	7.11	6.44	6.79	6.99	72.67	11	20	1.54	77.20	17.52	27	89.83	96.01
EL:FR2	1.40	69.91	6.79	5.88	6.67	6.83	73.82	18	20	1.68	84.17	17.20	24	83.07	96.63
EL:FR1	1.35	67.33	4.73	7.03	7.23	11.04	69.96	15	20	1.68	84.17	17.20	24	80.00	95.17
FR2:FR1	1.11	55.65	15.85	2.42	9.69	6.44	65.59	19	19	1.47	73.61	20.86	33	75.60	92.70
Total	1.22	61.23	0.44	4.61	12.36	26.94	55.66	2	13	1.68	84.17	17.20	24	72.75	89.48
PE:EL	1.18	58.86	2.38	7.47	12.95	21.53	55.66	7	24	1.54	77.20	17.52	27	76.25	87.60
CM:FR1	1.37	68.26	1.39	5.96	9.65	15.49	67.50	3	10	1.68	84.17	17.20	24	81.11	95.39
PE:FR2	1.23	61.53	0.68	4.77	12.59	25.59	56.38	4	10	1.68	84.17	17.20	24	73.11	89.53

See Table 4.14.for notes.

4.8.2.4. Distribution of Kite Operationality

The distribution of kite operationality was compared between the various models available and is seen in Figure 4.53. The alternative positions predict a larger percentage of kites operating for a longer duration, as does the factored HYCOM data. The factored HYCOM and Alternative points show a closer relationship regarding kite operationality over the duration. The Reanalysis tends to predict that higher numbers of kites will be functioning for shorter durations, and predicts kites operational for more time than the other models for all intervals except 90 – 100% where it drops well below the other models. The probability of non-exceedance for the percentage of kites operational is shown in Figure 4.54 for the various datasets.

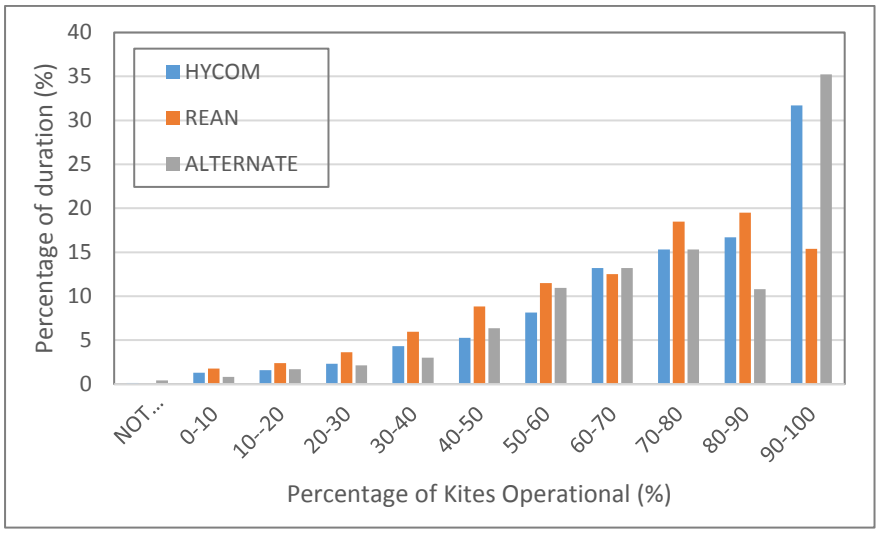

Figure 4.53. The distribution of kites working for certain percentages of the duration compared across the 3 datasets: factored HYCOM, factored HYCOM Reanalysis and the Alternate positions extracted from HYCOM.

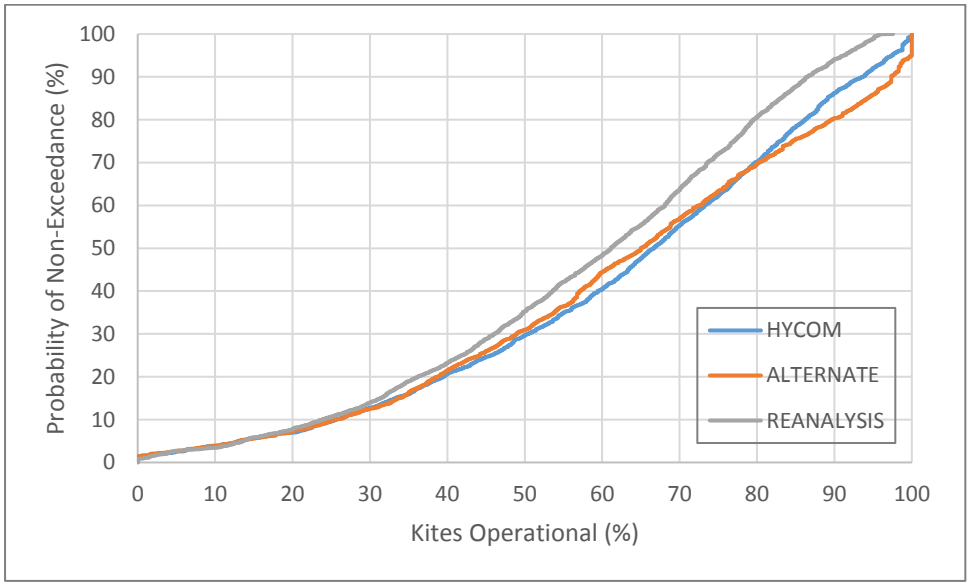

Figure 4.54. The probability of non-exceedance of working kites using all data sets i.e. there is an 80% probability that not more than 80% of the kites will be operational observing data from the Reanalysis.

Observing the distribution of percentage kites operating for the percentage duration for a cut-in speed of 1.0 m/s, there is a more even distribution with lower percentages of kites working for a longer duration and higher percentages of kites in operation for less of the time. However, the same relationships between the various data sets are held, this can be seen in the Appendix D.

Overall, it is seen that in using all locations, placing one hydro-kite per kilometre will not yield a KEF as high as using the best positions available, but it will result in a system that operates for a larger percentage of the duration. Therefore, it may be beneficial to implement a hydro-kite system designed for lower velocities to accommodate all points so they can operate efficiently, and a more constant supply of power will be able to be achieved in this manner.

Regardless of cut-in speed the percentage of KEF using all points relative to the best location did not alter significantly. The amount of KEF available for all points is lower than that for the optimum site which will always provide more power but has a more inconsistent nature. In general, using more locations increases the consistency of power supply, as adding more positions with energy producing potential at different locations decreases the duration that kites will not functional.

4.9. Potential Power

The hydro-kites can be designed to meet a stipulated desired power output. A 100 MW system would be able to generate enough electricity to supply over 112, 300 residential households accounting for approximately 0.35 % of the entire South African electricity consumption per year based on values from 2014 consumption. However, this is only achievable if the system operates at constant maximum capacity, actual energy generated will be much lower.

Due to the Loyd equation producing the theoretical maximum power that can be achieved and not the actual power. It is estimated that the power calculated would only account for approximately 50% of the maximum value (Olinger & Wang, 2015). Therefore, if the flight properties of the kite remained the same, the kite wing area would need to double in size to achieve the required power output, or scale the number of kites required by two as these are the only variable parameters. The factored HYCOM model is used for power calculations for concentrated and distributed systems.

4.9.1. Power of a Distributed System

The average KEF using all locations along the Agulhas from Port Edward to Port Alfred in a distributed system is 1.35 kW/m^2, determined from calculations using the factored HYCOM model dataset. The density of seawater is constant at 1027 kg/m^3. A C_L of 1 and a lift to drag ratio of 15 will be assumed.

A maximum power output of 250 kW is needed if 400 kites are used at intervals of 1 km to achieve a capacity of 100 MW. The wing area required to produce the desired maximum power is 2.11m^2, if fewer kites are used then larger kites will be needed at a larger spacing. Due to the presence of the Pondoland MPA, there is approximately 90 km within the proposed area that cannot be utilised. The location of other MPAs within the proposed usable region further restrict hydro-kite placement and spacing. Using hydro-kites with a wing area of 3m^2 would yield a maximum power output of 355 kW with an average power of 67.5 kW calculated from the average KEF using all locations. Approximately 282 kites would be required in a distributed system to attain a 100 MW power capacity. This is calculated assuming that kites within a line segment of the distributed array would at one time all be working to produce their maximum power output.

In reality, the previous assumption would not hold as the power generated at one location is not equal to that generated in another location within the same connected line. The maximum power output could be created by one kite but not necessarily by all at the same time as some kites within the line segment may not be in operation. Each line of hydro-kites within the distributed system will have the potential to produce different amounts of power due to the variability in ocean current velocity experienced along the coast. One line further north may produce more energy than a line located further south. The Agulhas current flows closer to the shore further north and separates more from

the coast as it moves south, different line segments will require different lengths of cable to connect them to the shore and therefore also different sizes. It is necessary to calculate the actual maximum load that could potentially be generated by each line of hydro-kites, designing each line segment for its specific load characteristics and distance offshore.

4.9.2. Power of a Concentrated System

Using only the location that experiences the highest velocities would require fewer hydro-kites to produce the same amount of electricity. The average KEF experienced at the prime location offshore of Morgan's Bay is 2.11 kW/m^2 from the factored HYCOM model. To produce a maximum capacity of 100MW would require 282 kites with an area of 3m^2. The area of the kite can be increased to produce the same power output with fewer kites, reducing the area of the kite farm. Increasing the area of the kite by a factor of 2 would produce twice the power using only half the number of kites. At this location with the highest current velocities, a 6m^2 kite could be used to generate a maximum of 710 kW of power requiring only 141 kites to attain the 100 MW maximum load capacity. The average power produced by one hydro-kite in this area is 211 kW. If the desired total energy output rather than the maximum capacity was 100 MW, 474 kites would be required with a maximum load capacity of 337 MW.

4.10. Cable Calculations

Various kite configurations and cable types should be investigated to determine the most feasible hydro-kite arrangement regarding power production, consistency of power, energy losses incurred as well as the overall economics of the project regarding material cost and installation. Cables with higher rated voltages reduce the current and the losses incurred but require more insulation which adds to the material cost. A compromise must be made regarding cable size, overall cable length and potential ohmic losses that would occur through the transmission process to find the best hydro-kite and cable configuration.

The technology available is limited, cables connecting the hydro-kites are restricted to an MV, only with the use of an offshore substation is it possible to increase the voltage to a high voltage (HV). The options remain to either incorporate an offshore substation that can use HV cables to the shore or connect the kites to land solely by the use of MV cables. Installing an offshore substation would increase the cost of the overall project but would reduce the number of cables required and the losses incurred. If only MV cables are used, long lengths of cable would be required, and losses would be slightly higher. An offshore substation can only be used with the concentrated array as a distributed array would need multiple substations at various locations which would not be economically feasible.

The length of cable needed to transport the power produced to the shore is assumed to be the distance from the site of the offshore hydro-kites to the shore with an additional 5 km allowed for transport on shore to a substation where the power can be fed into the grid system. The grid system and locations of substations must be examined to determine the most feasible installation locations regarding the distance to grid feed-in points.

4.10.1. Concentrated Array

One large hydro-kite farm is referred to as a concentrated array, it should be located at the best location, situated between East London and Cape Morgan near Morgan's Bay approximately 20 km offshore with high current velocities. To lower the cost of installation, larger kites can be used that produce more electricity which would reduce the overall material cost including that of turbines and step-up transformers, also reducing the area the farm covers, decreasing the extent of any possible environmental impact. The design assumptions for the concentrated array use a kite wingspan of $6m^2$.

The spacing between kites within the array is assumed at 150m. Due to ADCP EL305, which is closest to the best model location and shows a seabed depth of 90m. Kites are designed to fly at a depth of 20 m but with ocean current influencing the tether it would remain perpendicular to the seabed but at an angle and therefore required to be longer than 70 m to remain at a depth of 20 m below the surface. Kites are to be spaced at safe distances relative to each other to avoid interference, entanglement or damage. Therefore, a spacing of 150 m was assumed. Kite arrays must be thoroughly investigated regarding efficiency and ideal spacing to make use of blockage effects.

This location is found approximately 20 km from the shore. The total length from the array to its distribution point is assumed to be 25 km. The concentrated farm should be situated close enough to an HV substation for ease of grid access. Proximity to a substation reduces the length of overland cables required. Utilising the location with the highest velocities may produce more power but may incur more losses with regards to transmitting power through long length cables. A compromise could be made between sourcing a location that experiences relatively high ocean current velocities with a short distance to an electrical substation onshore.

There may be issues with this site as there is an MPA inshore of it so the connecting cables cannot be installed perpendicular to the shore. Cables must be placed to the right of the MPA to reduce the distance to shore. There is also a lack of substations in this region observing Figure 2.4. Therefore, cables over land must be used to connect to the nearest substations further south. Another promising location with a high KEF of 1.99 kW/m^2 further south should be used instead with shorter distances to onshore substations.

4.10.1.1. Option 1:

The first scenario to be considered is a concentrated hydro-kite farm near Morgan's Bay with the highest velocities observed. MV cables link the array to an offshore substation located close to the array approximately 200m away from the central most inshore point of the arrangement. The voltage is increased at the substation to a high transmission voltage which can transport electricity to the shore over a longer distance at a relatively small current thus minimising energy losses. The layout of options 1A and 1B can be seen in Figure 4.55 with option 1C in Figure 4.56.

A. Kite array 10 lines x 14 kites

The kite array is a rectangular configuration consisting of kites in a 10 x 14 formation. 140 kites are used producing a total of 99.4 MW which is taken as 100 MW as a margin of safety. The area of the concentrated farm is 2.63 km^2, 24 m of 24 kV 240 mm^2 conductor area submarine cabling is required to connect all hydro-kites to the offshore substation. A cable size of 95 mm^2 conductor area at a voltage of 36 kV is also suitable. The 24 kV cable has a slightly larger outside diameter, the difference between the conductor sizes is significant, but the 36 kV cable requires more insulation, so the difference between the outer diameters is not as significant. However, the weight of the 24 kV is substantially higher than the equivalent capacity 36 kV cable by almost one and a half times due to the larger conductor area of the 24 kV cable.

A high voltage cable of 170 kV with an area of 500 mm^2 is required for the connection from the substation to the shore over a distance of 25 km. The ohmic losses calculated throughout the entire cable arrangement are 2.43 % and 2.54 % of the total anticipated load for the 24 kV and 36 kV cables respectively. Other high voltage cables are also suitable for this array.

B. Kite array 12 lines x 11 kites

Kite array 1B is a similar concept to Kite array 1A except kites are arranged in a different formation. Kites are organised in a rectangular 12 x 11 configuration supplying more lines featuring fewer kites per line. An equal length of MV cable as in 1A will be required to connect the kites within the array to the substation. The reduction in the number of kites within each line results in a smaller cable size required compared to that in 1A.

This configuration incorporates 132 kites producing 7810 kW per line, taken as 7.9 MW generating a combined maximum of 94.8 MW of energy. The area of this farm is 2.48 km^2, only slightly smaller than kite array 1A. The length of MV cable required is 24 km, if the voltage of the cable is 24 kV a cable size of 150 mm^2 is needed. Another possibility is to use a smaller cable of 70 mm^2 conductor area at a higher voltage of 36 kV. Losses are calculated from the substation to the shore and are 2.94 % and 2.88 % using the 24 kV and 36 kV cables respectively incorporating the same 170 kV HV cable as in kite array 1A but with a size of 400 mm^2. The difference in losses between using the different MV cables is

relatively negligible. Both cable sizes are similar regarding overall outer diameter, but the weight of the 24 kV cable is 1.2 times higher than that for the 36 kV cable.

C. Kite array 8 lines x 17 kites

Kite array 1C uses 136 kites, an arrangement involving fewer lines to transport the load of more kites. This scenario will comprise of slightly less cable length when compared to the previous two but will require a larger cable size to transport the added load.

The area of the kite farm is 2.52 km^2, the cable size required is a 150 mm^2 conductor at a voltage of 36 kV over a combined length of 22 km. There is no conductor size at a 24 kV rating specified in the NEXANS catalogue with the capacity to carry the specified load. This scenario was tested using different HV lines and their relevant losses. Using one cable run at a voltage of 245 kV and conductor size of 240 mm^2 incurred a loss of 2.27 %, incorporating the same HV cable as used in kite array 1B of 400 mm^2 at a 170 kV rating produced slightly larger losses than the 245 kV cable at 2.64 %.

The sizing of HV cables is limited to the current capacity and not the voltage drop. A cable size of 630 mm^2 is also acceptable at a voltage of 145 kV for all scenarios, the 240 mm^2 245 kV cable is also suited and can be used in all Option 1 arrays. The 240 mm^2 245 kV cable has a very similar slightly lower outer diameter than both 400 mm^2 and 500 mm^2 170kV cables but the weight of both 170 kV cables is less than that of the 245 kV cable.

Only one HV cable is specified to transmit power to the shore, any possible damage that occurs to the cable would result in failure of power transmission to the shore where no energy would be available for use. To improve security of supply, two HV cables could be installed at safe distances apart to reduce the risk of damage to both. If one cable was damaged and unable to operate all the load would be placed onto the other cable so both cables must be designed for the maximum possible load. Losses would be less if two runs of HV cable are used as there would be half the current through each run of the cable. Ohmic losses are a function of the current squared so the loss in using two HV cables would be half the loss expected from using only one cable assuming cables are identical. The losses expected using 2 runs of 170 kV high voltage cable in kite array 1C would be 1.72 % of the total load generated.

All kite farms are relatively the same size due to the designed load to be transmitted. Kite farm area is not a limiting factor and should be neglected. Using Option 1 will result in low ohmic losses through the conductors. Cable lengths are restricted where less length is required due to the use of HV cables to the shore and MV cables are only needed in connections within the array. The cost of building an offshore substation must be investigated to determine the most economically feasible option. This overall configuration is suitable for potential expansion where kites can be added to the array and connected with additional MV cables to the substation. More HV cables to the shore would need to

be installed to transport the additional load to the shore if the initial design did not allow for expansion.

Table 4.17. Properties of cable configurations in Option 1 showing relative cable sizes, lengths and losses.

OPTION	1A			1B			1C		
DESCRIPTION	10 lines of 14 kites			12 lines of 11 kites			8 lines of 17 kites		
RUNS OF HV CABLE	1	1		1	1		1	1	2
FARM AREA (km^2)	2.63			2.48			2.52		
Load (MW)	100.00			94.8			96.8		
MV CABLE VOLTAGE (kV)	24	36		24	36		36		
MV CABLE SIZE (mm^2)	240 NEXANS	95 NEXANS		150 NEXANS	70 NEXANS		150 NEXANS		
MV CABLE LENGTH (km)	24.21			24.31			22.4		
HV CABLE VOLTAGE (kV)	170			170			245	170	170
HV CABLE SIZE (mm^2)	500 ABB			400 ABB			240 ABB	400 ABB	400 ABB
HV CABLE LENGTH (km)	25			25			25	25	50
MV LOSSES (kW)	918.95	1021.06		1094.55	1033.74		771.85		
HV LOSSES (kW)	1521.30			1708.99			1429.85	1781.86	890.93
TOTAL LOSSES (kW)	2434.40	2535.86		2787.54	2727.62		2200.09	2552.10	1661.17
PERCENTAGE LOSS (%)	2.43	2.54		2.94	2.88		2.27	2.64	1.72

NEXANS and ABB refer to cable brand.

4.10.1.2. Option 2:

This kite array is similar to that of Option 1 in that it consists of one hydro-kite farm using the same configurations as Kite array 1A, 1B and 1C. However, instead of an offshore substation with HV cables to the shore, only MV cables are used throughout to transmit energy to the shore. Farm areas and designed loads for all cases in Option 2 are identical to those for Option 1. The kite layout for option 2A can be seen in Figure 4.56 and the layouts for options 2B and 2C can be seen in Figure 4.57.

A. Kite array 10 lines x 14 kites

This layout includes 10 lines of MV cable that connect 14 kites each. The cables used in each line are 400 mm^2 conductor area at a rated voltage of 36 kV. The length of each line is 27 km, requiring an overall cable length of 270 km. Losses incurred are 4.85 % of the total energy produced which is

approximately twice that calculated for Option 1. This loss is due to the use of MV cables where the current is higher and losses are current dependent.

B. Kite array 12 lines x 11 kites

Connecting the kites as in Kite array 1B with the use of MV cables transmitting energy from the kite farm to the shore results in the use of smaller cable sizes compared to kite array 2A; requiring a 240 mm^2 conductor at a voltage of 36 kV. Due to the added cable lines, the required length of cable is much higher than that of Kite array 2A, the total length needed is 318 km. Losses are also greater than Kite Array 2A at 6.21 %, larger cable sizes could be used to reduce the losses but would increase the cost.

C. Kite array 8 lines x 17 kites

This scenario requires larger cable sizes compared to the other two with a conductor area of 630 mm^2 at the same 36 kV rating, but requires the least length of cable at 219 km. The losses experienced within this cable system are 3.81 %, lower than those experienced for kite array 1A and 1B.

This scenario involves the use of relatively large MV cables compared to Option 1 and requires long lengths of cable connecting the hydro-kites to the shore. If more kites are connected to each other within the area, the number of cable runs required to travel to the shore is reduced. However, this would increase the size of the cable required as larger cables would be necessary to transmit more energy over the distance to the shore to satisfy the voltage drop requirements.

There is the possibility for expansion where more hydro-kites could be added parallel to existing lines, but more MV cables would be required to transmit energy to shore. As stated previously, it would be impossible to add kites to existing lines unless the initial design incorporated future demand, as the permissible voltage drop would be exceeded which is not acceptable.

Table 4.18. Properties of cable configurations in Option 2 showing sizes, lengths and losses.

OPTION	2A		2B		2C
DESCRIPTION	10 lines of 14 kites		12 lines of 11 kites		8 lines of 17 kites
FARM AREA (km^2)	2.63		2.48		2.52
Load (MW)	100.00		94.80		96.80
MV CABLE VOLTAGE (kV)	36		36		36
MV CABLE SIZE (mm^2)	400 NEXANS		240 NEXANS		630 NEXANS
MV CABLE LENGTH PER LINE (km)	26.95		26.5		27.4
MV CABLE LENGTH (km)	269.50		318.00		219.20
MV LOSSES (kW)	4849.41		5886.53		3688.37
PERCENTAGE LOSS (%)	4.85		6.21		3.81

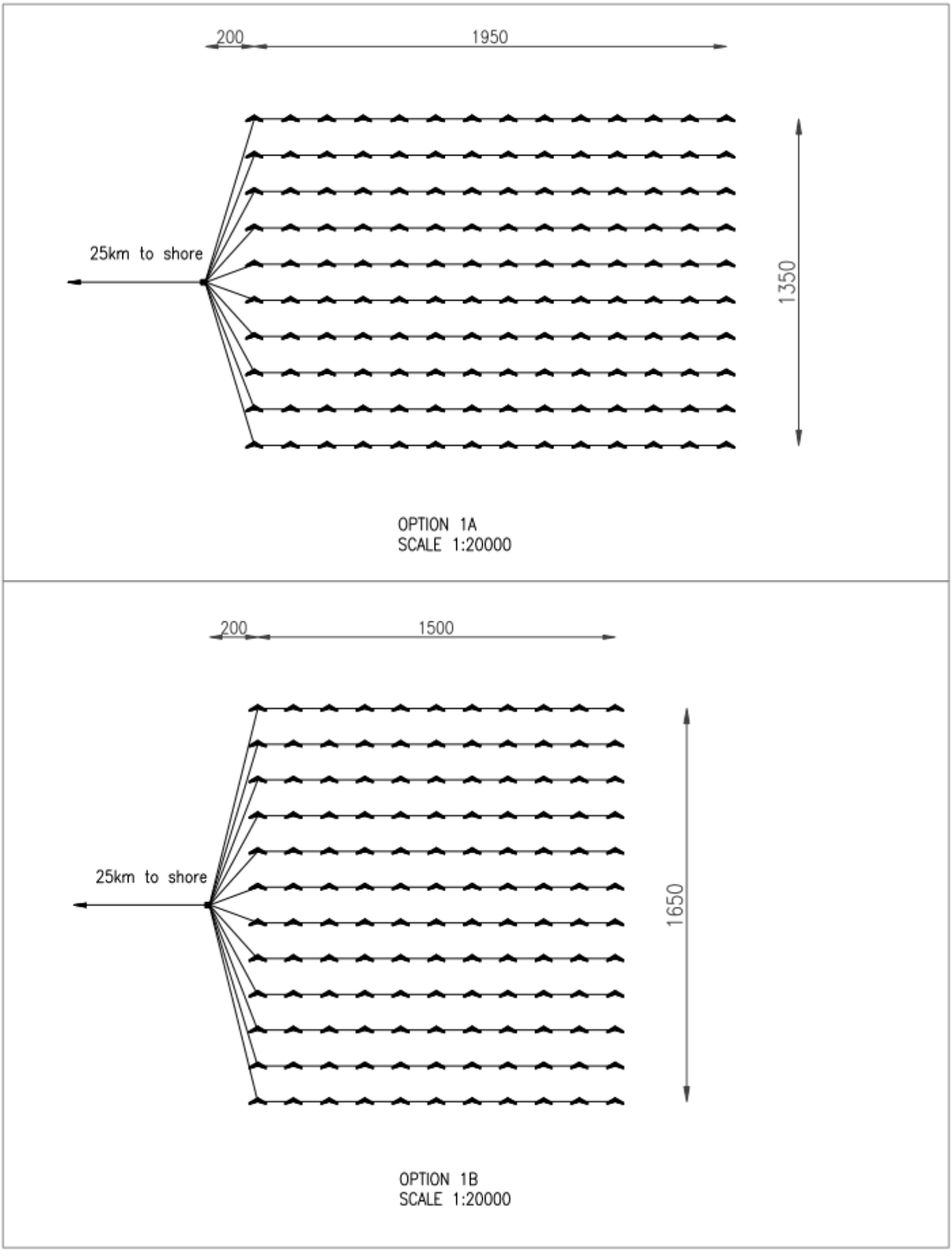

Figure 4.55. Layout drawing showing kite arrays for option 1A (top) and option 1B (bottom).

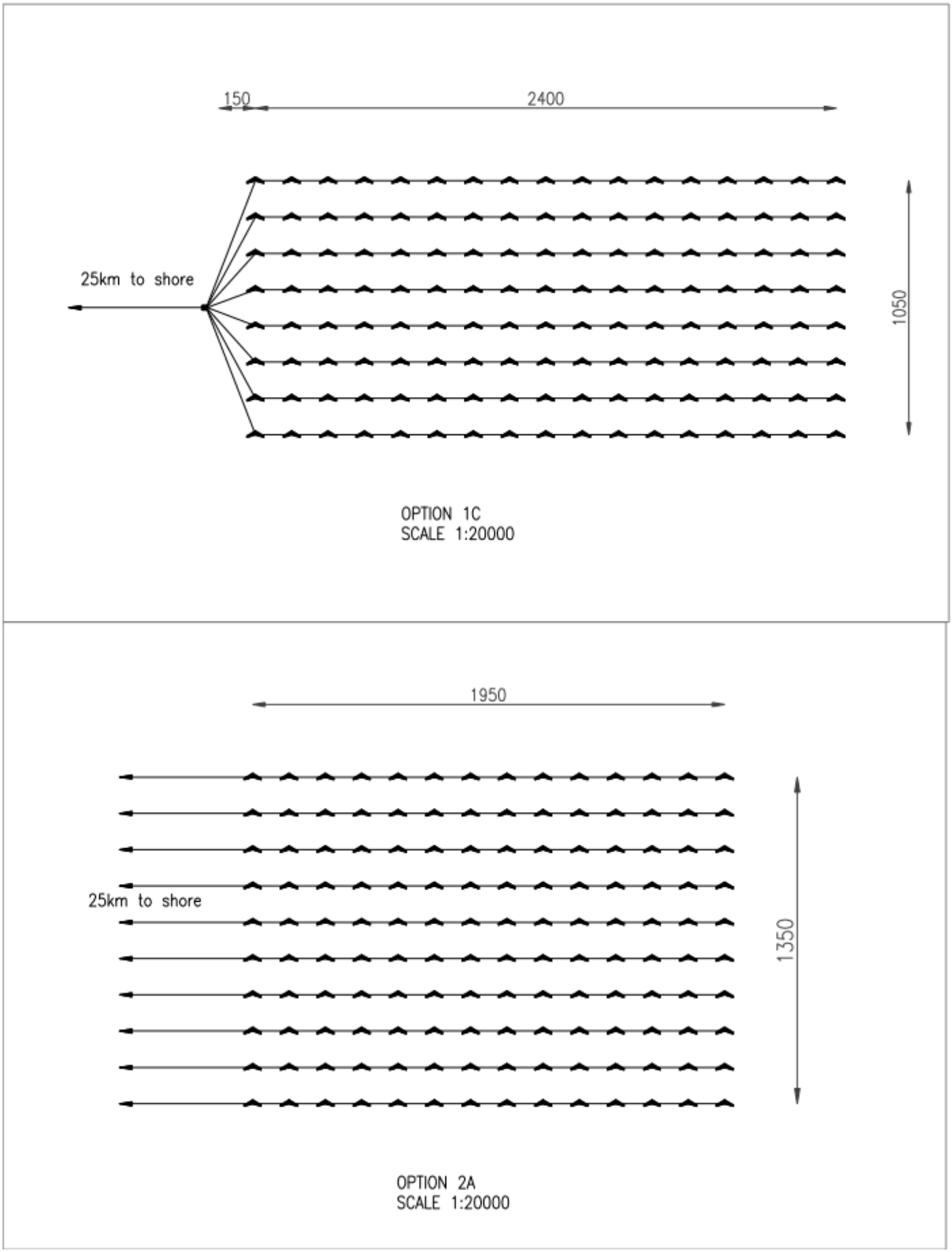

Figure 4.56.Layout drawing showing kite array for option 1C (top) and option 2A (bottom).

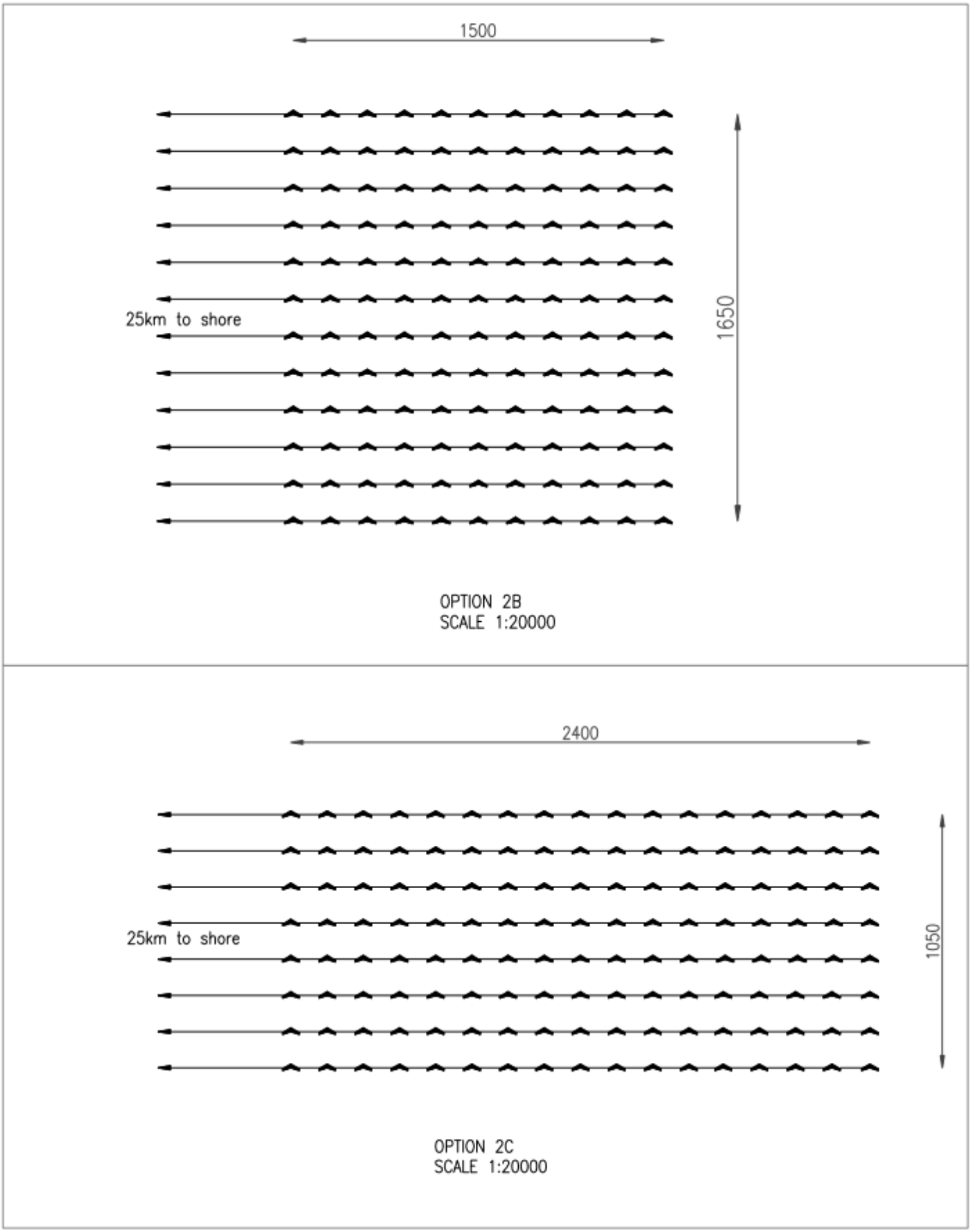

Figure 4.57. Layout drawing for kite array options 2B (top) and 2C (bottom).

4.10.2. Distributed Kite System:

The following scenarios involve a distributed system of smaller hydro-kites along the Agulhas current instead of one concentrated array. The distributed system is an attempt to provide a more consistent supply of energy in an effort to compensate for the effect of Natal Pulses. To produce the desired maximum power output as in the concentrated system, more kites are required which have a wing area of $3m^2$, each kite is capable of producing a maximum power of 355kW with an average power of 67.5kW per kite.

As the kites are spread over a long distance along the coast it is not feasible to incorporate an offshore substation. Therefore, MV cables are required to transport all energy to the shore. There are more kites involved in this system so there will be an increased cost in installation through both material cost for each kite as well as the expense of the cabling system and installation.

The number of kites required is dependent on the maximum power generated by the system at one time. To determine the maximum power that a line segment of kites can produce, all locations within that section must be investigated and the maximum power capacity must be determined. Approximately 340 kites are required within a distributed system to reach the 100 MW maximum power capacity. These calculations can be found in the Appendix D.

Kites were initially to be placed between Port Edward and the Fish River at a spacing of approximately 1 km, but due to the presence of a large MPA, kites can only be placed from Port St. Johns along the coast. There is also the presence of smaller MPAs along the coast within the placement area which must also be avoided. The location of the MPAs can be seen in Figure 4.58. The same number of kites can be placed along the coast from Port St. Johns to the Fish River at a reduced spacing. 340 kites can be situated along the coast with a spacing of 800 m between kites within line segments. The spacing between line segments may vary due to their positions and the attempt to avoid MPAs and find the shortest cable path to the shore.

4.10.2.1. Option 3:

All cable arrangements within Option 3 will not have the same requirements and will be designed specific to their maximum potential load and relative distance to the shore required. All cables used in the distributed system are at a 36kV rating.

A. Distributed Array: 10 lines to shore of 34 kites

This distributed array incorporates the use of 10 segments that transport the combined power output of 34 hydro-kites each to the shore, 340 kites are used in total. Each section consists of one MV cable

that runs to the shore with 17 hydro-kites connected on either side of it with one main cable from the centre to the shore. The distributed array can be seen in Figure 4.58.

The total design load capacity transported to the shore is 101 MW. The total length of cable required is 508 km where cable sizes and lengths can be seen in Table 4.19. The weighted average cable size used for this system is around 460 mm^2. The total losses for this system assuming the maximum load capacity is 6.11 %. The average power produced by one hydro-kite is approximately 72 kW, the total energy generated by this system arrangement is 214 GWh in one year that can potentially power just over 27, 000 homes assuming an average household consumption of 650 kWh.

Table 4.19. The total length and losses for the various size cables according to distance offshore and number of lines required for Option 3A.

OPTION 3A						
DESCRIP.	10 LINES 34 KITES EACH; SPACING 800m					
LINE NO.	LOAD (MW)	DIST. TO SHORE (km)	CABLE SIZE (mm^2)	CABLE LENGTH (km)	LOSSES (kW)	PERCENTAGE LOSS (%)
LINE 1	10	22	300	48.4	632.74	6.327405
LINE 2	9.5	21	240	47.4	691.73	7.28
LINE 3	9	19	150	45.4	921.69	10.24
LINE 4	11.5	18	240	44.4	842.52	7.33
LINE 5	9.5	18	150	44.4	963.83	10.15
LINE 6	10	26	400	52.4	554.76	5.55
LINE 7	10.5	28	630	54.4	419.62	4.00
LINE 8	10.5	29	630	55.4	433.15	4.13
LINE 9	10.5	31	800	57.4	368.08	3.51
LINE 10	10	32	800	58.4	346.70	3.47
Total	**101**			**508**	**6174.83**	**6.11**

Figure 4.58. Option 3A shows the electrical cable arrangement connecting hydro-kites positioned within the Agulhas current. One of ten main cables to shore transmits the power generated by 34 kites spread evenly on either side of the cable.

B. Distributed Array: 12 lines to shore of 28 kites

This scenario is similar to Option 3A comprising of 336 kites made up of 12 identical segments transmitting power of 28 hydro-kites each to the shore. Each MV cable to shore carries the combined energy output of each group of 14 hydro-kites connected on either side of it. The cable configuration can be seen in Figure 4.59.

Smaller cable sizes and longer cable lengths are required compared to Option 3A to carry the total design load of 102 MW. A total cable length of 551 km is required where sizes and lengths is shown in Table 4.20. The weighted average cable size is approximately 280 mm^2, less than that for option 3A. The total maximum losses experienced within this system are 7.4 %.

Table 4.20. The total length and losses for the various size cables according to distance offshore and number of lines required for Option 3B.

OPTION 3B						
DESCRIP.	12 LINES 28 KITES EACH; SPACING 800m					
LINE NO.	LOAD (MW)	DIST. TO SHORE (km)	CABLE SIZE (mm^2)	CABLE LENGTH (km)	LOSSES (kW)	PERCENTAGE LOSS (%)
LINE 1	9	21	185	42.6	756.29	8.40
LINE 2	8.5	21	185	42.6	682.60	8.03
LINE 3	8	19	120	40.6	860.71	10.76
LINE 4	9.5	18	150	39.6	891.92	9.39
LINE 5	8	18	120	39.6	821.39	10.27
LINE 6	8	21	150	42.6	753.65	9.42
LINE 7	8.5	26	300	47.6	515.89	6.07
LINE 8	8.5	28	300	47.6	552.01	6.49
LINE 9	8.5	29	400	50.6	431.60	5.08
LINE 10	8.5	30	400	51.6	445.28	5.24
LINE 11	8.5	31	400	52.6	458.96	5.40
LINE 12	8.5	32	500	53.6	381.65	4.49
Total	**102**			**551.2**	**7551.94**	**7.40**

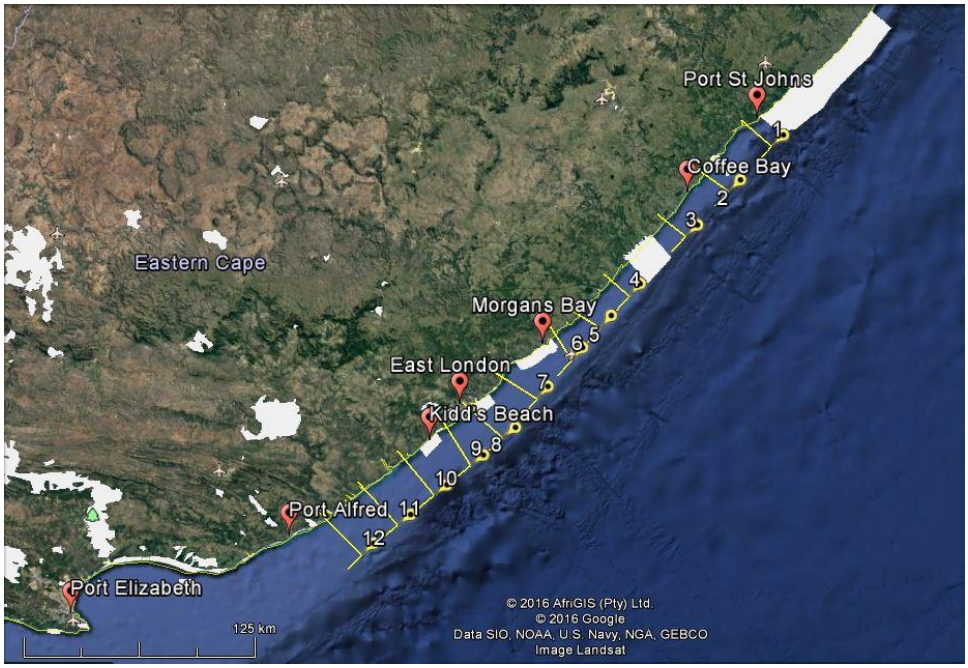

Figure 4.59. Option 3B shows the power cable configuration connecting hydro-kites located within the Agulhas current. One of twelve main cables to shore transmits the power generated by 28 kites spread evenly on either side of the cable.

C. Distributed Array: 8 lines to shore of 42 kites

Option 3C would consist of 8 cable segments carrying the power produced by 42 hydro-kites each to the land. Every MV cable carrying the combined energy to the shore transferring the power of the 21 hydro-kites located on both sides and the one central hydro-kite.

It is assumed that a line would carry approximately one-eighth of the load, 12.5 MW, over a maximum length of 30 km to the shore. A 1000 mm^2 cable fails the 5 % voltage drop specified, where the load could potentially be more than the assumed average for some segments. The 1000 mm^2 size cable is the largest cable size specified from the ABB catalogue. However, larger cables could be manufactured on request but would be costly. Therefore, this hydro-kite array and cable configuration are not viable.

It could be possible to combine segments of different scenarios: arranging a few cable segments of this high load capacity placed further north where cable distances to shore are lower, with other cable segments as those in options 3A and 3B that can handle the longer distances with smaller loads.

Another concept was investigated where the cable line linking the kites to the shore was not situated in the centre of the segment but at end, resembling an L-shape. The only difference between this scenario and those previously investigated is the losses; losses are much higher using this method due to the greater distance from the kites to the end location. Losses are limited in the previous systems with kites on either side of the main cable as intermediate losses are eliminated. The maximum distance from the shore in previous scenarios is the length of the cable to the shore and the length of half the cable segment. In the other approach the total length to shore is made up of the cable link to shore and the entire length of the segment which means more length to incur losses.

Distributed systems require long lengths of cabling compared to concentrated arrays of Options 1 and 2. These configurations require larger cable sizes to transport the load with an acceptable voltage drop. Losses are found to be much higher than the concentrated array in Option 1 that makes use of a substation and HV cables. There are limited opportunities regarding expansion. Entire new segments would need to be installed as kites cannot be added to existing cable lines as this would exceed the voltage drop limit. However, the system can be designed with potential expansion in mind, increasing cable sizes to facilitate the transport of more energy so that in the future more kites could be added to the line. Kites could be added between existing hydro-kites as the 800m spacing can allow for it, otherwise, kites could also be placed parallel to existing kites further inshore or offshore of them.

Increasing the number of cable lines to the shore results in less load per line segment so cable sizes can be smaller, but more cable length will be required. Using more segments increases the reliability, if one line is damaged the others will still be in operation.

Comparing all scenarios for a distributed system the best option would be Distributed Array 3B which attempts to find a compromise between cable size, cable length and the lowest losses incurred.

4.10.3. Concentrated arrays at distributed locations

Three main concentrated hydro-kite farms are to be used at the best locations within each segment that produce relatively high velocities: between Port Edward and Cape Morgan, Cape Morgan and East London and East London and the Fish River. The more southern Fish River locations were excluded due to an uncertainty of actual current velocities and lower velocities experienced further south. The position of Farm 1 is north of the ADCPs located at Cape Morgan and south of Coffee Bay, Farm 2 is situated near Morgan's Bay and Farm 3 is positioned near Hamburg. There is a distance of approximately 90 km between each location. The relative positions of the three farms is shown in Figure 4.60.

Observing the KEF values for each position from the HYCOM model it can be seen that kites at Farm 1 will be operational for 75% of the time, kites at Farm 2 will be working for 77% of the duration with kites at Farm 3 functioning for 82%. Overall, using the three farms limits the amount of time when no power is being produced to only 4% which is much less than when only the best location is used, which does not operate for over 20% of the duration. Farm 2 experiences the highest average KEF value, 2.11 kW/m^2. Farm 1 and Farm 3 also experience high ocean current velocities with an average KEF of 1.98 kW/m^2 and 1.99 kW/m^2respectively. The maximum capacity of a kite in this scenario is 710 kW for a 6m^2 kite.

4.10.3.1. Option 4:

Option 4 was investigated using different kite configurations, varying the number of kites and layout to determine the best outcome. Each farm is connected to the shore through a series of MV cables similar to that in Option 2 but applied to all three kite farms. The length of cable to shore from the offshore kite farm positions are approximately calculated: a distance of 20 km is used from Farm 1 to the shore, 25 km from Farm 2 to the shore and a distance of 35 km is approximated from Farm 3 to the shore. All distances incorporate extra distance for onshore transportation. The location of Farm 3 is predicted further offshore due to the course resolution of the HYCOM model from where the point was extracted. Farm 3 is approximately 5km further offshore than the distributed kite array line therefore, the distance to shore is more likely in the range of 30km.

In each scenario Farm 1 and 3 are designated to have fewer hydro-kites than Farm 2. All farm locations experience relatively the same power generation potential, Farm 2 being slightly higher than the others is selected to contain more hydro-kites. Kites positioned at Farm 3 are also further away from the shore than the other locations requiring more cabling and larger cable sizes to transport energy. All MV cables used in this scenario are of a 36 kV rating.

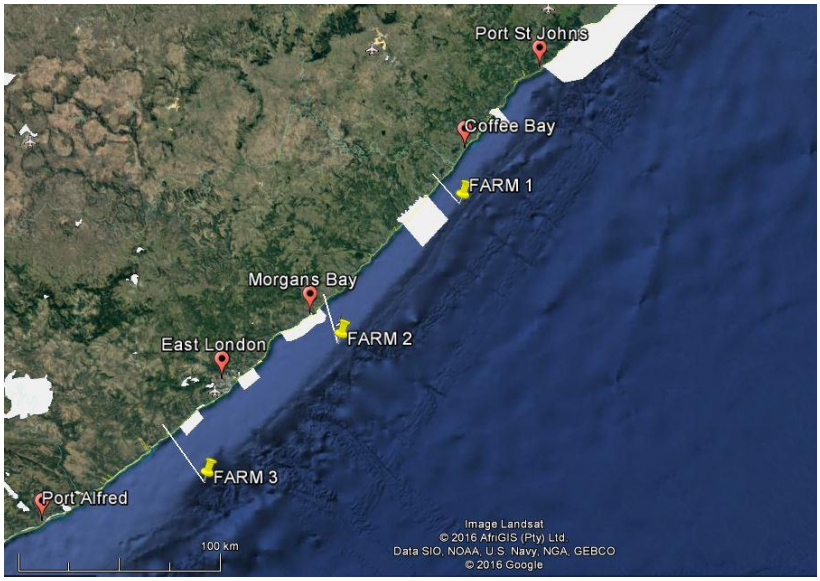

Figure 4.60. Map showing the relevant positions of the three kite farm locations within the Option 4 configuration

A. Farm 1: 4 x 11, Farm 2: 4 x 12, Farm 3: 4 x 11

Farm 1 is configured using 4 lines of 11 hydro-kites covering an area of 0.68 km^2. The cable size used is 150 mm^2 with a total length of 86 km. Farm 2 offshore of Morgan's Bay is also made up of 4 cables lines, each connects 12 hydro-kites, the area of the farm is 0.74 km^2, 240 mm^2 cables are required over a combined distance of 107 km. The third farm is the same configuration as Farm 1 with the same area, it requires much larger 500 mm^2 cables to transport the same energy as Farm 1 but over a longer distance of 146 km.

The total maximum power that this system is designed to transport is 97.6 MW from 136 hydro-kites covering a combined area of 2.09 km^2. The total length of MV cabling that is required is 339 km with a weighted average size of 329 mm^2 where losses are predicted at 6.36 % of the total anticipated load. The kite configurations for the various farms can be seen in Figure 4.61.

B. Farm 1: 5 x 9, Farm 2: 5 x 10, Farm 3: 5 x 9

Option 4B consists of Farm 1 and 3 again having the same configuration with 5 cable lines transporting the power of 9 hydro-kites each. Farm 2 also includes 5 cables lines that transport the power of 10 hydro-kites on each separate line. Farm 1 and 3 cover an area of 0.72 km^2, with Farm 2 making up 0.81 km^2. Farm 1 requires a 95 mm^2 cable at 36 kV over a total of 106 km, Farm 2 uses a 185 mm^2 cable

spanning a length of 132 km and Farm 3 requires an overall cable length of 181 km connected by a 300 mm^2 cable. The layout of the kite configurations for each farm can be seen in Figure 4.62.

A total maximum load of 101 MW can be transported by this system of 140 hydro-kites. The total area required is 2.25 km^2. A total cable length of 418.75 km is necessary to connect the farms to the shore with an average cable size of 212 mm^2. The losses incurred are 7.69 %.

C. Farm 1: 3 x 15, Farm 2: 3 x 16, Farm 3: 4 x 11

Option 4C attempts to use fewer lines connecting hydro-kites to the shore. Farm 1 uses only 3 lines transporting the load of 15 hydro-kites, a farm area of 0.63 km^2 is required with a 240 mm^2 cable over a distance of 66 km. Farm 2 also uses only 3 lines that connect 16 kites, a cable size of 500 mm^2 over a total distance of 82 km is needed, the farm size is 0.68 km^2. Farm 3 was initially designed to have the same configuration as Farm 1. However, the cable required to transport the required load over the specified distance exceeded 1000 mm^2 which is the largest cable available from the catalogue. Therefore, farm 3 was designed like that in Option 4A where 4 lines of 11 kites were used. The total area of the farm is the smallest of the three scenarios at 1.94 $km^{2,}$ the total length and losses are also the lowest at 294 km and 5.03 % loss using the total maximum load. However, this option uses larger cable sizes with an average cable size of 298 mm^2. Connecting more line with fewer hydro-kites that cable sizes are smaller but at the compromise of increasing the overall cable length and incurring slightly more losses. The arrangement of kites in each farm for this option can be seen in Figure 4.63.

There is a reduction in length of cable required when using Option 4 compared to Option 3 but similar when compared to Option 2. Ohmic losses are moderate and similar in comparison to those of Options 2 and 3 due to smaller cable sizes being used with higher resistances. This configuration increases the consistency of supply creating a compromise between the concentrated and distributed systems and should be viewed as a viable solution, offering benefits such as smaller cable sizes with reduced amounts of cabling required. Option 4 has the same potential for expansion as in Option 2 where lines can be added with hydro-kites parallel to existing lines, but hydro-kites cannot be added to existing lines unless initial design allows for expansion. Option 4A provides a system that attempts to compromise using less cable length and generating fewer losses but requires larger cable sizes.

Observing all cable configurations, utilising Option 1 would require the least amount of cabling and incur the least losses using an offshore substation and HV cables, but this is done at the expense of implementing that infrastructure. Option 2 makes use of small cable sizes and moderate cable lengths comparable to those of Option 4 with similar losses of a moderate magnitude, but does not possess the added reliability of Option 4. Losses predicted for Option 2B were the highest but can be reduced

by slightly increasing the cable size if necessary. Increasing the number of cable lines to shore reduces the cable size required but dramatically increases the length required. Option 3 required larger cable sizes over longer distances with similar losses to those of Option 4 but with improved reliability.

Load characteristics can be seen for all configurations in Table 4.21. The Sere Wind farm has a capacity of around 105 MW and it is predicted to produce 298 GWh in one year, which is not significantly higher than power estimations for the concentrated hydro-kite farms.

Table 4.21. Load characteristics of each cables configuration scenario and predicted power output.

OPTION		Total Load (MW)	Actual Power	Power in 1 year (GWh)	No. Homes	Percentage of Capacity (%)	No. Kites
	A	100	27.71	242.71	31117	27.71	140x6m^2
	B	94.8	26.12	228.84	29339	27.56	132x6m^2
1 and 2	C	96.8	26.92	235.78	30228	27.81	136x6m^2
	A	101	24.42	213.94	27428	24.18	340x3m^2
3	B	102	24.40	213.76	27405	23.92	336x3m^2
	A	97.6	27.60	241.82	31002	28.28	136x6m^2
	B	101	28.42	248.99	31922	28.14	140x6m^2
4	C	101	27.80	243.55	31224	27.53	137x6m^2

Table 4.22. Properties of cable configurations for Option 4 showing cable sizes, lengths and losses for each arrangement.

OPTION	4A					4B					4C				
FARM	1	2	3			1	2	3			1	2	3	3	
DESCRIP.	4 LINES 11 KITES	4 LINES 12 KITES	4 LINES 11 KITES	TOTAL		5 LINES 9 KITES	5 LINES 10 KITES	5 LINES 9 KITES	TOTAL		3 LINES 15 KITES	3 LINES 16 KITES	3 LINES 15 KITES	4 LINES 11 KITES	TOTAL
FARM AREA	0.68	0.74	0.68	2.09		0.72	0.81	0.72	2.25		0.63	0.68	0.63	0.68	1.94
LOAD(MW)	31.6	34.4	31.6	97.6		32.5	36	32.5	101		32.1	34.2	32.1	31.6	101
LOAD PER LINE (MW)	7.90	8.6	7.90			6.5	7.2	6.5			10.7	11.4	10.7	7.9	
CABLE VOLTAGE (kV)	36	36	36			36	36	36			36	36	36	36	
LENGTH TO SHORE (km)	20	25	35			20	25	35			20	25	35	35	
CABLE SIZE (mm^2)	150	240	500			95	185	300			240	500	exceeds 1000	500	
CABLE PER LINE (km)	21.5	26.65	36.5			21.2	26.35	36.2			22.1	27.25	37.1	36.5	
CABLE LENGTH (km)	86	106.6	146	338.6		106	131.75	181	418.75		66.3	81.75	111.3	146	294.05
LOSSES PER LINE (kW)	630.77	582.49	338.33			663.91	528.65	361.16			730.42	510.94		338.33	1579.69
TOTAL LOSSES (kW)	2523.08	2329.96	1353.32	6206.36		3319.54	2643.23	1805.81	7768.58		2191.25	1532.81		1353.32	5077.38
PERCENTAGE LOSS (%)	7.98	6.77	4.28	6.36		10.21	7.34	5.56	7.69		6.83	4.48		4.28	5.03

All cables sizes are based on NEXANS

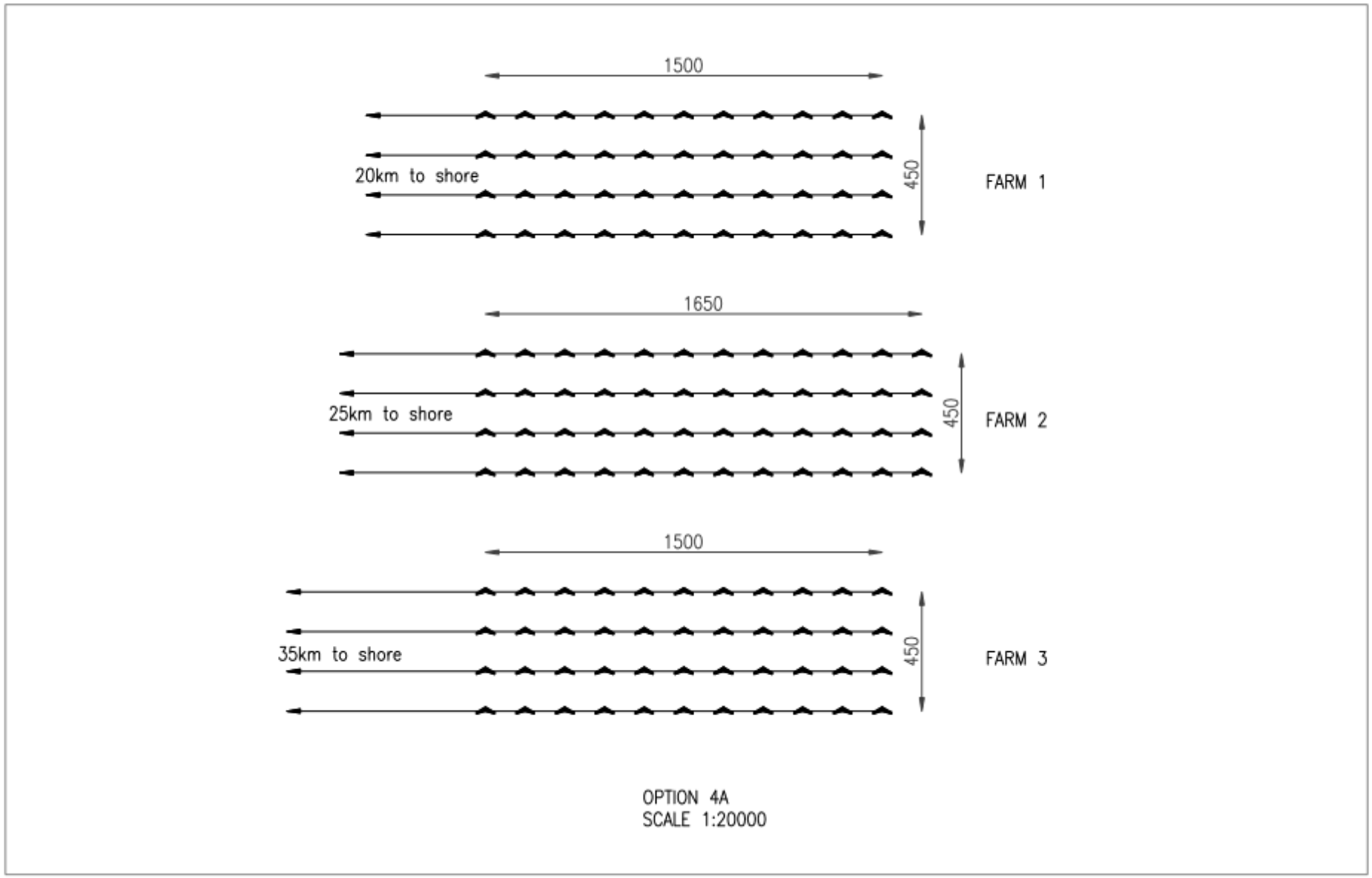

Figure 4.61.Layout drawing showing the kite configuration for each farm in option 4A.

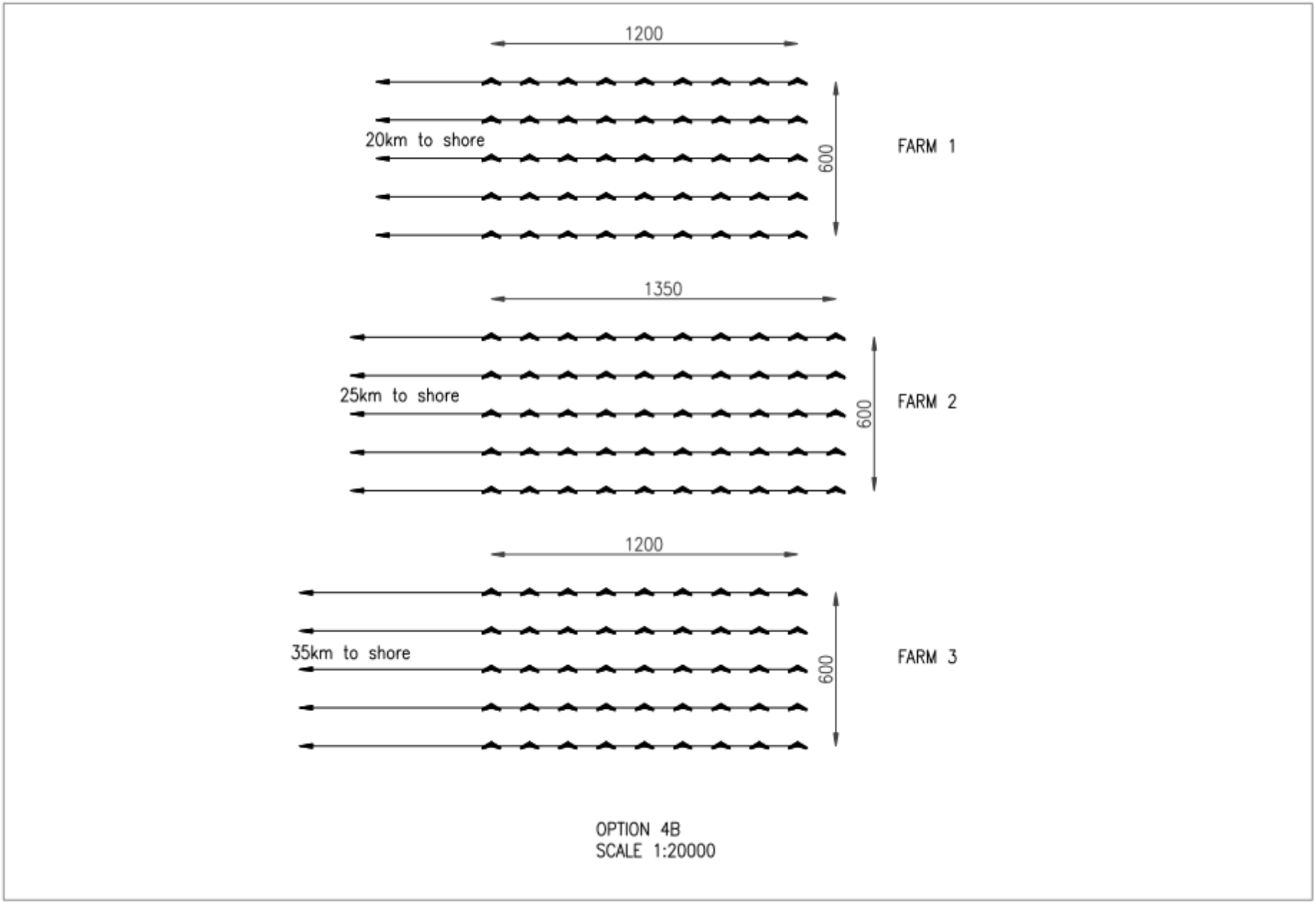

Figure 4.62.Layout drawing showing the kite configuration of each farm in option 4B.

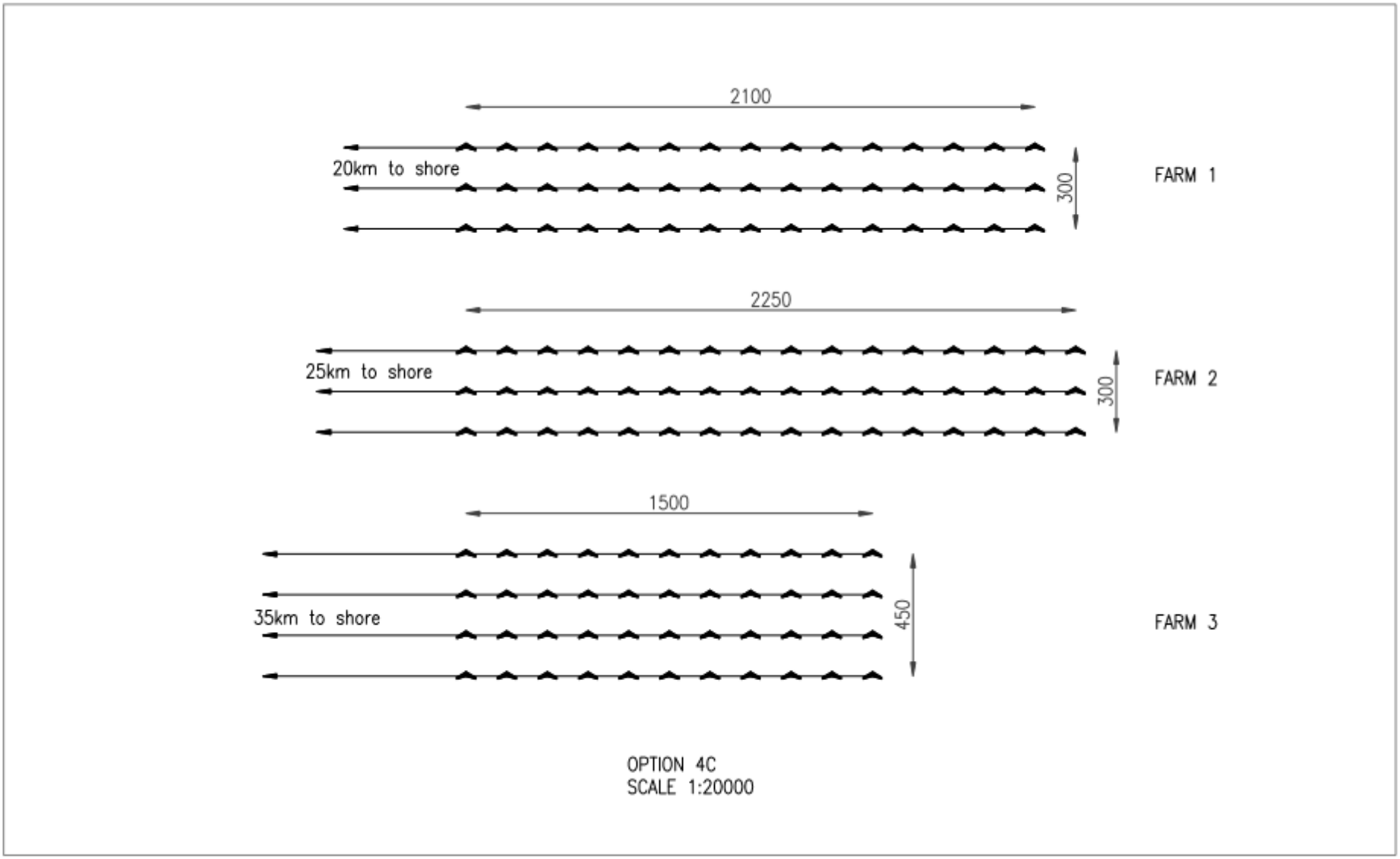

Figure 4.63.Layout drawing showing the kite configuration for each farm in option 4C.

4.10.4. Kite Array Efficiency

All configurations in the concentrated system were made up of multiple rows of hydro-kites in a centred arrangement at an equivalent spacing between turbines and between rows. Staggered arrangements appeared to generate more power than centred arrays for large stationary tidal turbines. Using one single row of turbines yielded the highest power, but it is not applicable to hydro-kite arrays as many kites are required. It may be more advantageous to stagger the hydro-kites instead of using a centred arrangement which would require offsetting every alternate row of kites by half a kite spacing further offshore for potentially more power production (Draper & Nishino, 2013).

The distributed array consists of small single centred kite devices spaced approximately 800m apart. The distance between the kites may be large enough, and the resistance to the flow and effects upstream may not be significant enough to cause a disturbance further downstream and affect the flow stream around those kites. However, to determine the efficiency of this configuration this must be investigated to determine the flow field around single centred kites and at what distance apart will kites have an impact on each other.

Large stationary marine turbine devices and their arrangement will offer different resistances to flow at a local level involving single turbine devices as well as at a global scale regarding the entire array. The outcomes of investigations into efficiency and optimal arrangement of large tidal turbines cannot be directly applied to small hydro-kite systems. Hydro-kites are of a much smaller and lighter design offering less resistance, they are constantly moving within a “figure of 8” shape influencing a greater area. The flow stream will be disturbed by the hydro-kite movements. The resulting wake region will vary compared to that of larger stationary turbines. The size of the system may have a significant impact, where effects might not be as great as those experienced in the larger stationary turbine systems.

Hydro-kite arrays need to be investigated to determine the optimum inter-kite spacing as well as the spacing for using multiple rows, investigating their local blockage, wake mixing effects and overall efficiency. Models should be developed, simulating the flow field around individual kite systems and the entire array.

4.10.5. Link from Kite

The maximum load that the $3m^2$ kite is capable of producing is 355 kW, assuming 360 kW as a safety measure. The length of the tether is taken as 150 m to account for the effect of current velocity on the tether, which will have to be verified. The voltage of the cable is dependent on the voltage at which the turbine generates energy which is an LV usually less than 1 kV. Submarine cables are armoured for protection which adds weight to the cable, this is advantageous when cables are laid on

the seabed and need to resist imposed forces. However, this is a disadvantage in the tether as the kite must then support the added weight. The tether cable was designed using both the armoured and unarmoured cables available.

A kite of wing area $3m^2$ with a thickness of 0.2 m is capable of supporting a load of 616.2 kg by displacement. The thickness of the kite is kept low to be aerodynamic, increasing performance and efficiency while minimising drag. A 315 kW 10000 rpm high speed brushless permanent magnet synchronous motor is available that runs at a voltage of 380 V with a current of 506 A, a maximum power of 450 kW and a weight of only 180 kg providing a ratio of 0.57 kg per kW generated. The weight of the on-board turbine is taken as 200kg in calculations. The maximum weight of the cable tether for this kite is 416.2 kg. The buoyancy force of the tether itself is not significant due to its small volume. The self-weight of the kite wing and nacelle have not been factored into calculations, but should be small due to small kite size and the use of lightweight material.

4.10.5.1. Armoured Tether Cable

The design of an armoured LV cable for the tether at a voltage of 1 kV requires a large 300 mm^2 cable to satisfy the current capacity. The cable weighs 1476 kg with an overall diameter of 65 mm. This cable does not satisfy the weight requirements and will not be able to be supported by the hydro-kite. The thickness of the kite required to support the weight of the cable is 0.55 m which would compromise the kite's flight properties and ability to generate power. Increasing the voltage of the cable would decrease the current to allow for a smaller cable to be used. The largest cable that can be used to satisfy the weight restrictions while keeping the kite dimensions constant, is a 70 mm^2 cable with a weight of 360 kg for a length of 150 m. This cable which would allow for an additional weight of approximately 50 kg. The voltage required to use this cable is 2.2 kV, due to the increase in voltage the cable used would need additional insulation which would add weight. The size required for a 1 kV cable cannot be supported by the hydro-kite. It is, therefore, impossible for a cable with a voltage of 380 V at which the specified turbine produces energy to be supported by the kite without changing its dimensions.

4.10.5.2. Unarmoured Tether Cable

The design of the tether cable using an unarmoured cable does not alter the cable size required, the only differences are the overall cable diameter and the weight. The weight of the tether required is 1361 kg for a 150 m length which is still inadequate for the kite to support it. Modifying the kite thickness to support the weight would require a depth of 0.51 m. The voltage required to use the 70 mm^2 unarmoured cable at a weight of 330 kg for a length of 150 m calculated as for the armoured cable is 2.2 kV. There is not a significant difference between using an armoured cable opposed to using an unarmoured cable.

4.10.5.3. Two Armoured Tether Cables

Another alternative to reduce the weight of the tether cable is to use two smaller cables and bind these together within a tether material. A current capacity of 208 A is required per cable. A 95 mm^2 cable operates at a current carrying capacity of 205 A with a total derating current of 232 A. The total weight of the tether using two cables is 960 kg which is less than using one larger cable but is still too heavy to be supported by the kite unless the kite thickness is adjusted to 0.38 m. To meet the weight requirement two 35 mm^2 cables would need to be used having a combined weight of 405 kg. The voltage required for these cables is 1.7 kV, but due to the added insulation required for higher voltage cables, the weight would probably increase above the maximum allowed weight. Therefore, two cables of a smaller size may be required at a higher voltage than 1.7 kV. Two 25 mm^2 cables weighing a combined 315 kg can be used at a voltage of 2.1 kV allowing for extra weight from insulation. The ohmic losses in using two cables instead of one are slightly higher by approximately 1 %, however, losses calculated are small.

Table 4.23. Properties of tether cables.

LINK	ARMOURED	UNARMOURED	2 CABLES ARMOURED
LOAD (kW)	360	360	360
LENGTH (m)	150	150	150
VOLTAGE (kV)	1	1	1
CABLE SIZE (mm2)	300	300	2 x 95
CURRENT (A)	416	416	208
WEIGHT (kg)	1476	1361	960
OVERALL DIAMETER (mm)	65	62	2 x 33
LOSSES (kW)	5.96	5.96	9.57
LOSSES (%)	1.66	1.66	2.66
KITE DEPTH REQ. (m)	0.55	0.51	0.38
CABLE SIZE REQ. (mm2)	70	70	2 x 35
WEIGHT (kg)	360	330	405
VOLTAGE REQ. (kV)	2.2	2.2	1.7
LOSSES (kW)	5.49	5.49	8.99
LOSSES (%)	1.53	1.53	2.50

HMPE is a tether material used in many TUSK systems. However, it is necessary for this system that the tether incorporates a power cable to transport power generated from the on-board turbine to the sea-bed. A cable could be embedded in a suitable tether material with adequate insulation properties. It is recommended that the tether weight not be in excess of more than 5% of the total kite weight

(Olinger & Wang, 2015). However, in this scenario, the LV submarine cable will have a large weight at a low voltage. The kite is small and will not have a significantly larger weight than that which it supports. The interactions of small size kite devices and tether systems must be further investigated to design an efficient connection.

A tether with an overall diameter of around 60 mm can make up 60 % of the drag force with a length of 100 m (Olinger & Wang, 2015). The diameter is approximately 10 mm using a 70 mm^2 cable, but the heavy weight of the cable may add to the drag experienced.

4.10.5.4. Low Voltage Step-Up Transformer

It is impossible for a cable tether to be supported by the small 3m^2 hydro-kite at a low voltage at which the turbine produces energy. The system could be feasible if a step up transformer is attached to the turbine, stepping up the voltage at the source in order to decrease the current and allow for smaller cable sizes to be used at reduced weights. However, the step up transformer would add increased weight to the system as it would be made of a metal core with wire around it. The voltage would then need to be increased above that calculated in order to compensate for the additional weight.

4.10.5.5. Buoyancy System

Alternatively, to reduce the need for a step-up transformer onto the kite which would add cost and weight, a buoyancy system could be implemented in either the kite's wing or the tether cable itself where it would be able to support its own weight not relying on the kite to support it.

4.10.5.6. Hydro-Kite without On-Board Turbine

The cable link from the hydro-kite system can be eliminated by either placing the turbine on the seabed or a floating buoy as described in Chapter 2. Potential power output will be reduced as the turbine is stationary and additional power is required to reel in the tether.

4.11. Economics

The requirements of the hydro-kite wing are that it is lightweight and of sound, unyielding design. Small hydro-kite wings can be low technology devices which could be manufactured in a labour intensive manner, avoiding the need for large and expensive machinery. The small kite wing can be manufactured using moulds, requiring unskilled labour that can be locally sourced. Larger kites may be more complicated to produce due to their larger size making them more difficult to handle and potentially requiring more time and more proficient skill as well as expensive machinery.

Long-term jobs are also set up to operate and maintain the project over its lifespan where people from local communities can be taught the relevant skills they require. This project could, therefore, have a positive effect on skills development. Projects appear more attractive to government involvement and investment if they can improve social conditions.

Due to the small size of the kite as well as its weight, maintenance can be performed by small boats. People from the local surrounding communities can be trained with regards to hydro-kite maintenance where they could commandeer small boats and perform repairs on site. Larger kites in a concentrated area might require the use of larger vessels that cannot be captained by unskilled persons. The maintenance would, therefore, need to be outsourced to a private company. A distributed system of smaller hydro-kites would allow for job creation regarding operation and maintenance where technicians are trained and are designated a certain number of hydro-kites in a region which they maintain.

Submarine power cables and their installation are expensive. The amount of cabling should be minimised to reduce costs substantially. Concentrated hydro-kite arrays require less cable length when compared to the distributed systems. It is advisable to transport a considerable amount of power from the kite farm to the shore in order to warrant the high expense of submarine cables as the installation of the cables is costly. It may prove better to install larger cables at an increased cost which can transmit larger amounts of power, therefore, warranting the high cost and making the system more economical.

It can be predicted that the use of fewer hydro-kites in a concentrated system can potentially incur less capital cost due to fewer elements being required: turbines, step up transformers, seabed anchors. Concentrated arrays require reduced lengths of submarine cabling which has high purchasing and installation costs. However, smaller kites can be manufactured and handled more easily than larger kites by unskilled local labour. Operation and maintenance of smaller kites has a higher potential for job creation which is critical in a country with such high unemployment rates and can improve the socio-economic situation in local communities. Initial capital costs may be higher in a

distributed system of small hydro-kites, but there is a greater potential for local job creation, community involvement, acceptance of the project and government interest and participation.

Due to uncertainty, risk and the high capital investment required in the marine energy market, a pilot project should be set up with a small kite array. The location for the pilot study could be near Morgan's Bay where high ocean current velocities are experienced, alternatively, sites should be investigated near East London close to onshore substations. The ocean current velocities in these regions should be confirmed with in situ ADCP measurements to verify the model predictions. The pilot study could incorporate two small kites and two larger kites to test the performance of each, this would provide a maximum capacity of 2.13 MW. Assuming the pilot study is successful the system can be expanded into a larger concentrated array as seen in Option 2. If the concentrated array is successful and the benefits of the renewable energy project are realised the project can be expanded further. Benefits of the project will include economic gain with return on investment as well as the upliftment of local communities with regards to development, job creation and access to electricity which will improve living standards.

A distributed system of hydro-kites along the coast may be branded as a higher risk due to the requirement for more infrastructure and material cost as well as the time required for construction and installation. However, the distributed system offers advantages over that of the concentrated system in terms of improved energy consistency. The project, dependent on the success of the previous phases, could then be extended to incorporate a distributed system in conjunction with the concentrated array, or more concentrated farms as in Option 4 could be incorporated The distributed system can act as more of a baseload power due to its higher consistency with the concentrated array capable of producing more energy but at a fluctuating intermittent level.

4.12. Kite Design

The dynamic loading of a TUSK system is considerably larger than that for an equivalent marine turbine or wind turbine, results can be seen in Appendix F. The type of wing design investigated is a swept and tapered wing as there are fewer limitations on design. The use of an untapered wing may present poor stall characteristics. Longitudinal stability can be created by adjusting the sweep angle and the amount of twist required. A swept wing is capable of efficiently operating over different speeds if the C_m is approximately zero and only a small twist is required. Any airfoil can be used with this wing design, due to swept and tapered wings having a high loading at the wing, an airfoil with a slight camber with a little reflex and small twist angle should be used. The airfoils investigated were symmetrical airfoils which incorporated a C_m of zero at 0° lift and slightly reflexed airfoils with small amounts of camber.

Four different kite designs of $1m^2$ area were designed varying the dimensions attaining different aspect and taper ratios for each. The amount of twist required for each design was calculated using different airfoils, this can be seen in Table 4.24 for airfoils: NACA 0009 and NACA 22112. The results for Kite 1 are shown in Table 4.25. Results for the other kites can be found in Appendix F. The various kite designs can be seen in Figure 4.64.

Table 4.24. Design parameters of various kite designs including twist and $C_{L\,max}$ calculated for airfoils NACA 0009 and NACA 22112.

	Design Parameters			NACA 0009		NACA 22112	
KITE ID	AR	PFW	z	ALPHA	CL max	ALPHA	CL max
KITE 1	5.65	28.90	0.42	-12.47	1.33	-11.43	1.25
KITE 2	8.57	20.97	0.75	-9.46	1.03	-9.46	1.05
KITE 3	9.23	16.26	0.86	-10.98	1.18	-10.98	1.21
KITE 4	16.00	9.93	1	-8.19	0.90	-8.19	0.93

For small c_m, observed in most of the investigated airfoils, the amount of twist required becomes more dependent on the PFW and predominantly the AR. A high AR can result in less twist needed to stabilise the kite.

The greater hydro-kite arrangement must also be taken into consideration when designing the kite wing. The kite design must be tailored to the design specifications where a nacelle is required with the on-board turbine, and a tether must be secured. The design must be as aerodynamic as possible to produce as much power as possible with limited drag. A kite design such as that of Kite 1 may be more suited to hydro-kite applications as the nacelle can be fitted underneath, limiting the drag unlike Kite 4 with the use of an untapered wing where the nacelle may protrude beyond the kite area and increase drag of the system and destabilising it. Kite 1 may also be easier to handle due to its more compact shape and shorter wingspan. Prototype kites should be designed using different kite dimensions and airfoils, and tested to determine actual performance regarding their environment and flight paths.

Table 4.25. Twist calculated for a 1m² kite (Kite 1) using various airfoils.

KITE 1	Max. Thick.	Max. Camber		z	k1	k2	STM	AR	PFW	C_L	R_e (root)	R_e (tip)	C_m (root)	C_m (tip)	α/ TWIST
NACA 1410	10% at 29.9% chord	1.0% at 50% chord	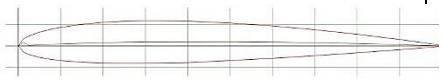	0.42	0.63	0.37	0.150	5.65	28.90	0.4	570556	237731	-0.023	-0.04	-18.56
NACA 63-212	12% at 34.9% chord	1.1% at 55% chord		0.42	0.63	0.37	0.150	5.65	28.90	0.4	570556	237731	-0.04	-0.037	-20.56
NACA 65(1)-212	12% at 40.0% chord	1.1% at 50% chord	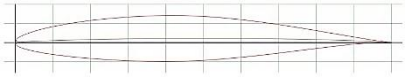	0.42	0.63	0.37	0.150	5.65	28.90	0.4	570556	237731	-0.04	-0.035	-20.40
NACA 0009	9% at 30.9% chord	0% - symmetric	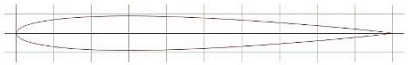	0.42	0.63	0.37	0.150	5.65	28.90	0.4	570556	237731	0	0	-12.47
NACA 0012	12% at 30.0% chord	0% - symmetric		0.42	0.63	0.37	0.150	5.65	28.90	0.4	570556	237731	0	0	-12.47
NACA 22112	12% at 29.5% chord	0.8% at 9.6% chord		0.42	0.63	0.37	0.150	5.65	28.90	0.4	570556	237731	0.008	0	-11.43
NACA 23112	12% at 29.5% chord	1.2% at 14.7% chord	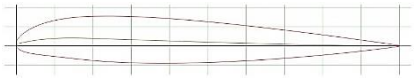	0.42	0.63	0.37	0.150	5.65	28.90	0.4	570556	237731	0.009	-0.005	-11.68
NACA 24112	12% at 29.4% chord	1.7% at 20.6% chord		0.42	0.63	0.37	0.150	5.65	28.90	0.4	570556	237731	0.01	-0.01	-11.93
NACA 25112	12% at 29.5% chord	2.0% at 27.2% chord	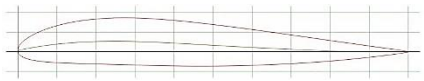	0.42	0.63	0.37	0.150	5.65	28.90	0.4	570556	237731	0.005	-0.027	-13.90

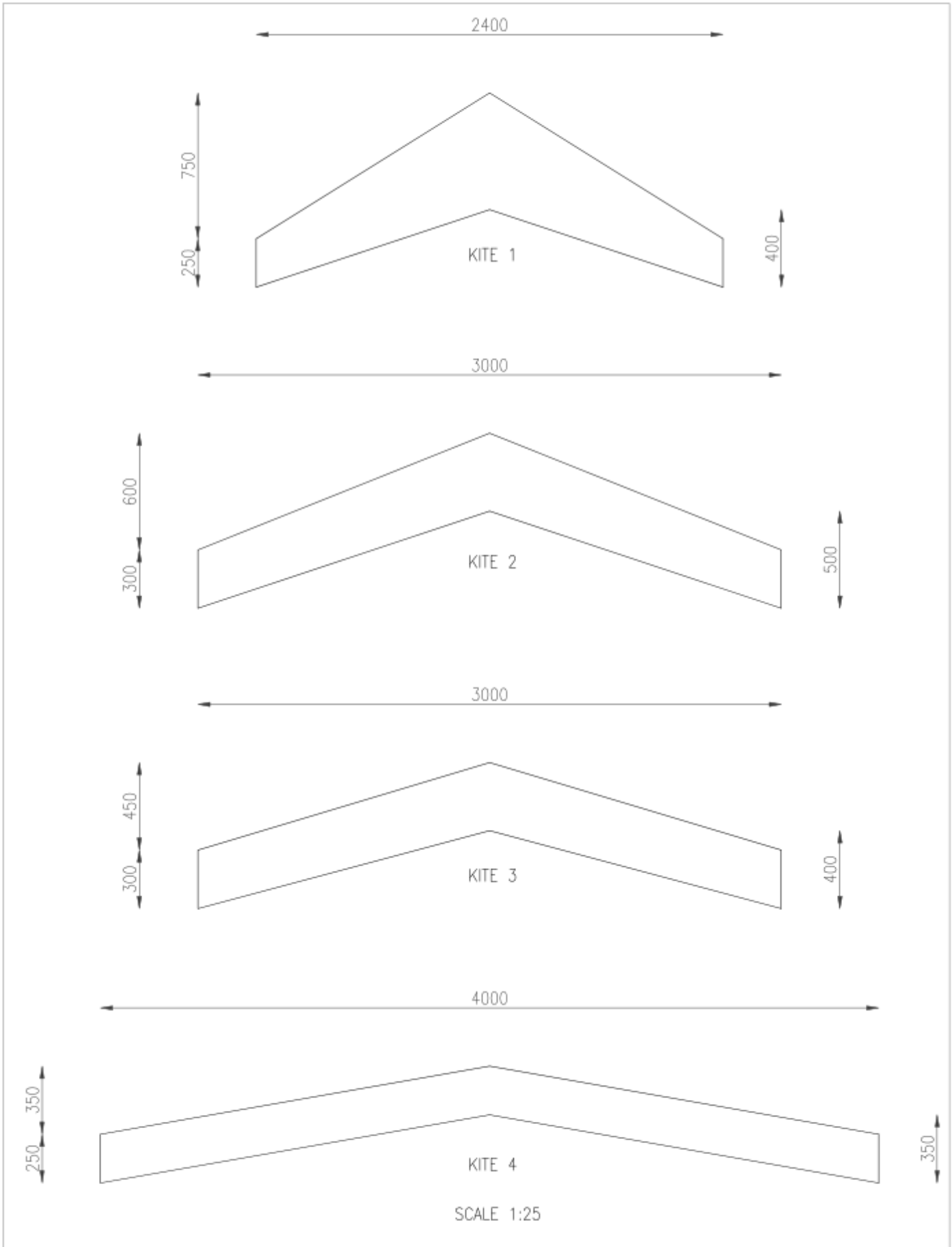

Figure 4.64. Diagrams showing various dimensions and design of each 1m² kite.

CHAPTER 5

5. CONCLUSION

This chapter presents the conclusion of this research including a summary of the results and recommendations for future research.

This study aimed to investigate the power producing potential of the Agulhas current using hydro-kite technology. The HYCOM model was used to predict ocean current velocities at various locations along the coast. The overall feasibility of implementing a hydro-kite system regarding kite array configurations and submarine power cables was examined.

5.1. Analysis of Agulhas Current

The Agulhas current was analysed for potential energy generation where available ADCP measurements were used between Port Edward and the Fish River. Cape Morgan was identified as the best location for energy extraction due to the high velocities experienced. East London also yielded high mean velocities and was located in proximity to onshore substations. At Port Edward data was only available for a short period but relatively high velocities were experienced further offshore but deeper mooring depths may prove more challenging. The more southern Fish River site also yielded a relatively high mean velocity but data was limited and no Natal Pulse events were present for the duration of the captured data which may have provided misleading results.

Natal pulse events were identified within the data and will undoubtedly inhibit power supply consistency as they were present at one location for up to 29 days, assuming a concentrated farm this means approximately one month without electricity from the kite system. Natal Pulses occurred between one and three times per year over the available data period. The speed of the current calculated from Natal Pulse events as they propagated south tended to vary considerably. Over a distance of approximately 100 km around Cape Morgan, Natal Pulse events were seen to occur at relatively the same time rendering a distributed system redundant within this area. The ocean current experiences fluctuating velocities even without the occurrence of a Natal Pulse with more fluctuations observed at locations further south. Meanders lasting approximately one day also have an effect on energy output. Ocean current energy from the Agulhas cannot be considered a baseload power due to the presence of Natal Pulses which cause variability within the current. A distributed system of hydro-kites is considered to overcome the issue of an intermittent power supply.

5.2. HYCOM Model

The performance of the HYCOM model was investigated and compared against the ADCP data to validate it. HYCOM underestimated current velocities at all locations for a depth of 20 m. Eskom

current velocities changed at a greater rate with regards to depth than the HYCOM model predictions in shallower depths, the gradient of the velocity with depth for Eskom was much steeper than that for HYCOM. HYCOM showed the worst predictions for the location at Cape Morgan which experienced the highest current velocities. HYCOM predictions between locations cannot be compared because the distribution of current velocities does not scale directly to the measured data. Factors were applied to the HYCOM data to attain a better representation of actual ocean events based on ADCP measurements. The location with the highest current velocities after the relevant factors were applied was between Cape Morgan and East London near Morgan's Bay. HYCOM cannot solely be used to identify locations with high power producing potential due to the model's inability to predict velocity magnitudes adequately.

Despite HYCOM's inefficiency at predicting ocean current magnitudes, the model was sufficient in identifying many Natal Pulse events. Overall, the HYCOM model showed a high correlation to the measured data with respect to velocity distributions at the locations that could be compared. Due to the coarse resolution of the HYCOM model, as stated in Backeberg et al. (2010) ocean model comparison, the model predicts the core of the Agulhas current further offshore than it is, refining the model may aid in producing better predictions. The presence of an undercurrent in the model also contributes to the Agulhas core forced further offshore.

The HYCOM Reanalysis was examined and compared with all ADCP locations. The Reanalysis further underpredicted the magnitude of the ocean current velocities in comparison with the HYCOM model. As seen in the HYCOM model, the distribution of ocean current velocities at different locations does not scale to the measured observations and individual factors were applied to each position. The factors applied scaled similarly with those used for the HYCOM model. The correlation of the Reanalysis data to the ADCP data was high for the sites investigated as in the HYCOM model but produced lower correlation coefficients for Port Edward and the southern Fish River region which were not able to be compared using HYCOM.

The alternative further offshore locations extracted from HYCOM confirmed that the HYCOM model predicts the current core further offshore as positions further offshore yielded better results regarding ocean current magnitude. Locations were extracted approximately 10km further offshore from the ADCP moorings for more northern regions where the current flow closer to the coastline. The alternative model predictions tended to underpredict velocity magnitudes, but underpredictions were less severe than in using the actual grid locations.

5.3. Power and Kite Array Configuration

The possibility of introducing a distributed kite array system compared with a concentrated system was investigated regarding KEF potential and the amount of time the system would not be in operation. A distributed system of hydro-kites dispersed along the coastline from Port Edward to the Fish River would generate approximately 60 % of the energy that could be produced from using the best location, near Morgan's Bay using the factored HYCOM model. The power generated is incredibly sensitive to the current velocity. Observing the best sites within each area segment, power would not be produced for approximately 20 % of the entire duration, whereas in a distributed system utilising many locations less than 1 % of the period experiences no power output. However, all hydro-kites are not always functional at the same time. To determine feasibility, the amount of time that a certain number of kites are working was considered. More than 50 % of the kites are functional for 82 % of the duration, with the majority of 56 % of the time more than 75 % of kites generating power.

Observing the outcomes of all models, the factored HYCOM model and the alternative HYCOM extraction produced similar results regarding the percentage of kites working over the duration. The Reanalysis data predicted less favourable results with fewer kites operational for a significant percent of the time. Results yielded that the best location generated more energy than that of the distributed system but at the disadvantage of inconsistent, unpredictable power generation as it is Natal Pulse dependent. A distributed system maintains a more reliable source of energy as Natal Pulse events can be present in one location but other areas will be unaffected so that the system can still generate power.

The distributed system requires more hydro-kites to attain the same capacity and approximately the same energy output of the concentrated system. Larger kites can be used within one large hydro-kite farm to minimise additional material costs regarding turbine, step-up transformers, cables and anchors. A concentrated array requires less cable lengths compared with the requirements for a distributed system where cable sizes used can also be smaller. Cable losses are not considered a deciding factor as losses incurred using the concentrated and distributed arrays show no substantial difference. Larger cables can be used if required to reduce losses but at an added expense. Submarine cable costs regarding purchasing and installation are incredibly high and will make up a significant percentage of the capital required for the project and must, therefore, be kept to a minimum. Kite deployment locations are not only reliant on KEF potential but are also dependent on the position of existing onshore substations and cable lines to connect the generated energy into the grid. Proposed new cable lines may increase the feasibility of this project improving access to the existing network system.

The tether cable link from the turbine to the seabed was investigated and designed for a small 3m^2 kite. The hydro-kite must support its own weight including the turbine and the weight of the tether. The turbine would need to be designed to generate energy at a higher voltage, or alternatively a buoyancy system can be implemented within the kite wing or within the tether so that the system can support itself and fly at the required depth. Alternatively, the generator can be located on the seabed removing the need for the cable within the tether.

The energy that could be generated using the concentrated array and distributed array of the same capacity is approximately the same but the distributed system uses more kites. This predicted energy is comparable to the output predicted by the Sere wind farm project initiated by Eskom. Eskom started the Sere wind farm venture to highlight the company's commitment to renewable energy with hopes of launching future renewable energy projects. Eskom showed interest in investigating ocean energy potential by deploying the ADCPs from which data was extracted.

5.4. Recommendations

The possibility of installing cables through the Pondoland MPA and other MPAs such as that near Morgan's Bay should be investigated to unlock a larger area of potential energy extraction. The seabed would only be disturbed for a short period during the installation process. A better indication of energy extraction potential can be gained through the collection of more data using ADCPs especially in areas where limited data was available. Areas that should be investigated include the more offshore locations near Port Edward, locations between Cape Morgan and East London and the more southern Fish River region. ADCPs could also be deployed north of Durban to examine if the area before the presence of the Natal Bight holds any significant energy potential. More data available can be beneficial in attaining a more refined representation of the Agulhas current ocean velocities and can be used to calibrate ocean models further in terms of scaling at various locations.

The ROMS SAfE ocean model could be investigated along with the HYCOM model to determine whether it yields a better correlation to measured data. The ROMS model does not predict the Agulhas Undercurrent as in HYCOM. Therefore, the Agulhas current core is not pushed further offshore, and more accurate velocity magnitudes at the relevant locations may be experienced. The ROMS model is still known to underpredict velocities where scaling factors may need to be applied to attain an accurate model.

It is imperative to the feasibility of this project that a prototype hydro-kite be designed and tested to further research and investigations. Small scale kite wing designs can be produced and tested using various airfoil designs. Designs should be tested and modified varying different parameters to attain

the most applicable power producing kite design. A symmetrical airfoil may be the easiest to manufacture and produce in bulk quantities. A kite prototype should be tested at sea to ascertain the actual amount of energy that could be generated and compare this with theoretical values from the Loyd power equation. A sensor or camera could be mounted on the prototype to monitor interactions within the marine environment.

The optimal arrangement of hydro-kites should be investigated to improve farm efficiency. The flow field around a single device should be determined and its effects on neighbouring devices. Wake regions and blocking effects should be explored with the effects on various configurations such as a multi-row array including staggered and centred formations as well as for a single row. A model should be set up with relevant parameters that can simulate flow around the devices and the array, predicting the power output of kite turbines within the array and the efficiency of the arrangement as a whole. Results could also be compared to large stationary turbines within an infinitely wide channel

A renewable energy development such as this can have a significant socio-economic impact in terms of local job creation and skills development, benefitting local communities as well as having a positive effect on the economy. Local jobs can be created during the lifespan of the project in manufacturing as well as through operations and maintenance. However, the renewable energy sector is still an emerging market in South Africa with projects carrying substantial risk and requiring significant investments in terms of the initial installations where government support is also necessary.

Assuming the success and power generating capability of a kite prototype, a full cost analysis should be performed including the added social benefits of implementing a distributed array compared with that of concentrated kite farms to determine the best scheme available. A pilot project should be conducted in an area located close to onshore substations and cable lines that has a high KEF for potential energy generation.

There is the possibility to combine a distributed array with that of a concentrated array, however, there may be more economic risk incurred with implementing a distributed array. Based on the success of the pilot study, a concentrated array could be initially implemented, the project should then be evaluated in terms of economic return and the social effects on local communities. If the outcome of the project appears favourable, the next phase of the project development could include the installation of a distributed array where less risk is then involved making it a more economically feasible initiative for investors.

References

ABB, 2013. *XLPE Submarine Cable Systems.* [Online]
Available at:
http://www04.abb.com/global/seitp/seitp202.nsf/0/badf833d6cb8d46dc1257c0b002b3702/$file/XLPE+Submarine+Cable+Systems+2GM5007+.pdf
[Accessed 25 May 2016].

Actforlibraries.org, 2008. *Elevons and how they function.* [Online]
Available at: http://www.actforlibraries.org/elevons-and-how-they-function/
[Accessed 4 February 2016].

Airfoil Tools, 2016. *Airfoil Database Search.* [Online]
Available at: http://airfoiltools.com/search/index
[Accessed 2 March 2016].

ALXION, 2011. *What is a Permanent Magnet Generator?.* [Online]
Available at: http://www.alxion.com/permanent-magnet-generator/
[Accessed 14 September 2016].

Attwood, J. R., 2000. Cable Design for Subsea Power Links. *IEEE Power Engineering Review,* 20(9), pp. 13-14,21.

Backeberg, B., Johannessen, J., Rouault, M. & Veitch, J., 2010. Preliminary Inter-Model Comparison of the Agulhas Current with Direct Range Doppler Velocity Estimated from ENVISAT's Advanced Synthetic Aperture Radar. *ESA Publication Division,* p. 7PP.

Bayworld Centre for Research and Education, 2005. *Sea Atlas - Reroflection.* [Online]
Available at: http://www.bcre.org.za/seaatlas/index.php?p=retroflection.php
[Accessed 20 October 2016].

Beal, L. & Bryden, H., 1999. The velocity and vorticity structure of the Agulhas Current at 32S. *Journal of Geophysical Research,* 104(C3), pp. 5151-5176.

Beal, L. M., deRuijter, D. P., Biastoch, A. & Zahn, R., 2011. On the role of the Agulhas system in ocean circulation and climate. *Nature,* 472(7344), pp. 429-436.

Bleck, R., 2002. An oceanic general circulation model framed in hybrid isopycnic cartesian coordinates. *Ocean Modelling,* Volume 37, pp. 55-88.

Boebel, O. et al., 2003. Path and variability of the Agulhas Return Current. *Deep Sea Research II,* Volume 50, pp. 35-56.

Bowditch, N., 2002. *American Practical Navigator: An Epitome of Navigation.* (Pub) Edition ed. s.l.:United States Government Printing.

Bryden, H., Beal, L. & Duncan, L., 2005. Structure and transport of the Agulas Current and its temporal variability. *Journal of Oceanography,* 61(3), pp. 479-492.

capetown.gov, 2016. [Online]
Available at: http://capetown.gov.za/en/EnvironmentalResource
[Accessed 17 October 2016].

Carbon Copy Communications, 2011. *Enabling offshore wind and connecting countries.* [Online]
Available at: http://carboncopycommunications.com/business-trade-press/enabling-offshore-wind-and-connecting-countries/
[Accessed 12 September 2016].

Carnegie, 2015. *Carnegie Wave Energy.* [Online]
Available at: http://carnegiewave.com/
[Accessed 20 September 2015].

Carnegie, 2015. *CETO 6 (Garden Island).* [Online]
Available at: http://carnegiewave.com/projects/ceto-6/
[Accessed 20 September 2015].

Comsol, 2012. *Simulating permanent megnet generators.* [Online]
Available at: https://www.comsol.com/blogs/simulating-permanent-magnet-generators/
[Accessed 5 October 2016].

Department of Energy, 2003. *The White Paper on Renewable Energy.* [Online]
Available at: http://www.energy.gov.za/files/policies/whitepaper_renewables_2003.pdf

deRuijter, W. P., Leeuven, P. J. v. & Lutjeharms, J. R., 1999. Generation and evolution of Natal Pulses: Solitary meanders in the Agulhas Current. *Journal of Physical Oceanography,* 29(12), pp. 3043-3055.

deRuijter, W. P. et al., 2002. Observations of the flow in the Mozambique Channel. *Geophysical Research Letters,* 29(10), p. 1502.

Dickins, S., 2015. *£25m sea 'kite' energy project launched off Holyhead.* [Online]
Available at: http://www.bbc.com/news/uk-wales-north-west-wales-32798276
[Accessed 15 June 2016].

Donohue, E., Firing, E. & Beal, L., 2000. Comparison of the three velocity sections of the Agulhas Curent and the Agulhas Undercurrent. *Journal of Geophysical Research,* 105(C12), pp. 28585-28593.

Draper, S. & Nishino, T., 2013. Centred and Staggered Arrangements of TIdal Turbines. *Journal of Fluid Mechanics,* Volume 739, pp. 72-93.

Drives & Controls, 2015. *Record-breaking motor is 'five times more powerful'.* [Online]
Available at:
http://drivesncontrols.com/news/fullstory.php/aid/4758/Record_breaking_motor_is_91five_times_more_powerful_92.html
[Accessed 21 September 2016].

Electronic Design, 2013. *Interface Connection.* [Online]
Available at: http://electronicdesign.com/site-files/electronicdesign.com/files/uploads/2013/10/1107InterfaceConnectionFig2.jpg
[Accessed 9 October 2016].

Eskom Holdings Limited, 2009. *Annual Report 2009.* [Online]
Available at: http://www.financialresults.co.za/eskom_ar2009/ar_2009/downloads/01_profile.pdf

ESKOM, 2011. *Renewable Energy: Sere wind farm.* [Online]
Available at: http://www.eskom.co.za/AboutElectricity/FactsFigures/Documents/Sere_Wind.pdf
[Accessed 15 October 2016].

ESKOM, 2014. *Renewable Energy - Sere Wind Farm Project.* [Online]
Available at: http://www.eskom.co.za/Whatweredoing/NewBuild/Pages/SereWindFarmProject.aspx
[Accessed 16 October 2016].

ESRU, University of Strathclyde, 2002. *Electricity.* [Online]
Available at: http://www.esru.strath.ac.uk/EandE/Web_sites/98-9/offshore/elec.htm
[Accessed 18 September 2016].

Fripp, C., 2016. *Here is how much you'll pay for Eskom's electricity from today.* [Online]
Available at: http://www.htxt.co.za/2016/04/01/here-is-how-much-youll-pay-for-electricity-from-today/
[Accessed 14 August 2016].

Gets, A., 2013. *Powering the Future: Renewable Energy Roll-out in South Africa,* Cape Town, South Africa: Prepared for Greenpeace Africa by AGAMA Energy (Pty) Ltd.

Global Carbon Atlas, 2015. *CO2 Emissions.* [Online]
Available at: http://www.globalcarbonatlas.org/?q=en/emissions
[Accessed 28 July 2015].

Gyory, J. et al., 2016. *The Agulhas Current.* [Online]
Available at: http://oceancurrents.rsmas.miami.edu/atlantic/agulhas.html
[Accessed 20 June 2016].

Haas, J., 2014. *Step-by step design procedure for flying wing R/C model aircraft without any vertical stabilisation aid (no fin, no rudder, no winglet).* [Online]
Available at: http://www.rcsoaringdigest.com/OTW/on-the-wing3/156-Jochen-Haas/Haas-software-Windows/Design-Procedure.DOC

Hepperle, M., 2002. *Basic Design of Flying Wing Models.* [Online]
Available at: http://www.mh-aerotools.de/airfoils/flywing1.htm
[Accessed 15 June 2015].

hycom.org, 2015. *Current Experiments.* [Online]
Available at: https://hycom.org/dataserver/glb-analysis
[Accessed 9 August 2015].

HYCOM, 2015. *HYCOM + NCODA 1/12 Analysis.* [Online]
Available at: http://hycom.org/dataserver/glb-analysis
[Accessed 8 August 2015].

HYCOM, 2015. *HYCOM + NCODA GLOBAL 1/12 REANALYSIS.* [Online]
Available at: http://hycom.org/dataserver/glb-reanalysis
[Accessed 10 September 2015].

HydroRun, 2014. *HydroRun Technology.* [Online]
Available at: http://hydrorun.ca/technology/
[Accessed 20 June 2015].

Hyperphysics, 2016. *Seawater.* [Online]
Available at: http://hyperphysics.phy-astr.gsu.edu/hbase/Chemical/seawater.html
[Accessed 12 October 2016].

Internation Energy Agency, 2014. *South Africa: Renewabkes and Waste for 2014.* [Online]
Available at:
https://www.iea.org/statistics/statisticssearch/report/?country=SOUTHAFRIC&product=renewablesandwaste&year=2014
[Accessed 15 October 2016].

Jansson, A., 2015. *Reflections from breakthrough marine energy trials.* [Online]
Available at: http://minesto.com/reflections-from-breakthrough-marine-energy-trials/
[Accessed 15 June 2016].

Kaluza, P., Kolzsch, A., Gastner, M. & Blasius, B., 2010. The complex network of global cargo ship movements. *Journal of the Royal Society Interface,* Volume 7, pp. 1093-1103.

Leber, G. M. & Beal, L. M., 2014. Evidence that Agulhas Current transport is maintained during a meander. *Journal of Geophysical Research,* Volume 119, pp. 3806-3817.

Leeuven, P. J. v. & deRuijter, W. P. M., 2000. Natal Pulses and the formation of Agulhas Rings. *Journal of Geophysical Research,* Volume 105, pp. 6425-6436.

Loyd, M. L., 1980. Crosswind Kite Power. *Journal of Energy,* 4(3), pp. 106-111.

Lutjeharms, J., 1988. Remote sensing corroboration of retroflection of the East Madagascar Curent. *Deep Sea Research Part A. Oceanographic Research Papers,* 35(12), pp. 2045-2050.

Lutjeharms, J., Boebel, O. & Rossby, H., 2003. Agulhas cyclones. *Deep-sea Research II,* 50(1), pp. 13-34.

Lutjeharms, J. R. E. & Roberts, H. R., 1988. The Natal Pulse: AN extreme transient on the Agulhas Current. *Journal of Geophysical Research,* 93(C1), pp. 631-645.

Marine Living Resources Act of 1988, 1988. s.l.:(Gazette No. 18930, Notice No. 747. Commencement date: 1 September 1998 [Proc. No. 80, Gazette No. 19148]).

McAllister, D., 1982. *Electric Cables Handbook.* illustrated ed. Great Britain: Granada Publishing.

McFadyen, S., 2009. *Three Phase Current - Simple Calculation.* [Online]
Available at: http://myelectrical.com/notes/entryid/8/three-phase-power-simple-calculations
[Accessed 17 May 2016].

Meyer, I., Reinecke, J. & Van Niekerk, J., 2014. *Resource Assessment of the Agulhas Current for the Purpose of Marine Energy Extraction.* Halifax, Internaional Conference on Ocean Energy.

Minesto, 2011. *Minesto.* [Online]
Available at: http://www.minesto.com/deep-green
[Accessed 15 April 2015].

Minesto, 2015. *Holyhead Deep.* [Online]
Available at: http://minesto.com/holyhead-deep/
[Accessed 14 June 2016].

Moodley, R., Nthontho, M., Chowdhury, S. & Chowdhury, S., 2012. A technical and economic analysis of energy extraction from the Agulhas Current on the East coast of South Africa. *2012 IEEE Power and Energy Society General Meeting.*

NEXANS, 2013. *Submarine Power Cables.* [Online]
Available at: http://www.nexans.co.za/Germany/2013/SubmPowCables_FINAL_10jun13_engl.pdf
[Accessed 22 May 2016].

Nirman, S. K., 2014. *Class VII: Chapter 5 - Water.* [Online]
Available at:
http://www.nirmancare.com/blog/index.php?controller=post&action=view&id_post=40
[Accessed 17 July 2015].

Nishino, T., 2013. Beyond the Betz Theory - Blockage, Wake Mixing and Turbulence. *2nd Oxford Tidal Energy Workshop.*

Nishino, T. & Draper, S., 2015. Local Blockage Effect for Wind Turbines. *Journal of Physics Conference Series.*

Nishino, T. & Wilden, R. H., 2013. The Efficiency of Tidal Fences: A brief review and further discusion on the effect of wake mixing. *Proc. ASME 2013 32nd International Conference on Ocean, Offshore and Arctic Engineering (Nantes) OMAE2013.*

NOAA, 2016. *Ocean Explorer.* [Online]
Available at: http://oceanexplorer.noaa.gov/facts/currents.html
[Accessed 14 April 2016].

Ocean Instruments, 2004. *Acoustic Doppler Current Profiler (ADCP).* [Online]
Available at: https://www.whoi.edu/instruments/viewInstrument.do?id=819
[Accessed 12 April 2015].

Ocean Motion, 2006. *Eastern Boundary Currents.* [Online]
Available at: http://oceanmotion.org/western-boundary-sst.htm
[Accessed 20 June 2016].

Ocean Motion, 2007. *Ocean in motion: Ekman Transport background.* [Online]
Available at: http://oceanmotion.org/html/background/ocean-in-motion.htm
[Accessed 25 November 2016].

Ocean Motion, 2007. *Wind Driven Surface Currents: Western Boundary Currents.* [Online]
Available at: http://oceanmotion.org/html/background/western-boundary-currents.htm
[Accessed 20 June 2016].

Olinger, D. & Wang, Y., 2015. Hydrokinetic energy harvesting using tethered undersea kites. *Journal of Renewable and Sustaincable Energy,* 7(4), p. 043114.

Open Electrical, 2012. *Cable Insulation Materials.* [Online]
Available at: http://www.openelectrical.org/wiki/index.php?title=Cable Insulation Materials
[Accessed 3 April 2016].

Parmar, J., 2014. *An example how to calculate volatge drop and size of electrical cable.* [Online]
Available at: http://myelectrical.com/notes/entryid/8/three-phase-power-simple-calculations
[Accessed 7 April 2016].

Penton, 2012. *What's the Difference Between AC Induction, Permanent Magnet, and Servomotor Technologies?.* [Online]
Available at: http://machinedesign.com/motorsdrives/whats-difference-between-ac-induction-

permanent-magnet-and-servomotor-technologies
[Accessed 15 September 2016].

Penven, P., Chang, N. & Shillington, F., 2006. Modellling the Agulhas Current using SAfE (Southern Africa Experiment). *Geophysical Research Abstract,* 8(Abstract 04225).

PM, 2013. *PMG Advantage.* [Online]
Available at: http://www.permanentmagnetgenerator.net/pages/Advantages%20of%20PMG.pdf
[Accessed 14 September 2015].

Price, J. F., Weller, R. A. & Schudlich, R. R., 1987. Wind-Driven Ocean Currents and Ekman Transport. *Science,* 238(4833), pp. 1534-1538.

Ragheb, M. & Ragheb, A. M., 2011. Wind Turbines Theory - The Betz Equation and Optimal Rotor Tip Speed Ratio. In: D. R. Carriveau, ed. *Fundamental and Advanced Topics in Wind Power.* s.l.:InTech.

Rouault, M. & Penven, P., 2011. New perspectives on Natal Pulses from satellite observations. *Journal of Geophysical Research,* Volume 116.

Rutovitz, J., 2010. *South African Energy Sector Jobs to 2030,* s.l.: Institute for Sustainable Futures, University of Technology Sydney prepared for Greenpeace.

Schouten, M. W., deRuijter, W. P. & Leeuven, P. J. v., 2002. Upstream control of Agulhas Ring shedding. *Journal of Geophysical Research,* 107(C8), p. 3109.

Sea Generation LTD, 2013. *Project Background.* [Online]
Available at: http://www.seageneration.co.uk/
[Accessed 23 June 2015].

Sentinel, 2013. *RDI Instruments.* [Online]
Available at: http://rdiinstruments.com/_documents/Brochures/sentinel_datasheet_lr.pdf
[Accessed 13 August 2015].

Shchepetkin, A. & McWilliams, J. C., 2003. A method for computing horizontal pressure-gradient force in an oceanic model with a nonaligned vertical coordinate. *Journal of Geophysical Research,* 108(C3).

Siemens, 2012. *Siemens Wind Turbine SWT-2.3-108.* Erlangden, Germany: Siemens AG Energy Sector.

Smithsonian National Air and Space Museum, 2015. *Roll, Pitch and Yaw.* [Online]
Available at: https://howthingsfly.si.edu/flight-dynamics/roll-pitch-and-yaw

South African Tourism, 2011. *Pondoland Marine Protected Area.* [Online]
Available at: http://www.southafrica.net/za/en/articles/entry/article-southafrica.net-pondoland-marine-protected-area
[Accessed 13 Spetember 2016].

Subsea Cables UK, 2014. *Submarine Power Cables Ensuring the lights stay on!.* [Online]
Available at: http://www.kis-orca.eu/media/72705/scuk_The_Importance_Of_Subsea_POWER_Cables_18092014.pdf
[Accessed 4 May 2016].

The Aviation History Online Museum, 2002. *Flight Control Surfaces - Elevons.* [Online]
Available at: http://www.aviation-history.com/theory/elevon.htm
[Accessed 4 February 2016].

Thue, W. A., 2005. *Electrical Power Cable Engineering.* Second Edition ed. New York: Marcel Dekker Inc..

Time for Change, 2007. *Pros and cons of nuclear power.* [Online]
Available at: http://timeforchange.org/pros-and-cons-of-nuclear-power-and-sustainability
[Accessed 18 June 2015].

Tripp Lite, 2015. *Single-phase vs. three-phase power explained.* [Online]
Available at: https://www.tripplite.com/products/singlevs3phase
[Accessed 8 June 2016].

Triton Renewable Energy, 2016. *How CETO works.* [Online]
Available at: http://www.tritonrenewableenergy.com/technology/ceto-works/
[Accessed 24 October 2016].

Tsugawa, M. & Hasumi, H., 2010. Generation and growth mechanism of the Natal Pulse. *Journal of Physical Oceanography,* 40(7), pp. 1597-1612.

Vaart, P. C. F. V. d. & deRuijter, W. P. M., 2001. Stability of western boundary currents with an application to pulse like behaviour of the Agulhas Current. *Journal of Physical Oceanography,* 31(9), pp. 2625-2644.

VanZweiten, J., Meyer, I. & Alsenas, G., 2014. Evaluation of HYCOM as a Tool for Ocean Current Energy Assessment. *Proceedings of the 2nd Marine Energy Technology Symposium.*

Whale Route, 2014. *Whale Watching South Africa Humpbacks, southern rights, Bryde's whales, orcasWatching Whales.* [Online]
Available at: http://whaleroute.com/areas/southafrica/
[Accessed 4 June 2016].

Windenergie-Institut, D., 2001. *Wind Turbine Grid Connection and Interaction,* Germany: ENERGIE.

Windows To the Universe, 2016. *Density of Ocean Water.* [Online]
Available at: http://www.windows2universe.org/earth/Water/density.html
[Accessed 4 March 2016].

Xinda Green Energy Co., LTD, 2016. *Products.* [Online]
Available at: http://www.xindaenergy.com/315kw-10000rpm-high-speed-brushless-PM-sychronous-motor-p381.html
[Accessed 4 October 2016].

A. Appendix A

Table A.1. Renewable energy production in South Africa in 2014 (IEA)

Renewable Energy	Electricity (GWh)	Percentage of Total Renewables (%)
Biofuel	303	4.61
Hydro	4082	62.08
Solar PV	1120	17.03
Wind	1070	16.27
Tide, Wave and Ocean	0	0.00
Total Renewables	6575	
Production from Coal	232020	
Total Electricity Production	252578	
Total Electricity Domestic Supply	249919	

B. Appendix B

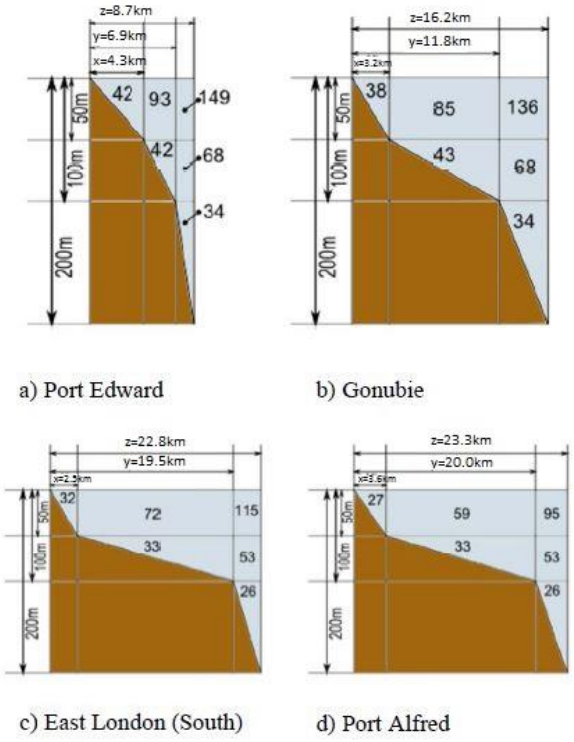

Figure B.1. Cross-sections showing study locations and average current speed per block (Moodley).

C. Appendix C

C.1. ADCP List

Table C.1. Deployment details of all ADCPs in the Agulhas Current between September 2005 and September 2010.

SQ	Filename	ADCP Type	Pressure sensor	Latitude (S)	Longitude (E)	Deployment date	Recovery date	Ship sounding (m)	Position
1	PE751	RDI 75	yes	-31.22263	30.20273	8-Sep-2005 16:44	11-Dec-2005 10:25	156	offshore
2	PE301	RDI 300 + waves	yes	-31.19722	30.17517	8-Sep-2005 17:06	11-Dec-2005 11:20	60	midshelf
3	PE601	RDI 600	yes	-31.17855	30.15253	8-Sep-2005 17:30	11-Dec-2005 12:05	31.8	inshore
4	PE602	RDI 600	no	-31.17860	30.15263	11-Dec-2005 13:58	10-Apr-2006 10:40	32.98	inshore
5	PE302	RDI 300 + waves	yes	-31.19732	30.17480	11-Dec-2005 14:54	10-Apr-2006 09:36	61.74	midshelf
6	PE752	RDI 75	yes	-31.22303	30.20270	13-Dec-2005 17:02	06-Apr-2006 08:22	173.4	offshore
7	EL1901	Nortek	yes	-32.50997	28.83000	14-Dec-2005 02:15	07-Apr-2006 09:10	83.25	midshelf
8	PE603	RDI 600	yes	-31.17865	30.15245	10-Apr-2006 17:30	09-Sep-2006 09:00	32.11	inshore
9	PEM03	RDI 600	no	-31.19753	30.17460	10-Apr-2006 17:50	09-Sep-2006 08:30	62.11	midshelf
10	EL201	Nortek	yes	-32.50717	28.83242	11-Apr-2006 14:45	02-Sep-2006 16:00	82.95	midshelf
11	EL303	RDI 300 + waves	yes	-32.32363	29.02225	11-Apr-2006 17:10	02-Sep-2006 07:00	96	midshelf
12	EL403	RDI 75	yes	-32.96595	28.30622	1-May-2006 19:06	08-Sep-2006 06:45	96	midshelf
13	EL754	RDI 75	yes	-32.57633	28.75208	8-Sep-2006 14:55	12-Dec-2006 08:40	91.99	midshelf
14	EL301	Nortek	yes	-32.50763	28.83210	8-Sep-2006 15:55	12-Dec-2006 10:45	84.78	midshelf
15	EL304	RDI 300	yes	-32.47545	28.79237	8-Sep-2006 16:27	12-Dec-2006 11:45	90	midshelf
16	EL401	Nortek	yes	-32.50753	28.83292	13-Dec-2006 11:28	07-Mar-2007 13:26	81.3	midshelf
17	EL755	RDI 75	yes	-32.64985	28.69545	13-Dec-2006 14:57	07-Mar-2007 15:25	102	offshore
18	EL305	RDI 300	yes	-32.87433	28.43367	13-Dec-2006 20:26	07-Mar-2007 18:02	88.8	midshelf
19	EL501	Nortek	yes	-32.50743	28.83293	8-Mar-2007 06:29	17-Aug-2007 15:34	85.5	midshelf
20	EL756	RDI 75	yes	-32.43732	28.94465	8-Mar-2007 08:45	17-Aug-2007 17:05	196	offshore
21	EL306	RDI 300	yes	-33.15012	28.11602	8-Mar-2007 14:49	14-Aug-2007 11:26	98.7	midshelf
22	EL601	Nortek	yes	-32.50735	28.83287	18-Aug-2007 10:20	06-Dec-2007 15:40	84.84	midshelf
23	EL757	RDI 75	yes	-32.51000	28.83287	18-Aug-2007 10:37	06-Dec-2007 14:52	83.86	midshelf
24	EL307	RDI 300	yes	-33.15005	28.09953	18-Aug-2007 15:19	06-Dec-2007 06:45	83.5	midshelf
25	FR301	RDI 300	yes	-33.85170	27.08120	18-Aug-2007 21:33	05-Dec-2007 16:44	89.6	midshelf
26	EL701	Nortek	yes	-32.50802	28.83293	07-Dec-2007 17:47	30-Mar-2008 08:20	85	midshelf
27	EL308	RDI 300	yes	-33.14983	28.09905	07-Dec-2007 21:07	30-Mar-2008 16:00	85	midshelf
28	FR752	RDI 75	yes	-33.85070	27.08023	08-Dec-2007 01:30	29-Mar-2008 08:30	88	midshelf
29	EL801	Nortek	yes	-32.50754	28.83314	01-Apr-2008 06:05	12-Jul-2008 07:30	87	midshelf
30	EL309	RDI 300	no	-33.14990	28.09933	01-Apr-2008 11:24	11-Jul-2008 15:03	88.7	midshelf
31	FR303	RDI 300	yes	-33.70283	27.29817	1-Apr-2008 16:01	13-Jul-2008 07:24	97	midshelf
32	EL310	RDI 300	yes	-33.14970	28.09903	11-Jul-2008 16:32	10-Dec-2008 17:30	82	midshelf
33	EL901	Nortek	yes	-32.50495	28.83143	12-Jul-2008 13:45	13-Dec-2008 06:50	84.5	midshelf
34	CM301	RDI 300	yes	-32.50737	28.83185	12-Jul-2008 14:06	13-Dec-2008 06:05	82.7	midshelf
35	FR304	RDI 300	no	-33.70290	27.29782	13-Jul-2008 09:41	09-Dec-2008 08:30	96	midshelf
36	FR305	RDI 300	no	-33.70310	27.29803	12-Dec-2008 09:38	4-Feb-2009 03:57	91.72	midshelf
37	EL311	RDI 300	yes	-33.15115	28.09700	12-Dec-2008 17:25	22-Mar-2009 08:30	83.12	midshelf
38	EL1910	Nortek	yes	-32.50560	28.83183	13-Dec-2008 13:23	23-Mar-2009 09:20	86	midshelf
39	CM302	RDI 300	yes	-32.49923	28.82348	13-Dec-2008 13:41	23-Mar-2009 10:10	86	midshelf
40	FR306	RDI 300	yes	-33.70322	27.29727	21-Mar-2009 14:20	24-Aug-2009 08:20	91.5	midshelf
41	EL312	RDI 300	yes	-33.15160	28.08072	23-Mar-2009 11:10	26-Aug-2009 07:20	86.6	midshelf
42	CM303	RDI 300	yes	-32.50638	28.83150	23-Mar-2009 11:10	25-Aug-2009 08:07	83.7	midshelf
43	CM304	RDI 300	no	-32.50790	28.83100	25-Aug-2009 09:15	5-Dec-2009 10:37	83	midshelf
44	EL313	RDI 300	yes	-33.15203	28.08727	26-Aug-2009 08:54	4-Dec-2009 14:30	82.7	midshelf
45	FR307	RDI 300	yes	-33.70333	27.29677	26-Aug-2009 15:24	4-Dec-2009 06:20	84	midshelf
46	EL314	RDI 300	yes	-33.15145	28.00866	4-Dec-2009 14:58	3-Mar-2010 13:15	89.02	midshelf
47	FR308	RDI 300	yes	-33.70335	27.29750	4-Dec-2009 20:06	4-Mar-2010 06:50	93.3	midshelf
48	CM305	RDI 300	no	-32.50733	28.83183	5-Dec-2009 13:39	3-Mar-2010 06:20	85.94	midshelf
49	CM306	RDI 300	no	-32.50725	28.83179	3-Mar-2010 09:10	13-Sep-2010 06:45	84	midshelf
50	EL315	RDI 300	yes	-33.15140	28.08651	3-Mar-2010 15:25	13-Sep-2010 11:30	88	midshelf
51	FR309	RDI 300	yes	-33.71332	27.29745	4-Mar-2010 08:15	3-Sep-2010 15:50	93.2	midshelf

Table C.2. List of ADCPs and bin depths, actual depths and percentage of data lost in each.

ADCP	BIN	Depth	% Data lost		ADCP	BIN	Depth	% Data lost
FR 301	34	20	2.163921869		EL306	38	20	2.36
FR752	29	21	6.05		EL307	31	21	0.70
					EL308	32	20	1.88
PE601	6	21	0		EL309	33	23	12.67
PE602	7	20	0		EL310	31	21	1.12
PE603	6	21	0		EL311	30	21	1.15
					EL312	32	21	2.05
PE301	21	19.95	0		EL313	33	20	7.90
PE302	21	19.53	0		EL314	32	20	3.48
PEM03	22	20	1.97		EL315	33	21.56	0.02
PE751	66	23	5.87		FR303	36	20	2.49
PE752	68	23	8.19		FR304	37	20	4.43
					FR305	36	20	3.51
EL1901	32	20.85	Nortek		FR306	35	22	8.41
EL201	33	19.88	Nortek		FR307	35	21.59	16.86
EL301	32	20.88	Nortek		FR308	35	21	7.20
EL401	33	18.97	Nortek					
EL501	33	19.54	Nortek		FR309	34	20.95	0.77
EL601	32	20.05	Nortek					
EL701	32	20.52	Nortek		EL303	38	20.19	0.00
EL801	33	19.89	Nortek		EL756	79	30	21.30
CM301	31	21	3.91		EL757	27	22	8.89
CM302	33	21	13.65		EL304	34	21	2.73
CM303	32	21	0.03		EL754	32	22	7.66
CM304	31	21	1.89		EL755	37	22	9.97
CM305	32	20	0.21		EL305	35	20	1.44
CM306	32	20	0.05		EL403	33	22	5.25

C.2. Data from ADCPs

Table C.3. Data for normal distribution curve at each location.

Position	Mean velocity (m/s)	Standard deviation σ (m/s)
Location 3	1.27	0.57
Location 1	1.44	0.58
Location 2	1.31	0.61
Location 4	0.96	0.55
Location 4 South	1.29	0.50

Table C.4. Distribution of current velocities at various locations of concentrated ADCPs. Equal intervals are used to compare the distributions. Highlighted cells show the maximum distribution and surrounding distributions of approximately 50% of the data.

Interval	PE751-752	PE301-M03	PE601-PE603	EL201-EL801	CM303-CM306	EL1901-EL801	CM301-CM306	EL306-EL311	EL312-EL315	FR301-752	FR303-FR305	FR306-308	FR303-309
0-0.2	5.60	5.80	13.96	2.21	3.44	2.16	4.85	4.32	5.84	1.32	5.76	7.30	7.81
0.2-0.4	6.27	6.25	19.21	4.14	5.64	4.03	7.12	5.85	6.73	3.64	11.10	10.86	11.70
0.4-0.6	5.46	11.02	30.95	3.45	5.13	3.31	5.60	5.42	7.59	5.40	12.27	12.80	12.55
0.6-0.8	6.29	13.99	25.25	3.36	3.44	3.23	4.19	5.18	8.39	8.58	12.54	13.38	12.56
0.8-1.0	6.13	16.96	8.55	4.24	3.86	3.94	4.77	4.74	9.04	10.30	10.78	11.01	10.24
1.0-1.2	7.36	16.22	1.72	7.33	5.17	6.90	5.76	6.83	9.93	12.15	11.07	12.07	11.40
1.2-1.4	13.16	16.37	0.37	11.01	9.64	10.58	9.33	9.36	11.84	15.18	11.59	10.61	11.01
1.4-1.6	15.74	10.32	0.00	15.31	14.31	14.85	13.42	13.48	13.99	15.77	9.50	9.02	8.87
1.6-1.8	15.42	2.80	0.00	18.62	17.49	18.86	16.24	15.83	11.66	11.72	6.90	5.84	6.19
1.8-2.0	13.04	0.26	0.00	16.76	16.09	17.86	14.81	14.03	8.66	8.31	5.01	4.55	4.58
2.0-2.2	4.77	0.01	0.00	9.09	10.20	9.79	9.23	9.44	4.73	5.19	2.44	2.10	2.36
2.2-2.4	0.71	0.00	0.00	3.55	4.45	3.59	3.77	4.06	1.25	1.98	0.88	0.30	0.59
2.4-2.6	0.04	0.00	0.00	0.92	0.84	0.88	0.71	1.34	0.24	0.36	0.14	0.10	0.10
2.6-2.8	0.00	0.00	0.00	0.03	0.28	0.03	0.19	0.14	0.12	0.09	0.02	0.06	0.03
2.8-3.0	0.00	0.00	0.00	0.00	0.01	0.00	0.01	0.00	0.00	0.00	0.00	0.00	0.00
highlighted	57.36	49.54	56.20	50.69	47.89	51.57	44.47	43.34	37.48	65.12	69.35	70.74	69.47
1.0-2.0m/s	64.71	45.96	2.09	69.03	62.70	69.04	59.56	59.52	56.07	63.14	44.07	42.08	42.04
1.0-2.4m/s	70.20	45.97	2.09	81.67	77.36	82.43	72.56	73.02	62.05	70.31	47.39	44.48	45.00

C.3. MRSU SST Imagery

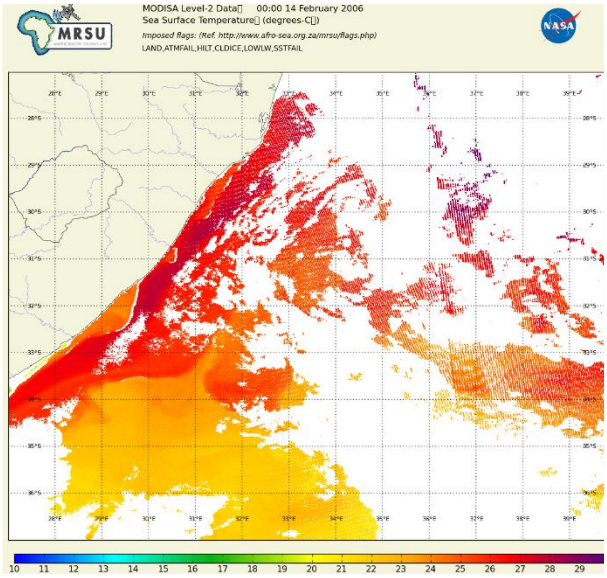

Figure C.1.Image from MRSU showing sea surface temperature along East Coast of South Africa during a Natal Pulse for 14 February 2006.

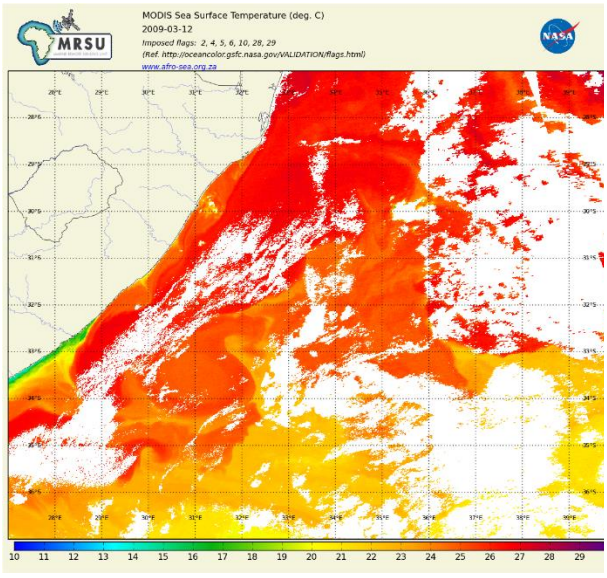

Figure C.2. Image from MRSU showing sea surface temperature along South Africa's East Coast during a Natal Pulse for 12 March 2009.

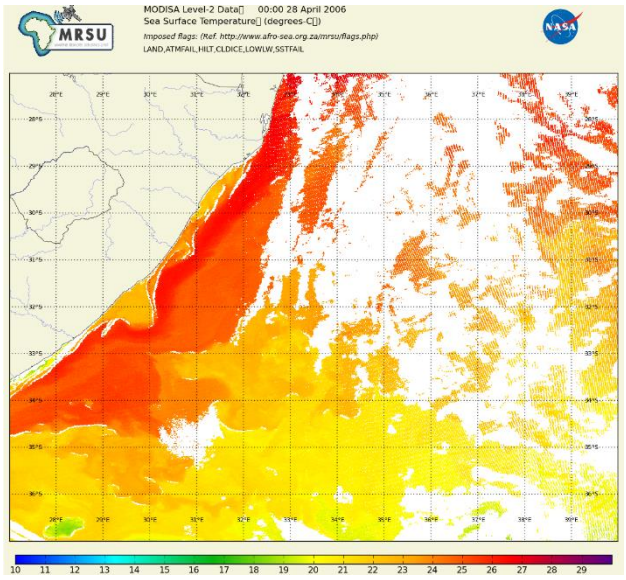

Figure C.3. Image from MRSU showing sea surface temperature along East Coast of South Africa during a Natal Pulse for 28 April 2006.

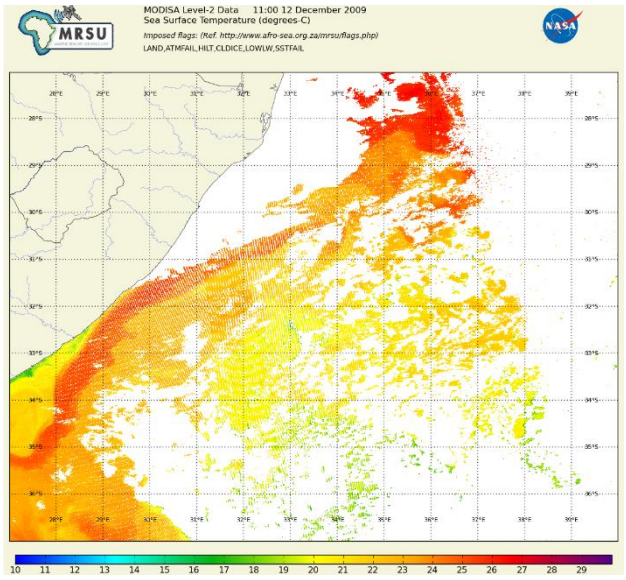

Figure C.4.MRSU image displaying sea-surface temperature on the East coast of South Africa during a Natal Pulse event for 12 December 2009.

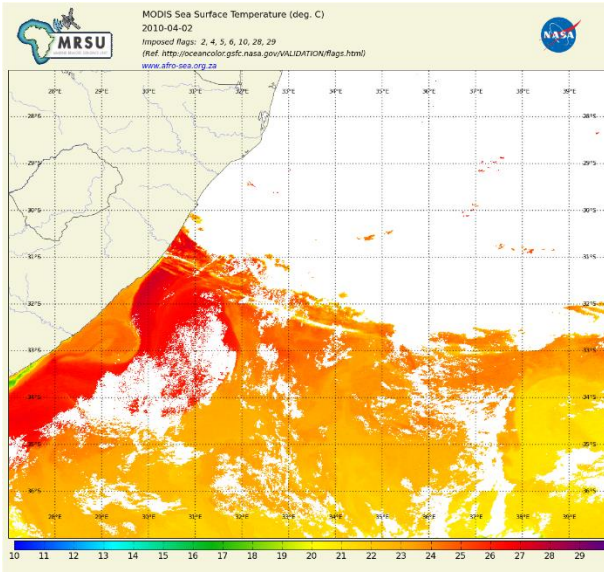

Figure C.5. Image of sea surface temperature along the East coast of South Africa from MRSU during a Natal Pulse during 2 April 2010.

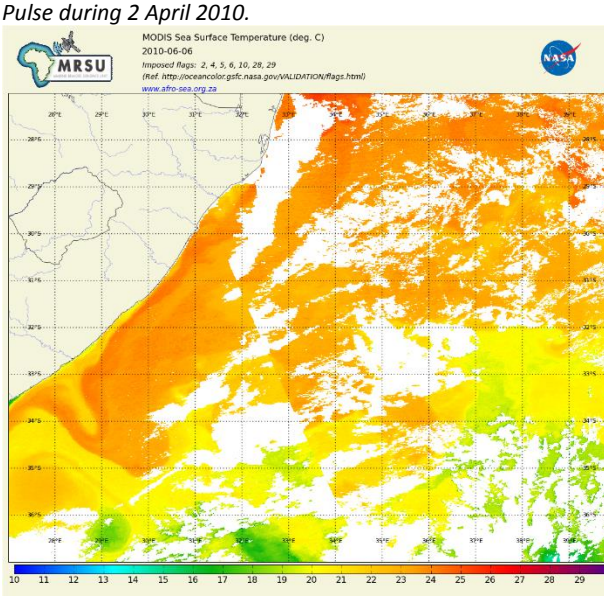

Figure C.6. Image from MRSU displaying sea surface temperature along the East coast of South Africa for 6 June 2010 during a Natal Pulse event.

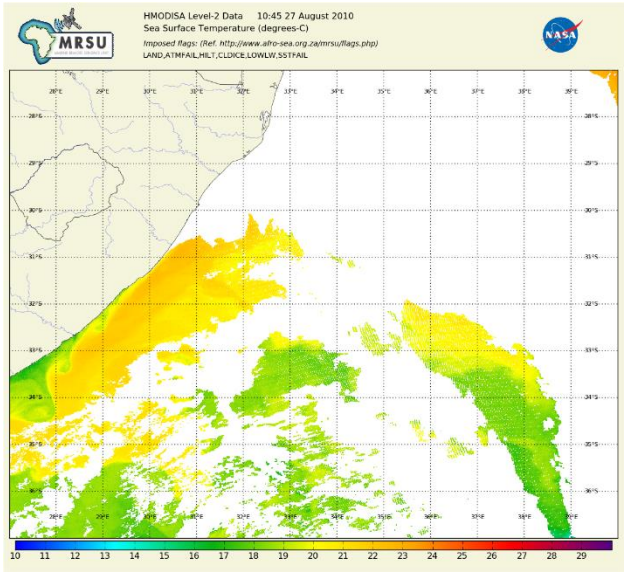

Figure C.7. Image from MRSU showing the sea surface temperature on the East coast of South Africa for 27 August 2010 during a Natal Pulse event.

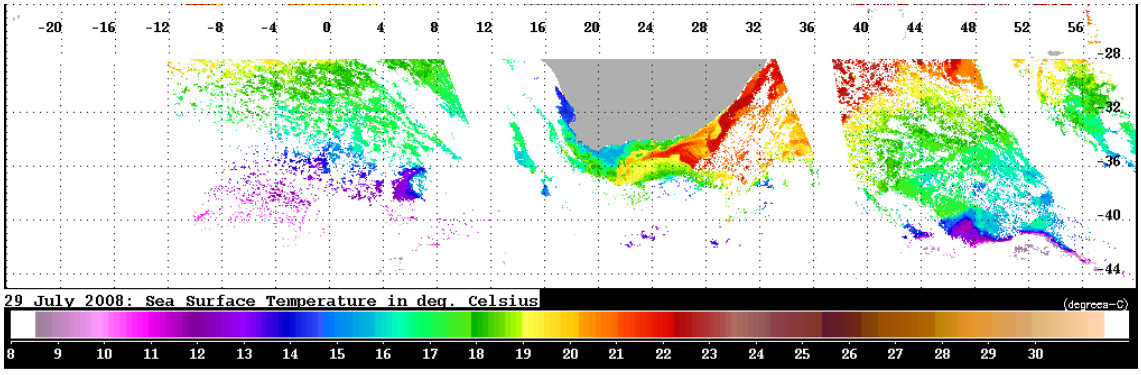

Figure C.8. Image from MRSU displaying the sea surface temperature around the coast of South Africa during a Natal Pulse for 29 July 2008.

D. Appendix D

D.1. Potential Power Output and Kite Operationality

Table D.1. Power output when varying velocity and kite wing area

Power (kW)	**Velocity (m/s)**						
Area (m^2)	**0.8**	**1**	**1.2**	**1.4**	**1.6**	**1.8**	**2**
0	0.00	0.00	0.00	0.00	0.00	0.00	0.00
1	8.76	17.12	29.58	46.97	70.11	99.82	136.93
2	17.53	34.23	59.16	93.94	140.22	199.65	273.87
3	26.29	51.35	88.73	140.90	210.33	299.47	410.80
4	35.05	68.47	118.31	187.87	280.44	399.30	547.73
5	43.82	85.58	147.89	234.84	350.55	499.12	684.67

Table D.2. Power output varying the lift to drag ratio with a change in area and a change in velocity based on the Loyd Equation.

POWER	Power 1		Power 2		Power 3	
	$A_1(m^2)$	$v_1(m/s)$	$A_2(m^2)$	$v_2(m/s)$	$A_3(m^2)$	$v_3(m/s)$
C_L/C_D	3	1	3	1.5	6	1
0	0.00		0.00		0.00	
2	0.91		3.08		1.83	
4	3.65		12.32		7.30	
6	8.22		27.73		16.43	
8	14.61		49.30		29.21	
10	22.82		77.03		45.64	
12	32.86		110.92		65.73	
14	44.73		150.97		89.46	
16	58.42		197.18		116.85	
18	73.94		249.56		147.89	
20	91.29		308.10		182.58	

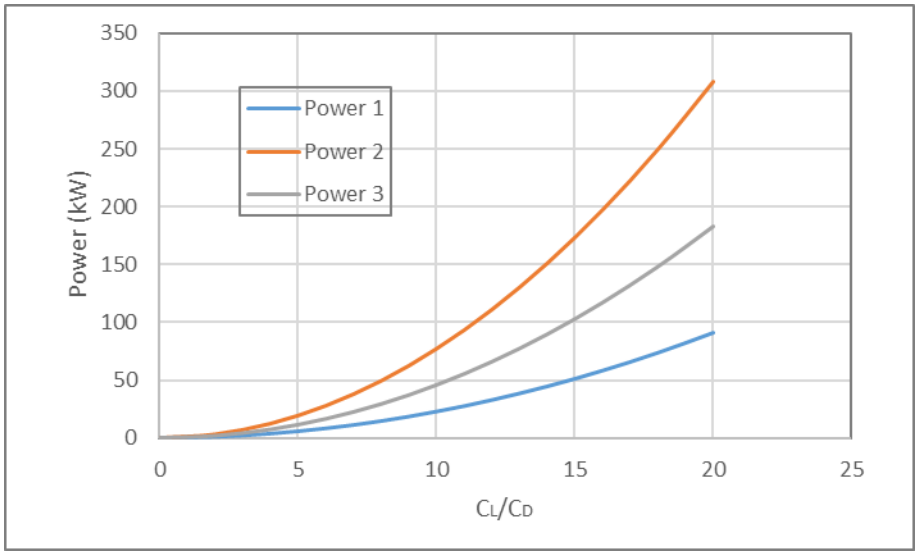

Figure D.1. Graph showing the power output when varying the lift to drag ratio with a change in area and a change in velocity to compare.

Table D.3. Power produced for various cut-in current speeds applying the Loyd equation to the factored HYCOM model dataset.

CUT-IN SPEED (m/s)	Power (kW)
0	137.43
0.2	137.42
0.4	137.33
0.6	136.85
0.8	135.23
1	131.14
1.2	122.55
1.4	107.61
1.6	85.59
1.8	59.22
2	33.34
2.4	0.00

Table D.4.Percentage of locations in operation for time series 1.

cut-in speed(m/s)	0.8	1
Location	Working (%)	Working (%)
CM	91.93	90.58
EL	92.83	89.69
FR1	79.19	71.95

Table D.5.Percentage of locations in operation for timeseries2.

cut-in speed(m/s)	0.8	1
Location	Working (%)	Working (%)
CM	76.56	72.76
EL	70.29	62.24
FR2	56.93	48.24

Table D.6. Frequency and percentage of number of locations working at the same time for time series 1 with a cut-in speed of 0.8m/s.

Time series 1	Frequency	Percentage
not working	0	0
1 working	9	4.07
2 working	62	28.05
3 working	150	67.87

Table D.7.Frquency and percentage of number of locations working at the same time for time series 1 with a cut-in speed of 1.0m/s.

Time series 1	Frequency	Percentage
Not working	0	0
1 working	17	7.69
2 working	72	32.58
3 working	132	59.73

Table D.8. Frequency and percentage for number of locations operational for time series 2 at a cut-in speed of 0.8m/s.

Time series 2	Frequency	Percentage
Not working	43	5.85
1 working	173	23.54
2 working	241	32.79
3 working	278	37.82

Table D.9. Frequency and percentage for number of locations operational for time series 2 at a cut-in speed of 1.0m/s.

Time series 2	Frequency	Percentage
not working	67	9.12
1 working	208	28.3
2 working	247	33.61
3 working	213	28.98

Table D.10. KEF and operationality for the factored HYCOM dataset using a cut-in speed of 1.0m/s.

cut-in speed = 1.0	All Points									Best Point					
FACTORED HYCOM	Avg. KEF	Power (kW)	Not working (%)	0<x<25%	25<x<50%	50<x<75%	75<x<100%	Consecutive Days Inoperational	Consecutive Days Op.<25%	Avg. KEF	Power (kW)	Not working (%)	Consecutive Days Inoperational	KEF (%)	Working (%)
PE:CM	1.25	62.73	7.39	11.56	14.54	25.78	40.72	23	37	1.95	97.64	32.30	39	64.25	88.79
CM:EL	1.54	76.90	11.68	9.93	8.30	11.44	58.64	13	18	2.09	104.30	28.96	25	73.73	94.71
EL:FR2	1.30	64.79	14.26	8.34	9.57	17.16	50.66	19	24	1.97	98.37	25.15	26	65.87	86.40
EL:FR1	1.21	60.65	13.51	11.12	8.22	18.87	48.27	19	25	1.97	98.37	25.15	26	61.66	83.99
FR2:FR1	0.84	41.92	38.66	2.07	4.73	3.06	51.49	33	33	0.98	49.09	45.05	33	85.40	99.57
Total	1.31	65.57	1.03	8.54	20.22	32.46	37.74	3	8	2.09	104.30	28.96	25	62.87	88.14
PE:EL	1.35	67.49	2.98	10.01	17.52	29.36	40.13	7	14	2.09	104.30	28.96	25	64.70	88.00
CM:FR1	1.36	68.17	5.56	11.84	13.11	19.51	49.98	10	14	2.09	104.30	28.96	25	65.36	91.38
PE:FR2	1.34	66.84	1.15	8.90	18.83	31.62	39.49	3	10	2.09	104.30	28.96	25	64.08	88.74

Table D.11. KEF and operationality for the factored reanalysis HYCOM dataset using a cut-in speed of 1.0m/s.

cut-in speed = 1.0	All Points									Best Point					
FACTORED REAN	Avg. KEF	Power (kW)	Not working (%)	0<x<25%	25<x<50%	50<x<75%	75<x<100%	Consecutive Days Inoperational	Consecutive Days Op.<25%	Avg. KEF	Power (kW)	Not working (%)	Consecutive Days Inoperational	KEF (%)	Working (%)
PE:CM	1.25	62.46	4.76	11.88	17.82	38.93	26.61	15	21	2.14	107.13	34.32	21	58.30	84.93
CM:EL	1.29	64.56	13.10	8.86	12.32	16.83	48.89	13	18	2.09	104.41	28.19	22	61.83	86.92
EL:FR2	1.01	50.72	15.83	13.28	12.58	12.14	46.16	15	20	1.67	83.53	28.23	28	60.71	80.27
EL:FR1	1.00	50.10	14.80	15.09	11.29	14.83	43.99	15	21	1.67	83.53	28.23	22	59.98	80.16
FR2:FR1	0.95	47.31	37.23	0.30	5.39	0.41	56.68	27	27	1.03	51.48	39.26	27	91.90	94.17
Total	1.19	59.50	0.81	9.85	24.65	36.72	27.97	1	9	2.14	107.13	34.32	21	55.55	88.12
PE:EL	1.26	63.17	1.73	11.59	20.92	35.39	30.37	7	16	2.14	107.13	34.32	21	58.96	88.32
CM:FR1	1.14	56.80	6.42	13.80	15.65	23.06	41.07	8	15	2.09	104.41	28.19	22	54.40	83.27
PE:FR2	1.20	60.16	0.81	10.30	23.69	36.94	28.27	1	9	2.14	107.13	34.32	21	56.15	88.17

Table D.12.KEF and operationality using the alternative offshore locations from HYCOM for a cut-in speed of 1.0m/s.

cut-in speed = 1.0	All Points									Best Point					
ALT HYCOM	Avg. KEF	Power (kW)	Not working (%)	0<x<25%	25<x<50%	50<x<75%	75<x<100%	Consecutive Days Inoperational	Consecutive Days Op.<25%	Avg. KEF	Power (kW)	Not working (%)	Consecutive Days Inoperational	KEF (%)	Working (%)
PE:CM	1.02	51.22	13.87	13.39	15.34	16.21	41.20	25	37	1.36	67.77	32.90	44	75.58	84.22
CM:EL	1.35	67.26	12.83	9.77	9.06	8.14	60.19	16	25	1.51	75.46	26.50	31	89.14	93.00
EL:FR2	1.36	68.06	11.84	8.62	8.58	8.38	62.57	19	26	1.65	82.56	25.59	26	82.43	94.55
EL:FR1	1.31	65.37	9.14	10.17	10.21	12.91	57.57	19	25	1.65	82.56	25.59	26	79.18	92.22
FR2:FR1	1.06	53.24	25.90	3.14	12.32	7.47	51.17	33	33	1.43	71.60	31.43	34	74.36	88.61
Total	1.18	59.06	1.47	8.22	21.26	32.34	36.71	4	15	1.65	82.56	25.59	26	71.54	84.35
PE:EL	1.13	56.61	5.05	12.63	18.39	25.51	38.42	9	41	1.51	75.46	26.50	31	75.01	82.30
CM:FR1	1.32	66.25	3.97	11.01	12.67	19.23	53.12	5	19	1.65	82.56	25.59	26	80.24	92.05
PE:FR2	1.19	59.37	2.19	8.22	21.10	30.67	37.82	7	15	1.65	82.56	25.59	26	71.91	84.49

Table D.13. The percentage of kites operational for certain percentage of the duration intervals using

CUT-IN SPEED = 0.8	HYCOM	REAN	ALTERNATE		CUT-IN SPEED = 1.0	HYCOM	REAN	ALTERNATE
NOT WORKING	0.14	0.00	0.41		NOT WORKING	1.16	1.10	1.37
0-10	1.30	1.78	0.82		0-10	2.74	2.87	2.26
10-20	1.57	2.40	1.71		10-20	2.81	4.86	2.81
20-30	2.33	3.63	2.12		20-30	4.72	7.05	5.20
30-40	4.31	5.95	3.01		30-40	6.71	9.72	8.28
40-50	5.27	8.83	6.37		40-50	9.65	13.62	10.34
50-60	8.15	11.50	10.95		50-60	11.36	13.55	15.40
60-70	13.21	12.53	13.21		60-70	15.47	16.02	12.66
70-80	15.33	18.48	15.33		70-80	14.17	14.24	12.80
80-90	16.70	19.51	10.81		80-90	16.43	11.70	10.27
90-100	31.69	15.40	35.25		90-100	14.78	5.27	18.62

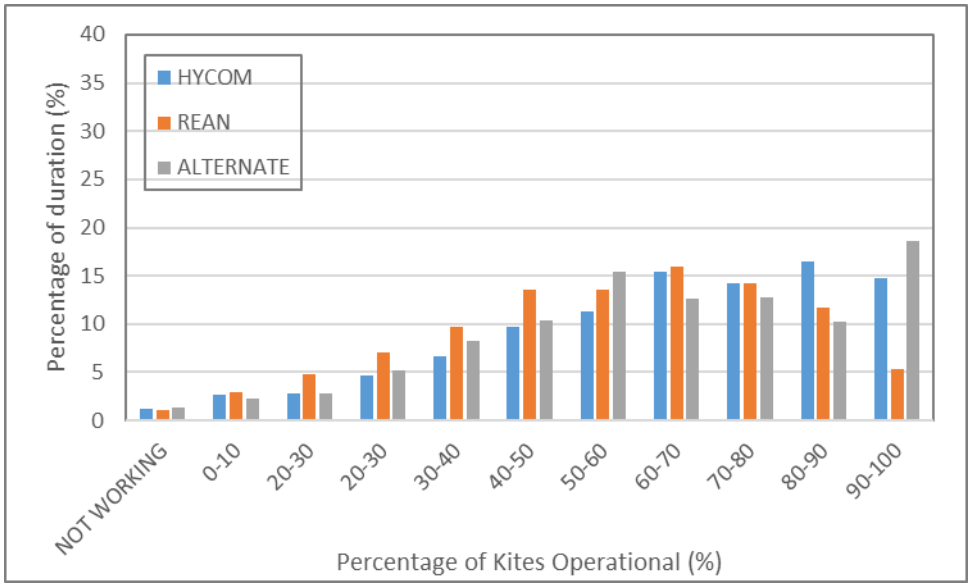

Figure D.2. The percentage of kites operational over the specified percentage of duration intervals using all datasets with a cut-in speed of 1.0m/s.

E. Appendix

Average household power consumption is estimated at between 500 and 750 kWh per month (Fripp, 2016). The total electricity consumption of South Africa during 2014 was 249, 919 GWh (Internation Energy Agency, 2014).

100MW system assuming it operates continuously for one year:

$$Energy = 100 \times 365 \times 24$$
$$= 876000\ MWh$$
$$= 876\ GWh$$

$$Percentage\ of\ Total\ Consumption = \frac{876}{249919} \times 100$$
$$= 0.35\%$$

$$No.households = \frac{876 \times 10^6}{650 \times 12}$$
$$= 112308$$

E.1. Distributed Hydro-Kite Array

Initial hydro-kite array assumption: 400 hydro-kites spaced at 1km intervals along the coast.

The maximum capacity of each kite is 250 kW to provide 100 MW. Maximum power produced is calculated using the highest velocity at which the kite can operate at, cut-out speed of 2.40 m/s. To attain more realistic power outputs a factor of 0.5 is applied to the Loyd equation.

Kite wing area required:

$$P = 0.5 \times \left(\frac{2}{27} \times \rho \times v^3 \times A \times C_L \times \frac{{C_L}^2}{C_D}\right)$$

$$A = \left(\frac{27 \times 2 \times P}{2 \times \rho \times v^3 \times C_L \times \frac{{C_L}^2}{C_D}}\right)$$
$$= 2.11\ m^2$$

If the wing area was increased the number of kites required would be reduced while maintaining the same power output.

Maximum power produced by one hydro-kite with a kite wing area of 3m^2:

$$P = 0.5 \times \left(\frac{2}{27} \times 1027 \times 10^{-3} \times 2.4^3 \times 3 \times 1 \times 15^2\right)$$
$$= 355\ kW$$

Average power produced by one hydro-kite with a wing area of 3m^2 using average KEF of 1.35kW/m^2:

$$P = 0.5 \times \left(\frac{4}{27} \times KEF \times A \times C_L \times \frac{{C_L}^2}{C_D}\right)$$
$$= 67.5\ kW$$

Number of kites required in a distributed system assuming all kites can produce maximum power at the same time:

$$Number\ of\ Kites = \frac{Required\ Power\ Capacity\ (kW)}{Maximum\ Power\ from\ one\ hydro-kite\ (kW)}$$
$$= \frac{100000}{355}$$
$$= 282\ kites$$

More kites are required due to the maximum power not being applied to all kites within the system at the same time.

Average energy produced by one hydro-kite in one year:

$$Energy = 67.5 \times 365 \times 24$$
$$= 591300\ kWh$$

E.2. Concentrated Hydro-Kite Array

Table E.1. Power and energy generated in one year from using the location with the highest average KEF for 3m² and 6m² kites.

Kite Area (m^2)	**3**	**6**
Average Power (kW)	105.5	211
Energy in 1 year (kWh)	924180	1848360
Maximum Power (kW)	355	710
Number kites for 100MW capacity	282	141

Table E.2. Co-ordinates for lines segments of hydro-kites within Option 3A

Name	Latitude	Longitude		Name	Latitude	Longitude
LINE 1 START	-31.6986	29.69618		LINE 6 START	-32.894	28.38012
LINE 1 MID	-31.7824	29.60262		LINE 6 MID	-32.9802	28.28776
LINE 1 END	-31.8716	29.50321		LINE 6 END	-33.0718	28.18963
LINE 2 START	-31.8978	29.47397		LINE 7 START	-33.0772	28.18386
LINE 2 MID	-31.9817	29.38041		LINE 7 MID	-33.1634	28.0915
LINE 2 END	-32.0708	29.281		LINE 7 END	-33.2407	27.98039
LINE 3 START	-32.097	29.25177		LINE 8 START	-33.3128	27.87238
LINE 3 MID	-32.1809	29.15821		LINE 8 MID	-33.3849	27.76437
LINE 3 END	-32.27	29.0588		LINE 8 END	-33.4615	27.64962
LINE 4 START	-32.4063	28.90677		LINE 9 START	-33.466	27.64287
LINE 4 MID	-32.4902	28.81321		LINE 9 MID	-33.5381	27.53486
LINE 4 END	-32.5815	28.71491		LINE 9 END	-33.6147	27.4201
LINE 5 START	-32.5869	28.70914		LINE 10 START	-33.6192	27.41335
LINE 5 MID	-32.6731	28.61678		LINE 10 MID	-33.6913	27.30534
LINE 5 END	-32.7647	28.51865		LINE 10 END	-33.7747	27.20001

Table E.3. Co-ordinates for lines segments of hydro-kites within Option 3B

Name	Latitude	Longitude		Name	Latitude	Longitude
LINE 1 START	-31.6986	29.69618		LINE 7 START	-32.894	28.38012
LINE 1 MID	-31.7667	29.62016		LINE 7 MID	-32.9641	28.30508
LINE 1 END	-31.8401	29.53829		LINE 7 END	-33.0395	28.22426
LINE 2 START	-31.9135	29.45643		LINE 8 START	-33.0772	28.18386
LINE 2 MID	-31.9817	29.38041		LINE 8 MID	-33.1473	28.10882
LINE 2 END	-32.0551	29.29855		LINE 8 END	-33.2136	28.02089
LINE 3 START	-32.1285	29.21668		LINE 9 START	-33.2181	28.01414
LINE 3 MID	-32.1966	29.14066		LINE 9 MID	-33.2767	27.92638
LINE 3 END	-32.27	29.0588		LINE 9 END	-33.3398	27.83188
LINE 4 START	-32.4116	28.90092		LINE 10 START	-33.3578	27.80488
LINE 4 MID	-32.4797	28.8249		LINE 10 MID	-33.4164	27.71712
LINE 4 END	-32.5545	28.74377		LINE 10 END	-33.4795	27.62261
LINE 5 START	-32.5599	28.738		LINE 11 START	-33.4975	27.59561
LINE 5 MID	-32.63	28.66296		LINE 11 MID	-33.5561	27.50786
LINE 5 END	-32.7054	28.58215		LINE 11 END	-33.6192	27.41335
LINE 6 START	-32.7108	28.57637		LINE 12 START	-33.6372	27.38635
LINE 6 MID	-32.7808	28.50133		LINE 12 MID	-33.6958	27.29859
LINE 6 END	-32.8563	28.42052		LINE 12 END	-33.7645	27.21232

E.3. Load Capacity for Distributed System

Table E.4. The maximum power produced by various hydro-kite arrangements using model predictions for locations from the factored HYCOM model

	750 KITES			375 KITES			340 KITES	
LINE	Max. Power (MW)	Design Capacity (MW)		Max. Power (MW)	Design Capacity (MW)		Max. Power (MW)	Design Capacity (MW)
1	20.99	21		10.49	11		9.51	10
2	20.81	21		10.40	10.5		9.43	9.5
3	19.66	20		9.83	10		8.91	9
4	23.67	24		11.83	12		10.73	11
5	19.58	20		9.79	10		8.88	9
6	22.21	22.5		11.11	11.5		10.07	10.5
7	22.02	22.5		11.01	11.5		9.98	10
8	22.06	22.5		11.03	11.5		10.00	10.5
9	21.75	22		10.87	11		9.86	10
10	21.84	22		10.92	11		9.90	10
TOTAL	214.57	217.5		107.29	110		97.27	99.5

Table E.5.Design load capacity for distributed array Option 3A using proposed kite placement locations and data extracted from the factored HYCOM model.

340 KITES	Loyd Equation Power Calculation				Realistic Power Output ≈ 50%				
LINE	Average Power per kite (kW)	Max Power per line (kW)	Max Power per kite (kW)		Average Power per kite (kW)	Max Power per line (kW)	Max Power per kite (kW)		Design Load Capacity (MW)
1	150.34	19013.70	559.23		75.17	9506.85	279.61		10
2	145.72	18513.98	544.53		72.86	9256.99	272.26		9.5
3	151.20	17625.08	518.38		75.60	8812.54	259.19		9
4	132.47	22233.52	653.93		66.23	11116.76	326.96		11.5
5	159.99	18248.54	536.72		79.99	9124.27	268.36		9.5
6	169.22	19566.02	575.47		84.61	9783.01	287.74		10
7	161.72	20548.48	604.37		80.86	10274.24	302.18		10.5
8	143.50	20508.07	603.18		71.75	10254.04	301.59		10.5
9	121.70	20374.27	599.24		60.85	10187.13	299.62		10.5
10	100.74	19369.27	569.68		50.37	9684.64	284.84		10
TOTAL		196000.92			71.83	98000.46			101

Table E.6. Design load capacity for distributed array Option 3B using proposed kite placement locations and data extracted from the factored HYCOM model.

336 KITES	Loyd Equation Power Calculation				Realistic Power Output ≈ 50%				
LINE	Average Power per kite (kW)	Max Power per line (kW)	Max Power per kite (kW)		Average Power per kite (kW)	Max Power per line (kW)	Max Power per kite (kW)		Design Load Capacity (MW)
1	147.22	17240.76	615.74		73.61	8620.38	307.87		9
2	144.28	16263.92	580.85		72.14	8131.96	290.43		8.5
3	158.19	15381.53	549.34		79.10	7690.77	274.67		8
4	133.90	18605.03	664.47		66.95	9302.52	332.23		9.5
5	148.96	15412.82	550.46		74.48	7706.41	275.23		8
6	166.48	15218.19	543.51		83.24	7609.10	271.75		8
7	173.71	16959.18	605.68		86.86	8479.59	302.84		8.5
8	160.94	16883.18	602.97		80.47	8441.59	301.49		8.5
9	151.44	16472.48	588.30		75.72	8236.24	294.15		8.5
10	141.69	16141.32	576.48		70.85	8070.66	288.24		8.5
11	115.04	16206.59	578.81		57.52	8103.29	289.40		8.5
12	101.11	16583.77	592.28		50.55	8291.89	296.14		8.5
TOTAL		197368.79			72.62	98684.39			102

Table E.7.Average power, energy and number of households that can be powered using options 3A and 3B of a distributed hydro-kite system.

Option	3A	3B
Total Average Power Produced (kW)	24422	24400
Energy Produced in one year (MWh)	213938	213747
No. of Households Powered	27428	27403

E.4. Distributed Concentrated Farms

Table E.8. Percentage working of locations where farms will be placed for a cut-in speed of 0.8m/s.

Cut-in speed = 0.8m/s	FARM 1	FARM 2	FARM 3
HYCOM Grid Ref.	(41, 126)	(32, 118)	(23, 109)
Frequency	1879	1937	2058
Percentage Working	74.65	76.96	81.76

Table E.9. Percentage working of locations where farms will be placed for a cut-in speed of 1.0m/s.

Cut-in speed = 1.0m/s	FARM 1	FARM 2	FARM 3
HYCOM Grid Ref.	(41, 126)	(32, 118)	(23, 109)
count	1704	1788	1884
Percentage Working	67.70	71.04	74.85

Table E.10. Percentage that a certain number of kites will be working using the three main location for a cut-in speed of 1.0m/s.

Cut-in speed = 1.0m/s	FREQUENCY	PERCENTAGE WORKING
3 WORKING	1200	47.68
2 WORKING	670	26.62
1 WORKING	436	17.32
NONE WORKING	211	8.38

Table E.11. Percentage that a certain number of kites will be working using the three main locations for a cut-in speed of 0.8m/s.

Cut-in speed = 0.8m/s	FREQUENCY	PERCENTAGE WORKING
3 WORKING	1418	56.34
2 WORKING	633	25.15
1 WORKING	354	14.06
NONE WORKING	112	4.45

E.5. Submarine Cable Data

E.5.1. Derating Factor

Table E.12. Ground temperature correction factor

Ground Temperature Correction Factor (F2)	
Ground Temperature (°C)	Insulation: XLPE/EPR
10	1.07
15	1.04
20	0.96
25	0.93
35	0.89
40	0.85
45	0.8
50	0.76
55	0.71
60	0.65
65	0.6
70	0.53
75	0.46
80	0.38

Table E.13. Soil thermal resistivity factor.

Soil Thermal Resistivity Factor (F3)	
Resistivity (Km/W)	F3
1	1.18
1.5	1.1
2	1.05
2.5	1
3	0.96

Table E.14. Cable laying depth correction factor.

Cable Depth Correction Factor (F5)	
Laying Depth (m)	F5
0.5	1.1
0.7	1.05
0.9	1.01
1	1
1.2	0.98
1.5	0.96

E.5.2. MV Cables

Table E.15.Constructional and electrical data for MV submarine cables from NEXANS for conductor areas from between 35mm² and 240mm² for voltage ratings of 24kV and 36kV.

2XS(FL)2YRAA 12/20(24) kV — **Constructional Data**

1	2	3	4	5	6		7	8	9	10	11
Nominal cross sectional area of conductor (mm²)	Conductor copper round stranded diameter over conductor (mm)	Insulation XLPE wall thickness (mm)	Screen copper wires and counter helix cross sectional area (mm²)	Metallic tape aluminium wall thickness (mm)	Core sheath PE black wall thickness (mm)	diameter (mm)	Bedding wall thickness (mm)	Armour steel wires round galvanized diameter (mm)	Serving bitumen fib. material and lime wash wall thickness (mm)	Outer diameter of cable (mm)	Cable weight (t/km)
35	7.0	5.5	16	0.2	2.5	28	2	3.15	3.5	78	8.8
50	8.2	5.5	16	0.2	2.5	30	2	3.15	3.5	83	9.3
70	9.9	5.5	16	0.2	2.5	31	2	4.0	3.5	87	11.4
95	11.5	5.5	16	0.2	2.5	33	2	4.0	3.5	89	12.7
120	13.0	5.5	16	0.2	2.5	34	2	4.0	4.0	94	14.1
150	14.5	5.5	25	0.2	2.5	36	2	4.0	4.0	97	15.3
185	16.1	5.5	25	0.2	2.5	37	2	5.0	4.0	102	18.6
240	18.6	5.5	25	0.2	2.5	40	2	5.0	4.0	108	21.1

2XS(FL)2YRAA 12/20(24) kV — **Electrical Data**

1		2	3	4	5	6	7	8	9	
Nominal cross sectional area conductor (mm²)	screen (mm²)	Conductor resistance DC 20°C (Ω/km)	Conductor resistance AC 90°C (Ω/km)	Screen resistance 20°C (Ω/km)	Capacitance (μF/mm)	Inductance (mH/km)	Current rating (A)	Losses (W/m)	1s short circuit current after full load at 90°C conductor temperature conductor (kA)	screen (kA)
35	16	0.524	0.67	1.15	0.17	0.47	171	60	5.0	3.3
50	16	0.387	0.49	1.15	0.18	0.44	199	60	7.1	3.3
70	16	0.268	0.34	1.15	0.20	0.41	243	63	10.0	3.3
95	16	0.193	0.25	1.15	0.22	0.40	292	67	13.6	3.3
120	16	0.153	0.20	1.15	0.24	0.38	328	68	17.1	3.3
150	25	0.124	0.16	0.73	0.26	0.37	364	70	21.4	5.1
185	25	0.0991	0.13	0.73	0.28	0.35	408	72	26.5	5.1
240	25	0.0754	0.10	0.73	0.31	0.34	467	75	34.3	5.1

2XS(FL)2YRAA 18/30(36) kV — **Constructional Data**

1	2	3	4	5	6		7	8	9	10	11
Nominal cross sectional area of conductor (mm²)	Conductor copper round stranded diameter over conductor (mm)	Insulation XLPE wall thickness (mm)	Screen copper wires and counter helix cross sectional area (mm²)	Metallic tape aluminium wall thickness (mm)	Core sheath PE black wall thickness (mm)	diameter (mm)	Bedding wall thickness (mm)	Armour steel wires round galvanized diameter (mm)	Serving bitumen fib. material and lime wash wall thickness (mm)	Outer diameter of cable (mm)	Cable weight (t/km)
50	8.2	8.0	16	0.2	2.5	35	2	3.15	3.5	93	11.1
70	9.9	8.0	16	0.2	2.5	36	2	4.0	4.0	99	12.8
95	11.5	8.0	16	0.2	2.5	38	2	4.0	4.0	102	14.9
120	13.0	8.0	16	0.2	2.5	39	2	4.0	4.0	105	16.2
150	14.5	8.0	25	0.2	2.5	41	2	4.0	4.0	108	17.6
185	16.1	8.0	25	0.2	2.5	42	2	5.0	4.0	113	21.0
240	18.6	8.0	25	0.2	2.5	45	2	5.0	4.0	119	23.4

2XS(FL)2YRAA 18/30(36) kV — **Electrical Data**

1		2	3	4	5	6	7	8	9	
Nominal cross sectional area conductor (mm²)	screen (mm²)	Conductor resistance DC 20°C (Ω/km)	Conductor resistance AC 90°C (Ω/km)	Screen resistance 20°C (Ω/km)	Capacitance (μF/mm)	Inductance (mH/km)	Current rating (A)	Losses (W/m)	1s short circuit current after full load at 90°C conductor temperature conductor (kA)	screen (kA)
50	16	0.387	0.49	1.15	0.14	0.48	202	62	7.1	3.3
70	16	0.268	0.34	1.15	0.15	0.45	245	65	10.0	3.3
95	16	0.193	0.25	1.15	0.17	0.42	291	67	13.6	3.3
120	16	0.153	0.20	1.15	0.18	0.41	330	69	17.1	3.3
150	25	0.124	0.16	0.73	0.19	0.39	366	71	21.4	5.1
185	25	0.0991	0.13	0.73	0.21	0.38	411	74	26.5	5.1
240	25	0.0754	0.10	0.73	0.23	0.36	470	77	34.3	5.1

Table E.16. Data provided for three core submarine cables with copper wire screen from ABB for voltages of 12kV, 24kV and 36kV.

Cross-section of conductor	Diameter of conductor	Insulation thickness	Diameter over insulation	Cross section of screen	Outer diameter of cable	Cable weight (Aluminium)	Cable weight (Copper)	Capacitance	Charging current per phase at 50 Hz	Inductance
mm²	mm	mm	mm	mm²	mm	kg/m	kg/m	µF/km	A/km	mH/km
Table 41										
Three-core cables, nominal voltage 10 kV (Um = 12 kV)										
70	9.6	3.4	18.8	16	80.7	13.7	15.0	0.31	0.6	0.41
95	11.2	3.4	20.4	16	84.2	14.4	16.2	0.34	0.6	0.39
120	12.6	3.4	21.8	16	87.2	14.9	17.2	0.37	0.7	0.37
150	14.2	3.4	23.4	16	90.6	15.7	18.5	0.40	0.7	0.36
185	15.8	3.4	25.0	16	94.1	16.5	19.9	0.44	0.8	0.35
240	18.1	3.4	27.3	16	99.1	17.7	22.2	0.48	0.9	0.33
300	20.4	3.4	29.6	16	104.0	18.9	24.5	0.53	1.0	0.32
400	23.2	3.4	32.4	16	110.1	20.8	28.2	0.59	1.1	0.31
500	26.2	3.4	35.8	16	117.4	22.7	32.1	0.66	1.2	0.30
Table 42										
Three-core cables, nominal voltage 20 kV (Um = 24 kV)										
70	9.6	5.5	23.0	16	89.8	15.1	16.4	0.21	0.8	0.44
95	11.2	5.5	24.6	16	93.2	15.8	17.6	0.23	0.9	0.41
120	12.6	5.5	26.0	16	96.2	16.6	18.8	0.25	0.9	0.40
150	14.2	5.5	27.6	16	99.7	17.3	20.1	0.27	1.0	0.38
185	15.8	5.5	29.2	16	103.2	18.2	21.6	0.29	1.1	0.37
240	18.1	5.5	31.5	16	108.1	19.3	23.7	0.32	1.2	0.35
300	20.4	5.5	33.8	16	113.1	20.6	26.2	0.35	1.3	0.34
400	23.2	5.5	36.6	16	119.1	22.5	29.9	0.39	1.4	0.33
500	26.2	5.5	40.0	16	126.5	24.5	33.8	0.43	1.6	0.32
630	29.8	5.5	43.6	16	134.3	26.7	38.5	0.48	1.7	0.31
Table 43										
Three-core cables, nominal voltage 30 kV (Um = 36 kV)										
70	9.6	8.0	28.0	16	100.6	16.9	18.2	0.16	0.9	0.46
95	11.2	8.0	29.6	16	104.0	17.7	19.5	0.18	1.0	0.44
120	12.6	8.0	31.0	16	107.0	18.4	20.7	0.19	1.0	0.42
150	14.2	8.0	32.6	16	110.5	19.3	22.1	0.21	1.1	0.41
185	15.8	8.0	34.2	16	114.0	20.1	23.6	0.22	1.2	0.39
240	18.1	8.0	36.5	16	118.9	21.4	25.9	0.24	1.3	0.38
300	20.4	8.0	38.8	16	123.9	22.6	28.2	0.26	1.4	0.36
400	23.2	8.0	41.6	16	129.9	24.6	32.0	0.29	1.6	0.35
500	26.2	8.0	45.0	16	137.3	26.7	36.0	0.32	1.7	0.34
630	29.8	8.0	48.6	16	145.1	29.2	40.9	0.35	1.9	0.32
800	33.7	8.0	52.5	16	154.4	32.2	47.2	0.38	2.1	0.31

Table E.17.Current ratings specified by voltage for ABB cables. 10-90kV corresponds to cables in Table E.16

10-90 kV XLPE 3-core cables		
Cross section mm²	Copper conductor	Aluminium conductor
	A	A
95	300	235
120	340	265
150	375	300
185	420	335
240	480	385
300	530	430
400	590	485
500	655	540
630	715	600
800	775	660
1000	825	720

100-300 kV XLPE 3-core cables		
Cross section mm²	Copper conductor	Aluminium conductor
	A	A
300	530	430
400	590	485
500	655	540
630	715	600
800	775	660
1000	825	720

Table E.18.Adjusted current ratings to obtain equivalent current rating for larger size NEXANS submarine cables based on data provided from ABB.

CONDUCTOR AREA (mm^2)	CURRENT RATING NEXANS (A)	CURRENT RATING ABB (A)	CURRENT ADJUSTED (A)
95	291	300	291
120	330	340	331
150	366	375	366
185	411	420	410
240	470	480	470
300		530	520
400		590	580
500		655	645
630		715	705
800		775	764
1000		825	814

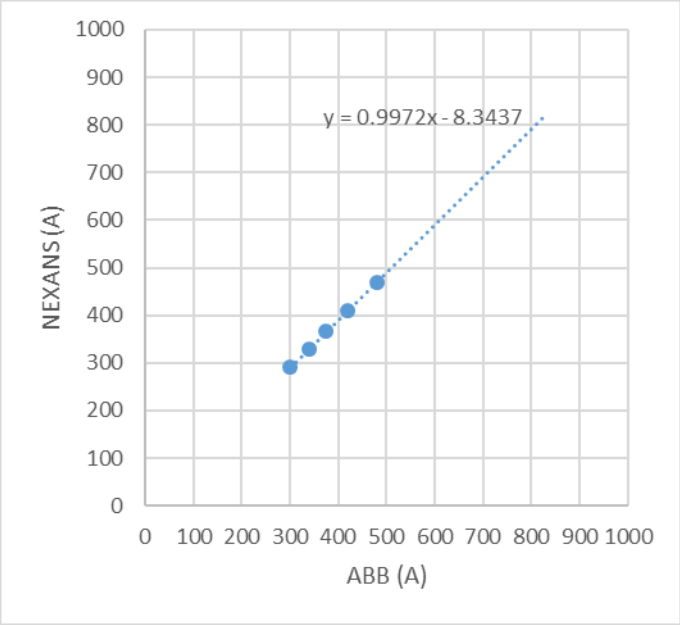

Figure E.1. Scatter plot showing the relationship between the current rating of ABB cables and NEXANS cables for a voltage of 36 kV.

Table E.19. Adjusted inductance to obtain equivalent inductance for larger size NEXANS submarine cables based on data provided from ABB.

CONDUCTOR AREA (mm^2)	INDUCTANCE NEXANS (mH/km)	INDUCTANCE ABB (mH/km)	INDUCTANCE ADJUSTED (mH/km)
95	0.42	0.44	0.423128
120	0.41	0.42	0.403654
150	0.39	0.41	0.393917
185	0.38	0.39	0.374443
240	0.36	0.38	0.364706
300		0.36	0.345232
400		0.35	0.335495
500		0.34	0.325758
630		0.32	0.306284
800		0.31	0.296547
1000		0.3	0.28681

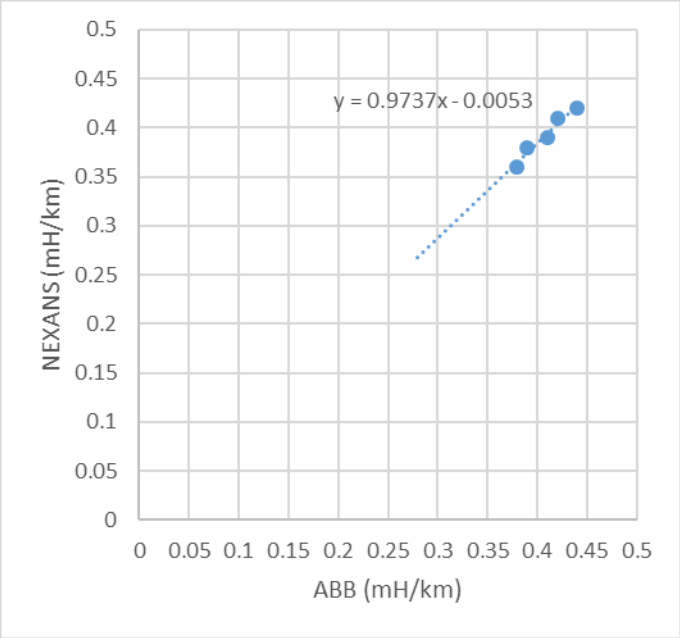

Figure E.2. Scatter plot showing the relationship between inductance of ABB cables and NEXANS cables at a voltage of 36 kV.

Table E.20. Equivalent conductor diameter for larger size NEXANS submarine cables based on data provided from ABB for larger cable sizes and compared with NEXANS.

CONDUCTOR AREA (mm^2)	CONDUCTOR DIAMETER NEXANS (mm)	CONDUCTOR DIAMETER ABB (mm)	CONDUCTOR DIAMETER ADJUSTED (mm)
95	11.5	11.2	11.50
120	13	12.6	12.93
150	14.5	14.2	14.56
185	16.1	15.8	16.19
240	18.6	18.1	18.53
300		20.4	20.88
400		23.2	23.73
500		26.2	26.79
630		29.8	30.46
800		33.7	34.43
1000		37.9	38.72

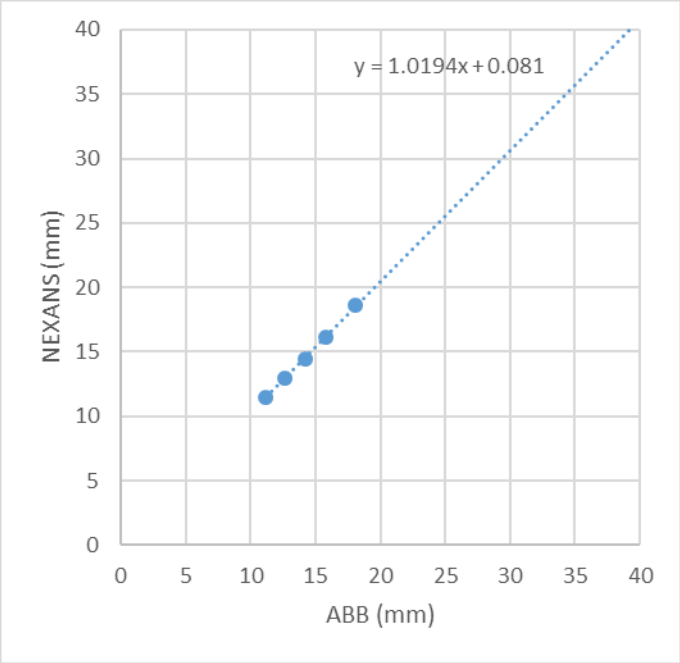

Figure E.3. Scatter plot showing the relationship between conductor diameter of ABB cable and NEXANS cables.

Table E.21. Diameter over insulation estimated for larger size NEXANS cable based on data from ABB and compared with NEXANS data for smaller cable sizes.

CONDUCTOR AREA (mm^2)	DIAMETER OVER INSULATION NEXANS (mm)	DIAMETER OVER INSULATION ABB (mm)	DIAMETER OVER INSULATION ADJUSTED (mm)
95	38	29.6	37.80
120	39	31	39.21
150	41	32.6	40.82
185	42	34.2	42.43
240	45	36.5	44.75
300		38.8	47.07
400		41.6	49.89
500		45	53.32
630		48.6	56.95
800		52.5	60.88
1000		57.3	65.72

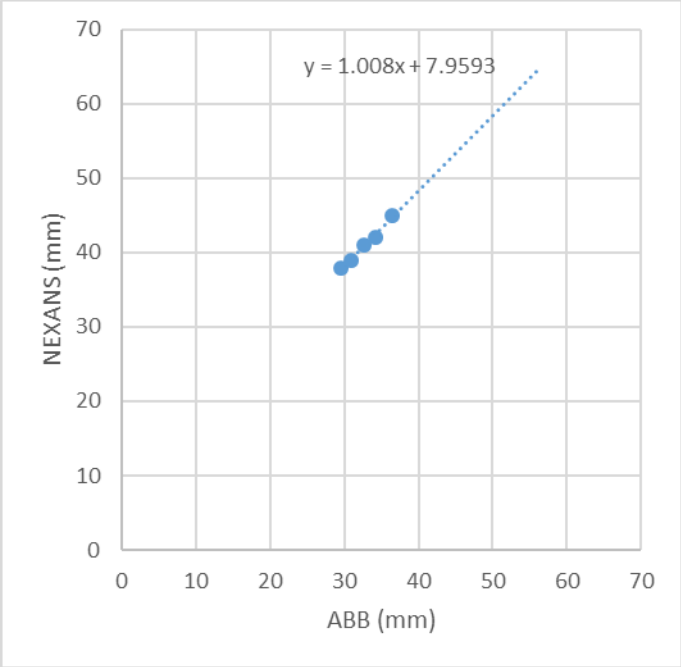

Figure E.4. Scatter plot showing the relationship between the diameter over the insulation for ABB and NEXANS cables.

Table E.22. Resistance calculated using adjusted values equivalent for a NEXANS cable.

CONDUCTOR AREA (mm^2)	CURRENT ADJUSTED (A)	INDUCTANCE ADJUSTED (mH/km)	DC Resistance at 20°C (Ω/km)	DC Resistance at 90°C (Ω/km	x_s^2	y_s	x_p^2	CONDUCTOR DIAMETER ADJUSTED (mm)	DIAMETER OVER INSULATION ADJUSTED (mm)	s	y_p	AC RESISTANCE AT 90°C
95	291	0.423	0.181	0.231	5.431E-	1.536E-	5.431E-	11.50	37.80	37.80	6.717E-	0.231
120	331	0.404	0.144	0.183	6.860E-	2.451E-	6.860E-	12.93	39.21	39.21	1.072E-	0.183
150	366	0.394	0.115	0.147	8.575E-	3.829E-	8.575E-	14.56	40.82	40.82	1.676E-	0.147
185	410	0.374	0.093	0.119	1.058E-	5.825E-	1.058E-	16.19	42.43	42.43	2.550E-	0.119
240	470	0.365	0.072	0.092	1.372E-	9.803E-	1.372E-	18.53	44.75	44.75	4.293E-	0.092
300	520	0.345	0.057	0.073	1.715E-	1.532E-	1.715E-	20.88	47.07	47.07	6.713E-	0.073
400	580	0.335	0.043	0.055	2.287E-	2.723E-	2.287E-	23.73	49.89	49.89	1.194E-	0.055
500	645	0.326	0.034	0.044	2.858E-	4.255E-	2.858E-	26.79	53.32	53.32	1.868E-	0.044
630	705	0.306	0.027	0.035	3.601E-	6.755E-	3.601E-	30.46	56.95	56.95	2.970E-	0.035
800	764	0.297	0.022	0.027	4.573E-	1.089E-	4.573E-	34.43	60.88	60.88	4.795E-	0.027
1000	814	0.287	0.017	0.022	5.716E-	1.702E-	5.716E-	38.72	65.72	65.72	7.502E-	0.022

Table E.23.Adjusted values for AC resistance for larger size NEXANS cables based on the relationship between NEXANS AC resistance and the resistance calculated for the larger cables using assumed electrical and conductor properties.

CONDUCTOR AREA (mm^2)	AC RESISTANCE AT 90°C NEXANS (Ω/km)	AC RESISTANCE AT 90°C (Ω/km)	AC RESISTANCE AT 90°C ADJUSTED(Ω/km)
95	0.25	0.231	0.251
120	0.2	0.183	0.199
150	0.16	0.147	0.160
185	0.13	0.119	0.130
240	0.1	0.092	0.101
300		0.073	0.081
400		0.055	0.061
500		0.044	0.050
630		0.035	0.040
800		0.027	0.032
1000		0.022	0.026

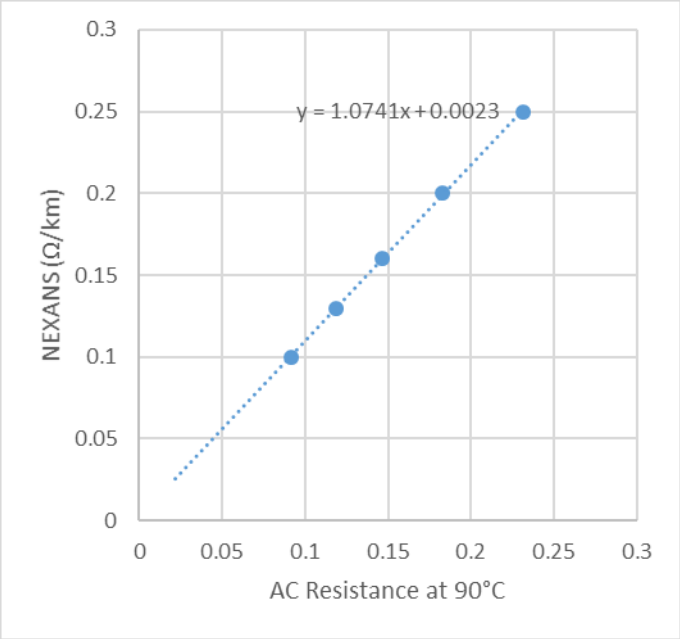

Figure E.5. Scatter plot showing the relationship between the calculated AC resistance of a cable using the adjusted values equating ABB cables to NEXANS and the resistance of the NEXANS cables.

E.5.3. HV Cables

Table E.24. Properties of ABB HV cables using three core cables with a lead sheath.

Cross-section of conductor	Diameter of conductor	Insulation thickness	Diameter over insulation	Lead sheath thickness	Outer diameter of cable	Cable weight (Aluminium)	Cable weight (Copper)	Capacitance	Charging current per phase at 50 Hz	Inductance
mm²	mm	mm	mm	mm	mm	kg/m	kg/m	µF/km	A/km	mH/km
Table 47										
Three-core cables, nominal voltage 132 kV (Um = 145 kV)										
185	15.8	18.0	54.2	2.1	165.0	41.4	44.9	0.13	3.0	0.47
240	18.1	17.0	54.5	2.1	166.0	41.8	46.3	0.14	3.4	0.44
300	20.4	16.0	54.8	2.1	167.0	42.4	48.0	0.16	3.8	0.42
400	23.2	15.0	55.6	2.1	168.0	43.6	51.1	0.18	4.3	0.40
500	26.2	15.0	59.0	2.3	176.0	48.6	58.0	0.20	4.6	0.38
630	29.8	15.0	62.6	2.4	185.0	53.3	65.2	0.21	5.1	0.37
800	33.7	15.0	66.5	2.5	194.0	59.0	74.0	0.23	5.6	0.36
1000	37.9	15.0	71.3	2.7	206.0	66.6	85.4	0.25	6.1	0.35
Table 48										
Three-core cables, nominal voltage 150 kV (Um = 170 kV)										
240	18.1	21.0	62.5	2.4	184.0	51.1	55.5	0.13	3.4	0.47
300	20.4	20.0	62.8	2.4	185.0	51.7	57.3	0.14	3.7	0.44
400	23.2	19.0	63.6	2.4	187.0	52.9	60.5	0.15	4.1	0.42
500	26.2	18.0	65.0	2.5	190.0	55.7	65.1	0.17	4.7	0.40
630	29.8	17.0	66.6	2.5	194.0	57.8	69.7	0.19	5.3	0.38
800	33.7	17.0	70.5	2.7	204.0	64.7	79.8	0.21	5.7	0.37
1000	37.9	17.0	75.3	2.8	215.0	71.6	90.5	0.23	6.3	0.36
Table 49										
Three-core cables, nominal voltage 220 kV (Um = 245 kV)										
500	26.2	24.0	77.6	2.9	219.0	71.8	81.3	0.14	5.7	0.43
630	29.8	23.0	79.2	3.0	224.0	74.9	86.7	0.16	6.4	0.41
800	33.7	23.0	83.1	3.1	234.0	80.2	95.3	0.17	6.9	0.40
1000	37.9	23.0	87.3	3.1	241.0	85.1	104.0	0.19	7.4	0.38

Table E.25. AC Resistance calculation for a 145 kV ABB cable.

ABB SUBMARINE CABLES 145 kV			ρ = 1.724 x 10^-11Ωkm	α = 0.00393								
CONDUCTOR AREA (mm^2)	CURRENT RATING (A)	INDUCTANCE (mH/km)	DC RESISTANCE (Ω/km) at 20°C	DC Resistance at 90°C (Ω/km)	xs^2	ys	xp^2	CONDUCTOR DIAMETER (mm)	DIAMETER OVER INSULATION (mm)	s	yp	AC RESISTANCE at 90°C
185	365	0.47	0.093	0.119	1.058E-03	5.825E-09	1.058E-03	15.8	54.2	54.2	2.547E-08	0.119
240	440	0.44	0.072	0.092	1.372E-03	9.803E-09	1.372E-03	18.1	54.5	54.5	4.288E-08	0.092
300	530	0.42	0.057	0.073	1.715E-03	1.532E-08	1.715E-03	20.4	54.8	54.8	6.704E-08	0.073
400	590	0.4	0.043	0.055	2.287E-03	2.723E-08	2.287E-03	23.2	55.6	55.6	1.193E-07	0.055
500	655	0.38	0.034	0.044	2.858E-03	4.255E-08	2.858E-03	26.2	59	59	1.865E-07	0.044
630	715	0.37	0.027	0.035	3.601E-03	6.755E-08	3.601E-03	29.8	62.6	62.6	2.963E-07	0.035
800	755	0.36	0.022	0.027	4.573E-03	1.089E-07	4.573E-03	33.7	66.5	66.5	4.783E-07	0.027
1000	825	0.35	0.017	0.022	5.716E-03	1.702E-07	5.716E-03	37.9	71.3	71.3	7.481E-07	0.022

Highlighted cells, no actual data for current for those conductor sizes so they were extrapolated and assumed.

Table E.26. AC Resistance calculated for a 170 kV ABB cable.

ABB SUBMARINE CABLES 170 KV			ρ = 1.724 x 10^-11Ωkm	α = 0.00393								
CONDUCTOR AREA (mm^2)	CURRENT RATING (A)	INDUCTANCE (mH/km)	DC RESISTANCE (Ω/km) at 20°C	DC Resistance at 90°C (Ω/km)	xs^2	ys	xp^2	CONDUCTOR DIAMETER (mm)	DIAM19ETER OVER INSULATION (mm)	s	yp	AC RESISTANCE at 90°C
240	440	0.47	0.072	0.092	1.372E-03	9.803E-09	1.372E-03	18.1	62.5	62.5	4.287E-08	0.092
300	530	0.44	0.057	0.073	1.715E-03	1.532E-08	1.715E-03	20.4	62.8	62.8	6.700E-08	0.073
400	590	0.42	0.043	0.055	2.287E-03	2.723E-08	2.287E-03	23.2	63.6	63.6	1.192E-07	0.055
500	655	0.4	0.034	0.044	2.858E-03	4.255E-08	2.858E-03	26.2	65	65	1.863E-07	0.044
630	715	0.38	0.027	0.035	3.601E-03	6.755E-08	3.601E-03	29.8	66.6	66.6	2.961E-07	0.035
800	755	0.37	0.022	0.027	4.573E-03	1.089E-07	4.573E-03	33.7	70.5	70.5	4.778E-07	0.027
1000	825	0.36	0.017	0.022	5.716E-03	1.702E-07	5.716E-03	37.9	75.3	75.3	7.472E-07	0.022

Table E.27. AC Resistance calculated for a 245 kV ABB cable.

ABB SUBMARINE CABLES 245 kV			ρ = 1.724 x 10^-11Ωkm	α = 0.00393								
CONDUCTOR AREA (mm^2)	CURRENT RATING (A)	INDUCTANCE (mH/km)	DC RESISTANCE (Ω/km) at 20°C	DC Resistance at 90°C (Ω/km)	xs^2	ys	xp^2	CONDUCTOR DIAMETER (mm)	DIAMETER OVER INSULATION (mm)	s	yp	AC RESISTANCE at 90°C
240	440	0.4529	0.071833	0.091595	1.372E-03	9.803E-09	1.372E-03	20.457	52.192	52.192	4.292E-08	0.091595
300	530	0.4475	0.057467	0.073276	1.715E-03	1.532E-08	1.715E-03	21.849	55.762	55.762	6.706E-08	0.073276
400	590	0.4385	0.0431	0.054957	2.287E-03	2.723E-08	2.287E-03	24.169	61.712	61.712	1.192E-07	0.054957
500	655	0.43	0.03448	0.043965	2.858E-03	4.255E-08	2.858E-03	26.2	77.6	77.6	1.861E-07	0.043965
630	715	0.41	0.027365	0.034893	3.601E-03	6.755E-08	3.601E-03	29.8	79.2	79.2	2.956E-07	0.034893
800	755	0.4	0.02155	0.027478	4.573E-03	1.089E-07	4.573E-03	33.7	83.1	83.1	4.770E-07	0.027478
1000	825	0.38	0.01724	0.021983	5.716E-03	1.702E-07	5.716E-03	37.9	87.3	87.3	7.457E-07	0.021983

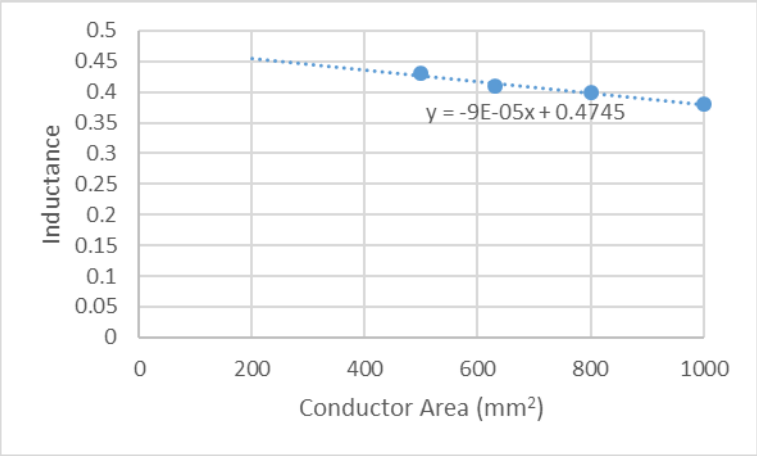

Figure E.6. Relationship between conductor area and inductance for a 245kV ABB cable to extrapolate inductance values for smaller conductor sizes.

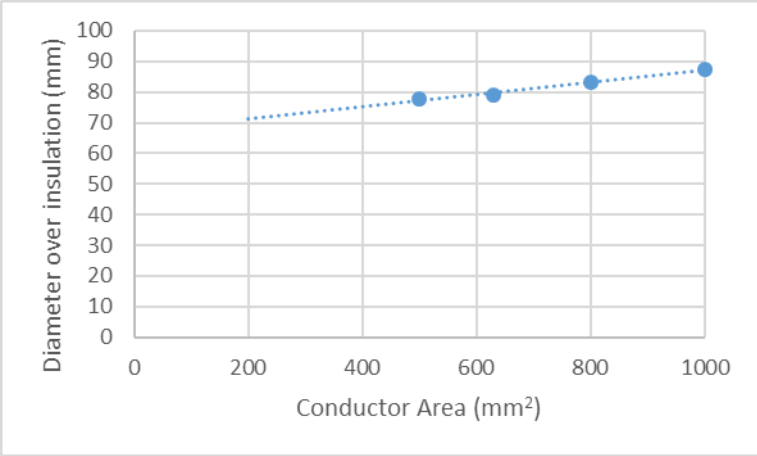

Figure E.7. Relationship between conductor area and diameter over the insulation for a 245kV ABB cable to extrapolate inductance values for smaller conductor sizes.

E.5.4. LV Cables

Table E.28. Current rating for Prysmian LV cables of 1kV based in on number of cores.

Conductor cross section	Current rating for continuous service. Conductor temperature max. +90°C, ambient max +45°C. According to IEC 60092-352, Table B.4 for 0,6/1 kV cables. Up to 6 cables bunched together.									
Cores	1	2	3	4	5	7	12	19	27	37
Reduction	1,00	0,85	0,70	0,70	0,58	0,52	0,44	0,37	0,33	0,30
(mm²)	(A)	(A)	(A)	(A)	(A)	(A)	(A)	(A)	(A)	(A)
1,5	23	20	16	16	13	12	10	9	8	7
2,5	30	26	21	21	18	16	13	11	10	9
4	41	34	28	28	24					
6	52	44	36	36	30					
10	72	61	50	50	42					
16	96	82	67	67	56					
25	127	108	89	89	74					
35	157	133	110	110	92					
50	196	167	137	137						
70	242	206	169	169						
95	293	249	205	205						
120	339	288	237	237						
150	389	331	272	272						
185	444	377	311	311						
240	522	444	365	365						
300	601	511	421	421						

Table E.29. Constructional data provided for Prysmian LV armoured 1kV cables

Size (n x mm²) or (n G mm²)	Conductor Diameter/Height approx. (mm)	Conductor Width approx. (mm)	Diameter over Braid approx. (mm)	Cable Diameter approx. (mm)	Cable Weight approx. (kg/km)	Bending Radius min. (mm)
POWER CABLES						
1x16	5,0	–	8,5	11,0	270	90
1x25	5,8	–	9,5	12,5	365	100
1x35	6,8	–	10,5	13,5	470	110
1x50	7,9	–	12,0	15,0	620	120
1x70	9,6	–	14,0	17,5	850	140
1x95	11,3	–	16,0	19,0	1130	150
1x120	12,7	–	17,5	21,0	1400	170
1x150	14,1	–	19,5	23,0	1700	180
1x185	15,7	–	21,5	25,0	2070	200
1x240	18,1	–	24,0	28,0	2650	220
2x1,5	1,6	–	7,5	10,0	130	60
2x2,5	2,0	–	8,5	11,0	160	65
3x1,5 3G1,5	1,6	–	8,0	10,5	155	65
3x2,5 3G2,5	2,0	–	9,0	11,5	195	70
3x4	2,6	–	10,0	13,0	270	80
3x6	3,1	–	11,0	14,0	320	85
3x10	4,0	–	13,5	16,5	520	100
3x16	5,0	–	16,0	19,0	740	115
3x25	5,8	–	18,5	22,0	1050	135
3x35	5,6	9,2	19,0	23,0	1350	185
3x50	6,5	10,7	21,5	25,5	1750	205
3x70	7,9	12,8	25,0	29,0	2400	230
3x95	9,3	15,1	28,0	33,0	3200	260
3x120	10,5	17,0	31,5	36,5	4100	290
3x150	11,6	18,9	35,0	41,0	5000	330

Table E.30.Constructional data provided for Prysmian LV unarmoured 1kV cables

Size (n x mm²) or (n G mm²)		Conductor Diameter/Height approx. (mm)	Conductor Width approx. (mm)	Cable Diameter approx. (mm)	Cable Weight approx. (kg/km)	Bending Radius min. (mm)
POWER CABLES						
1x16		5,0		9,0	200	70
1x25		5,8	–	10,5	290	85
1x35		6,9	–	11,5	385	90
1x50		8,0	–	13,0	510	100
1x70		9,7	–	15,0	720	120
1x95		11,3	–	16,5	970	130
1x120		12,7	–	18,5	1210	150
1x150		14,1	–	20,5	1490	160
1x185		15,7	–	23,0	1840	180
1x240		18,1	–	25,5	2390	200
1x300		20,2		29,0	3100	230
2x1,5		1,6	–	8,5	80	35
2x2,5		2,0	–	9,5	105	40
3x1,5	3G1,5	1,6	–	9,0	100	40
3x2,5	3G2,5	2,0	–	10,5	140	45
3x4	3G4	2,6	–	11,5	200	45
3x6	3G6	3,1	–	12,5	260	50
3x10		4,0	–	14,5	420	60
3x16		5,0	–	17,5	620	70
3x25		5,8	–	20,0	940	80
3x35		5,6	9,2	20,5	1170	160
3x50		6,5	10,7	23,0	1550	185
3x70		7,9	12,8	27,0	2200	215
3x95		9,3	15,1	31,0	2950	250
3x120		10,5	17,0	34,0	3700	270
3x150		11,6	18,9	38,0	4600	300

Table E.31. Electrical data provided for Prysmian LV 1kV cables.

Cable Type LM-HF, LSM-HF, LM-FRHF, LSM-FRHF (n x mm²)	Cross Section (mm²)	Conductor Resistance (IEC 60228) R (Ω/km) at +20 °C	at +45 °C	at +85 °C	Inductance L (mH/km)
1 x 35	35	0,524	0,575	0,658	0,316
1 x 50	50	0,387	0,425	0,486	0,315
1 x 70	70	0,268	0,294	0,336	0,303
1 x 95	95	0,193	0,212	0,242	0,292
1 x 120	120	0,153	0,168	0,192	0,284
1 x 150	150	0,124	0,136	0,156	0,286
1 x 185	185	0,0991	0,109	0,124	0,281
1 x 240	240	0,0754	0,083	0,095	0,276
1 x 300	300	0,0601	0,066	0,075	0,288
2 x 1,5	1,5	12,1	13,289	15,191	0,336
2 x 2,5	2,5	7,41	8,138	9,303	0,313
3 x 1,5	1,5	12,1	13,289	15,191	0,336
3 x 2,5	2,5	7,41	8,138	9,303	0,313
3 x 4	4	4,61	5,063	5,788	0,293
3 x 6	6	3,08	3,383	3,867	0,281
3 x 10	10	1,83	2,010	2,297	0,266
3 x 16	16	1,15	1,263	1,444	0,254
3 x 25	25	0,727	0,798	0,913	0,211
3 x 35	35	0,524	0,575	0,658	0,202
3 x 50	50	0,387	0,425	0,486	0,200
3 x 70	70	0,268	0,294	0,336	0,197
3 x 95	95	0,193	0,212	0,242	0,190
3 x 120	120	0,153	0,168	0,192	0,189
3 x 150	150	0,124	0,136	0,156	0,191
3 x 185	185	0,0991	0,109	0,124	0,193
3 x 240	240	0,0754	0,083	0,095	0,190
3 x 300	300	0,0601	0,066	0,075	0,188

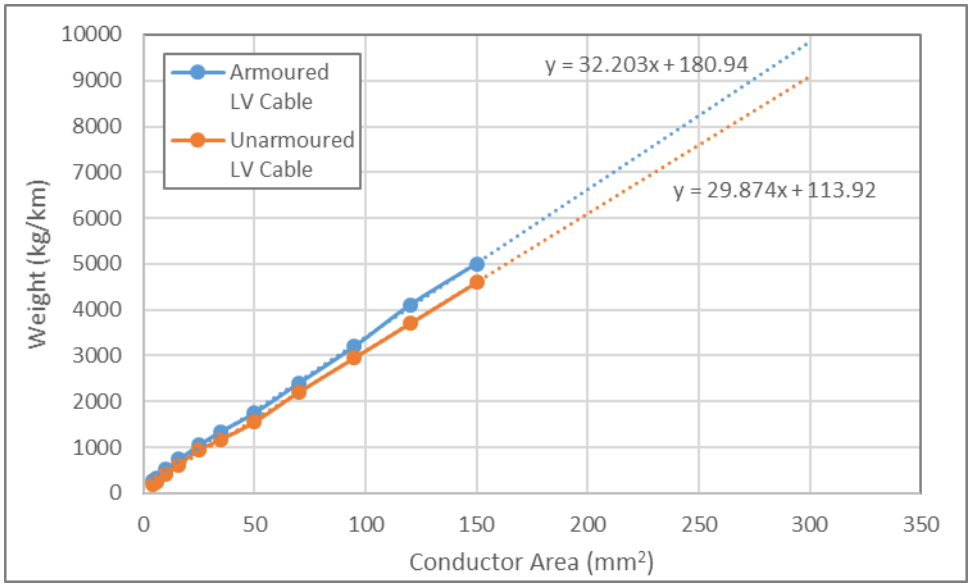

Figure E.8. Graph of conductor area vs. weight for LV armoured and unarmoured cables from Prysmian used to estimate weight of larger cable sizes.

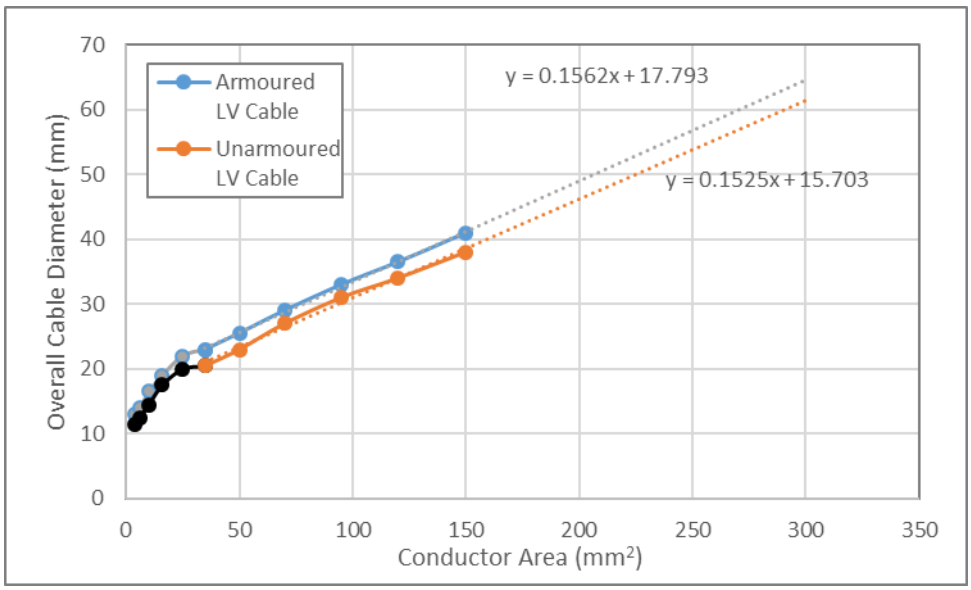

Figure E.9. Graph of conductor area vs. overall cable diameter for LV armoured and unarmoured cables from Prysmian to find diameters for larger cable sizes. The relationship between conductor area and cable diameter appears linear after a conductor size of 35mm², but not for conductor areas less than 35mm² which can be seen by the different colours.

Weight displaced by a 3m² kite assuming a depth of 0.2m:

$$Volume = Area \times depth$$
$$= 3 \times 0.2$$
$$= 0.6m^3$$

$$Displaced\ weight = Volume \times \rho$$
$$= 0.6 \times 1027$$
$$= 616.2\ kg$$

$$Tether\ Weight_{max} = Displaced\ Weight - Weight_{Turbine}$$
$$= 616.2 - 200$$
$$= 416.2\ kg$$

300mm^2 cable with a weight of 1476.28kg.

Kite thickness required to support the weight of the 300mm^2 cable:

$$Kite\ Thickness_{REQ.} = \frac{Total\ Weight\ (kg)}{Kite\ Area\ \times \rho}$$
$$= \frac{1476.28 + 200}{3 \times 1027}$$
$$= 0.55m$$

The voltage required if kite dimensions remain constant:

70mm^2 cable used weighing 360kg for 150m, total derating current for the cable is 191A.

$$V = \frac{Load\ (kVA) \times 1000}{\sqrt{3} \times I \times 1000}$$
$$= \frac{720 \times 1000}{\sqrt{3} \times 191 \times 1000}$$
$$= 2.18\ kV$$

Table E.32. Resistance calculations for armoured LV cables including weight and overall cable diameter and weight.

Conductor Area(mm²)	Current Rating (A)	Inductance (mH/km)	Resistance (Ω/km) DC 20	Resistance (Ω/km) DC 90	xs^2	ys	xp^2	Conductor Ø (mm)	Ø over braid (mm)	s	yp	Resistance (Ω/km) AC 90	Weight per km (kg)	Weight of 150m (kg)	Overall Ø (mm)
4	28	0.293	4.610	5.878	2.14E-05	2.38E-12	2.14E-05	2.60	10.00	5.00	1.04E-11	5.878	270	41	13
6	36	0.281	3.080	3.927	3.20E-05	5.33E-12	3.20E-05	3.10	11.00	5.50	2.33E-11	3.927	320	48	14
10	50	0.266	1.830	2.333	5.39E-05	1.51E-11	5.39E-05	4.00	13.50	6.75	6.61E-11	2.333	520	78	17
16	67	0.254	1.150	1.466	8.57E-05	3.83E-11	8.57E-05	5.00	16.00	8.00	1.67E-10	1.466	740	111	19
25	89	0.211	0.727	0.927	1.36E-04	9.57E-11	1.36E-04	5.80	18.50	9.25	4.19E-10	0.927	1050	158	22
35	110	0.202	0.524	0.668	1.88E-04	1.84E-10	1.88E-04	5.60	19.00	9.50	8.06E-10	0.668	1350	203	23
50	137	0.200	0.387	0.493	2.55E-04	3.38E-10	2.55E-04	6.50	21.50	10.75	1.48E-09	0.493	1750	263	26
70	169	0.197	0.268	0.342	3.68E-04	7.04E-10	3.68E-04	7.90	25.00	12.50	3.08E-09	0.342	2400	360	29
95	205	0.190	0.193	0.246	5.11E-04	1.36E-09	5.11E-04	9.30	28.00	14.00	5.94E-09	0.246	3200	480	33
120	237	0.189	0.153	0.195	6.44E-04	2.16E-09	6.44E-04	10.50	31.50	15.75	9.45E-09	0.195	4100	615	37
150	272	0.191	0.124	0.158	7.95E-04	3.29E-09	7.95E-04	11.60	35.00	17.50	1.44E-08	0.158	5000	750	41
185	311	0.193	0.099	0.126	9.94E-04	5.15E-09	9.94E-04					0.126	6138	921	47
240	365	0.190	0.075	0.096	1.31E-03	8.90E-09	1.31E-03					0.096	7910	1186	55
300	421	0.188	0.060	0.077	1.64E-03	1.40E-08	1.64E-03					0.077	9842	1476	65

Table E.33. Resistance calculations for unarmoured LV cables including weight and overall cable diameter and weight.

Conductor Area(mm²)	Current Rating (A)	Inductance (mH/km)	Resistance (Ω/km) DC 20	Resistance (Ω/km) DC 90	xs^2	ys	xp^2	Conductor Ø (mm)	Ø over braid (mm)	s	yp	Resistance (Ω/km) AC 90	Weight per km (kg)	Weight of 150m (kg)	Overall Ø (mm)
4	28	0.293	4.610	5.878	2.14E-05	2.38E-12	2.14E-05	2.6	11.5	5.75	1.04E-11	5.878	200	30	12
6	36	0.281	3.080	3.927	3.20E-05	5.33E-12	3.20E-05	3.1	12.5	6.25	2.33E-11	3.927	260	39	13
10	50	0.266	1.830	2.333	5.39E-05	1.51E-11	5.39E-05	4	14.5	7.25	6.60E-11	2.333	420	63	15
16	67	0.254	1.150	1.466	8.57E-05	3.83E-11	8.57E-05	5	17.5	8.75	1.67E-10	1.466	620	93	18
25	89	0.211	0.727	0.927	1.36E-04	9.57E-11	1.36E-04	5.8	20	10	4.19E-10	0.927	940	141	20
35	110	0.202	0.524	0.668	1.88E-04	1.84E-10	1.88E-04	5.6	20.5	10.25	8.05E-10	0.668	1170	176	21
50	137	0.200	0.387	0.493	2.55E-04	3.38E-10	2.55E-04	6.5	23	11.5	1.48E-09	0.493	1550	233	23
70	169	0.197	0.268	0.342	3.68E-04	7.04E-10	3.68E-04	7.9	27	13.5	3.08E-09	0.342	2200	330	27
95	205	0.190	0.193	0.246	5.11E-04	1.36E-09	5.11E-04	9.3	31	15.5	5.94E-09	0.246	2950	443	31
120	237	0.189	0.153	0.195	6.44E-04	2.16E-09	6.44E-04	10.5	34	17	9.45E-09	0.195	3700	555	34
150	272	0.191	0.124	0.158	7.95E-04	3.29E-09	7.95E-04	11.6	38	19	1.44E-08	0.158	4600	690	38
185	311	0.193	0.099	0.126	9.94E-04	5.15E-09	9.94E-04					0.126	5641	846	44
240	365	0.190	0.075	0.096	1.31E-03	8.90E-09	1.31E-03					0.096	7284	1093	52
300	421	0.188	0.060	0.077	1.64E-03	1.40E-08	1.64E-03					0.077	9076	1361	61

F. Appendix F

F.1. Dynamic Loading

Table F.1. The dynamic loading for TUSK systems, a wind turbine and a marine turbine.

	ρ (kg/m^3)	v_{max} (m/s)	v_a (m/s)	q (KN/m^2)
TUSK	1027	2.4	24	295.78
Wind Turbine	1.184	25	25	0.37
Marine Turbine	1027	2.4	2.4	2.96

Table F.2. Design parameters of the various kite designs

DESIGN PARAMETERS	z	k1	k2	STM	AR	PFW	CL	Re(root)	Re(tip)
KITE 2	0.75	0.55	0.45	0.15	8.57	20.97	0.4	380370	285278
KITE 3	0.86	0.53	0.47	0.15	9.23	16.26	0.4	332824	285278
KITE 4	1	0.5	0.5	0.15	16.00	9.93	0.4	237731	237731

Table F.3. Twist calculated using various airfoils and kite designs.

	KITE 2			KITE 3			KITE 4		
AIRFOIL	$C_{m\ root}$	$C_{m\ tip}$	ALPHA	$C_{m\ root}$	$C_{m\ tip}$	ALPHA	$C_{m\ root}$	$C_{m\ tip}$	ALPHA
NACA 0009	0	0	-9.46	0	0	-10.98	0	0	-8.19
NACA 0012	0	0	-9.46	0	0	-10.98	0	0	-8.19
NACA 22112	0	0	-9.46	0	0	-10.98	0	0	-8.19
NACA 23112	-0.005	-0.005	-10.25	-0.005	-0.005	-11.90	-0.005	-0.005	-8.87
NACA 24112	-0.01	-0.01	-11.04	-0.01	-0.01	-12.81	-0.01	-0.01	-9.56
NACA 25112	-0.027	-0.027	-13.72	-0.027	-0.027	-15.92	-0.027	-0.027	-11.88

G. Appendix G

G.1. Python Scripts

G.1.1. Wind rose Script

```
import csv
cr = csv.reader(open('E:\python\current rose\PE csv.csv','rb'))
cr2 = csv.reader(open('E:\python\current rose\PE csv.csv','rb'))

list1 = [x[0] for x in cr] #column 1: Direction extracted from csv file
list2 = [x[1] for x in cr2] #column 2: Velocity magnitude extracted from csv file

def conv(list):
    ""conv takes a list of strings as input and returns a list of floats""
    newL = []
    for i in list:
        newL = newL + [float(i)]


    return newL

list3 = conv(list1) #Direction values as list of floats
list4 = conv(list2) #Velocity magnitude values as list of floats

import windrose
from windrose import WindroseAxes
from matplotlib import pyplot as plt
import matplotlib.cm as cm
import numpy as np
from numpy import arange

wd = list3 #direction specified
ws = list4 #speed specified

ax = WindroseAxes.from_ax()
ax.bar(wd,ws, normed=True, opening=0.8, edgecolor='white',bins=np.arange(0,2.5,0.5)
)

ax.set_legend()
plt.show()
```

G.1.2. Distance between Co-ordinates

http://stackoverflow.com/questions/4913349/haversine-formula-in-python-bearing-and-distance-between-two-gps-points

```
from math import*
def haversine(lon1, lat1, lon2, lat2):
    """
    Calculate the great circle distance between two points
    on the earth (specified in decimal degrees)
    """
    # convert decimal degrees to radians
    lon1, lat1, lon2, lat2 = map(radians, [lon1, lat1, lon2, lat2])

    # haversine formula
    dlon = lon2 - lon1
    dlat = lat2 - lat1
    a = sin(dlat/2)**2 + cos(lat1) * cos(lat2) * sin(dlon/2)**2
    c = 2 * asin(sqrt(a))
    r = 6371 # Radius of earth in kilometers. Use 3956 for miles
    return c * r
```

G.1.3. Export Datapoints

```
import numpy as np
from netCDF4 import Dataset
file4 = Dataset('E:/Masters/Hycom data/GLBa0 (4).nc4')
file3 = Dataset('E:/Masters/Hycom data/GLBa0 (3).nc4')

lats4 = file4.variables['Latitude'][:]
lons4 = file4.variables['Longitude'][:]
time4 = file4.variables['MT'][:]
depth4 = file4.variables['Depth'][:]
velu4 = file4.variables['u'][:]
velv4 = file4.variables['v'][:]

PElat = -31.211
CMlat = -32.501999
ELlat = -33.174198
FR2lat = -33.708199
FR1lat = -33.841202

PElon = 390.239990
CMlon = 388.800049
ELlon = 388.079956
FR2lon = 387.280029
FR1lon = 387.119995

def listgen(startlat, endlat,n):
    """list gen takes in a starting latitude point and ending latitude point
        and number of posistions required it calculates the difference between
        these and calculates the step required between each location based on
        the number of locations required and generated an output list of all
        latitude values"""
    pointlist = []
    #incl. startlat in Pointlist if first segment
    a = (startlat-endlat)/(n)
    #start incl. (n-1)
    while len(pointlist) < (n):
        startlat = startlat - a
        pointlist = pointlist + [startlat]
    return pointlist
Point = listgen(CMlat,ELlat,100)

def listgenlon(startlon, endlon,n):
    """same principles as listgen but using longitude values"""
    startlon = startlon
    endlon = endlon
    pointlist2 = []
    #incl. startlat in Pointlist if incl.
    a = (startlon-endlon)/(n-1)
    #start incl. (n-1)
    while len(pointlist2) < (n):
        startlon = (startlon - a)
        pointlist2 = pointlist2 + [startlon]
    return pointlist2
Point2 = listgenlon(CMlon,ELlon,100)

def getclosest_ij(lats,lons,latpt,lonpt):
    """determines the closest grid point in HYCOM to provided co-ors"""
    dist_sq = (lats-latpt)**2 + (lons-lonpt)**2
    minindex_flattened = dist_sq.argmin()
    return np.unravel_index(minindex_flattened,lats.shape)

def extractlist(list1,list2,n,extract=[]):
    """provides the grid locations of all points to be extracted from
        latitude and longitude points"""
```

```
    if len(extract) == n:
        return extract
    else:
        extract = extract + [getclosest_ij(lats4, lons4, list1[0],list2[0])]
        return extractlist(list1[1:],list2[1:],n,extract)
Extract = extractlist(Point,Point2,100)

def removepoint(L,newlist=[]):
    """removes duplicate grid reference names from list"""
    if L ==[]:
        return newlist
    elif L[0] in newlist:
        return removepoint(L[1:],newlist)
    else:
        newlist = newlist + [L[0]]
        return removepoint(L[1:],newlist)
Extractonly = removepoint(Extract)

def countlist(List1, List2, extractlist=[], count=0):
    """counts the number of times a grid reference needs to be used for each
        grid reference within the list"""
    while List2 != []:
        if List2[0] == List1[0]:
            count += 1
            if len(List1)==1:
                extractlist = extractlist + [count]
                break
            return countlist(List1[1:],List2,extractlist,count)
        else:
            extractlist = extractlist + [count]
            return countlist(List1,List2[1:],extractlist, count=0)
    return extractlist

counted = countlist(List1, List2)
```

G.1.4. Longest duration

```
import sys
sys.setrecursionlimit(2750)

import csv
cr = csv.reader(open('E:\HYCOM vs ESKOM\FINAL RESULTS\Factored\LONDUR\LONDUR ALT PC
.csv','rb'))
cr2 = csv.reader(open('E:\HYCOM vs ESKOM\FINAL RESULTS\Factored\LONDUR\LONDUR ALT P
C.csv','rb'))

rows = [x for x in cr2]
row_1 = rows[0] #list elements in row1 of csv file

def indexlist(List):
    """creates a list of indeces of elements in row1"""
    R = []
    for i in row_1:
        R+= [row_1.index(i)]
    return R
Indexes = indexlist(row_1)


arr = range(2517) #adjust to needed

def listofcol(index):
    """creates a list for column specified by the index within the csv file"""
    extr = [x[index] for x in cr]

    return extr
```

```
ColList = listofcol(25)


def csvtolist(column):
    """creates a new list from csv column"""
    L=[]
    x=0

    for row in column:

        arr[x] = row

        L += [arr[x]]

    L=L[1:2518]
    return L
StrList = csvtolist(ColList)

def strtofloat(List):
    """converts list of strings to new list of floats"""
    newL =[]
    for i in List:
        i = float(i)
        newL += [i]
    return newL
FloatList = strtofloat(StrList)


def longestdur(L,count,newcount=0):
    """takes in a list of floats and returns the longest duration that kites
        will not be operational for under the specified parameters"""

    while len(L) != 0:
        if L[0] == 0:   #0 indicates no operationality; can use any value -
                        #<25 will give the longest duration that less than 25% kite
s not operational
            newcount +=1

            return longestdur(L[1:],count,newcount)
        else:
            if count >= newcount:
                count = count

            else:
                count = newcount

            return longestdur(L[1:],count,newcount=0)
    if count >= newcount:
        return count
    return newcount

LonDur = longestdur(FloatList,0)
```

G.1.5. List to Matrix

```
latlist = lats.tolist()
lonlist = lons.tolist()

matrix = [lonlist]*len(latlist)
longitude = np.asarray(matrix)

matrix2 = [latlist]*len(lonlist)
rmatrix2 = np.asarray(matrix2)
latitude = rmatrix2.transpose()
```